Republic of Iraq
Ministry of Higher Education
and Scientific Research
University of Babylon
College of Engineering

Nonlinear Static and Dynamic Analysis of Laminated Plates Under In-plane Forces

A Thesis
Submitted to the College of Engineering
of the University of Babylon in Partial fulfillment of the
Requirements for the Degree of Doctor of Philosophy
in Civil Engineering
(Structural Engineering)

By

Haider Kadhem Ammash
M.Sc.

Supervised by

Prof. Dr. Husain M. Husain
Assist. Prof. Dr. Nameer A. Alwash

January 2008
Moharram 1429

جمهورية العراق

وزارة التعليم العالي والبحث العلمي

جامعة بابل/ كلية الهندسة

قسم الهندسة المدنية

التحليل اللاخطي الاستاتيكي والديناميكي للالواح الطبقية تحت أحمال محورية

أطروحة

مقدمة الى كلية الهندسة في جامعة بابل

جزءاً من متطلبات نيل شهادة دكتوراه فلسفة

في الهندسة المدنية

(الهندسة الانشائية)

حيدر كاظم عماش

ماجستير هندسة مدنية

إشراف

الاستاذ الدكتور حسين محمد حسين الاستاذ المساعد نمير عبد الامير علوش

كانون الثاني 2008 محرم 1429

ز

هُوَ الَّذِي بَعَثَ فِي الْأُمِّيِّينَ رَسُولًا مِنْهُمْ يَتْلُو عَلَيْهِمْ آيَاتِهِ وَيُزَكِّيهِمْ وَيُعَلِّمُهُمْ الْكِتَابَ وَالْحِكْمَةَ وَإِنْ كَانُوا مِنْ قَبْلُ لَفِي ضَلَالٍ مُبِينٍ

صدق الله العلي العظيم

سورة الجمعة، الاية (2)

الخلاصة

تـم تقـديم طريقـة العناصـر المحـددة اللاخطيـة لتحليـل الازاحـة الكبيـره المـرن-اللـدن الاسـتاتيكي والـديناميكي للصـفائح غيـر متماثلـة الخـواص تحـت حمـل ضـغط فـي المسـتوي. تبنـت هـذه الدراسـة طريقة الطبقة ثنائي البعد(two-dimensional layered approach) واعتمدت نظرية التشوهات القصية الكلاسيكية وذات المرتبـة العليـا (classical and higher order shear deformation theory) مـع خمس،وسـبع وتسـع درجـات حريـة لكـل عقـدة، تـم توظيـف عنصـر لاكـرانج (Lagrangian) ذي العقد التسع لتمثيل الصفائح الطبقية. تم فرض ترابط تام بين الطبقات المتعددة (لا يحدث التَرقُق(انفصال الطبقات)).

قسمت هذة الدراسة الى جزئين، يتضـمن الجـزء الاول تحليل الازاحـة الكبيـره المـرن-اللـدن الاستاتيكي للصفائح الحديدية والُطبقية تحت حمل ضغط في المستوي. وقد أُخذ بنظـر الاعتبـار تـأثير التقوسات الابتَدائية ونَسب النحافة ونَسب الأبعاد وظروف الاسناد وتعامد الخواص للطبقات المنفردة وزاوية تدوير الالياف وتموج الالياف على تحليل الازاحة الكبيره المرن-اللدن الاستاتيكي. تم تحليل الصفيحة مع مجال من نَسب التقوس الابتدائي (0.0-1.0) ومجال من نَسب النحافة (0.5-4.242)، ومجال من تسلسل الالياف المتموجة (1-12)، ومجال من ارتفاع قمة الالياف المتموجة(0.0-0.5).

يتضمن الجزء الثاني تحليل الازاحـة الكبيـرة المـرن-اللـدن للصـفائح الحديديـة والطبقيـة تحـت احمـال ديناميكيـة فـي المسـتوي. تـم اسـتعمال مصـفوفة الكتلـة المتوافقـة والكتلـة المتكومـة فـي هـذه الدراسة. كذلك، تم استخدام مصفوفة إخماد رايلي (Rayleigh type damping matrix) للتعبير عن خواص الاخماد. تم استخدام طريقتين (Newmark integration method) و(harmonic acceleration method) لحل معادلـة التوازن الديناميكي. وقد أُخذ بنظـر الاعتبـار تـأثير التقوس الابتدائي وخطوة الوقت وظروف الاسناد وتعامد الخـواص للطبقـات المنفردة وزاويـة تـدوير الالياف ونوع الحمل وقيمة الحمل ومعامل التخميد وتموج الالياف علـى تحليل الازاحـة الكبيـره المـرن-اللـدن الديناميكي.

تم فحص بعض الامثلة بأستخدام برنامج الحاسبة (FENSDAAP)الذي كتب في الدراسة الحالية وكذلك قورنت مع دراسة سابقة لبعض الباحثين.

من النتائج المستحصلة، يمكن ملاحظة التالي:-1المقاومة القصوى للصفائح تحت حمل ضغط في المستوي يتناقص مع زيادة عدد درجات الحرية(الصفيحة تصبح اكثر مرونـة)’2) تصـرف الصـفائح الُطبقيـة حسـاس جداً لشكل الالياف (مستقيم او متموج). تصرّف الصفائح ذات الالياف المتموجة معتمد على ارتفاع قمة الالياف وعدد تسلسل التموجات’3) قابلية التحمل للصفائح المُطّبقة والمتموجة الالياف وتحت حمل ضغط في اتجاه التموج اكثر من قابلية التحمل للصفائح الطبقية والمتموجة

الالياف وتحت حمل ضغط عمودي على التموج بحوالي (42%)’4) الصفائح التي لا تمتلك تقوساً ابتدائياً لا تظهر اي تذبذب لاحمال ديناميكية في المستوي اقل من حمل الانبعاج الاستاتيكي لتلك الصفيحة’5) قابلية التحمل الديناميكية للصفيحة وفترة الوقت تتناقص مع زيادة نسبة الحمل(P_x/P_u)’ 6) الصفائح الطبقية المتعامدة غير تناظرياً(antisymmetric cross-ply) تمتلك معدل تخميد اعلى من معدل تخميد الصفائح الطبقية المتعامدة تناظرياً (symmetric cross-ply)’7) اذا اخذ التخميد بنظر الاعتبار وتصرف الصفيحة اظهر عدم اي تذبذب حول موضع الهطول الاستاتيكي، فهذا يعني أن معامل التخميد تحت معامل التخميد الحرج.

Abstract

A nonlinear finite element method is adopted for the large displacement elastic-plastic static and dynamic analysis of anisotropic plates under in-plane compressive loads. The analysis is based on the two-dimensional layered approach with classical and higher order shear deformation theory with five, seven, and nine degrees of freedom per node, nine-node Lagrangian isoparametric quadrilateral elements are used for the discretization of the laminated plates. A complete bond between the layers is assumed (no delamination occurs).

This study is divided into two parts; the first part includes the large displacement elastic-plastic static analysis of steel and laminated composite plates under in-plane compressive loads. The effects of initial imperfection, slenderness ratio, aspect ratio, boundary conditions, orthotropy of individual layers, fiber's orientation angle, and fiber waviness on the large displacement elastic-plastic static analysis are considered. The plate is analyzed with a range of initial imperfection ratios ($\boldsymbol{w_o/h}$) (0.0-1.0), range of slenderness ratios ($\left(\frac{b}{h}\sqrt{\frac{\sigma_o}{E}}\right)$)(0.5-4.242), range of number of sequences ($\boldsymbol{k}$) of sine wave fiber (1-12) and with a range of the amplitude of fiber path ($\boldsymbol{\Delta}$) of sine wave fiber (0.0-0.5).

The second part includes the large displacement elastic-plastic dynamic analysis of plain and laminated composite plates under in-plane dynamic loading. Both consistent and lumped mass matrices are used in the present study. Damping property is considered by using Rayleigh type damping which is linearly related to the mass and the stiffness matrices. **Newmark** integration method and Harmonic acceleration method are used for solving the dynamic equilibrium equations. The effects of initial imperfection, time step, boundary conditions, orthotropy of individual layers, fiber's orientation angle, type of loading, load magnitude, damping factor, and fiber waviness on the large displacement elastic-plastic dynamic analysis are considered.

Several examples have been investigated using a computer program which is named herein as (FENSDAAP) and the results are compared with those obtained by other researchers.

From these results, the following points are noticed: 1) The ultimate strength of the plates under in-plane compressive loads decreases with increasing the number of degrees of freedom (the plate becomes more flexible), 2) The behavior of the laminated plate is very sensitive to the shape of fibers (straight or sine wave). The behavior of the plate with sine wave fiber depends on the amplitude of the fiber and the number of sequences of the fiber, 3) the capacity of the laminated plate with sine wave fiber and under in-plane compressive load in the direction of waviness is higher than the capacity of the plate with sine wave fiber and under in-plane compressive load orthogonal to the direction of waviness by approximate value (42%), 4) the perfect plate does not reveal any oscillation for in-plane dynamic loading less than the static buckling load of this plate, 5) the dynamic capacity of the plate and the time duration will decrease as the loading ratio (applied in-plane load to the static ultimate in-plane load)($\boldsymbol{P_x/P_u}$) increases, 6) the antisymmetric cross-ply laminated plate has a damping rate faster than the symmetric cross-ply laminated plate, 7) if damping is considered and if the response of the plate shows no oscillation about the static deflection position, it means that the damping factor is below the critical damping factor.

Acknowledgements

Praise be to ALLAH, the Most Gracious, the Most Merciful, Who gave me the ability and desire to complete this study work.

I wish to express my continual thanks and deepest gratitude to my supervisors **Dr. Husain M. Husain** and **Dr. Nameer A. Alwash** for their suggestion of the problem, and their valuable assistances and continuous guidance.

I am grateful to the Dean of the College of Engineering and the Head of the Civil Engineering Department in the University of Babylon for their co-operation and assistance.

Special thanks are due to **Mr. Nabeel H.** for his help during the research.

Always, great thanks for my family, especially for my parents for their support to carry out this work, for my brothers, for my sisters, and for my wife.

Finally, all my words cannot express my thanks for all my friends for their interest and support during carrying out this study.

Haider Kadhem Ammash

2007

Certification

We certify that this thesis titled "**Nonlinear Static and Dynamic Analysis of Laminated Plates Under In-plane Forces**", was prepared by "**Haider Kadhem Ammash**" under our supervision at Babylon University in partial fulfillment of the requirements for the degree of Doctor of Philosophy in Civil Engineering.

Signature:

Name: Dr. Husain M. Husain

Date: / /2007

Signature:

Name: Dr. Nameer A. Alwash

Date: / /2007

CERTIFICATE

We certify as an examining committee that we have read this thesis entitled **"Nonlinear Static and Dynamic Analysis of Laminated Plates Under In-plane Forces",** and examined the student **Haider Kadhem Ammash** in its content and what related to it, and found it meets the standard of thesis for the degree of Doctor of Philosophy in Civil Engineering.

Signature:
Name: Asst. Prof. Dr. Ihsan Al-Shaarbaf
(Member)
Date: / / 2008

Signature:
Name: Asst. Prof. Dr. Raad K. Shukur
(Member)
Date: / / 2008

Signature:
Name: Prof. Dr. Sabeeh Z. Al -Sarraf
(Chairman)
Date: / / 2008

Signature:
Name: Asst. Prof.Dr. Haitham H. Aldaami
(Member)
Date: / / 2008

Signature:
Name: Asst. Prof. Dr. Mustafa B. Dawood
(Member)
Date: / / 2008

Signature:
Name: Prof. Dr. Husain M. Husain
(Member)
Date: / / 2008

Signature:
Name: Asst. Prof. Nameer A. Alwash
(Member)
Date: / / 2008

Approval of the Civil Engineering Department
Signature:
Asst. Prof. Dr. Ammar Yaser Ali
Head of the Civil Engineering Department
Date: / / 2008

Approval of the College of Engineering
Signature:
Prof. Dr. Nabeel –Al
Dean of the College of Engineering
Date: / / 2008

Contents Pages

Chapter Five
Nonlinear Dynamic Analysis of Plate

Chapter Six
Applications and Discussions on Nonlinear Static Analysis

Notations

Symbol	Description
a, b	Plate dimensions in x and y-directions, respectively.
$[B]$	Strain-nodal displacement matrix.
c_{ij}	Element of elasticity matrix with respect to material coordinate system.
D	Flexural rigidity = $Et^3/12(1-\nu^2)$.
$\{d\}$	Displacement vector.
$\{\dot{d}\}$	Velocity vector.
$\{\ddot{d}\}$	Acceleration vector.
E_i	Modulus of elasticity in i-direction.
E_f	Modulus of elasticity of fiber.
E_m	Modulus of elasticity of matrix.
F_i, F_{ij}	Strength tensors of the first and second order, respectively.
$\{F\}$	External load vector.
F	Yield function.
$\{F_D\}$	Damping force vector.
$\{F_I\}$	Inertia force vector.
$\{F_S\}$	Elastic force vector.
$\{F(t)\}$	Dynamic external force vector.
G	Shear modulus.
h_L-h_{L-1}	Distance from plate middle surface to the upper and lower surface of L^{th} lamina.
h	Plate thickness.
$[K_o]$	Constant linear elastic stiffness matrix
$[K_L]$	Initial or large displacement matrix
$[K_\sigma]$	Initial stress stiffness matrix
$[K_T]_0$	Tangent stiffness matrix.
M_x, M_y, M_{xy}	Bending and twisting moments (per unit width) (on yz, xz, and both yz and xz-sections).
M_x^*, M_y^*, M_{xy}^*	Higher order bending and twisting moments (per unit width) (on yz, xz, and both yz and xz-sections).
N_x, N_y, N_{xy}	In-plane stress resultants (per unit width) (on yz, xz, and both yz and xz-sections).

N_x^*, N_y^*, N_{xy}^*	Higher order in-plane stress resultants (per unit width) (on ***yz***, ***xz***, and both ***yz*** and ***xz***-sections).
P_x	In-plane applied load in ***x***-direction.
$\{P\}$	Internal load vector.
Q_{ij}	Element of elasticity matrix with respect to Cartesian coordinate system
Q_x, Q_y	Transverse shearing forces (per unit width) (on ***yz*** and ***xz***-sections).
Q	Uniformly distributed load (per unit area).
$\{\Delta R\}$	Residual load vector.
$[T]$	Transformation matrix.
u,**v**,***w***	Displacement components in ***x***,***y*** and ***z*** direction, respectively.
w_o	Amplitude of initial imperfection.
x,y,z	Coordinates.
γ_{ij}^o	Shear strain in ij-plane at middle surface.
γ_{ij}^{o*}	Higher order shear strain in ij-plane at middle surface.
$\{\varepsilon\}$	Strain vector.
$\{\varepsilon_o\}$	Middle surface strain vector.
ε_i	Normal strain in i-direction.
ε_i^o	Normal strain in i-direction at middle surface.
ε_i^{o*}	Higher order normal strain in i-direction at middle surface.
ξ, η	Curvilinear coordinates system.
θ	Fiber's orientation angle.
θ_x, θ_y	Rotations of transverse normals in the (***xz***) and (***yz***) planes.
θ_x^*, θ_y^*	Higher order rotations of transverse normals in the (***xz***) and (***yz***) planes.
κ_i^o	Bending curvature in i-plane at middle surface.
κ_{ij}^o	Bending curvature in ij-plane at middle surface.
κ_i^{o*}	Higher order bending curvature in i-plane at middle surface.
κ_{ij}^{o*}	Higher order bending curvature in ij-plane at middle surface.
ν_i	Poisson's ratio in i-direction.
$\{\sigma\}$	Stress vector at sampling point.
$\sigma_{m(\max)\,\varepsilon_f}$	Matrix stress at a matrix strain equal to the maximum tensile strain in the fiber
σ_o	Yield stress of steel

Abbreviations

Symbol	Description
AIAA	American institute of aeronautics and astronautics
ASCE	American society of civil engineers.
ASME	American society of mechanical engineers.
Comp.&Struct.	Computers and structures.
D.O.F.	Degree of freedom.
Eng.struct.	Engineering structure.
ICE	Institution of civil engineers.
Int.J.Mech.Sci.	International journal of mechanical sciences.
Int.J.Num.Meth. Eng.	International journal of numerical methods in engineering.
Int.J.Struct.Eng. and Mech.	International journal of structural engineering and mechanics.
J. Appl. Mech	Journal of applied mechanics.
J.Eng.Mech.	Journal of engineering mechanics.
J.Eng.Mech.Div.	Journal of engineering mechanic division.
J.Eng.Strcut.	Journal of engineering structures.
NASA	National aeronautics and space administration.
NDOF	Number of degree of freedom.

CHAPTER ONE

Introduction

1.1 General

All real physical structures, when subjected to quickly applied loads or displacements, behave dynamically. The additional inertia forces, from Newton's second law, are equal to the mass times the acceleration of the oscillating bodies. If the loads or displacements are applied very slowly, then the inertia forces can be neglected and a static load analysis can be justified. In engineering practice, however, plate problems often involve consideration of dynamic disturbances, produced by time-dependent external forces or displacements. Dynamic loads may be created by moving vehicles, wind gusts, seismic disturbances, unbalanced mechanics, wave impacts, flight loads, shock or blast, sound, etc.

Structural dynamics deals with time-dependent motions of structures and an analysis of the internal forces associated with them. Thus, the objective is to determine the effect of vibrations on the performance of the structure [**Szilard, 1974**][(103)].

The computation of natural frequencies and modes comprises a significant element in the dynamic analysis of structures, and it is important in the design of structures subjected to vibratory loading as from earthquakes and moving vehicles. It is generally considered that the structural response of structures subjected to any kind of dynamic loads is dependent on both of lower and higher modes. In designing these structures, it is essential that the natural frequencies and modes be determined accurately. In the case of static loading, stability analysis over the years has been a very useful tool for design. The primary reason for this is that the type of analysis yields somewhat limited but still useful information at a significant reduction in cost. The definition of buckling load is useful, also because it makes possible the use of design charts for simple structural configurations. Such charts, although are now in a lesser degree of use, due to the availability of high speed computers, are still valuable in the preliminary design phase.

1.2 Steel Plate Structures

Plate structures such as the plate, box and multi-cellular girders were fabricated from an assemblage of individual plates. This allows the designers to select the most effective disposition of material in the cross-section to carry the specific loading. Structures of high strength/weight ratio can then be achieved which are practically well suited to long-span bridges, aircrafts, Figure(1.1), ships, and other situations where the reduction of self-weight is an important design objective [**Mathlum,1997**][(66)].

Figure (1.1): An aircraft wing idealized as a plate structure

To maximize the saving in self-weight, the component plates of the structural member are designed to be of slender properties. They will then have a low elastic critical load and will normally operate in the post-buckling range, so that advantage must take their post-buckling reserve of strength. Thus, the design of the plate panels is based on post-buckling compressive strength with consideration of buckling load. Therefore, it is necessary to study the post-buckling behavior of the plate panels besides their buckling behavior. The buckling characteristics of such panels are of crucial importance for overall structural strength. The post-buckling behavior is especially important because of the reserved capacity which exists after the initial buckling. However, looking at the deflection behavior of actual plate panels, it is clear that a column model does not provide the best representation of the real structural response. Usually, local

deformations dominate, while lateral deflection in the global mode is less significant.

The compressive strength of plate panels is of primary concern to the designer. As a sequence, the evaluation of plate compressive strength has mainly been achieved through laboratory experiments in the past few decades. For a realistic assessment of the buckling and post-buckling behavior of plates, large deflection theory must be used because small deflection theory is of limited practical value for the analysis of plate at loads comparable to their ultimate loads. The large deflection mechanics of plates is a highly nonlinear problem whose solution relies on the use of a numerical technique such as the nonlinear finite element analysis.

Although the linear buckling loads provide a measure of the compressive load carrying capacity of the plate panels, the test results indicate that the panels can undergo substantial nonlinear transverse deformations prior to failure.

Traditionally, such structures have been designed according to the allowable stress principles so that a linear elastic analysis of the stress distribution was sufficient to be used by employing simplified linear numerical analysis such as the finite difference and the finite element methods. The improved nonlinear analysis is applicable to different plates which continue to operate in the post-buckling range. Therefore, the effect of geometric nonlinearity arising from the plate buckling, must be taken in account.

1.3 Composite Material

The composite material is made of two or more macro-constituent's materials essentially soluble or mixable into each other, usually a reinforcing material supported in a compatible matrix, where the sum of properties of each constituent taken separately, are assembled in prescribed amounts to achieve specific physical and chemical properties [**Jones,1999**][(50)].

The reinforcement materials may form as continuous or discontinuous fibers, flakes, fillers or particles embedded in the matrix material. Fibers in various forms (mat yarn, woven roving, and chopped strands) are inherently much stiffer and stronger than the same material in bulk form. The matrix material works as a binder material giving the composite a protection and supports its bulk

form and stress transfer when the fiber is broken. Typically, the matrix is of considerably lower density, stiffness and strength than those of the fibers.

Composite materials have many characteristics that are different from many conventional engineering materials. Most common engineering materials are homogeneous and isotropic while the composite materials are often heterogeneous and anisotropic. Such materials have physical properties varying with respect to position and orientation.

Layered composite material plates are extensively used in the construction of aerospace, civil, marine, automotive and other high performance structures, and during the operation of this structure, it is subjected to static and dynamic loads, Figure (1.2). Therefore, there exists a need for investigating the response of layered (laminated) composite material plates subjected to such types of loading.

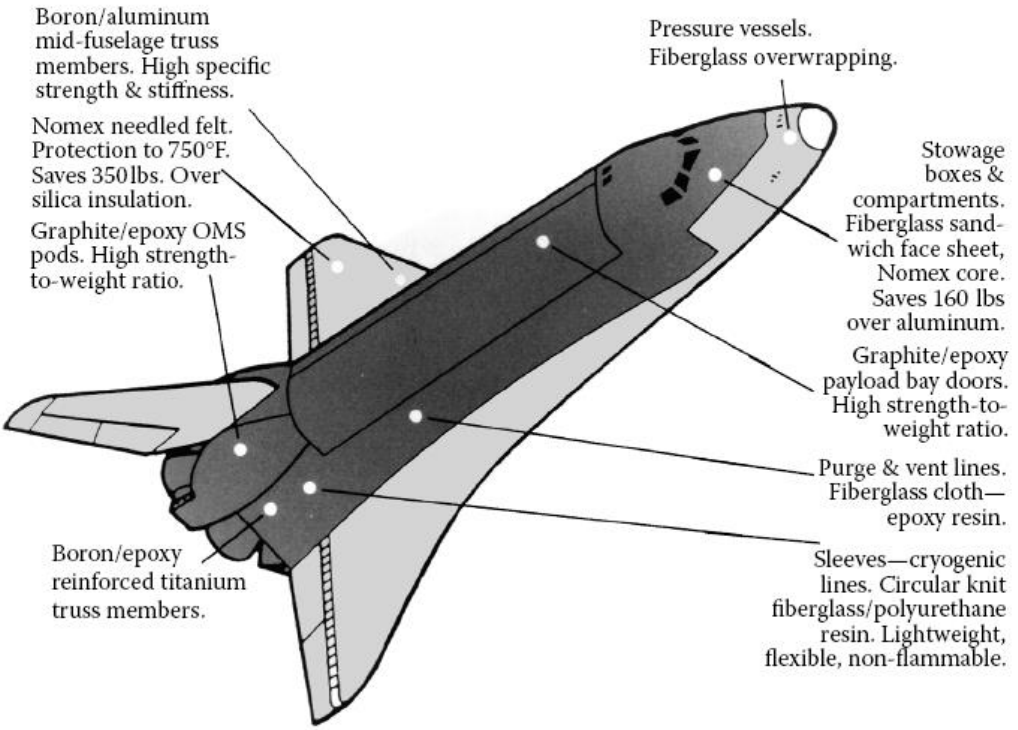

Figure (1.2): Use of composites in the space shuttle [**Kaw,2006**][53]

1.4 Classification of Composite Materials

In order to classify and characterize the composite materials, a distinction between the following four types is commonly accepted [**Stegman** and **Lund,2001**][46]:

A. Fibrous composite materials that consist of fibers in a matrix, e.g.:

- Orthotropically aligned reinforced materials: stiffners, wires, and fibers in matrix.

B. Laminated composite materials that consist of layers of various materials, e.g.:

- Laminated glass, plywood, clad metals, bimetals, and laminated fibrous composites.

C. Particulate composite materials that are composed of particles in a matrix, e.g.:

- Quasi-isotropic random reinforced materials: powder or particles in a matrix like ceramics.

D. Combination of some or all of the first three types, e.g.:

- Laminated fiber reinforced materials: orthotropic lamina bonded together to form an anisotropic material.
- Sandwich constructions: face sheets bonded to a lightweight core.

The fiber reinforced laminates have been increasingly found in many engineering structures because of their anisotropic material properties that can be tailored through the variation of the fiber orientation and stacking sequence of lamina that gives the designer added degree of flexibility.

1.5 Analysis of Composite Materials

The analytical methods that are used for composite materials are divided into two main categories, micromechanics and macromechanics.

Firstly, micromechanics are the study of properties of a monolayer in a composite material in the microscopic or constituent level in order to determine the principal strength, elastic and thermal properties of the monolayer.

The filament (fiber) matrix array, void inclusions and fiber volume fraction are the important factors in the micromechanical study of the composite fiber reinforced materials.

The modulus of elasticity ($\boldsymbol{E_1}$) in the longitudinal direction (at fiber direction) and the modulus of elasticity ($\boldsymbol{E_2}$) in transverse direction (at perpendicular direction to fibers) in terms of fiber and matrix volume fractions with respect to the rule of mixtures are given as follows [**Abid-Ali,2000**][(4)]:

$$E_1 = E_f V_f + E_m V_m \quad \textbf{(1.1)}$$

$$E_2 = \frac{E_f E_m}{\left(V_m E_f + V_f E_m\right)} \quad \textbf{(1.2)}$$

where

E_f: modulus of elasticity of fiber.
E_m: modulus of elasticity of matrix.
V_f: volume fraction of fiber.
V_m: volume fraction of matrix.

In addition, all mechanical and physical properties are depending upon fiber volume fractions. Figure (1.3) represents strength of a composite fiber reinforced material with respect to volume fraction of fibers and the critical volume fraction needed to give any strengthening, whereas Figure (1.4) shows the stress-strain relationship and mechanical behavior of the composite material.

Secondly, macromechanics is the study of the composite material behavior wherein the material is presumed homogeneous and the effects of the constituent materials are detected only as average apparent properties of the composite. It is a very helpful tool to the designer and analyst of the composite material structures.

In macromechanics study, strength, stiffness, and other properties are based on fiber orientation, number of lamina (layer), thickness of each layer, and all other structural design parameters.

The modeling techniques associated with the finite element method for the analysis of composite plates have been based on the following approaches [**Ali,2004**][(6)].

A. Equivalent single-layer theories (2D-layered approach).

- Classical lamination theory (CLT).
- First order shear deformation theory (FSDT).
- High order shear deformation theory (HSDT).

B. Three-dimensional elasticity theory (3D-approach)

- Traditional three-dimensional elasticity formulation.
- Layer-wise theories.

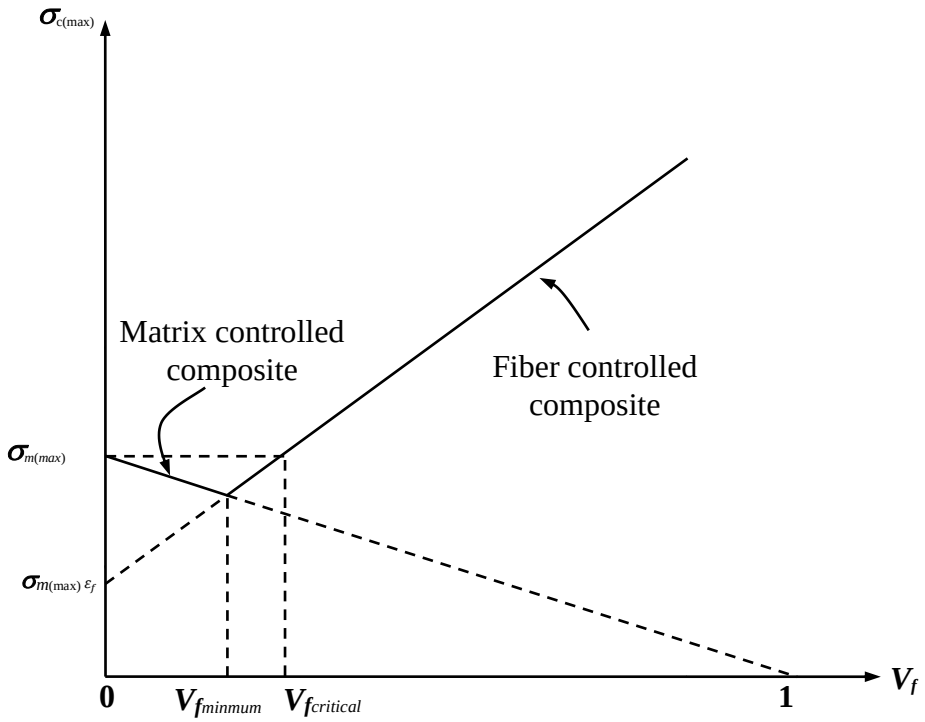

Figure (1.3): Effect of fiber volume fraction on the strength of composite [**Jones,1999**](50)

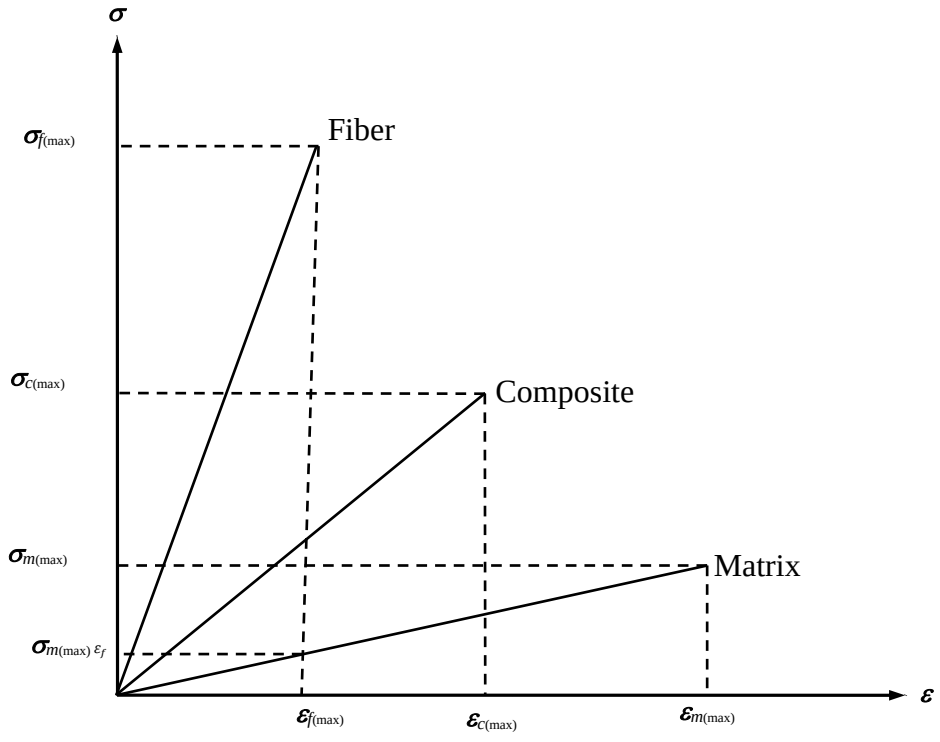

Figure (1.4): Stress-strain curve of fiber, matrix, and composite [**Jones,1999**](50)

The equivalent single-layer theories are derived from the three dimensional and elasticity theory by making suitable assumptions concerning the kinematics of deformation and the stress state through the thickness of the composite plates.

These assumptions allow the reduction of the three dimensional problems to two dimensional problems. The equivalent single-layer theories are suitable for thin to moderately thick layer composite plates. In the three dimensional or layer-wise theories, each layer is treated as a three dimensional solid, thus these theories are suitable for thick composite plates.

In the present study, Nine-node Lagrangian isoparametric quadrilateral finite element method has been employed for the discretization of the plates under in-plane loading. The effect of shear deformation was considered in this study. Constant shear deformation effect through thickness was considered for thin isotropic plate where this type needs for the shear correction factor (5/6). Parabolic shear deformation through thickness for a laminated composite plate was also considered where this type does not need a shear correction factor. Three types of degrees of freedom per node was considered in the present study, five degrees of freedom was used for the thin isotropic plate while in the higher order shear deformation theory of the [**Kommineni** and **Kant, 1993**][57] seven and nine degrees of freedom per node were adopted.

1.6 Types of Laminated Composite Plate

Laminated composite plate can be pre-classified according to the configuration of fibers in the laminate into two main useful types illustrated in the following [**Jones**,**1999**][50]:

1.6.1 Symmetric lamination

This type of lamination is symmetric in both geometry and material properties about the middle surface of the laminated composite. The symmetric lamination includes two configurations as follows:

1. Symmetric cross-ply lamination

[$0^o/90^o/0^o$] cross-ply lamination is an example for this type, as shown in Figure (1.5). Symmetric cross-ply lamination consists of an odd or an even number of orthotropic layers that have principal material directions aligned with the axes of

the lamina and laminated (built) symmetrically about the middle surface [**Jones**,**1999**] [50].

2. Symmetric angle-ply lamination

Symmetric angle-ply laminas include an odd or an even number of orthotropic layers that are symmetrically disposed about the middle surface of the laminated composite. For example, In[30º/75º/30º], the principal material directions are not aligned with the lamina axes. Both types are shown in Figure (1.6).

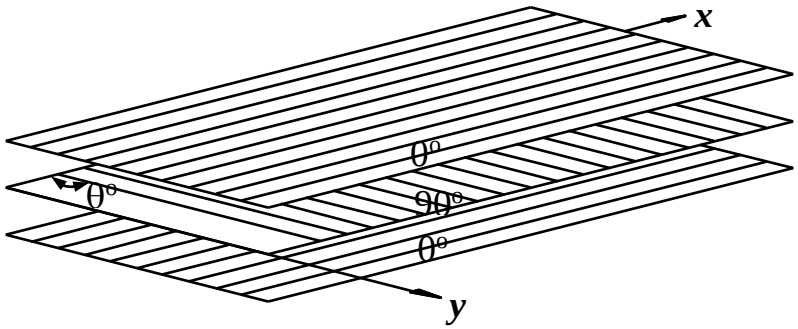

Figure (1.5): Symmetric cross-ply lamination of composite plates

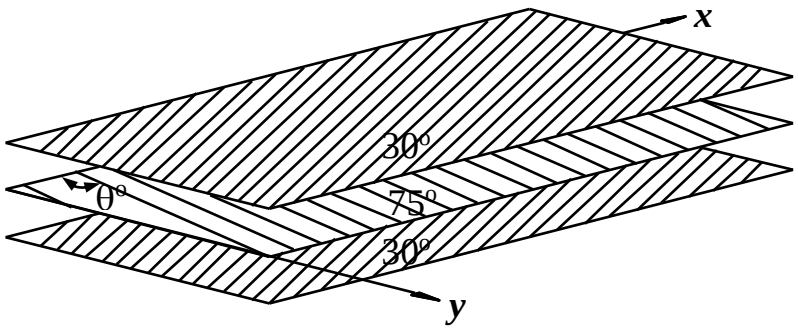

Figure (1.6): Symmetric angle-ply lamination of composite plates

1.6.2 Antisymmetric lamination

This type of lamination is very effectively used in practical applications of laminated plates and shells. Material properties of the individual layers are not symmetric about the middle surface of the laminated plate. The antisymmetric lamination has bending-extension coupling and bend-twist coupling. Both bending-extension coupling effects are illustrated as an example by antisymmetric laminated plates after curing. The laminate is flat before curing but thermally

induced residual stresses cause the laminate to become highly curved, as shown in Figure (1.7).

Figure (1.7): An antisymmetric laminated plate after curing

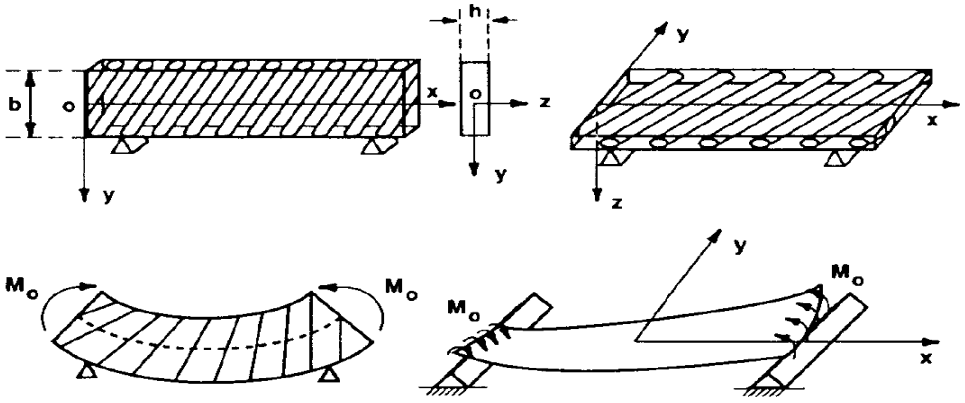

Figure (1.8): Effect of bend-twist coupling on plate bending [**Jones, 1999**][50]

The effect of bend-twist coupling on plate bending is shown in Figure (1.8). Utilization from this coupling in advanced design is illustrated in the design of forward-swept wings subjected to aerodynamic loads which tend to twist the wing about an axis that is along the wing and off perpendicular to the fuselage. The wings are designed by using composite laminates at various angles to the wing axis and this results in bend-twist coupling that causes the wing to have deflection in the opposite sense by the aerodynamic wing twisting effect.

Similarly to symmetric lamination, the antisymmetric lamination includes two configurations as follows:

1. Antisymmetric cross-ply lamination

Antisymmetric cross-ply laminate consists of an even number of orthotropic layers laid on each other with principal material directions alternating at 0^o and 90^o to the lamina axes. $[0^o/90^o/0^o/90^o]$ is an example, as shown in Figure (1.9).

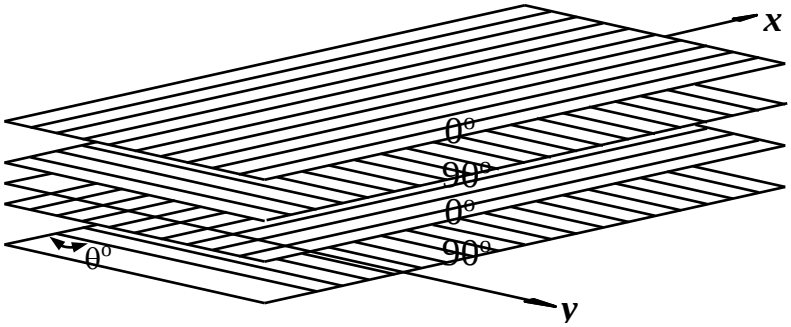

Figure (1.9): Antisymmetric angle-ply lamination of composite plates

2. Antisymmetric angle-ply lamination

This is the most general configuration type of a laminate. It contains an even number of orthotropic layers laid on each other with principal material directions not aligned with the lamina axes. [30°/75°/30°/75°] is an example, as shown in Figure (1.10).

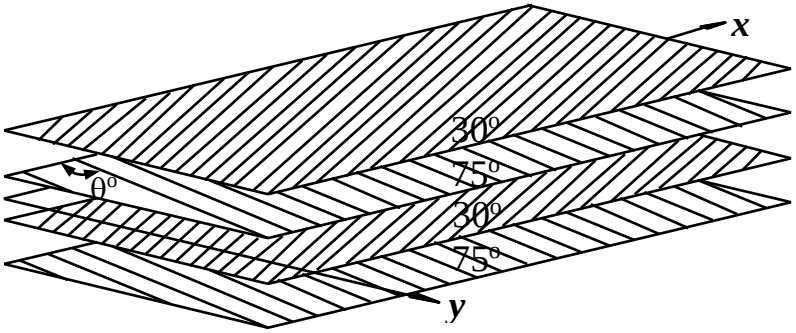

Figure (1.10): Antisymmetric angle-ply lamination of composite plates

1.7 Application of Composite Materials

The processional road in the ancient Babylon, one of the Wonders of the ancient world, was made of bitumen reinforced with straw. Straw and horsehair were used to reinforce mud bricks at least 5000 years ago [**Abid-Ali, 2000**][(4)]. More recently industries use extensively the composite materials. Composite materials have grown rapidly in the past fifty years with development of fibrous composites; to begin with glass fiber-reinforced polymers and more recently with carbon fiber-reinforced polymers. Fiber-reinforced polymer composites with high strength to weight and high stiffness to weight ratios have become more important in necessary lightweight applications such as in aircraft, aerospace, sports and boats application, etc. Their use in such composite material applications today are listed in Table (1.1) [**Kaw,2006**][(53)].

Table (1.1): Applications of composite materials in some industries,[**Kaw,2006**][53]

Application	Part
Marine	Boats, deck houses, gears, tanks, deep submergence boxes, vehicles, etc.
Aircraft	Rudder, fuselage, landing-gear, fairings, etc.
Automobile	Tires, drive shaft, window glass, etc.
Chemical industries	Pipes, pressure vessels, tank, etc.
Sport	Tennis rackets, sport equipments, etc.
Medical	Dental material, joints in human body, denture bases, etc.
Effective passive control system	Slider crank mechanism, peculiar tools, etc.

1.8 Buckling Behavior of Thin Plates

Thin plate elements are extensively used in naval and aeronautical structures and they are often subjected to normal and shearing forces acting in the plane of the plate, as shown in Figure (1.11). If these in-plane forces are sufficiently small, the equilibrium is stable and the resulting deformations are characterized by the absence of lateral displacements ($w=0, u\neq 0, v\neq 0$). As the magnitude of these in-plane forces increases to at certain load intensity, a marked change in the character of the deformation pattern takes place. That is, simultaneously with in-plane deformations lateral displacements are introduced. In this condition the originally stable equilibrium becomes unstable and the plate is said to have buckled. The load producing this condition is called the critical load. The importance of the critical load is the initiation of a deflection pattern, which, if the load is further increased, rapidly leads to very large lateral deflections and eventually to complete failure of the plate. This is a dangerous condition, which must be avoided. Besides this buckling behavior, the behavior of a flat plate after buckling is of considerable practical interest. The post-buckling of plates is usually difficult in analysis since it is basically a nonlinear problem. Slightly curved plates, subjected to simultaneous action of in-plane compressive forces and lateral loads, may undergo what is called "snap-through" buckling, which is characterized by reversal deflections produced by the nonlinear relationship between the buckling load and the deflections. During continuous loading, the plate may begin to deflect in one

direction, but at a certain load, it buckles in the reverse direction, assuming again a stable shape [**Paik, et al., 2000**][79].

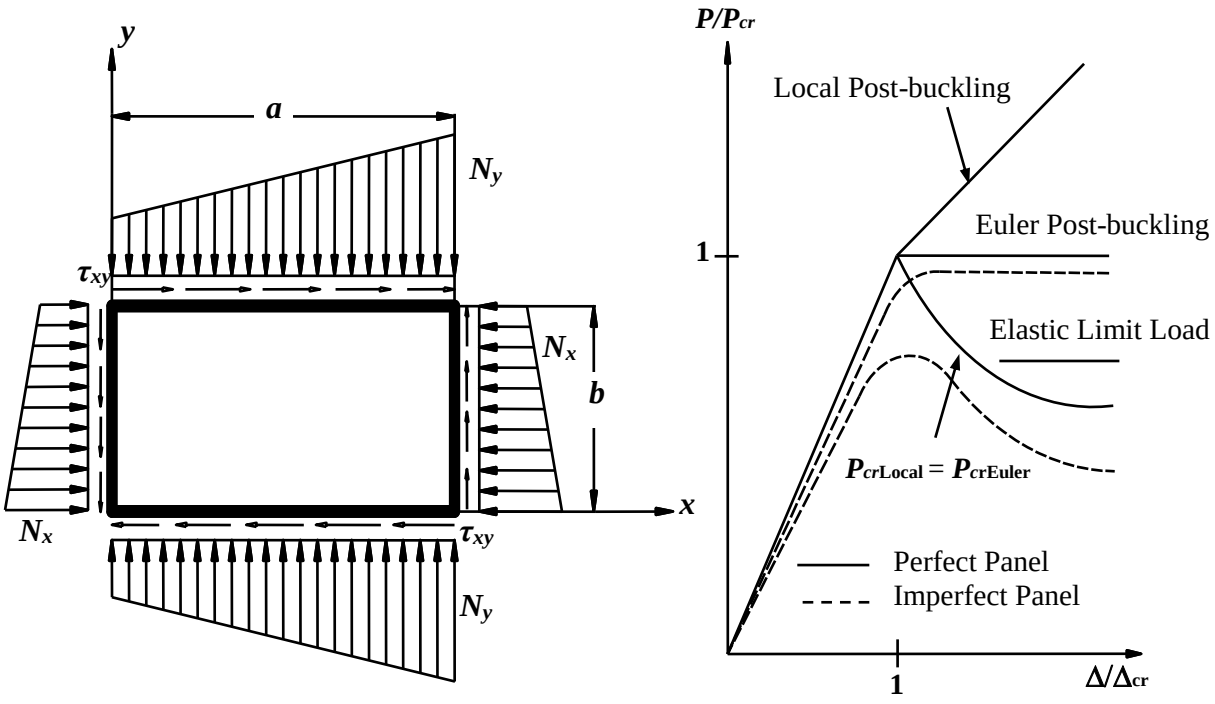

a: Plate under a general pattern of combined external in-plane loads

b: Nonlinear elastic behavior of steel panels

Figure (1.11): Buckling and post-buckling elastic behavior of plate under combined external in-plane loads

1.9 Initial Imperfection

Structural imperfections can be grouped into two geometric derivations and residual stresses. The geometric imperfections include derivations in axial out-of-straightness and cross-sectional parameters such as plate thickness, stiffener profile, and initial distortions. The out-of-straightness is particularly due to structural fabrication where the plate is fabricated in a factory which will not be able to produce a perfectly flat surface for plates and thus the plates but they will have very small initial imperfections [**Paik, et al.,2000**][79]. Residual stresses arise from manufacturing of the profile as well as fabrication of the structure; they are mainly caused by processes such as welding, flame cutting, and hot rolling for plates. All these processes create heat affected zones which cause expansion. The expansion is prevented by the adjacent cold regions in the expense of elastic stress mobilization in the cold region. This leads to plastic deformations in the heated zones with reduced yield stress. During the cooling process, the heated zones

contracts and are usually too short under normal temperature conditions. As a result, tension zones of residual stresses and permanent deformations are created. Figure (1.12) shows a schematic of the post-weld initial deflections in a ship stiffened plate structure. The measurements of welding induced initial deflection in plates in merchant structures reveal a complex multi-wave shape in two directions [**Paik, et al.,2000**][79].

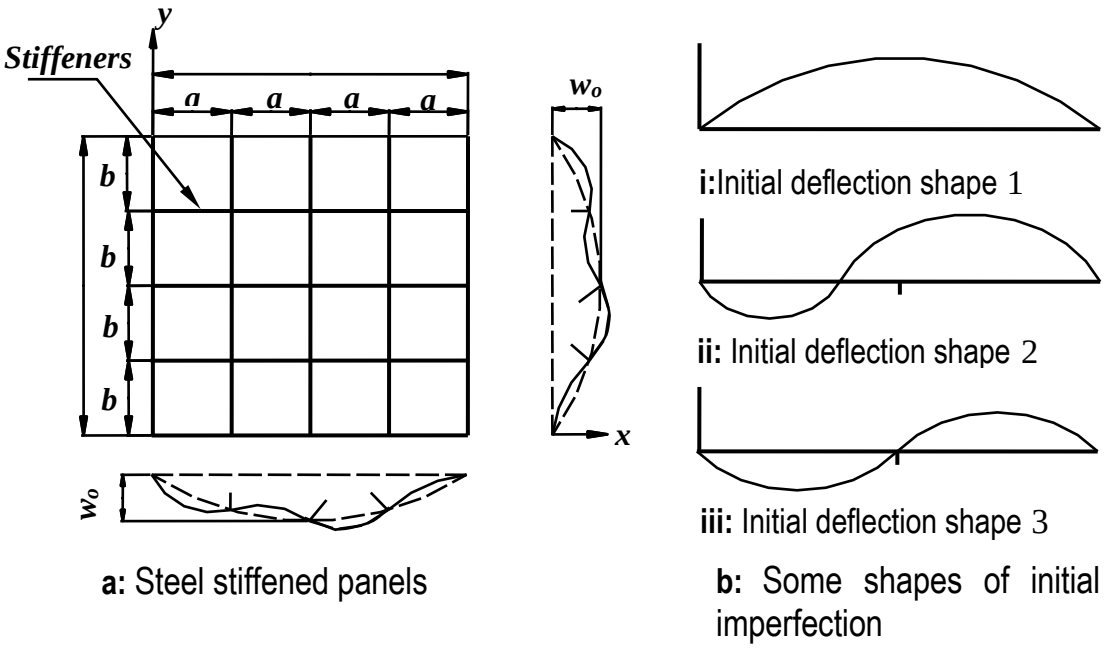

Figure (1.12): Fabrication related initial deflection in steel stiffened panels

1.10 Dynamic Stability

Dynamic stability or instability of elastic structures has drawn considerable attention in the past four decades. The class of problems falling in the category of parametric excitation, or parametric resonance, includes the best defined, conceived, and understood problems of dynamic stability [**Ali,2004**][5].

The problem of dynamic stability is best defined in terms of an example, like an Euler column, which is loaded at one end by a periodic axial force, as shown in Figure (1.13); the other end is immovable. It can be shown that for a certain relationship between the exciting frequency and the column natural frequency of transverse vibration, transverse vibrations occur with rapidly increasing amplitudes. This is called parametric resonance and the system is said to be dynamically unstable, moreover, the loading is called parametric excitation load.

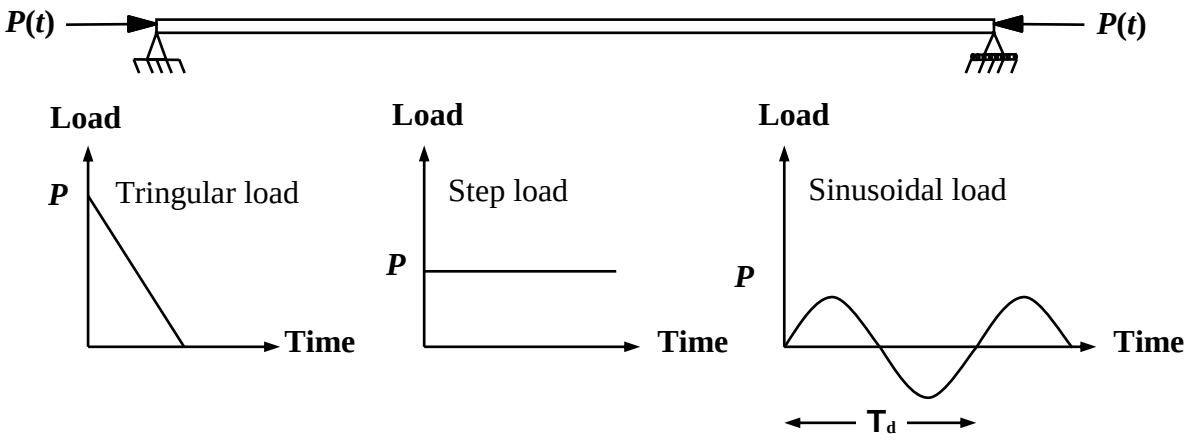

Figure (1.13): A simply supported beam subjected to a dynamic load

Other examples of parametric resonance include (1) a thin flat plate parametrically loaded by in-plane forces, which may cause transverse plate vibrations; (2) parametrically loaded shallow arches (symmetric loading) which under certain conditions vibrate asymmetrically with increasing amplitude; (3) long cylindrical, thin shells (or thin rings) under uniform but periodically applied pressure, which can excite vibrations in an asymmetric mode [**Ali, 2004**] [(5)].

1.11 Objectives and Scope

This study deals with static and dynamic analysis of plates under many types of in-plane loading. Isotropic and orthotropic plates have been considered in the analysis. Nine-node isoparametric quadrilateral finite elements were employed for analysis of these types of plates. The analysis is based on the two-dimensional layered approach. The transverse shear deformation effect was considered in the present study. Five degrees of freedom were employed for thin isotropic plates with higher order shear deformation, while seven and nine degrees of freedom per node were considered for laminated composite plates. This study is divided into two parts; in the first part, there is an attempt for formulating a simplified nine-node isoparametric finite element of rectangular plate based on two-dimensional layered approach. Post-buckling and post-yielding static analysis of isotropic and orthotropic materials for plates were considered in this part. The effect of initial imperfection, slenderness ratio, aspect ratio, boundary conditions, type of loading, orientation of fiber, and number of layers, type of fiber, stacking sequence, number of degrees of freedom were considered.

The second part deals with nonlinear dynamic analysis of rectangular plates under in-plane loading. Also, in this part, the analysis of both isotropic and orthotropic plate was considered. Two types of integration method were used (Newmark method and Harmonic acceleration method) for solving the dynamic equilibrium equations. The effect of initial imperfection, aspect ratio, boundary conditions, type of fiber, orientation of fiber, stacking sequence, type of axial loading, number of degrees of freedom, damping effect, and material nonlinearity were considered.

1.12 Layout of the Thesis

A general introduction to the main ideas involved in the thesis about the isotropic and composite plates is presented in Chapter One, with the objective and scope of the investigation. In Chapter Two, a brief review of early studies and the more advanced studies on the subject are given with an interpretation of the results as possible. Chapter Three, presents a description of different theories to analyze layered plates and establish the derivation of the basic equations of the macromechanical behavior of such structures. Chapter Four includes details about geometrical nonlinearity (strain-displacement relationships) and material nonlinearity with tangential stiffness and numerical solution of nonlinear equations. Chapter Five contains a complete formulation of mass and damping matrices with a discussion of the solution techniques which are adapted to solve nonlinear equations and eigenvalue problems as well as nonlinear dynamic equilibrium equations.

Chapter Six includes an application and results of static post-buckling analysis of plates with group of effects. Chapter Seven includes an application and results of dynamic analysis of plates with different effects. Finally, Chapter Eight gives the conclusions and the recommendations for further studies.

CHAPTER TWO

Literature Review

2.1 General

The analysis of dynamically loaded structures has received a continuous but varying levels of attention over the past 50 years. Due to the infinite number of permutations of structural parameters and due to the costs of performing tests on such structures, the amount of available experimental data, while broad, is also scant relative to any particular combination of structure and dynamic load.

The finite element method has been applied with great success to geometrical and material nonlinearities in continuum and structural problems. The geometric nonlinearity is modeled by well-known formulations, the total or updated Lagrangian coordinates, while success in modeling the material nonlinearities depends on the validity of the constitutive models to be used.

The review presented here aims at showing the most important developments and steps that have been taken on the path leading to the knowledge of today in this subject.

In this chapter a literature survey is divided into two major scopes: -

1. **Static Analysis of Plate**

This part includes two branches:-

a- Large deflection analysis of an isolated plate.

b- Elastic-plastic large deflection analysis of an isolated plate.

2. **Dynamic Analysis of Plate**

This part also includes two branches:-

a- Large deflection dynamic analysis of an isolated plate.

b- Elastic-plastic large deflection dynamic analysis of an isolated plate.

2.2 Static Analysis of Plate

Any load when applied very slowly on structures can be as a considered static load and the effects of acceleration and velocity forces will be neglected.

2.2.1 Large deflection analysis of an isolated plate

The large deflection theory of isolated plates is more complicated than the small deflection theory because of the nonlinearity. The nonlinearity arises because the deflection increases the membrane stresses and they are redistributed and begin to dominate over flexural action. This problem was treated by von-Karman's equations and by Marguerre's equations [**Szilard, 1974**][(103)].

Coan [**1951**][(23)] solved Marguerre's equations to study the post-buckling behavior of plates by assuming the deflected shape of a rectangular simply supported plate as a double Fourier series and overcame the restriction on Levy's solution. Edge pull-in of three kinds was allowed for by adding further complementary functions to the expressions for the stress function (**Φ**). The theory was applied to a square plate with the central initial deflection (w_o=0.1h) and the results were compared with the experimental values.

Yamaki [**1959**][(120)] gave an extension of Levy and Coan's works by solving the problem with different boundary conditions, combining two kinds of loading conditions [**case (1)**, the edges where kept straight by the distribution of the normal stresses, while in **case (2)**, the edges are free from stresses]. The solution of Marguerre's fundamental equations for large deflections of thin plates with slight initial curvature was presented in his study for the case of a rectangular plate subjected to edge compressive load by using a double trigonometric series with calculated coefficients to solve these equations. The conclusions from this study were as follows: -

1. The deflection in **case (1)** is always smaller than the corresponding one in **case (2)**.

2. Under loads which are much greater than the critical load, the net deflection for the initially deflected plate is smaller than that for the initially flat plate.

Stein [**1960**][(100)] proposed a purely mathematical approach that had been presented to explain the possibility of a change of buckling wave form. He converted the nonlinear large deflection equations of von-Karman for plates into a set of linear equations by expanding the displacements into a power series in terms of arbitrary parameters. He investigated the post-buckling behavior of simply supported rectangular plates in end compressive load by solving the first few equations and presented non-dimensional load-shortening curves for plates with various length-width ratio (***a***/***b***) (1 to 5). These curves were obtained by using the values of (***m***).(where ***m*** is the integer in the power series method), which intersect with these basic curves for the range plotted. The intersections of the load- shortening curves indicate possible changes in buckle pattern, as shown in Figure (2.1).

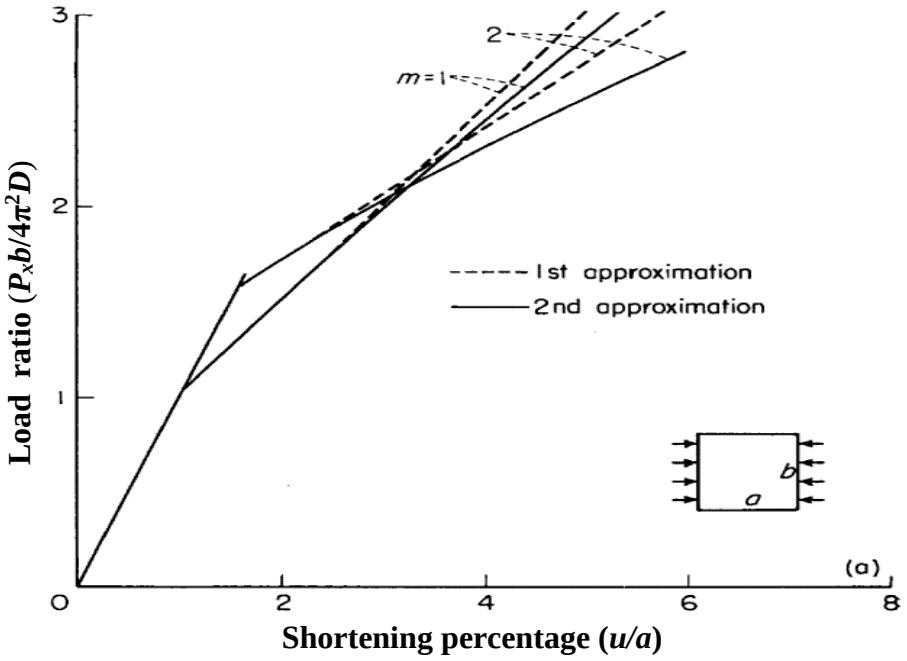

Figure (2.1): Non-dimensional load-shortening curves of square simply supported plates in compression, (***a***/***b***=1) [**Stein,1960**] [(100)]

Rushton [**1969**][96] demonstrated the dynamic relaxation method to analyze the post-buckling behavior of plates with variable thickness and with edge restrained against lateral expansion. In this approach the nodes had been considered to have a constant thickness different from the thickness of the previous node. A variable thickness plate (each node has thickness different from those of other nodes) was considered, in which the thickness was defined by:

$$h_x = h_o\, e^{\lambda x} \qquad \textbf{(2.1)}$$

with λ was chosen ($\lambda = \ln 2/a$) so that at the thicker end at $x=a$, $h_a = 2h_o$.

He observed that the finite difference method tends to underestimate the initial buckling load by about 3% when compared with the exact solution

Colville, et al. [**1973**][24] used a general method of solution of the von-Karman plate equations by using a direct iterative finite element procedure. Their study included all applicable nonlinearity in the strain displacement equations. The use of fully compatible finite element for both the in-plane and bending action results in monotonic convergence to the theoretical solution of the structure idealization. This procedure gave minimum computational time.

Colville and **Shye** [**1979**][25] used the finite element method to investigate post-buckling behavior of plates. In that study, the finite element solution procedure was employed for the large deflection problems based on the theory developed by **Colville**, who had shown that for post-buckling applications the uncoupled equilibrium equations may be written as: -

$$[K_w + K_N]\{w\} = \{q\} - [K_g]\{w\} \qquad \textbf{(2.2)}$$

$$[K_u]\{u\} = \{f\} - \{G_N\} \qquad \textbf{(2.3)}$$

in which K_w = bending stiffness of the undeformed plate; K_g = the geometric stiffness of the plate; K_N = the nonlinear stiffness matrix; w= nodal bending displacements; q = applied bending loads; K_u= in-plane

stiffness of the undeformed plate; $\boldsymbol{G_N}$ = a nonlinear membrane correction force vector; $\boldsymbol{u}$= nodal in-plane displacements; $\boldsymbol{f}$ = applied in-plane loads. Their main conclusions were the following: (1) The finite element procedure was capable of giving the initial and secondary critical buckling loads and corresponding buckling modes; (2) The magnitude of initial disturbing deflection does not affect the final converged deflected shape; (3) The magnitude of the initial disturbing deflection does affect the number of iterations required to achieve convergence.

Pica, et al. [**1979**][87] presented a finite element analysis of the geometrically nonlinear behavior of plates using a Mindlin formulation with the assumption of small rotations. A comparison of the performance of linear, Serendipity, Lagrangian and Hetrosis elements was given for square, skew, circular and elliptical plates subjected to distributed and point loading with other numerical thin plate solutions. The formulation presented was extended to include shallow shells allowing for investigating post-buckling behavior of plates with initial imperfections. Their conclusion is that the higher order elements give good results although no particular element emerges as being "best".

Pica and Wood [**1980**][88] presented a geometrically nonlinear analysis of shallow shells using finite element formulation. The nine-node Lagrangian element was used for a number of post-buckling solutions and it was important to observe the ability of the element to model curved boundaries. Both local and global instability phenomena were included as in the simple truss example shown in Figure (2.2). Newton-Raphson iteration process was used to solve the nonlinear equations. Their conclusion was that the present total Lagrangian approach provided a ready means of analyzing the nonlinear behavior of an important class of structures, namely, plates with initial imperfections.

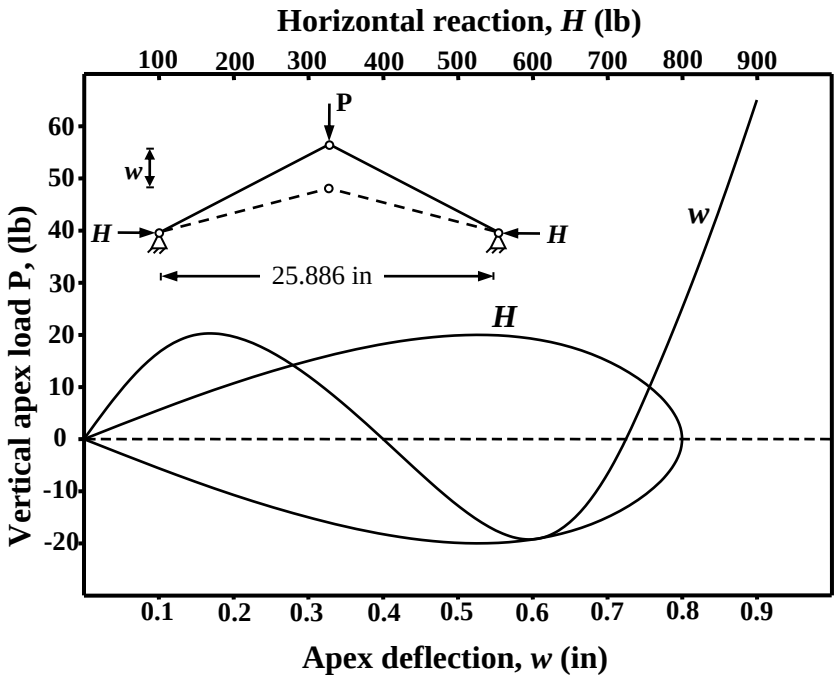

Figure (2.2): Hinged truss-load versus deflection and horizontal reaction [**Pica** and **Wood**, **1980**][88]

Fok [**1984**][32] presented two numerical methods for estimating the experimental critical load and the initial imperfection of rectangular plates loaded in edge compressive load from recordings of load and deflection. The three-point technique makes use of three sets of such readings to form a system of nonlinear simultaneous equations, the solution of which yields the critical load, initial imperfection, and the constant governing the curvature of the load-deflection curve. The least square technique was applicable to neutral bifurcation. Both two techniques were applied to various experimental results and it was found that the calculated values were very close to the experimental values.

Galerkin method had been widely applied to both static and dynamic problems in the area of solid mechanics. The idea of the method is the minimization of error by orthogonalizing with respect to a set of given functions [**Chia,1980**][21].

Ueda, et al. [**1987**][110] studied the large deflection behavior of a rectangular plate by an efficient semi-analysis method. An incremental form of the governing differential equations of plates and stiffened plate

with initial deflection had been derived. For each load increment, these equations were solved by the Galerkin method with especial consideration of simply supported boundaries. These equations take the following form: -

$$D\nabla^4(\Delta w)=\left(\begin{array}{l}\dfrac{\partial^2\Phi_{i-1}}{\partial y^2}\dfrac{\partial^2(\Delta w)}{\partial x^2}+\dfrac{\partial^2(\Delta\Phi)}{\partial y^2}\dfrac{\partial^2 w^t_{i-1}}{\partial x^2}\\ +\dfrac{\partial^2\Phi_{i-1}}{\partial x^2}\dfrac{\partial^2(\Delta w)}{\partial y^2}+\dfrac{\partial^2(\Delta\Phi)}{\partial x^2}\dfrac{\partial^2 w^t_{i-1}}{\partial y^2}\\ -2\dfrac{\partial^2\Phi_{i-1}}{\partial x\partial y}\dfrac{\partial^2(\Delta w)}{\partial x\partial y}-2\dfrac{\partial^2(\Delta\Phi)}{\partial x\partial y}\dfrac{\partial^2 w^t_{i-1}}{\partial x\partial y}\\ +\dfrac{\Delta q}{t}\end{array}\right) \tag{2.4}$$

$$\nabla^4(\Delta\Phi)=Et\left(2\frac{\partial^2 w^t_{i-1}}{\partial x\partial y}\frac{\partial^2(\Delta w)}{\partial x\partial y}-\frac{\partial^2 w^t_{i-1}}{\partial x^2}\frac{\partial^2(\Delta w)}{\partial y^2}-\frac{\partial^2 w^t_{i-1}}{\partial y^2}\frac{\partial^2(\Delta w)}{\partial x^2}\right) \tag{2.5}$$

where w_{i-1}= total deflection at the end of the load increment (i-1), Φ_{i-1}= stress function at the end of load increment (i-1), Δw_i= increment deflection through current load increment, $\Delta\Phi_i$= increment stress function through current load increment. A procedure of equilibrium correction at intermediate load steps must maintain that good accuracy of the solution may be maintained with larger load steps because of the small quantities of higher order of (Δw, and $\Delta\Phi$) being neglected.

Elseifi [**1998**][(31)] presented nonlinear finite element method for the post-buckling analysis of stiffened composite panels with geometric imperfections. A four node, six degrees of freedom per node, rectangular, conformal element was used. Transverse shear effects were neglected since the width to thickness ratio of the panels under consideration is over 500. A maximum stress failure criterion was added to the finite element code to predict the panel post-buckling failure load. The element was validated by using several standard examples problems where the results were compared with both available analytical and experimental results. A new integration technique that mixes symbolic closed-form function manipulation and Gaussian quadrature numerical

integration had been introduced in order to reduce the required computation time for each analysis. His study did not take the effect of fiber orientation, number of fibers, and type of initial imperfection.

Shukla and **Nath** [**2000**][98] presented a post-buckling analysis of shear deformable cross-ply laminated rectangular plate subjected to the combination of in-plane edge compressive mechanical loading and thermal loads due to a linearly varying temperature across the thickness. Their formulation was based on the first order shear deformation theory and von-Karman type nonlinearity. The analysis used a quadratic extrapolation technique for linearization and Chebyshev polynomials for spatial discretization. They studied the effect of aspect ratio, lamination scheme, the number of layers, types of boundary condition (simply supported edge, clamped edge, and free edge), and the modular ratio on the critical load/limit load and post-buckling behavior. Their conclusion was that the buckling and post-buckling strength decreases with an increase in temperature and its effect is similar to the effect of initial geometric imperfections. They also concluded that the effect of aspect ratio on the limit load and post-buckling response is significant. They observed that their present method was quite efficient in obtaining the buckling and post-buckling response of a laminated composite plate under thermomechanical loading.

Mohammed [**2001**][69] used the finite element method to study the buckling and post-buckling behavior of rectangular isolated steel plates under in-plane shear load. This study considered the effect of initial imperfection and the boundary condition on the overall behavior of the plate. His study was divided into two parts. The first part included the analysis of isolated plates under in-plane shear load with different values of initial shapes. The second part included analysis of isolated plates under in-plane shear load with different cases of condition support. His conclusion was that the behavior of a thin-walled structure is usually sensitive to the nature and magnitude of initial imperfection.

More recently, **Zou** and **Qiao** [**2002**][(125)] presented a higher order finite strip method for post-buckling behavior of imperfect composite plates subjected to progressive end shortening. The arbitrary nature of initial geometric imperfection induced during manufacturing was accounted for in the analysis. The nonlinear equilibrium equations were solved by Newton-Raphson method. That study showed that the post-buckling behavior of an imperfect composite plate depends not only on the material lay up, snap-to-thickness and anisotropy of the laminate, but also on the direction of induced out-of-plane imperfection.

2.2.2 Elastic-plastic large deflection analysis of an isolated plate

Most engineering structural materials such as steel and aluminum are ductile where their strains near ultimate strength are much more than the strains at elastic limit, as the structure is loaded beyond the elastic limit. Plastic strain occurs and causes a redistribution of stress. The computation of this distribution of stress has been noticed to be complicated; and a simplified method to compute the ultimate strength of the structure under a monotonic proportional load has been given by many investigators. This method, known as limit analysis, is to calculate the upper bound and the lower bound of the system of loads, in which the structure can take without collapse. In the limit analysis, the material is generally assumed to be ideally plastic and the strain hardening effect is usually neglected.

In the upper bound theorem: if a collapse configuration is assumed, the external loads computed by the principle of "virtual velocities $\dot{w}_i$" will be equal to or greater than the true collapse load.

In the lower bound theorem: if a stress configuration can be found which exceeds yields nowhere in the structure and which is in equilibrium with the external loads, these external loads will be equal to or less than the true collapse limit [**Mathlum,1997**][(66)].

Wah [**1958**][(114)] introduced a closed form solution for the deflections, residual deflection, residual membrane tensions, and other quantities of engineering interest for infinitely long clamped rectangular

plates with large deflections under uniform pressure. The analysis assumed infinite rigidity, in the plane of the plate, of the boundary supports. His formula based on several idealizations, which cannot be exactly duplicated in practice.

Lin, et al. [**1972**][(63)] introduced an analytical method for predicting the elasto-plastic bending of rectangular plates with large deflection. The effects of the plastic strain and the large deflection on plate deformation were shown to be the same as a set of applied external forces on the plate in the classical elastic small deflection theory. Their observation was that the deflection increased only slightly by plastic strain and the maximum extreme fiber stress is relieved by plastic yielding.

Crisfield [**1975**][(27)] used a finite element formulation for the large deflection elasto-plastic analysis of thin mild steel plates subjected to in-plane compressive load. This method was used to trace the behavior of imperfect steel panels over the full load range, including the unloading stage following collapse. A series of simply supported thin plates under uniaxial compression were analyzed to study different in-plane boundary conditions, levels of geometric imperfection and residual stress. The load-shortening curves to predict the behavior of stiffened plates subjected to uniaxial compression with wide eccentricity had been derived. He obtained good correlation with experimental results and showed that the imposition of straight edge constraint to the unloaded edges had no influence on the behavior of moderately stocky plates whereas increases in the collapse load of (5-10%) were achieved for thinner plates.

Little [**1977**][(64)] used a simple formulation of the minimum energy principle for analysis of plate collapse. This method is rigorous and yet economical in its use of the computer. His collapse analysis included a procedure which makes allowance for the effect of a large shortening increment where his results showed, surprisingly, that the predicted load-shortening response of a typical plate was only marginally dependent on the increment size. He presented results for biaxial in-plane compression

and compared his results with previous theoretical work, both elastic and elasto-plastic behaviors and good agreement was obtained.

Bathe and **Bolourchi** [**1980**][(16)] presented a displacement based versatile and effective finite element for linear and geometrically and materially nonlinear analysis of plates and shells. The element was formulated by interpolating the element geometry using the mid-surface nodal point coordinates and mid-surface nodal point normal. They presented a total and updated Lagrangian formulation in order to allow for very large displacements and rotations. In linear analysis of plates, the element reduces to the well established plate bending elements based on classical plate theory, whereas in linear analysis of shells and in geometrically nonlinear analysis of plates and shells by the use of the element, in essence, a general shell theory was employed.

Ueda and **Yao** [**1982**][(109)] presented a new mechanism of plastic hinge based on the incremental theory of plasticity and derived the elastic-plastic and plastic stiffness matrices for one-dimensional members. Using this plastic hinge, a method of elastic-plastic analysis of space frame structures was well developed with the inclusion of the effect of large deflection. This basic idea of plastic hinge method was extended for plates and solid bodies. The basic theory of the new method was made by using the finite element method.

In this theory, the yield condition at the ***i*** th node of an element is described as follows: "the ***i*** th node becomes plastic when the resultant stresses at this node satisfy appropriate plasticity condition and plastic deformation is developed only at the nodes".

For the element with ***k*** plastic nodes, the relation between the increments of the nodal force, ***df***, and the nodal displacement, ***du***, is derived in the following form:

$$df = k^p du \qquad \textbf{(2.6)}$$

where k^p is plastic stiffness. In this equation, either elastic-plastic or plastic stiffness matrix exists and this was expressed in explicit form.

When an element is subjected to a constant strain, the element becomes plastic in the entire volume if the yield condition is satisfied at any point. Simultaneously, the plastic node is formed at every node of the element. Completely the same plastic stiffness matrix is obtained by either the ordinary finite element method or by the plastic node method. From these facts the accuracy of the solution by this method is anticipated to be of the same order as that by the ordinary finite element method when the element division increases.

Paik and **Kim** [**1989**][(76)] presented a new and simplified rectangular finite element having only four corner nodal points to analyze the elastic-plastic large deformation behavior up to the ultimate limit state of plates with initial imperfections. The finite element contains the geometric nonlinearity caused by both in-plane and out-of-plane large deformation because for very thin plates the influence of the former is not negligible. Simple matrix operation was derived for elastic-plastic large deflection to treat the expanded plastic zone in the plate thickness direction of the element based upon the concept of plastic node method.

Li and **Owen** [**1989**][(62)] presented a refined finite element shell model for the numerical analysis of thick or thin anisotropic laminated shells. A layered approach was adopted for solution with displacement variables assumed at each laminated interface. Elastic-plastic numerical analysis was performed based on the flow theory and Huber-Mises yielding surface extended by Hill for fully three dimensional anisotropic materials. Their numerical results were presented for non-laminated and laminated shells and the effect of boundary constrains on the load-boundary deformation characteristics and on the spread of plastic zones was discussed. There was a tendency that plastic zones spread along weaker layers in both thick and thin laminates and this effect was more noticeable in composite shells than in plate structures. They also observed that the number of lamina had a small influence on the load carrying response.

Usami [**1993**][113] proposed a formula based on extensive numerical results of elastic-plastic large deflection analysis of simply supported imperfect plates in compression as well as in combined compression and bending. This formula was expressed as functions of the magnitudes of compressive residual stress and initial out-of-flatness and was used to compute the ultimate strength of welded built up beam-column segments. He also studied the effective width concept of locally buckled plates in both compression and bending.

Mirambell, et al. [**1994**][67] presented experimental investigations and numerical solutions of the behavior of steel plates under pure compression. The measurements were concentrated on the strains at several characteristic points of the panel displacements. A numerical model was developed for the analysis of the geometrical and material non-linearity of steel plate structures, based on the finite element method. Their study showed that the numerical and the experimental stress values were close.

Mathlum [**1997**][66] presented a large deflection elasto-plastic analysis by finite element method to analyze rectangular thin plates under compressive and shear load as well as the ultimate strength of plate girders with longitudinal and diaphragm stiffeners. His study was divided into three parts, the first part, included the analysis of isolated plate under compressive load. The second part included analysis of isolated plates under shear load. The last part contained analysis of ultimate load of plate girders with transverse and longitudinal stiffeners. His conclusion was that a plate girder without any stiffeners gives lower strength and a plate girder with transverse stiffeners has a larger strength than that with the longitudinal stiffener. This finding indicated that for plates in plane shear load the transverse stiffeners are more effective than the longitudinal stiffeners.

Lee and **Yoo** [**1999**][58] introduced an experimental study on ultimate shear strength of web panels. In this study, 10 scaled plate girder models were tested to investigate the shear behavior of web panels

up to failure. The following conclusions are drawn with regard to the behavior of the plate girder web panels:

1. The boundary condition at the flange-web juncture in practical design is much closer to the fixity.
2. In all existing failure mechanisms, the through–thickness bending stress effect on the ultimate shear strength is negligible. However, it has been found that very high bending stresses may develop at failure.
3. An anchoring system, such as flanges, is not needed for the development of the post-buckling strength.

More recently, **Turvy** and **Salehi** [**2001**][(107)] introduced a finite difference implementation of the dynamic relaxation algorithm to solve the governing equations for an elasto-plastic large deflection behavior of a pressure loaded sector, based on the Ilyusion full- section yield criterion and the flow theory of plasticity. This study showed that the effect of the in-plane edge restraint to be more significant in changing the post-yielding response of slender simply supported plates with substantial stiffness increases by accompanying the presence of full in-plane restraint. It showed that for slender sector plates the development of plasticity within the plate is quite complicated. At the maximum pressure applied, a plastic membrane state is approached in the slender sector plates under simply supported in-plane fixed edge conditions, whereas in the case of clamped in-plane fixed edge plates a residual interior elastic zone remains.

Amash [**2003**][(11)] presented a finite difference method for post-buckling and post-yielding problems of rectangular thin plates with constant and variable thickness. The basic (governing) differential equation for membrane actions of plate with variable thickness was derived. His study was divided into two parts. The first part included the post-buckling analysis of rectangular thin plate under the action of in-plane compressive loading. The second part included the elasto-plastic analysis of rectangular plate under the action of in-plane compressive

loading. In this part, the geometrical and material nonlinearity were included. His study considered the effect of initial imperfections, boundary conditions, slenderness ratios, aspect ratios, and tapering ratios on the ultimate strength. His conclusion was that the post-buckling behavior of a thin plate is very sensitive to the magnitude of initial imperfection and magnitude of tapering ratio. He also observed that the ultimate strength decreases with the increase of initial imperfection.

2.3 Dynamic Analysis of Plate

2.3.1 Large deflection dynamic analysis of an isolated plate

Dynamic buckling of structures under dynamic loading has become a significant research and has received increasing attention in the last decade from designers of modern engineering metal structures. Most past investigations focused on simple structures such as columns, plates and cylindrical shells.

Stricken, et al. [**1971**][(101)] presented a formulation and a computer program for the geometrically nonlinear dynamic analysis of shells of revolution under symmetric and asymmetric loads. The nonlinear strain energy expression was evaluated by using a linear function for all displacements. Five different procedures were examined for solving the equations of equilibrium, with Houbolt's method proving to be the most suitable. Solutions were presented for the symmetric and asymmetric buckling of shallow caps under step pressure loadings. In the formulation, the nonlinear term were taken to the right-hand side of the equations of equilibrium and treated as additional generalized forces. These forces were evaluated under the assumption that all displacements may be represented by linear functions in the meridional distance.

Kao and **Perrone** [**1978**] [(45)] presented a dynamic buckling analysis for axisymmetric spherical caps with initial imperfections. Their study considered two types of loading, namely, step loading with infinite duration and right triangular pulse. Solution of perfect spherical caps under step loading was in excellent agreement with previous findings.

Their results showed that the initial imperfection reduce the buckling capacity for both dynamic and static responses. From the solutions obtained for triangular pulse situations, it was revealed that pulse duration had a very significant impact on the magnitude of the dynamic buckling load. Their conclusion was that the step loading with infinite duration is the limiting case of a triangular pulse, and that the step loading provided the most severe loading situation for dynamic analysis.

Akay [**1980**][(10)] developed a four-node isoparametric mixed quadrilateral element for large deflection dynamic analysis of plates. Dynamic von-Karman plate equations were modified to include the effect of transverse shear deformations as Ressiner plate theory. Finite element equations of motion were obtained via a mixed Galerkin approach with three moments and three displacement components as dependent variables. Nonlinear time dependent equations were solved by using Newmark's step by step direct integration algorithm in conjunction with Picard type successive iterations within each time step. His study investigated the effect of thickness and the effect of applying Ressiner type boundary conditions, on the dynamic response of simply supported plates.

Houlston [**1989**][(42)] presented the theory of finite strip method with its application to nonlinear analysis of air-blast loaded plates and stiffened panels. The method was mainly applicable to plate and shell analyses which involve significant bending and membrane action in only one direction. From his analysis, it was observed that the strips are to be oriented in the direction of weak bending and membrane action. The degrees of freedom available could be advantageously used to obtain accurate interpolations where required. His results showed reasonable agreement of peak displacement with that from ADINA software backage.

Weller, **et al.** [**1989**] [(116)] used the ADINA computer code for determining the dynamic load amplification factor (DLF) for beams and plates under in-plane impact loads. Good agreement was found in

comparisons with self-developed finite difference computer codes and available experimental results. Though the problem that had been studied was of a wave propagation nature, a relatively small number of time steps were found to be enough to describe the phenomenon quite accurately. This can be attributed to the relatively short time duration of the applied loading (around the natural period of the structure). They observed that the DLF was usually larger than unity, both for beams and plates. In the presence of certain values of relatively large initial geometric imperfections and combined with periods of the applied load which were close to the first period of natural lateral vibrations of either the beam or the plate, DLF would be smaller than unity.

In [**1993**][(50)], **Kommineni** and **Kant** presented a C^o-continuous finite element formulation of a higher order displacement theory for predicting linear and geometrically nonlinear behavior in the sense of von-Karman transient response of composite and sandwich plates. The displacement model accounts for nonlinear cubic variation of the tangential displacement components through the thickness of the laminated plate and the theory requires no shear correction coefficients. The parametric effects of the time step, finite element mesh, lamination scheme, and orthotropy on the linear and geometrically nonlinear responses were investigated. Their numerical results for central transverse deflection, stress, and stress resultant were presented for rectangular composite and sandwich plates under various boundary conditions and loadings. The conclusion of their study was that the refined shear deformation theory is essential for predicting accurate responses of layered composite and sandwich laminates.

Azevedo and **Awruch** [**1999**][(12)] presented a geometric nonlinear dynamic analysis of plates and shells using eight-node hexahedral isoparametric elements. The main features of their study are: (1) the element matrices were obtained by using reduced integrations with hourglass control; (2) an explicit Taylor-Galerkin scheme was used to

carry out the dynamic analysis by solving the corresponding equations of motion in terms of velocity components.

Tao, et al. [**2004**][(105)] presented a simple solution of the dynamic buckling of stiffened plates under impact loading. Based on large deflection theory, a discretely stiffened plate model had been used. The tangential stresses of stiffeners and their in-plane displacements were neglected. The motion equations of stiffened plates were obtained by using Lagrange-Hamilton's principle. The deflection of the plate was expressed as Fourier series, and by using Galerkin method the discrete equations were solved by Runge-Kutta method. Their results were in excellent agreement with the finite element method. They observed that the Budiansky-Roth criterion was partially applicable for detecting the dynamic buckling of a stiffened plate. The conclusion of their study was that an appropriate shape of initial imperfection would avoid local buckling of the structure under impact load.

2.3.2 Elastic-plastic large deflection dynamic analysis of an isolated plate

Dynamic buckling analysis of plate structures has been a subject of intense study. Plate structures designed according to quasi-static analysis may fail under conditions of dynamic loading. For a more realistic prediction of the load carrying capacity of these plates, in addition to the dynamic effect, considerations should include other factors such as nonlinearities in material and geometry, initial imperfections, etc, as these factors, in a different manner, may also affect the magnitude of this capacity. Large deformation dynamic buckling analysis was studied by several researchers;the studies are given in the following:

Bathe, **et al.** [**1975**][(15)] derived a finite element incremental formulation for nonlinear static and dynamic analysis of shells. Their study considered elastic, hyperelastic (rubber-like), hypoelastic, and elastic-plastic materials in static and dynamic analysis. Their observation was on the provision of the constitutive tensors which were defined appropriately, all formulations give the same numerical results. The only

advantage of using one formulation rather than the others was in its better numerical effectiveness. Theory and sample analyses show that in small strain but large displacement analyses the differences which arise by using the same material constants in the formulations because of a clear definition of the constants may not be considerable and could be expected to be small. The conclusion of their study was that the update and total lagrangian formulations can effectively be used in a general nonlinear analysis program. It depends largely on the program designed and the material constants available by which the formulation becomes most effective.

Bathe and **Ozdemir** [**1975**][14] presented a formulation and a numerical method implementing the finite element elastic-plastic large deformation of shells for static and dynamic response. Their study presented two consistent formulations for elastic-plastic large deformation analysis in which either the initial configuration or the current configuration was used for the description of statics and kinematics variables. They observed that the difference between update and total lagrangian solutions become smaller as the number of load steps is increased.

Nagarajan and **Popov** [**1975**][74] derived incremental equations of motion from a Lagrangian variational formulation for the large displacement elastic-plastic and elastic-viscoplastic dynamic analysis of deformable bodies. They used degenerate isoparametric elements, permitting relaxation of the Kirchhoff-Love hypothesis in the finite element formulation specialized for the analysis of shells of revolution subjected to axisymmetric loading. The linearized incremental equations of motion were solved by using direct integration procedures, with added accuracy obtained from application of equilibrium correction at each step. The effectiveness of the numerical techniques was illustrated by the dynamic response analyses carried out on a shallow spherical cap subjected to uniform external step pressure loading.

Kao [**1980**][46] developed a finite difference method for the large deflection elastic-plastic dynamic buckling analysis of axisymmetric spherical caps with initial imperfections. His problem formulation was based on governing differential equations of motion, treating the plastic deformation as an effective plastic load. His results of large deformation elastic-plastic dynamic response of a spherical cap compared very suitable with other studies. He observed that the plastic yielding and the initial imperfection play significant roles in reducing the load carrying capacity of shell structures. His conclusion is that the dynamic effect had an influence of lowering the load carrying capacity where the dynamic effect cuts down the elastic-plastic loads ($\boldsymbol{P}_{cr}$) from (0.31 to 0.26) and from (0.5 to 0.36) of the static $\boldsymbol{P_{cr}}$ for shells (A and B), respectively as shown in the following Figure (2.3).

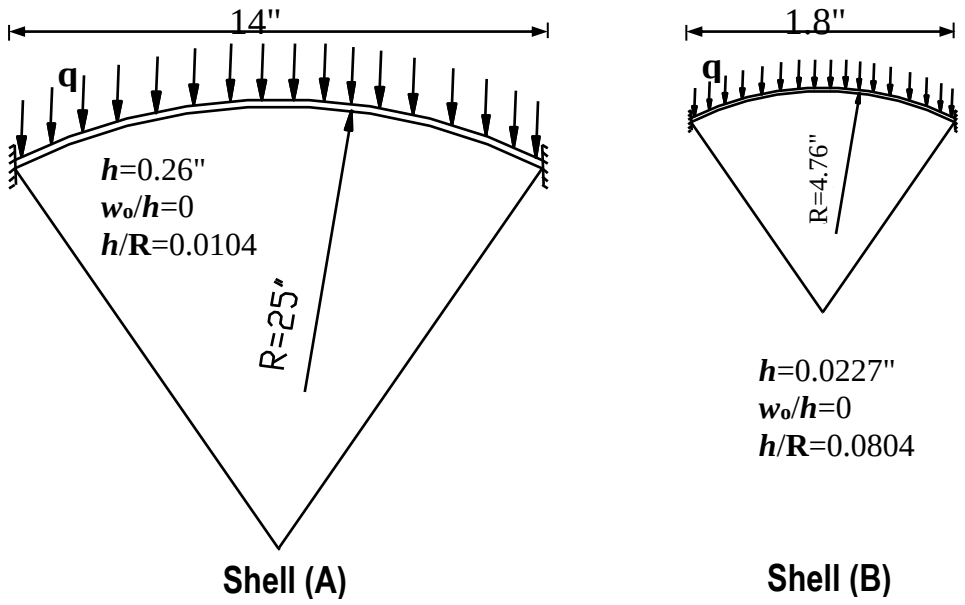

Figure (2.3): Shells under dynamic distributed load

Ishizoki and **Bathe** [**1980**][44] developed a finite element procedure for dynamic analysis of shell structures. The geometric and material nonlinearity were considered. Their analysis predicted the nonlinear response of a shallow cap, an impulsively loaded cylindrical shell and a complete spherical shell. The effect of various finite element modeling

characteristics and effect of initial imperfection on the static and dynamic buckling behavior of shells were investigated. The conclusion of their study was that the dynamic buckling load was significantly smaller than the static buckling load for ($0<w_o<0.2''$) where w_o=initial imperfection, but the difference in the buckling loads becomes small when w_o is greater than $0.2''$.

Rudrapatna, **et al.** [**1999**][(94)] presented a finite element formulation of thin square steel plates subjected to blast loading with the inclusion of the nonlinear effect of geometry and material as well as strain rate sensitivity. They proposed a phenomenological interactive failure criterion comprising bending, tension and transverse shear to predict the various modes of failure. A node release algorithm was developed to simulate the progression of plate rupture from the boundary. Their analysis was continued in the post-failure phase to account for the free flight deformation of a torn plate. Their results compared well with previous published experimental data. Their study showed the importance of the interaction effects of tensile and bending strains on the shear failure of blast loaded plates.

More recently, in [**2007**][(48)], **Khante**, **et al.** presented a formulation of higher-order shear deformation theory for damped elasto-plastic dynamic bending analysis of plates. They developed a finite element model based on a C^0-higher order shear deformation theory. Nine-node Lagrangian elements with five degrees of freedom per node (w,θ_x, θ_y, θ_x^*, θ_y^*) were used. Von-Mises and Tresca yield criteria were incorporated along with associated flow rules. Explicit central difference time stepping scheme was employed to integrate temporal equations. The mass matrix was diagonalized by using an efficient proportional mass lumping scheme. Rayleigh (a_1) factor was neglected, as the damping matrix consists of (a_0) factor multiplied by the mass matrix. They

observed that for sensitive plates, with increase in damping coefficient α the central displacement decreases without affecting the effective period of vibration of the plate. In contrast to the damped behavior of an elastic plate, where the central displacement response approaches the equilibrium or steady state position of oscillations, the elasto-plastic response was characterized by rigid body shift on lower side. One important conclusion was that in the case of elastic plates, damping only reduces the period for which the plate will continue to vibrate while the equilibrium position or permanent deformation becomes independent of damping. For plates with lower damping factor, damping introduces varying degrees of elasto-plasticity. The sensitivity to damping is independent of boundary conditions. No unexpected qualitative response was observed for elastic and elasto-plastic plates with change in boundary conditions.

From the preceding review of literature, it is clear that there is no study which considers the nonlinear dynamic analysis of isolated laminated plate under axial compression load by taking into account the effect of damping, effect of initial imperfection, property of material (isotropic or orthotropic), slenderness ratio, type of boundary conditions, type of loading, and type of fiber (straight or wavy). There is also a little amount of literature that takes into account the higher order displacement model of nine degrees of freedom per node with different types of lamination. Accordingly, the following chapters are devoted to cover the above additional research fields.

CHAPTER THREE

Theory and Derivation of The Basic Constitutive Relations

3.1 General

In this chapter, the stress-strain relationship for isotropic and orthotropic materials is summarized. Stress and stress resultant formulations and types of finite elements with derivations of [***B***] matrix in linear strain-nodal displacement matrix are presented.

3.2 Stress-Strain Relations for a Composite Lamina

The basic building block of a laminated fiber-reinforced composite material is the composite lamina. A lamina is a flat (sometimes curved as in a shell) arrangement of unidirectional or woven fibers in a supporting matrix.

The following demands must be made on fibers used in reinforced composite materials [**Jones, 1999**][(50)].

- High tensile strength.
- High modulus of elasticity.
- Lower ultimate elongation than the matrix.
- Good adhesion to the matrix.
- Good resistance to the matrix and its additions.

While the influence of the matrix on the composite is as follows:

- Binding the reinforcement and distributing the load.
- Protecting the fibers from physical and chemical damage.
- Dominant factor in determining the transverse shear and through-thickness properties.
- Dominant factor in determining the impact resistance and fracture toughness.
- Dominant factor in determining the long time (creep) response.
- Dominant factor in determining the service temperature.

The purpose of this section is to provide a basic understanding of the macromechanical behavior of a lamina when the averaged apparent mechanical properties are considered.

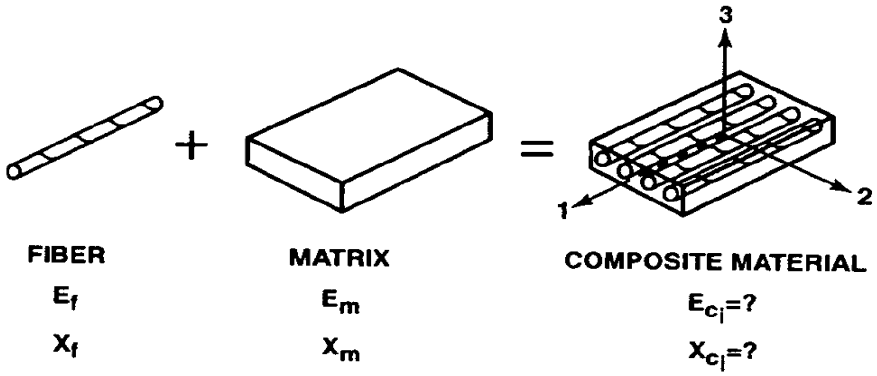

Figure (3.1): Basic questions of lamina macromechanics [**Jones, 1999**][50]

The basic questions of lamina macromechanics as illustrated by Figure (3.1) are the following:

1- What are the characteristics of a lamina?

2- How does a lamina respond to loading?

The materials are assumed to behave linearly elastic, i.e., the generalized Hooke's law is used for relating the stresses to strains. A material coordinate system is **1-2-3**, and the Cartesian coordinate system is ***x-y-z***, as shown in Figure (3.2), which is introduced for the unidirectional reinforced lamina.

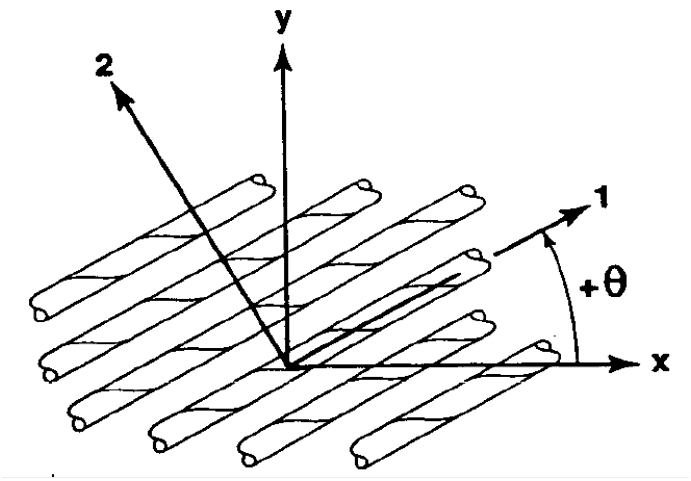

Figure (3.2): Positive rotation of principal material axes (**1-2**) from (***x-y***) axes[50]

The notation used in the following is described in Table (3.1).

Table (3.1): Tensor and contracted notation for stresses and strains[**Jones, 1999**][50]

Stresses		Strains	
Tensor notation	**Contracted notation**	**Tensor notation**	**Contracted notation**
σ_{11}	σ_1	ε_{11}	ε_1
σ_{22}	σ_2	ε_{22}	ε_2
σ_{33}	σ_3	ε_{33}	ε_3
$\sigma_{23}=\tau_{23}$	σ_4	$2\varepsilon_{23}=\gamma_{23}$	ε_4
$\sigma_{31}=\tau_{31}$	σ_5	$2\varepsilon_{31}=\gamma_{31}$	ε_5
$\sigma_{12}=\tau_{12}$	σ_6	$2\varepsilon_{12}=\gamma_{12}$	ε_6

The general anisotropic constitutive relation with respect to a material coordinate system (**1-2-3**) is given by Hooke's law as follows:

$$\begin{bmatrix}\sigma_1\\ \sigma_2\\ \sigma_3\\ \tau_{12}\\ \tau_{13}\\ \tau_{23}\end{bmatrix}=\begin{bmatrix}C_{11} & C_{12} & C_{13} & C_{16} & C_{14} & C_{15}\\ C_{21} & C_{22} & C_{23} & C_{26} & C_{24} & C_{25}\\ C_{31} & C_{32} & C_{33} & C_{36} & C_{34} & C_{35}\\ C_{61} & C_{62} & C_{63} & C_{66} & C_{64} & C_{65}\\ C_{42} & C_{42} & C_{43} & C_{46} & C_{44} & C_{45}\\ C_{51} & C_{52} & C_{53} & C_{56} & C_{54} & C_{55}\end{bmatrix}\begin{bmatrix}\varepsilon_1\\ \varepsilon_2\\ \varepsilon_3\\ \gamma_{12}\\ \gamma_{13}\\ \gamma_{23}\end{bmatrix} \qquad \textbf{(3.1)}$$

By assuming symmetry ($C_{ij}=C_{ji}$), thus twenty one independent material constants are used to describe the material. For the composite lamina illustrated in Figure (3.2), there are two orthogonal planes of material property symmetry and the material is termed orthotropic. The stress-strain relations in coordinates aligned with principal material directions are given by:

$$\begin{bmatrix}\sigma_1\\ \sigma_2\\ \sigma_3\\ \tau_{12}\\ \tau_{13}\\ \tau_{23}\end{bmatrix}=\begin{bmatrix}C_{11} & C_{12} & C_{13} & 0 & 0 & 0\\ C_{21} & C_{22} & C_{23} & 0 & 0 & 0\\ C_{31} & C_{32} & C_{33} & 0 & 0 & 0\\ 0 & 0 & 0 & C_{66} & 0 & 0\\ 0 & 0 & 0 & 0 & C_{44} & 0\\ 0 & 0 & 0 & 0 & 0 & C_{55}\end{bmatrix}\begin{bmatrix}\varepsilon_1\\ \varepsilon_2\\ \varepsilon_3\\ \gamma_{12}\\ \gamma_{13}\\ \gamma_{23}\end{bmatrix} \qquad \textbf{(3.2)}$$

i.e., nine independent material constants characterize the material.

If a plane stress assumption with transverse shear in direction **3** is used for the orthotropic composite lamina, the stress-strain relations are given as:

$$\begin{bmatrix}\sigma_1\\ \sigma_2\\ \tau_{12}\\ \tau_{13}\\ \tau_{23}\end{bmatrix}=\begin{bmatrix}C_{11} & C_{12} & 0 & 0 & 0\\ C_{12} & C_{22} & 0 & 0 & 0\\ 0 & 0 & C_{66} & 0 & 0\\ 0 & 0 & 0 & C_{55} & 0\\ 0 & 0 & 0 & 0 & C_{44}\end{bmatrix}\begin{bmatrix}\varepsilon_1\\ \varepsilon_2\\ \gamma_{12}\\ \gamma_{13}\\ \gamma_{23}\end{bmatrix} \qquad \textbf{(3.3)}$$

where

$$\begin{aligned}
C_{11} &= E_1/(1-\nu_{12}.\nu_{21})\\
C_{12} &= \nu_{12}.E_2/(1-\nu_{12}.\nu_{21}) = \nu_{21}.E_1/(1-\nu_{12}.\nu_{21})\\
C_{22} &= E_2/(1-\nu_{12}.\nu_{21})\\
C_{44} &= G_{23}/r\\
C_{55} &= G_{13}/r\\
C_{66} &= G_{12}
\end{aligned} \qquad \textbf{(3.4)}$$

Where r is the shear reduction factor and equal to (1.2) for plate analysis with constant transverse shear deformation effect, and equal to (1.0) for higher order transverse shear deformation effect as will described later. The number of independent material constants is now reduced to six.

To express the stress-strain relationship for the lamina of arbitrary orientation as illustrated in Figure (3.2), the transformation equations are used for expressing stresses in *x-y* coordinate system in terms of stresses in **1-2** coordinate system [**Jones, 1999**](50).

$$\begin{bmatrix}\sigma_x\\ \sigma_y\\ \tau_{xy}\\ \tau_{xz}\\ \tau_{yz}\end{bmatrix}=[T]^{-1}\begin{bmatrix}\sigma_1\\ \sigma_2\\ \tau_{12}\\ \tau_{13}\\ \tau_{23}\end{bmatrix} \qquad \textbf{(3.5)}$$

where

$$[T]=\begin{bmatrix}c^2 & s^2 & 2sc & 0 & 0\\ s^2 & c^2 & -2sc & 0 & 0\\ -sc & sc & (c^2-s^2) & 0 & 0\\ 0 & 0 & 0 & c & -s\\ 0 & 0 & 0 & s & c\end{bmatrix} \qquad \textbf{(3.6)}$$

and

$s = \sin(\theta)$

$c = \cos\theta)$

θ : is the orientation's angle of fibers.

Similarly, the strain transformation equations are:

$$\begin{bmatrix} \varepsilon_x \\ \varepsilon_y \\ \gamma_{xy} \\ \gamma_{xz} \\ \gamma_{yz} \end{bmatrix} = [T]^{-1} \begin{bmatrix} \varepsilon_1 \\ \varepsilon_2 \\ \gamma_{12} \\ \gamma_{13} \\ \gamma_{23} \end{bmatrix} \qquad \textbf{(3.7)}$$

Using the above transformations, the stress-strain relations for an arbitrary lamina orientation can be written as:

$$\begin{bmatrix} \sigma_x \\ \sigma_y \\ \tau_{xy} \\ \tau_{xz} \\ \tau_{yz} \end{bmatrix} = \begin{bmatrix} Q_{11} & Q_{12} & Q_{16} & 0 & 0 \\ Q_{12} & Q_{22} & Q_{26} & 0 & 0 \\ Q_{16} & Q_{26} & Q_{66} & 0 & 0 \\ 0 & 0 & 0 & Q_{55} & Q_{45} \\ 0 & 0 & 0 & Q_{45} & Q_{44} \end{bmatrix} \begin{bmatrix} \varepsilon_x \\ \varepsilon_y \\ \gamma_{xy} \\ \gamma_{xz} \\ \gamma_{yz} \end{bmatrix} \qquad \textbf{(3.8)}$$

where

$$[Q] = [T]^{-1}[C][T] \qquad \textbf{(3.9)}$$

Finally, in a general orthotropic composite lamina as an orthotropic lamina in which the principal material axes are not aligned with the structural axes, the constitutive matrix (Q) is as defined above in Equation (3.8). All the coefficients of the constitutive matrix are listed as follows:

$$\begin{aligned}
Q_{11} &= c^2\left(C_{11}c^2 + C_{12}s^2\right) + s^2\left(C_{12}c^2 + C_{22}s^2\right) + 4s^2c^2C_{66} \\
Q_{12} &= c^2\left(C_{11}s^2 + C_{12}c^2\right) + s^2\left(C_{12}s^2 + C_{22}c^2\right) - 4s^2c^2C_{66} \\
Q_{16} &= sc^3\left(C_{11} - C_{12} - 2C_{66}\right) + s^3c\left(C_{12} - C_{22} + 2C_{66}\right) \\
Q_{26} &= s^3c\left(C_{11} - C_{12} - 2C_{66}\right) + sc^3\left(C_{12} - C_{22} + 2C_{66}\right) \\
Q_{66} &= s^2c^2\left(C_{11} + C_{22} - 2C_{12} - 2C_{66}\right) + C_{66}\left(s^4 + c^4\right) \\
Q_{44} &= c^2C_{44} + s^2C_{55} \\
Q_{45} &= sc\left(C_{55} - C_{44}\right) \\
Q_{55} &= s^2C_{44} + c^2C_{55}
\end{aligned} \qquad \textbf{(3.10)}$$

3.3 Laminated Plate Theories

A laminated plate is a series of laminas bonded together to act as an integral structural element. Thus, a laminate is not a material but instead a structural element with essential features of both material properties and geometry. The stiffness and strength of such a composite material with structural configuration are obtained from the properties of the constituent laminas, and thus the macromechanical behavior of a laminate is the main topic of this section. The lamination so described can be considered as a single layer with "rule of mixtures" representation of the interaction between the multiple laminas in a plate or shell [**Jones, 1999**][(50)].

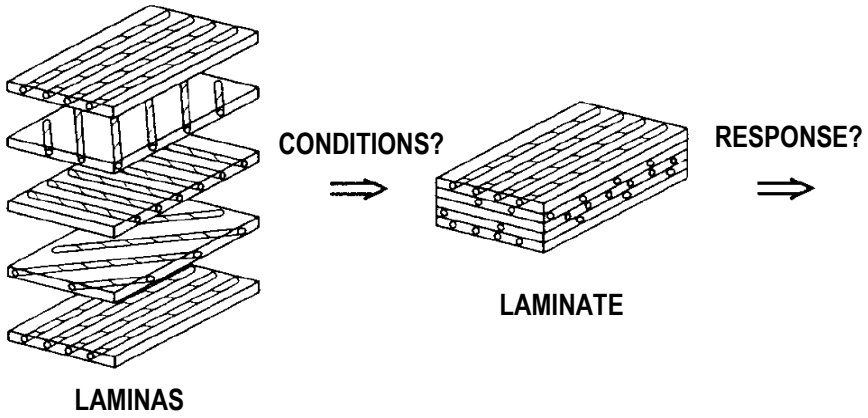

Figure (3.3): Laminated plate with several lamina orientations[**Jones, 1999**][(50)]

As mentioned previously that, in the analysis of the laminated plates, there are two categories of theories, equivalent single layer and three dimensional elasticity theories. In the first category, the material properties of the constituent layer are smeared to form a hypothetical single layer whose properties are equivalent to through thickness integrated sum of its constituents, and this category contains classical lamination theory, first order shear deformation theory, and higher order shear deformation theory as will be given in the following section:

3.3.1 Classical lamination theory

Classical laminated plate theory is also often called "classical laminated theory (CLT)" which is based on the Kirchhoff-Love hypothesis for plates and shells [**Jones, 1999**][(50)].

The assumptions of classical laminated plate theory are as follows:

1- The plate is thin. That is the thickness (***h***) is small compared to the other physical dimensions.
2- The displacements $u(x,y,z), v(x,y,z)$ and $w(x,y,z)$ are small compared to the plate thickness.
3- The in-plane strains $\varepsilon_x^o, \varepsilon_y^o$ and γ_{xy}^o are small compared to unity.
4- The transverse normal stress σ_z is negligible.
5- The transverse shear stresses τ_{xz}, τ_{yz} are negligible.

3.3.2 First order shear deformation theory (FSDT)

Timoshenko deep beam theory, which includes transverse shear deformation and rotary inertia effect, has been extended to isotropic plates by **Reissner** and **Mindlin**, and to laminate anisotropic plates by **Yang**, ***et. al***. and their theory, also called "First order shear deformation theory (FSDT)", takes into account the effect of transverse shear deformation and assume it constant through the plate thickness. Thus, a shear correction factor is used [**Stegman** and **Lind, 2001**][46].

The assumptions of First order shear deformation theory (FSDT) are as follows:

1- The in-plane displacements are linear functions of ***z*** (plane cross sections remaining plane after deflection).
2- The displacements $u(x,y,z), v(x,y,z)$ and $w(x,y,z)$ are small compared to the plate thickness.
3- The in-plane strains $\varepsilon_x, \varepsilon_y$ and γ_{xy} are small compared to unity.
4- The transverse normal stress σ_z is negligible.
5- The transverse shear stresses τ_{xz}, and τ_{yz} are considered to be constant through the plate thickness.

3.3.3 Higher order shear deformation theory (HSDT)

In general, a layered composite plate exhibits coupling between the in-plane displacements, transverse displacements and shear rotations. However, due to the low transverse shear modulus relative to the in-plane Young's modulus of each lamina, the transverse shear deformation effect

is more pronounced in composite than in isotropic plates. Hence, several types of shear deformation theories have been introduced.

The higher order shear deformation theories are more efficient to represent the transverse shear deformation, through-thickness displacement and strains. The assumption of a higher order plate theory can also be used within the equivalent layer formulation [**Jones, 1999**](50).

The assumptions of higher order shear deformation are as follows:

1- The plate may be moderately thick.
2- The in-plane displacements $u(x,y,z), v(x,y,z)$ are cubic functions of z.
3- The transverse shear stresses τ_{xz}, and τ_{yz} are parabolic in z, no shear correction factor is necessary.
4- The in-plane stresses σ_x, σ_y, and τ_{xy} are cubic functions of z.
5- The normals to the mid-surface before deformation are straight, but not necessarily remain normal to it the mid-surface after deformation.
6- The transverse normal stress σ_z is negligible.

Figure (3.4) briefly shows, the basic difference between the classical and the first order theories with the higher order theories.

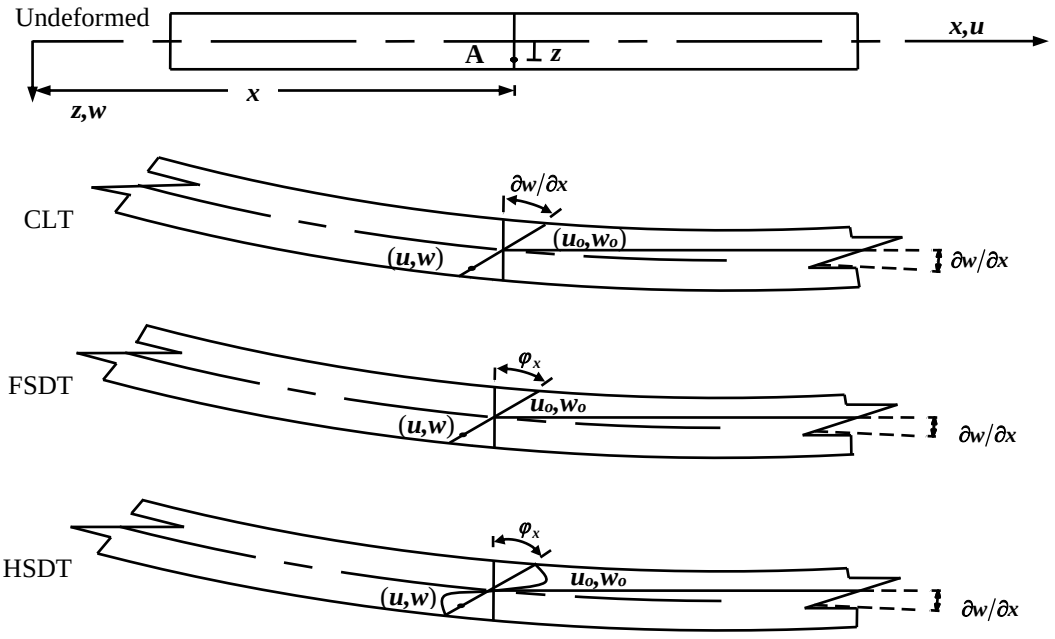

Figure (3.4): Kinematics of deformation of a plate in various plate theories[**Ali, 2004**](6)

All the prescribed theories are considered in the present study in order to study the effect of these theories on the accuracy and the time consumption in the analysis.

3.4 Displacement Field

The displacement at any point in the plate element is defined by a number of Cartesian components of the mid-surface nodal displacements and a number of rotations of the mid-surface depend on the type of considered theory. In the present study, three types of displacement equations were considered, as follows:

3.4.1 First order shear deformation theory (FSDT)

The displacement representation for this theory with five degrees of freedom per node is as follows:

$$\begin{aligned} u(x,y,z,t) &= u_o(x,y,t) + z\theta_x(x,y,t) \\ v(x,y,z,t) &= v_o(x,y,t) + z\theta_y(x,y,t) \\ w(x,y,z,t) &= w_o(x,y,t) \end{aligned} \qquad \textbf{(3.11)}$$

in which t denotes the time; and u_o, v_o, and w_o are the components of the mid-plane displacements for a generic point (x,y,z) having displacements u, v, and w in x, y, and z directions, respectively. Here, θ_x and θ_y are rotations of transverse normals in the (xz) and (yz) planes, respectively.

The strain-displacement relations after differentiating Equation (3.11) are:

$$\begin{aligned} \varepsilon_x &= \frac{\partial u}{\partial x} = \varepsilon_x^o + z\kappa_x \\ \varepsilon_y &= \frac{\partial v}{\partial y} = \varepsilon_y^o + z\kappa_y \\ \gamma_{xy} &= \frac{\partial u}{\partial y} + \frac{\partial v}{\partial x} = \gamma_{xy}^o + z\kappa_{xy} \\ \gamma_{xz} &= \frac{\partial u}{\partial z} + \frac{\partial w}{\partial x} = \varphi_x \\ \gamma_{yz} &= \frac{\partial v}{\partial z} + \frac{\partial w}{\partial y} = \varphi_y \end{aligned} \qquad \textbf{(3.12)}$$

where

$$\varepsilon_x^o = \frac{\partial u_o}{\partial x},\ \varepsilon_y^o = \frac{\partial v_o}{\partial y},\ \gamma_{xy}^o = \frac{\partial u_o}{\partial y} + \frac{\partial v_o}{\partial x}$$
$$\kappa_x = \frac{\partial \theta_x}{\partial x},\ \kappa_y = \frac{\partial \theta_y}{\partial y},\ \kappa_{xy} = \frac{\partial \theta_x}{\partial y} + \frac{\partial \theta_y}{\partial x} \qquad \textbf{(3.13)}$$
$$\varphi_x = \theta_x + \frac{\partial w_o}{\partial x}$$
$$\varphi_y = \theta_y + \frac{\partial w_o}{\partial y}$$

All the strains above are defined in the middle plane of the laminate. By substitution from Equation (3.12) into the stress-strain relations given by Equation (3.8), the stress-strain relations for L^{th} lamina are as follows:

$$\begin{bmatrix}\sigma_x\\ \sigma_y\\ \tau_{xy}\end{bmatrix}^L = \begin{bmatrix}Q_{11} & Q_{12} & Q_{16}\\ Q_{12} & Q_{22} & Q_{26}\\ Q_{16} & Q_{26} & Q_{66}\end{bmatrix}\left\{\begin{bmatrix}\varepsilon_x^o\\ \varepsilon_y^o\\ \gamma_{xy}^o\end{bmatrix} + z\begin{bmatrix}\kappa_x\\ \kappa_y\\ \kappa_{xy}\end{bmatrix}\right\} \qquad \textbf{(3.14)}$$

$$\begin{bmatrix}\tau_{xz}\\ \tau_{yz}\end{bmatrix}^L = \begin{bmatrix}Q_{55} & Q_{45}\\ Q_{45} & Q_{44}\end{bmatrix}\begin{bmatrix}\varphi_x\\ \varphi_y\end{bmatrix} \qquad \textbf{(3.15)}$$

The stress, moment and shear resultants of NL-layered laminate are:

$$\begin{bmatrix}N_x\\ N_y\\ N_{xy}\end{bmatrix}^L = \int_{-h/2}^{h/2}\begin{bmatrix}\sigma_x\\ \sigma_y\\ \tau_{xy}\end{bmatrix}dz = \sum_{L=1}^{NL}\begin{bmatrix}Q_{11} & Q_{12} & Q_{16}\\ Q_{12} & Q_{22} & Q_{26}\\ Q_{16} & Q_{26} & Q_{66}\end{bmatrix}^L\left(\int_{h_{L-1}}^{h_L}\left\{\begin{bmatrix}\varepsilon_x^o\\ \varepsilon_y^o\\ \gamma_{xy}^o\end{bmatrix} + z\begin{bmatrix}\kappa_x\\ \kappa_y\\ \kappa_{xy}\end{bmatrix}\right\}dz\right) \qquad \textbf{(3.16)}$$

and,

$$\begin{bmatrix}M_x\\ M_y\\ M_{xy}\end{bmatrix}^L = \int_{-h/2}^{h/2}\begin{bmatrix}\sigma_x\\ \sigma_y\\ \tau_{xy}\end{bmatrix}z\,dz = \sum_{L=1}^{NL}\begin{bmatrix}Q_{11} & Q_{12} & Q_{16}\\ Q_{12} & Q_{22} & Q_{26}\\ Q_{16} & Q_{26} & Q_{66}\end{bmatrix}^L\left(\int_{h_{L-1}}^{h_L}\left\{z\begin{bmatrix}\varepsilon_x^o\\ \varepsilon_y^o\\ \gamma_{xy}^o\end{bmatrix} + z^2\begin{bmatrix}\kappa_x\\ \kappa_y\\ \kappa_{xy}\end{bmatrix}\right\}dz\right) \qquad \textbf{(3.17)}$$

and,

$$\begin{bmatrix}Q_x\\ Q_y\end{bmatrix}^L = \int_{-h/2}^{h/2}\begin{bmatrix}\tau_{xz}\\ \tau_{yz}\end{bmatrix}dz = \sum_{L=1}^{NL}\begin{bmatrix}Q_{55} & Q_{45}\\ Q_{45} & Q_{44}\end{bmatrix}^L\left(\int_{h_{L-1}}^{h_L}\left\{\begin{bmatrix}\varphi_x\\ \varphi_y\end{bmatrix}\right\}dz\right) \qquad \textbf{(3.18)}$$

After the integration, the expressions above are rewritten in a matrix form which defines the stress-resultant/strain relations of the laminate as follows:

$$\begin{bmatrix} N_x \\ N_y \\ N_{xy} \\ M_x \\ M_y \\ M_{xy} \end{bmatrix} = \begin{bmatrix} A_{11} & A_{12} & A_{16} & B_{11} & B_{12} & B_{16} \\ A_{12} & A_{22} & A_{26} & B_{12} & B_{22} & B_{26} \\ A_{16} & A_{26} & A_{66} & B_{16} & B_{26} & B_{66} \\ B_{11} & B_{12} & B_{16} & D_{11} & D_{12} & D_{16} \\ B_{12} & B_{22} & B_{26} & D_{12} & D_{22} & D_{26} \\ B_{16} & B_{26} & B_{66} & D_{16} & D_{26} & D_{66} \end{bmatrix} \begin{bmatrix} \varepsilon_x \\ \varepsilon_y \\ \gamma_{xy} \\ \kappa_x \\ \kappa_y \\ \kappa_{xy} \end{bmatrix} \quad \textbf{(3.19)}$$

$$\begin{bmatrix} Q_x \\ Q_y \end{bmatrix} = \begin{bmatrix} A_{55} & A_{45} \\ A_{45} & A_{44} \end{bmatrix} \begin{bmatrix} \varphi_x \\ \varphi_y \end{bmatrix} \quad \textbf{(3.20)}$$

All the coefficients in ***A***, ***B***, and ***D*** will be defined later.

Equations (3.19) and (3.20) represent the relation between the stress resultant (membrane forces, bending moments and shear forces) and the strains.

3.4.2 Higher order shear deformation theory (HSDT) with seven degrees of freedom per node

The strain expressions derived from the displacement field was considered by **Mallikarjuna,** and **Kant** [**1988**][65]**,** and by **Ali** [**2004**][6] with seven degrees of freedom per node as follows:

$$\begin{aligned} u(x,y,z,t) &= u_o(x,y,t) + z\theta_x(x,y,t) + z^3\theta_x^*(x,y,t) \\ v(x,y,z,t) &= v_o(x,y,t) + z\theta_y(x,y,t) + z^3\theta_y^*(x,y,t) \\ w(x,y,z,t) &= w_o(x,y,t) \end{aligned} \quad \textbf{(3.21)}$$

in which (***u***, ***v***, ***w***, θ_x, and θ_y) are defined previously, θ_x^* and θ_y^* are the corresponding higher order terms in Taylor's series expression and also defined at the middle plane. The strain-displacement relations after differentiating Equation (3.21) are:

$$\begin{aligned} \varepsilon_x &= \frac{\partial u}{\partial x} = \varepsilon_x^o + z\kappa_x + z^3\kappa_x^* \\ \varepsilon_y &= \frac{\partial v}{\partial y} = \varepsilon_y^o + z\kappa_y + z^3\kappa_y^* \\ \gamma_{xy} &= \frac{\partial u}{\partial y} + \frac{\partial v}{\partial x} = \gamma_{xy}^o + z\kappa_{xy} + z^3\kappa_{xy}^* \\ \gamma_{xz} &= \frac{\partial u}{\partial z} + \frac{\partial w}{\partial x} = \varphi_x + z^2\varphi_x^* \\ \gamma_{yz} &= \frac{\partial v}{\partial z} + \frac{w}{\partial y} = \varphi_y + z^2\varphi_y^* \end{aligned} \quad \textbf{(3.22)}$$

where the parameters $(\varepsilon_x^o, \varepsilon_y^o, \gamma_{xy}^o, \kappa_x, \kappa_y, \kappa_{xy}, \varphi_x, \varphi_y)$ are defined previously at Equation (3.13).

$$\kappa_x^* = \frac{\partial \theta_x^*}{\partial x}, \kappa_y^* = \frac{\partial \theta_y^*}{\partial y}, \kappa_{xy}^* = \frac{\partial \theta_x^*}{\partial y} + \frac{\partial \theta_y^*}{\partial x}$$
$$\varphi_x^* = 3\theta_x^* \qquad \textbf{(3.23)}$$
$$\varphi_y^* = 3\theta_y^*$$

Also, all the strains above are defined in the middle-plane of the laminate. By substitution from Equation (3.22) into the stress-strain relations given by Equation (3.8), the stress-strain relations for L^{th} lamina are as follows:

$$\begin{bmatrix} \sigma_x \\ \sigma_y \\ \tau_{xy} \end{bmatrix}^L = \begin{bmatrix} Q_{11} & Q_{12} & Q_{16} \\ Q_{12} & Q_{22} & Q_{26} \\ Q_{16} & Q_{26} & Q_{66} \end{bmatrix} \left\{ \begin{bmatrix} \varepsilon_x^o \\ \varepsilon_y^o \\ \gamma_{xy}^o \end{bmatrix} + z \begin{bmatrix} \kappa_x \\ \kappa_y \\ \kappa_{xy} \end{bmatrix} + z^3 \begin{bmatrix} \kappa_x^* \\ \kappa_y^* \\ \kappa_{xy}^* \end{bmatrix} \right\} \qquad \textbf{(3.24)}$$

$$\begin{bmatrix} \tau_{xz} \\ \tau_{yz} \end{bmatrix}^L = \begin{bmatrix} Q_{55} & Q_{45} \\ Q_{45} & Q_{44} \end{bmatrix} \left\{ \begin{bmatrix} \varphi_x \\ \varphi_y \end{bmatrix} + 3z^2 \begin{bmatrix} \theta_x^* \\ \theta_y^* \end{bmatrix} \right\} \qquad \textbf{(3.25)}$$

The stress, moment and shear resultants of NL-layered laminate are:

$$\begin{bmatrix} N_x \\ N_y \\ N_{xy} \end{bmatrix}^L = \int_{-h/2}^{h/2} \begin{bmatrix} \sigma_x \\ \sigma_y \\ \tau_{xy} \end{bmatrix} dz = \sum_{L=1}^{NL} \begin{bmatrix} Q_{11} & Q_{12} & Q_{16} \\ Q_{12} & Q_{22} & Q_{26} \\ Q_{16} & Q_{26} & Q_{66} \end{bmatrix}^L \left(\int_{h_{L-1}}^{h_L} \left\{ \begin{bmatrix} \varepsilon_x^o \\ \varepsilon_y^o \\ \gamma_{xy}^o \end{bmatrix} + z \begin{bmatrix} \kappa_x \\ \kappa_y \\ \kappa_{xy} \end{bmatrix} + z^3 \begin{bmatrix} \kappa_x^* \\ \kappa_y^* \\ \kappa_{xy}^* \end{bmatrix} \right\} dz \right) \qquad \textbf{(3.26)}$$

$$\begin{bmatrix} M_x \\ M_y \\ M_{xy} \end{bmatrix}^L = \int_{-h/2}^{h/2} \begin{bmatrix} \sigma_x \\ \sigma_y \\ \tau_{xy} \end{bmatrix} z\, dz = \sum_{L=1}^{NL} \begin{bmatrix} Q_{11} & Q_{12} & Q_{16} \\ Q_{12} & Q_{22} & Q_{26} \\ Q_{16} & Q_{26} & Q_{66} \end{bmatrix}^L \left(\int_{h_{L-1}}^{h_L} \left\{ z \begin{bmatrix} \varepsilon_x^o \\ \varepsilon_y^o \\ \gamma_{xy}^o \end{bmatrix} + z^2 \begin{bmatrix} \kappa_x \\ \kappa_y \\ \kappa_{xy} \end{bmatrix} + z^4 \begin{bmatrix} \kappa_x^* \\ \kappa_y^* \\ \kappa_{xy}^* \end{bmatrix} \right\} dz \right) \qquad \textbf{(3.27)}$$

$$\begin{bmatrix} M_x^* \\ M_y^* \\ M_{xy}^* \end{bmatrix}^L = \int_{-h/2}^{h/2} \begin{bmatrix} \sigma_x \\ \sigma_y \\ \tau_{xy} \end{bmatrix} z^3\, dz = \sum_{L=1}^{NL} \begin{bmatrix} Q_{11} & Q_{12} & Q_{16} \\ Q_{12} & Q_{22} & Q_{26} \\ Q_{16} & Q_{26} & Q_{66} \end{bmatrix}^L \left(\int_{h_{L-1}}^{h_L} \left\{ z^3 \begin{bmatrix} \varepsilon_x^o \\ \varepsilon_y^o \\ \gamma_{xy}^o \end{bmatrix} + z^4 \begin{bmatrix} \kappa_x \\ \kappa_y \\ \kappa_{xy} \end{bmatrix} + z^6 \begin{bmatrix} \kappa_x^* \\ \kappa_y^* \\ \kappa_{xy}^* \end{bmatrix} \right\} dz \right) \qquad \textbf{(3.28)}$$

$$\begin{bmatrix} Q_x \\ Q_y \end{bmatrix}^L = \int_{-h/2}^{h/2} \begin{bmatrix} \tau_{xz} \\ \tau_{yz} \end{bmatrix} dz = \sum_{L=1}^{NL} \begin{bmatrix} Q_{55} & Q_{45} \\ Q_{45} & Q_{44} \end{bmatrix}^L \left(\int_{h_{L-1}}^{h_L} \left\{ \begin{bmatrix} \varphi_x \\ \varphi_y \end{bmatrix} + 3z^2 \begin{bmatrix} \theta_x^* \\ \theta_y^* \end{bmatrix} \right\} dz \right) \qquad \textbf{(3.29)}$$

$$\begin{bmatrix} Q_x^* \\ Q_y^* \end{bmatrix}^L = \int_{-h/2}^{h/2} \begin{bmatrix} \tau_{xz} \\ \tau_{yz} \end{bmatrix} z^2\, dz = \sum_{L=1}^{NL} \begin{bmatrix} Q_{55} & Q_{45} \\ Q_{45} & Q_{44} \end{bmatrix}^L \left(\int_{h_{L-1}}^{h_L} \left\{ z^2 \begin{bmatrix} \varphi_x \\ \varphi_y \end{bmatrix} + 3z^4 \begin{bmatrix} \theta_x^* \\ \theta_y^* \end{bmatrix} \right\} dz \right) \qquad \textbf{(3.30)}$$

After the integration, the above expressions are rewritten in a matrix form which defines the stress-resultant/strain relations of the laminate as follows:

$$\begin{bmatrix} N_x \\ N_y \\ N_{xy} \\ M_x \\ M_y \\ M_{xy} \\ M^*_x \\ M^*_y \\ M^*_{xy} \end{bmatrix} = \begin{bmatrix} A_{11} & A_{12} & A_{16} & B_{11} & B_{12} & B_{16} & E_{11} & E_{12} & E_{16} \\ A_{12} & A_{22} & A_{26} & B_{12} & B_{22} & B_{26} & E_{12} & E_{22} & E_{26} \\ A_{16} & A_{26} & A_{66} & B_{16} & B_{26} & B_{66} & E_{16} & E_{26} & E_{66} \\ B_{11} & B_{12} & B_{16} & D_{11} & D_{12} & D_{16} & F_{11} & F_{12} & F_{16} \\ B_{12} & B_{22} & B_{26} & D_{12} & D_{22} & D_{26} & F_{12} & F_{22} & F_{26} \\ B_{26} & B_{26} & B_{66} & D_{16} & D_{26} & D_{66} & F_{16} & F_{26} & F_{66} \\ E_{11} & E_{12} & E_{16} & F_{11} & F_{12} & F_{16} & H_{11} & H_{12} & H_{16} \\ E_{12} & E_{22} & E_{26} & F_{12} & F_{22} & F_{26} & H_{12} & H_{22} & H_{26} \\ E_{16} & E_{26} & E_{66} & F_{16} & F_{26} & F_{66} & H_{16} & H_{26} & H_{66} \end{bmatrix} \begin{bmatrix} \varepsilon_x \\ \varepsilon_x \\ \gamma_{xy} \\ \kappa_x \\ \kappa_y \\ \kappa_{xy} \\ \kappa^*_x \\ \kappa^*_y \\ \kappa^*_{xy} \end{bmatrix} \qquad \textbf{(3.31)}$$

and,

$$\begin{bmatrix} Q_x \\ Q_y \\ Q^*_x \\ Q^*_y \end{bmatrix} = \begin{bmatrix} A_{55} & A_{45} & D_{55} & D_{45} \\ A_{45} & A_{44} & D_{45} & D_{44} \\ D_{55} & D_{45} & F_{55} & F_{45} \\ D_{45} & D_{44} & F_{45} & F_{44} \end{bmatrix} \begin{bmatrix} \varphi_x \\ \varphi_x \\ \varphi^*_x \\ \varphi^*_y \end{bmatrix} \qquad \textbf{(3.32)}$$

All the coefficients in A, B, D, E, F, and H will be defined later.

3.4.3 Higher order shear deformation theory (HSDT) with nine degrees of freedom per node

The strain expressions derived from the displacement field were considered by **[Ali, 2004]**[(6)] with nine degrees of freedom per node as follows:

$$\begin{aligned} u(x,y,z,t) &= u_o(x,y,t) + z\theta_x(x,y,t) + z^2 u^*_o(x,y,t) + z^3\theta^*_x(x,y,t) \\ v(x,y,z,t) &= v_o(x,y,t) + z\theta_y(x,y,t) + z^2 v^*_o(x,y,t) + z^3\theta^*_y(x,y,t) \\ w(x,y,z,t) &= w_o(x,y,t) \end{aligned} \qquad \textbf{(3.33)}$$

in which the parameters (u, v, w, θ_x, θ_y, θ^*_x, and θ^*_y) are defined previously, u^*_o, and v^*_o are the corresponding higher order terms in Taylor's series expression and they are also defined at the middle plane. The strain-displacement relations after differentiating Equation (3.33) are:

$$\varepsilon_x = \frac{\partial u}{\partial x} = \varepsilon_x^o + z\kappa_x + z^2\varepsilon_x^{o^*} + z^3\kappa_x^*$$

$$\varepsilon_y = \frac{\partial v}{\partial y} = \varepsilon_y^o + z\kappa_y + z^2\varepsilon_y^{o^*} + z^3\kappa_y^*$$

$$\gamma_{xy} = \frac{\partial u}{\partial y} + \frac{\partial v}{\partial x} = \gamma_{xy}^o + z\kappa_{xy} + z^2\gamma_{xy}^{o^*} + z^3\kappa_{xy}^* \qquad \textbf{(3.34)}$$

$$\gamma_{xz} = \frac{\partial u}{\partial z} + \frac{\partial w}{\partial x} = \varphi_x + z\gamma_{xz}^o + z^2\varphi_x^*$$

$$\gamma_{yz} = \frac{\partial v}{\partial z} + \frac{\partial w}{\partial y} = \varphi_y + z\gamma_{yz}^o + z^2\varphi_y^*$$

where $(\varepsilon_x^o, \varepsilon_y^o, \gamma_{xy}^o, \kappa_x, \kappa_y, \kappa_{xy}, \kappa_x^*, \kappa_y^*, \kappa_{xy}^*, \varphi_x, \varphi_y, \varphi_x^*, \varphi_y^*)$ are defined previously.

$$\varepsilon_x^{o*} = \frac{\partial u_o^*}{\partial x},\ \varepsilon_y^{o*} = \frac{\partial v_o^*}{\partial y},\ \gamma_{xy}^{o*} = \frac{\partial u_o^*}{\partial y} + \frac{\partial v_o^*}{\partial x}$$

$$\gamma_{xz}^{o*} = 2u_o^* \qquad \textbf{(3.35)}$$

$$\gamma_{yz}^{o*} = 2v_o^*$$

Also, all the strains above are defined in the middle-plane of the laminate. By substitution from Equation (3.34) into the stress-strain relations given by Equation (3.8), in the same process as Equations ((3.24) to (3.30)) and after complete integration, the stress-resultant/strain relations of the laminate are as follows:

$$\begin{bmatrix} N_x \\ N_y \\ N_{xy} \\ N_x^* \\ N_y^* \\ N_{xy}^* \\ M_x \\ M_y \\ M_{xy} \\ M_x^* \\ M_y^* \\ M_{xy}^* \end{bmatrix} = \begin{bmatrix} A_{11} & A_{12} & A_{16} & D_{11} & D_{12} & D_{16} & B_{11} & B_{12} & B_{16} & E_{11} & E_{12} & E_{16} \\ A_{12} & A_{22} & A_{26} & D_{12} & D_{22} & D_{26} & B_{12} & B_{22} & B_{26} & E_{12} & E_{22} & E_{26} \\ A_{16} & A_{26} & A_{66} & D_{16} & D_{26} & D_{66} & B_{16} & B_{26} & B_{66} & E_{16} & E_{26} & E_{66} \\ D_{11} & D_{12} & D_{16} & F_{11} & F_{12} & F_{16} & E_{11} & E_{12} & E_{16} & G_{11} & G_{12} & G_{16} \\ D_{12} & D_{22} & D_{26} & F_{12} & F_{22} & F_{26} & E_{12} & E_{22} & E_{26} & G_{12} & G_{22} & G_{26} \\ D_{16} & D_{26} & D_{66} & F_{16} & F_{26} & F_{66} & E_{16} & E_{26} & E_{66} & G_{16} & G_{26} & G_{66} \\ B_{12} & B_{12} & B_{16} & E_{11} & E_{12} & E_{16} & D_{11} & D_{12} & D_{16} & F_{11} & F_{12} & F_{16} \\ B_{12} & B_{22} & B_{26} & E_{12} & E_{22} & E_{26} & D_{12} & D_{22} & D_{26} & F_{12} & F_{22} & F_{26} \\ B_{16} & B_{26} & B_{66} & E_{16} & E_{26} & E_{66} & D_{16} & D_{26} & D_{66} & F_{16} & F_{26} & F_{66} \\ E_{11} & E_{12} & E_{16} & G_{11} & G_{12} & G_{16} & F_{11} & F_{12} & F_{16} & H_{11} & H_{12} & H_{16} \\ E_{12} & E_{22} & E_{26} & G_{12} & G_{22} & G_{26} & F_{12} & F_{22} & F_{26} & H_{12} & H_{22} & H_{26} \\ E_{16} & E_{26} & E_{66} & G_{16} & G_{26} & G_{66} & F_{16} & F_{26} & F_{66} & H_{16} & H_{26} & H_{66} \end{bmatrix} \begin{bmatrix} \varepsilon_x^o \\ \varepsilon_y^o \\ \gamma_{xy}^o \\ \varepsilon_x^{o*} \\ \varepsilon_y^{o*} \\ \gamma_{xy}^{o*} \\ \kappa_x \\ \kappa_y \\ \kappa_{xy} \\ \kappa_x^* \\ \kappa_y^* \\ \kappa_{xy}^* \end{bmatrix} \qquad \textbf{(3.36)}$$

and,

$$\begin{bmatrix} Q_x \\ Q_y \\ S_x \\ S_y \\ Q_x^* \\ Q_y^* \end{bmatrix} = \begin{bmatrix} A_{55} & A_{45} & B_{55} & B_{45} & D_{55} & D_{45} \\ A_{45} & A_{44} & B_{45} & B_{44} & D_{45} & D_{44} \\ B_{55} & B_{45} & D_{55} & D_{45} & E_{55} & E_{45} \\ B_{45} & B_{44} & D_{45} & D_{44} & E_{45} & E_{44} \\ D_{55} & D_{45} & E_{55} & E_{45} & F_{55} & F_{45} \\ D_{45} & D_{44} & E_{45} & E_{44} & F_{45} & F_{44} \end{bmatrix} \begin{bmatrix} \varphi_x \\ \varphi_y \\ \gamma_{xz}^{o*} \\ \gamma_{yz}^{o*} \\ \varphi_x^* \\ \varphi_y^* \end{bmatrix} \quad \textbf{(3.37)}$$

All coefficients in ***A***, ***B***, ***D***, ***E***, ***F***, ***G***, and ***H*** groups are defined as follows:

$$A_{ij} = \sum_{L=1}^{NL} Q_{ij}(h_L - h_{L-1}) \qquad i, j = 1, 2, 6 \text{ or } i, j = 4, 5 \qquad \textbf{(3.38 a)}$$

$$B_{ij} = (1/2)\sum_{L=1}^{NL} Q_{ij}(h_L^2 - h_{L-1}^2) \qquad i, j = 1, 2, 6 \text{ or } i, j = 4, 5 \qquad \textbf{(3.38 b)}$$

$$D_{ij} = (1/3)\sum_{L=1}^{NL} Q_{ij}(h_L^3 - h_{L-1}^3) \qquad i, j = 1, 2, 6 \text{ or } i, j = 4, 5 \qquad \textbf{(3.38 c)}$$

$$E_{ij} = (1/4)\sum_{L=1}^{NL} Q_{ij}(h_L^4 - h_{L-1}^4) \qquad i, j = 1, 2, 6 \text{ or } i, j = 4, 5 \qquad \textbf{(3.38 d)}$$

$$F_{ij} = (1/5)\sum_{L=1}^{NL} Q_{ij}(h_L^5 - h_{L-1}^5) \qquad i, j = 1, 2, 6 \text{ or } i, j = 4, 5 \qquad \textbf{(3.38 e)}$$

$$G_{ij} = (1/6)\sum_{L=1}^{NL} Q_{ij}(h_L^6 - h_{L-1}^6) \qquad i, j = 1, 2, 6 \qquad \textbf{(3.38 e)}$$

$$H_{ij} = (1/7)\sum_{L=1}^{NL} Q_{ij}(h_L^7 - h_{L-1}^7) \qquad i, j = 1, 2, 6 \qquad \textbf{(3.38 g)}$$

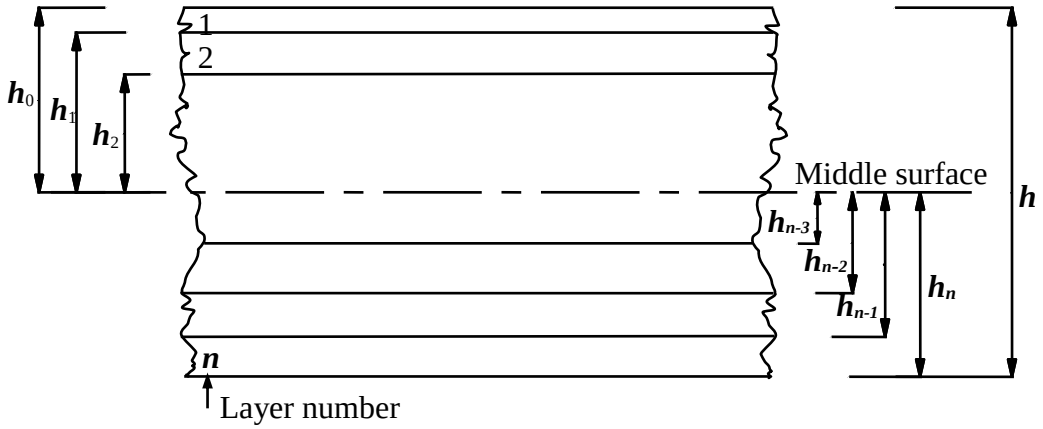

Figure (3.5): Geometry of an NL-layered laminate [**Jones**,**1999**](50)

3.5 Waviness of Fiber

In the conventional design of composite laminates, fibers with the matrix are placed as uniformly spaced with parallel straight lines, often inclined

at a constant angle with the laminate axis. Therefore, the fiber angle and the fiber volume fraction within the plane of a lamina can be considered constant. Thus, all the previous derivations for the stress-strain relations were performed according to straight fibers. The present study focuses on the concept of designing composite materials with optimized forms of inhomogeneity, obtained by tailoring the profile of reinforcing fibers, to further improve the buckling strength of the thin-walled laminates [**Pandey**,**1999**][(82)].

Kao, **et al**. **[1988]** as given by [**Pandey**,**1999**][(82)], analyzed the tensile response of laminates with a sinusoidal fiber pattern. **Hyer** and **Charette [1991]** as given by [**Pandey**,**1999**][(82)], studied the effect of curvilinear fibers on the tensile and compressive response of a plate with a circular hole. [**Pandey**,**1999**][(82)] studied the effect of sinusoidal fibers on the buckling behavior of a composite laminate.

The present study explores the idea of tailoring the profile of reinforcing fibers to improve the buckling strength of composite plates. This study investigates the effect of waviness of fibers on the dynamic buckling curves, as shown in Figure (3.6), and this waviness is of the form:

$$y(x) = \alpha \sin\left(\frac{k\pi x}{a}\right) \qquad \textbf{(3.39)}$$

such that the angle of fiber orientation θ varies along the longitudinal x-axis as:

$$\tan(\theta) = \frac{dy}{dx} = \frac{\alpha k\pi}{a}.\cos\left(\frac{k\pi x}{a}\right) = \Delta k\pi.\cos(k\pi\bar{x}) \qquad \textbf{(3.40)}$$

where a = plate length; k= number of half sine waves; and α= wave amplitude. Two normalized variables, $\Delta=\alpha/a$ and $\bar{x} = x/a$, are introduced.

The main objective is to study the effect of fiber waviness, characterized by k and Δ, on the static and dynamic buckling behavior of composite laminates. The fiber can also be rotated in any direction with the x-axis, as shown in Figure (3.6), by using the following expression:

$$x_n = x\cos(\beta) + y\sin(\beta) \qquad \textbf{(3.41)}$$

where x_n represent the x-coordinate for a rotated fiber, and β is the angle of the waviness fiber.

The angle of fiber orientation in Equation (3.40) is variable with x-coordinate and it is used in Equation (3.6) instead of the constant angle used for straight fibers.

Figure (3.7) shows the principal material directions aligned with the lamina axes by angle (β).

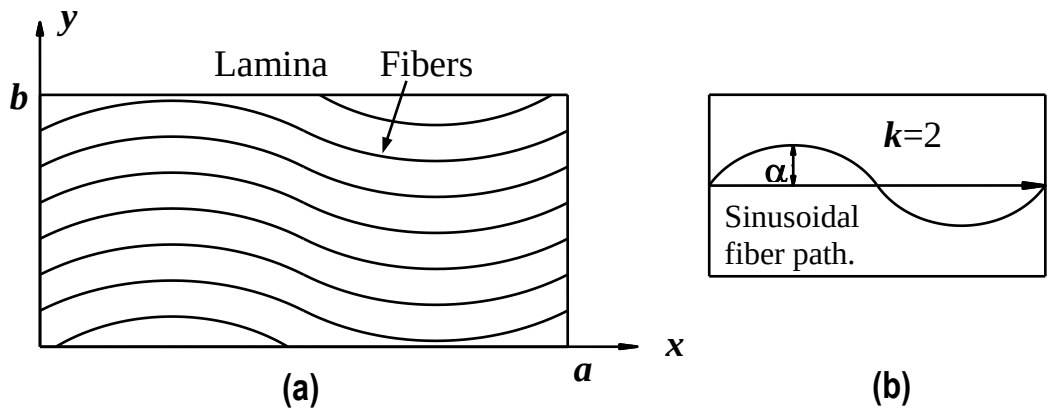

Fiber (3.6): (a) Lamina with variable fiber orientation; **(b)** Geometry of sinusoidal fiber path [**Pandey**,**1999**][82]

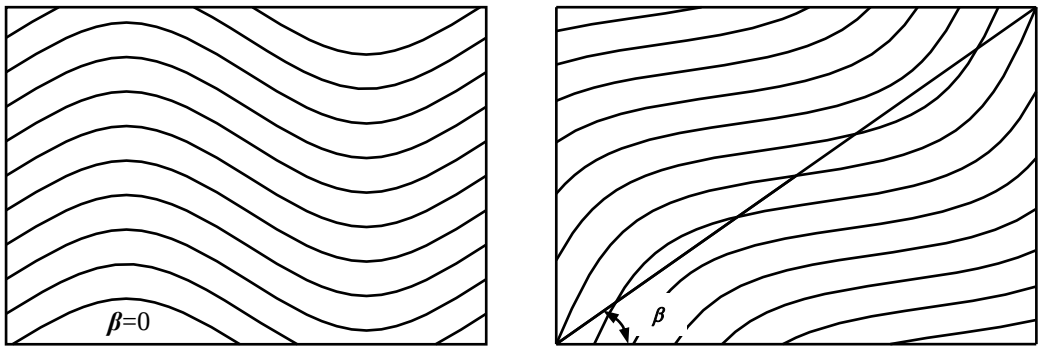

Figure (3.7): Laminate plate with sine wave fibers aligned with x-axis

3.6 Finite Element Concepts

In order to study the dynamic post-buckling behavior of plates with initial imperfection for different boundary conditions, load conditions, and fiber orientation, and because of the limitations on the boundary and load conditions and other effects that make the analytical methods intractable, it was decided to use the finite element method.

The finite element method has proved to be a powerful method of analysis in many fields of engineering.

Most of its early applications were used to adopted the solution of linear problems. However, for more than thirty years, the application of the finite element method to nonlinear problems has been under rapid development [**Mathlum**, **1997**][(66)].

The finite element method involves dividing (or discretizing) the continuum into a finite number of elements connected at nodal points. These elements have a simple shape (usually rectangular or triangular) and any complex structural shape can be approximately represented by a proper assemblage of these elements. Any difficulties due to complex loading conditions can be simplified by assuming that the load can be applied only at the nodes of the element. The accuracy of the method depends not only on the idealization of the continuum, but also on the properties of the shape functions assumed to represent the deformed shapes of the element.

3.7 Types of Quadratic Element

A brief description of the quadratic elements used in the present model is given below. The behavior of the elements discussed here is mainly based on studies of linear beam, plate and shell problems. The elements considered are eight-node Serendipity, Nine-node Lagrangian, and Heterosis elements as shown in Figure (3.8).

3.7.1 Eight-node Serendipity element

This element is the simplest element as shown in Figure (3.8 a) and it is considered in the original work of **Ahmed, et al**. [**Baka, 2002**][(13)]; their results obtained by using full integration rule, show that as the shell thickness is reduced the solution becomes stiff. This locking phenomenon is exhibited by this element even in moderately thin or thick situations. A great improvement of the results is achieved by using a reduced integration rule. In spite of the improvement, the locking may still occur. Despite the noted drawbacks above, the eight-node Serendipity element remains one most popular of the isoparametric elements.

3.7.2 Nine-node Lagrangian element

Investigations carried out by **Pugh**, **et al.**(as given by [**Baka**, **2002**][13]) as shown in Figure (3.8 b) is more optimal as a general plate element. The performance exhibited by the Lagrangian element appears to be superior to the Serendipity element when reduced or selective integration is adopted. However some drawbacks may arise when reduced integration is employed. The stiffness matrix exhibits rank deficiency, which causes the appearance of spurious mechanisms. This drawback is not exhibited by the eight-node Serendipity element with reduced integration [**Baka, 2002**][13].

3.7.3 Nine-node Heterosis element

The reasons which led to the development of this nine-node quadrilateral element shown in Figure (3.8 c) are to overcome the shortcomings mentioned above (the locking phenomena and the spurious mechanisms) because this element has improved characteristics when it is compared with the nine-node Lagrangian and the eight-node Serendipity elements. The locking problem is overcome by using selective integration, which leads to obtain a correct rank for the stiffness matrix of this element, and does not lock in very thin situation. The other problem (spurious mechanisms) can be overcome by using reduced integration. The element gives a better behavior compared with the nine-node Lagrangian element and makes the appearance of spurious mechanisms improbable. It is good to recall that, this element was initially developed for plates and employed Serendipity shape functions for vertical displacement (w) and Lagrangian shape function for rotations. Then, Heterosis concept has been extended to shell analysis (using Serendipity shape functions for the lateral displacement, w only)[**Baka, 2002**][13].

The nine-node Lagrangian element shown in Figure (3.8 b) is adopted in the present study. This element contains four nodes at the corners, four nodes at the mid-sides of the element boundaries and one node at the center of the element. The topology order is counter-clockwise in the sequence from 1 to 9.

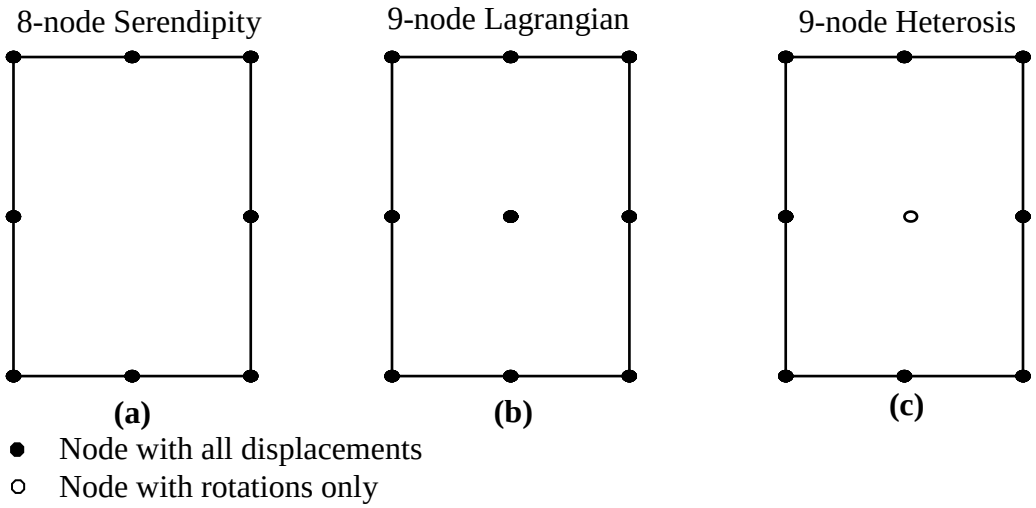

Figure (3.8): Nodal configuration of the three quadratic plate elements

The shape function, $N_i(\xi,\eta)$, at the ***i***-th node of this element and its derivatives are given in Table (3.1).

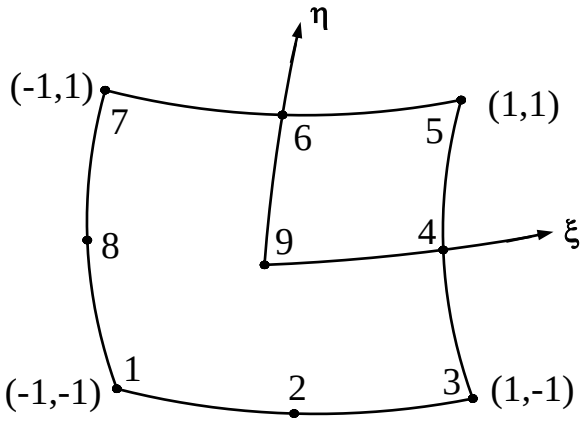

Figure (3.9): Nine-node quadrilateral isoparametric element

Table (3.1): Shape functions and their derivatives [**Bathe, 1996**][17]

Location	N_i	$\partial N_i/\partial\xi$	$\partial N_i/\partial\eta$
Corner Nodes (1, 3, 5, 7)	$\left(\frac{1}{4}\right)(1+\xi_o)(1+\eta_o)(\eta_o+\xi_o-1)$	$\left(\frac{\xi_i}{4}\right)(1+\eta_o)(2\xi_o+\eta_o)$	$\left(\frac{\eta_i}{4}\right)(1+\xi_o)(2\eta_o+\xi_o)$
Mid-side Nodes (2, 6)	$\left(\frac{1}{2}\right)(1-\xi^2)(1+\eta_o)$	$-\xi(1+\eta_o)$	$\left(\frac{\eta_i}{2}\right)(1-\xi^2)$
Mid-side Nodes (4, 8)	$\left(\frac{1}{2}\right)(1-\eta^2)(1+\xi_o)$	$(\xi_i/2)(1-\eta^2)$	$-\eta(1-\xi_o)$
Center Node (9)	$(1-\xi^2)(1+\eta^2)$	$-2\xi(1-\eta^2)$	$-2\eta(1-\xi^2)$

where $\xi_o=\xi\xi_i$, $\eta_o=\eta\eta_i$

ξ_i and η_i are the natural (local) coordinates of node (i).

3.8 Derivation of Linear Strain-Nodal Displacement Matrix

The engineering components of strain can be expressed in terms of the first partial derivatives of the displacement components. Therefore, the linear strain-nodal displacement matrix [$\boldsymbol{B}$] at any point within an element for a five, seven, and nine degrees of freedom per node can be written. For five degrees of freedom per node:

$$[\varepsilon]=\begin{bmatrix} \frac{\partial u_o}{\partial x} \\ \frac{\partial v_o}{\partial y} \\ \frac{\partial u_o}{\partial y}+\frac{\partial v_o}{\partial x} \\ \frac{\partial \theta_x}{\partial x} \\ \frac{\partial \theta_y}{\partial x} \\ \frac{\partial \theta_x}{\partial y}+\frac{\partial \theta_y}{\partial x} \\ \varphi_x \\ \varphi_y \end{bmatrix} = \sum_{i=1}^{9} \begin{bmatrix} \frac{\partial N_i}{\partial x} & 0 & 0 & 0 & 0 \\ 0 & \frac{\partial N_i}{\partial y} & 0 & 0 & 0 \\ \frac{\partial N_i}{\partial y} & \frac{\partial N_i}{\partial x} & 0 & 0 & 0 \\ 0 & 0 & 0 & \frac{\partial N_i}{\partial x} & 0 \\ 0 & 0 & 0 & 0 & \frac{\partial N_i}{\partial y} \\ 0 & 0 & 0 & \frac{\partial N_i}{\partial y} & \frac{\partial N_i}{\partial x} \\ 0 & 0 & \frac{\partial N_i}{\partial x} & N_i & 0 \\ 0 & 0 & \frac{\partial N_i}{\partial y} & 0 & N_i \end{bmatrix} \begin{bmatrix} u_o \\ v_o \\ w_o \\ \theta_x \\ \theta_y \end{bmatrix}_i \qquad \textbf{(3.42)}$$

Equation (3.42) represents the strain-nodal displacement [***B***] matrix for five degrees of freedom per node. Also, the strain-nodal displacement matrices of any point within an element for seven and nine degrees of freedom per node are:

$$[\varepsilon]=\begin{bmatrix} \frac{\partial u_o}{\partial x} \\ \frac{\partial v_o}{\partial y} \\ \frac{\partial u_o}{\partial x}+\frac{\partial u_o}{\partial x} \\ \frac{\partial \theta_x}{\partial x} \\ \frac{\partial \theta_y}{\partial y} \\ \frac{\partial \theta_x}{\partial y}+\frac{\partial \theta_y}{\partial x} \\ \frac{\partial \theta_x^*}{\partial x} \\ \frac{\partial \theta_y^*}{\partial y} \\ \frac{\partial \theta_x^*}{\partial y}+\frac{\partial \theta_y^*}{\partial x} \\ \varphi_x \\ \varphi_y \\ 3\theta_x^* \\ 3\theta_y^* \end{bmatrix} = \sum_{i=1}^{9} \begin{bmatrix} \frac{\partial N_i}{\partial x} & 0 & 0 & 0 & 0 & 0 & 0 \\ 0 & \frac{\partial N_i}{\partial y} & 0 & 0 & 0 & 0 & 0 \\ \frac{\partial N_i}{\partial y} & \frac{\partial N_i}{\partial x} & 0 & 0 & 0 & 0 & 0 \\ 0 & 0 & 0 & \frac{\partial N_i}{\partial x} & 0 & 0 & 0 \\ 0 & 0 & 0 & 0 & \frac{\partial N_i}{\partial y} & 0 & 0 \\ 0 & 0 & 0 & \frac{\partial N_i}{\partial y} & \frac{\partial N_i}{\partial x} & 0 & 0 \\ 0 & 0 & 0 & 0 & 0 & \frac{\partial N_i}{\partial x} & 0 \\ 0 & 0 & 0 & 0 & 0 & 0 & \frac{\partial N_i}{\partial y} \\ 0 & 0 & 0 & 0 & 0 & \frac{\partial N_i}{\partial y} & \frac{\partial N_i}{\partial x} \\ 0 & 0 & \frac{\partial N_i}{\partial x} & N_i & 0 & 0 & 0 \\ 0 & 0 & \frac{\partial N_i}{\partial x} & 0 & N_i & 0 & 0 \\ 0 & 0 & 0 & 0 & 0 & 3N_i & 0 \\ 0 & 0 & 0 & 0 & 0 & 0 & 3N_i \end{bmatrix} \begin{bmatrix} u_o \\ v_o \\ w_o \\ \theta_x \\ \theta_y \\ \theta_x^* \\ \theta_y^* \end{bmatrix}_i \quad \textbf{(3.43)}$$

$$
[\varepsilon]=\begin{bmatrix}
\frac{\partial u_o}{\partial x}\\
\frac{\partial v_o}{\partial y}\\
\frac{\partial u_o}{\partial y}+\frac{\partial v_o}{\partial x}\\
\frac{\partial u_o^*}{\partial x}\\
\frac{\partial v_o^*}{\partial y}\\
\frac{\partial u_o^*}{\partial y}+\frac{\partial v_o^*}{\partial x}\\
\frac{\partial \theta_x}{\partial x}\\
\frac{\partial \theta_x}{\partial y}\\
\frac{\partial \theta_x}{\partial y}+\frac{\partial \theta_y}{\partial x}\\
\frac{\partial \theta_x^*}{\partial x}\\
\frac{\partial \theta_y^*}{\partial y}\\
\frac{\partial \theta_x^*}{\partial y}+\frac{\partial \theta_y^*}{\partial x}\\
\varphi_x\\
\varphi_y\\
2u_o^*\\
2v_o^*\\
3\theta_x^*\\
3\theta_y^*
\end{bmatrix}
=\sum_{i=1}^{9}
\begin{bmatrix}
\frac{\partial N_i}{\partial x} & 0 & 0 & 0 & 0 & 0 & 0 & 0 & 0\\
0 & \frac{\partial N_i}{\partial y} & 0 & 0 & 0 & 0 & 0 & 0 & 0\\
\frac{\partial N_i}{\partial y} & \frac{\partial N_i}{\partial x} & 0 & 0 & 0 & 0 & 0 & 0 & 0\\
0 & 0 & 0 & 0 & 0 & \frac{\partial N_i}{\partial x} & 0 & 0 & 0\\
0 & 0 & 0 & 0 & 0 & 0 & \frac{\partial N_i}{\partial y} & 0 & 0\\
0 & 0 & 0 & 0 & 0 & \frac{\partial N_i}{\partial y} & \frac{\partial N_i}{\partial x} & 0 & 0\\
0 & 0 & 0 & \frac{\partial N_i}{\partial x} & 0 & 0 & 0 & 0 & 0\\
0 & 0 & 0 & 0 & \frac{\partial N_i}{\partial y} & 0 & 0 & 0 & 0\\
0 & 0 & 0 & \frac{\partial N_i}{\partial y} & \frac{\partial N_i}{\partial x} & 0 & 0 & 0 & 0\\
0 & 0 & 0 & 0 & 0 & 0 & 0 & \frac{\partial N_i}{\partial x} & 0\\
0 & 0 & 0 & 0 & 0 & 0 & 0 & 0 & \frac{\partial N_i}{\partial y}\\
0 & 0 & 0 & 0 & 0 & 0 & 0 & \frac{\partial N_i}{\partial y} & \frac{\partial N_i}{\partial x}\\
0 & 0 & \frac{\partial N_i}{\partial x} & N_i & 0 & 0 & 0 & 0 & 0\\
0 & 0 & \frac{\partial N_i}{\partial y} & 0 & N_i & 0 & 0 & 0 & 0\\
0 & 0 & 0 & 0 & 0 & 2N_i & 0 & 0 & 0\\
0 & 0 & 0 & 0 & 0 & 0 & 2N_i & 0 & 0\\
0 & 0 & 0 & 0 & 0 & 0 & 0 & 3N_i & 0\\
0 & 0 & 0 & 0 & 0 & 0 & 0 & 0 & 3N_i
\end{bmatrix}
\begin{bmatrix}
u_o\\ v_o\\ w_o\\ \theta_x\\ \theta_y\\ u_o^*\\ v_o^*\\ \theta_x^*\\ \theta_y^*
\end{bmatrix}_i
\qquad \textbf{(3.44)}
$$

Equation (3.43) represents the strain-nodal displacement [***B***] matrix for seven degrees of freedom per node. The strain-nodal displacement [***B***] matrix of any point within an element for nine degrees of freedom per node is given in Equation (3.44). The interpolation (shape) functions (N_i) depend on the spatial coordinates and are known collectivity as the shape function matrices, where the strain-nodal displacement matrix [***B***] is generally composed of derivatives of the shape functions, as described by the equations above. Since the shape functions (N_i) are functions of the

local coordinates rather than Cartesian coordinates, a relationship needs to be established between the derivatives in the two coordinates systems.

Chain rule is used to relate between the Cartesian coordinate and the natural coordinate and this relation is expressed in matrix form as [**Hinton** and **Owen**, **1977**][38]:

$$\begin{bmatrix} \frac{\partial N_i}{\partial \xi} \\ \frac{\partial N_i}{\partial \eta} \end{bmatrix} = \begin{bmatrix} \frac{\partial x}{\partial \xi} & \frac{\partial y_i}{\partial \xi} \\ \frac{\partial x}{\partial \eta} & \frac{\partial y}{\partial \eta} \end{bmatrix} \begin{bmatrix} \frac{\partial N_i}{\partial x} \\ \frac{\partial N_i}{\partial y} \end{bmatrix} \qquad \textbf{(3.45)}$$

The second matrix in the equation above is named **[J]** (**Jacobian** matrix) and its elements can be obtained by differentiating the following equations:

$$x(\xi,\eta) = \sum_{i=1}^{9} N_i(\xi,\eta).x_i$$
$$y(\xi,\eta) = \sum_{i=1}^{9} N_i(\xi,\eta).y_i \qquad \textbf{(3.46)}$$

Hence, the **Jacobian** matrix can be expressed as:

$$\mathbf{[J]} = \begin{bmatrix} \sum_{i=1}^{9} \frac{\partial N_i}{\partial \xi} x_i & \sum_{i=1}^{9} \frac{\partial N_i}{\partial \xi} y_i \\ \sum_{i=1}^{9} \frac{\partial N_i}{\partial \eta} x_i & \sum_{i=1}^{9} \frac{\partial N_i}{\partial \eta} y_i \end{bmatrix} \qquad \textbf{(3.47)}$$

Then, the derivatives of the shape function with respect to Cartesian coordinates can be given as:

$$\begin{bmatrix} \frac{\partial N_i}{\partial x} \\ \frac{\partial N_i}{\partial y} \end{bmatrix} = [\,\mathbf{J}\,]^{-1} \begin{bmatrix} \frac{\partial N_i}{\partial \xi} \\ \frac{\partial N_i}{\partial \eta} \end{bmatrix} \qquad \textbf{(3.48)}$$

where $[\mathbf{J}]^{-1}$ is the inverse of **Jacobian** matrix given as:

$$[\mathbf{J}]^{-1} = \begin{bmatrix} \frac{\partial \xi}{\partial x} & \frac{\partial \eta}{\partial x} \\ \frac{\partial \xi}{\partial y} & \frac{\partial \eta}{\partial x} \end{bmatrix} = \frac{1}{\det \mathbf{J}} \begin{bmatrix} \frac{\partial y}{\partial \eta} & -\frac{\partial y}{\partial \xi} \\ -\frac{\partial x}{\partial \eta} & \frac{\partial x}{\partial \xi} \end{bmatrix} \qquad \textbf{(3.49)}$$

CHAPTER FOUR

Nonlinear Analysis of Plates

4.1 General

If the deflection of a plate is of the order of magnitude of its thickness but is still small relative to the other dimensions, the analysis of the problem should include the strain of the middle plane of the plate. Classical formulation of this problem leads to a set of nonlinear equations which are characterized by the coupling of the dependent variables describing the membrane and the bending behavior of the plate. These equations are difficult to solve [**Paik** and **Kim**, **1989**][(76)]. In many technical fields of aircraft construction, ship building, and instrument manufacturing, plates are finding use with large deflections. The plate has usually inherent initial curvature during the fabricating process. The analysis is more complicated than those for ideally flat plates. In order to obtain more reliable design and safety assessment of plate structures, it is essential to have knowledge for the elastic-plastic large deformation behavior up to the failure of the plate elements with initial imperfections.

Finite element method is one of the most powerful approaches to analyze nonlinear behavior of structures but in usual it requires enormous computational efforts which are generally caused by a large number of unknowns and also by complicated numerical integration, especially for obtaining the elastic-plastic stiffness matrix of the element.

This chapter will be divided into three parts. The first part deals with geometrical nonlinearity of a plate with (five, seven, and nine) degrees of freedom per node for the nine-node element. The second part concerns the material nonlinearity for isotropic and anisotropic plates by using **Tsai-Wu** criterion. Finally, the third part deals with the numerical solution of nonlinear equations.

4.2 Geometrical Nonlinearity

There are two existing sources of geometric nonlinearity; the first is connected with the strain-displacement equations. Even if the strains are small in the conventional sense, rotation of the element adds nonlinear terms to the strain-displacement equation. As will be seen in the derivation of the plate element, if these nonlinear rotational terms are omitted, the derivation becomes incapable of yielding the nonlinear stiffness matrix [**Elseifi**, **1998**][31].

The second source of nonlinearity exists with respect to the equilibrium equations. It is necessary to keep the deformed geometry in mind when writing the equilibrium equations. This in turn, causes these equations to become nonlinear. The following formulation will describe the geometrical nonlinearity of plate elements.

4.2.1 Green-Lagrangian strains

The components of the Green-Lagrangian strain vector are known in terms of local derivatives of the displacements for the plate element as [**Pica**, **et al.**, **1979**][87]:

$$[\varepsilon]=\begin{Bmatrix}\varepsilon_x\\ \varepsilon_y\\ \gamma_{xy}\\ \gamma_{xz}\\ \gamma_{yz}\end{Bmatrix}=\begin{Bmatrix}\frac{\partial u}{\partial x}+\frac{1}{2}[(\frac{\partial u}{\partial x})^2+(\frac{\partial v}{\partial x})^2+(\frac{\partial \hat{w}}{\partial x})^2]\\ \frac{\partial v}{\partial y}+\frac{1}{2}[(\frac{\partial u}{\partial y})^2+(\frac{\partial v}{\partial y})^2+(\frac{\partial \hat{w}}{\partial y})^2]\\ \frac{\partial u}{\partial y}+\frac{\partial v}{\partial x}+[\frac{\partial u}{\partial x}\frac{\partial u}{\partial y}+\frac{\partial v}{\partial x}\frac{\partial v}{\partial y}+\frac{\partial \hat{w}}{\partial x}\frac{\partial \hat{w}}{\partial y}]\\ \frac{\partial u}{\partial z}+\frac{\partial w}{\partial x}+[\frac{\partial u}{\partial x}\frac{\partial u}{\partial z}+\frac{\partial v}{\partial x}\frac{\partial v}{\partial z}+\frac{\partial \hat{w}}{\partial x}\frac{\partial \hat{w}}{\partial z}]\\ \frac{\partial v}{\partial z}+\frac{\partial w}{\partial y}+[\frac{\partial u}{\partial y}\frac{\partial u}{\partial z}+\frac{\partial v}{\partial y}\frac{\partial v}{\partial z}+\frac{\partial \hat{w}}{\partial y}\frac{\partial \hat{w}}{\partial z}]\end{Bmatrix}-\begin{Bmatrix}\frac{1}{2}(\frac{\partial w_o}{\partial x})^2\\ \frac{1}{2}(\frac{\partial w_o}{\partial y})^2\\ \frac{\partial w_o}{\partial x}\frac{\partial w_o}{\partial y}\\ \frac{\partial w_o}{\partial x}\frac{\partial w_o}{\partial z}\\ \frac{\partial w_o}{\partial y}\frac{\partial w_o}{\partial z}\end{Bmatrix} \qquad \textbf{(4.1)}$$

where

$\hat{w}=(w+w_o)$

w: net deflection of plate.

w_o: initial deflection of plate.

4.2.2 Von-Karman assumptions

The von-Karman assumptions for large deflection of plates take the following form when used with a plate element [**Zienkiewicz**,**2000**][(124)].

1- The thickness is smaller than the length of the plate (this hypothesis is not restrictive since otherwise the displacements are not large).
2- The magnitude of the deflection (***w***) is of the order of thickness ***h***. Also ***w***=***w***(***x***,***y***) not a function of ***z***.
3- A Lagrange (fixed) coordinate system is used. This formulation is valid provided that the slopes should be $\frac{\partial w}{\partial x}, \frac{\partial w}{\partial y} << 1.0$.
4- The tangential displacements, ***u*** and ***v*** are small. Only nonlinear terms, which depend on $\frac{\partial w}{\partial x}$ and $\frac{\partial w}{\partial y}$ are to be retained in the strain-displacement relations.
5- All strain components are small.
6- The residual stresses resulting from the restraining effect of the welded edges after buckling are neglected.

Putting on the assumptions above, the Green-Lagrange strain vector Equation (4.1) for plate elements can be written as:

$$[\varepsilon]=\begin{Bmatrix} \frac{\partial u}{\partial x} \\ \frac{\partial v}{\partial y} \\ \frac{\partial u}{\partial y}+\frac{\partial v}{\partial x} \\ \frac{\partial u}{\partial z}+\frac{\partial w}{\partial x} \\ \frac{\partial v}{\partial z}+\frac{\partial w}{\partial y} \end{Bmatrix}+\begin{Bmatrix} \frac{1}{2}(\frac{\partial \hat{w}}{\partial x})^2 \\ \frac{1}{2}(\frac{\partial \hat{w}}{\partial y})^2 \\ \frac{\partial \hat{w}}{\partial x}\frac{\partial \hat{w}}{\partial y} \\ 0 \\ 0 \end{Bmatrix}-\begin{Bmatrix} \frac{1}{2}(\frac{\partial w_o}{\partial x})^2 \\ \frac{1}{2}(\frac{\partial w_o}{\partial y})^2 \\ (\frac{\partial w_o}{\partial x}\frac{\partial w_o}{\partial y}) \\ 0 \\ 0 \end{Bmatrix} \qquad \textbf{(4.2)}$$

Equation (4.2) displays the relation of strains with the displacements and also shows the relation of strains with the initial imperfection. Equation (4.2) is rewritten in another form to be remembered $\hat{w} = w + w_o$:

$$[\varepsilon]=\begin{Bmatrix} \frac{\partial u}{\partial x} \\ \frac{\partial v}{\partial y} \\ \frac{\partial u}{\partial y}+\frac{\partial v}{\partial x} \\ \frac{\partial u}{\partial z}+\frac{\partial w}{\partial x} \\ \frac{\partial v}{\partial z}+\frac{\partial w}{\partial y} \end{Bmatrix}+\begin{Bmatrix} \frac{1}{2}(\frac{\partial w}{\partial x})^2 \\ \frac{1}{2}(\frac{\partial w}{\partial y})^2 \\ \frac{\partial w}{\partial x}\frac{\partial w}{\partial y} \\ 0 \\ 0 \end{Bmatrix}+\begin{Bmatrix} \frac{\partial w}{\partial x}\frac{\partial w_o}{\partial x} \\ \frac{\partial w}{\partial y}\frac{\partial w_o}{\partial y} \\ \frac{\partial w_o}{\partial x}\frac{\partial w}{\partial y}+\frac{\partial w}{\partial x}\frac{\partial w_o}{\partial y} \\ 0 \\ 0 \end{Bmatrix} \quad \textbf{(4.3)}$$

Then, rewriting Equation (4.3) in a symbolic form as follows:

$$[\varepsilon]=\begin{Bmatrix} \varepsilon_x \\ \varepsilon_y \\ \gamma_{xy} \\ \gamma_{xz} \\ \gamma_{yz} \end{Bmatrix}=\begin{Bmatrix} \varepsilon_o^p \\ 0 \end{Bmatrix}+\begin{Bmatrix} z\varepsilon_o^b \\ \varepsilon_o^s \end{Bmatrix}+\begin{Bmatrix} \varepsilon_L^P \\ 0 \end{Bmatrix}+\begin{Bmatrix} \varepsilon_I^p \\ 0 \end{Bmatrix} \quad \textbf{(4.4)}$$

where the linear mid-plane strains are:

$$[\varepsilon_o^p]=\begin{Bmatrix} \frac{\partial u}{\partial x} \\ \frac{\partial v}{\partial y} \\ \frac{\partial u}{\partial y}+\frac{\partial v}{\partial x} \end{Bmatrix} \quad \textbf{(4.5)}$$

Equation (4.5) represents the in-plane strain. Also:

$$[\varepsilon_o^b]=\begin{Bmatrix} \frac{\partial \theta_x}{\partial x} \\ \frac{\partial \theta_y}{\partial y} \\ \frac{\partial \theta_x}{\partial y}+\frac{\partial \theta_y}{\partial x} \end{Bmatrix} \quad \textbf{(4.6)}$$

Equation (4.6) represents the bending strain. Also:

$$[\varepsilon_o^s]=\begin{Bmatrix} \varphi_x \\ \varphi y \end{Bmatrix} \quad \textbf{(4.7)}$$

Equation (4.7) represents the shear strain. Moreover:

$$[\varepsilon_L^p]=\begin{Bmatrix} \frac{1}{2}\left(\frac{\partial w}{\partial x}\right)^2 \\ \frac{1}{2}\left(\frac{\partial w}{\partial y}\right)^2 \\ \frac{\partial w}{\partial x}\frac{\partial w}{\partial y} \end{Bmatrix} \quad \textbf{(4.8)}$$

Equation (4.8) represents the nonlinear component of in-plane strain. Finally:

$$\left[\varepsilon_I^p\right]=\begin{Bmatrix} \dfrac{\partial w}{\partial x}\dfrac{\partial w_o}{\partial x} \\ \dfrac{\partial w}{\partial y}\dfrac{\partial w_o}{\partial y} \\ \dfrac{\partial w}{\partial x}\dfrac{\partial w_o}{\partial y}+\dfrac{\partial w_o}{\partial x}\dfrac{\partial w}{\partial y} \end{Bmatrix} \qquad \textbf{(4.9)}$$

Equation (4.9) represents the initial strain due to initial deflection. The vector components of Equation (4.4) represent the generalized strains. It can be noted that the vector ($\varepsilon_p^o+\varepsilon_L^p+\varepsilon_L^p$) reproduce the Marguerre strain expression for plate.

4.3 Variational Equation of Equilibrium

The total potential energy Π of a deformed plate with initial deflection of the order of magnitude of the thickness and with additional bending deflection of the same order, is defined as

$$\Pi = U - W \qquad \textbf{(4.10)}$$

where U is the potential energy of deformation (strain energy) and W is the potential energy of the external loading.

The state of equilibrium of a deformed plate can be characterized as that for which the first variation of the total potential energy of the system is equal to zero.

$$d\Pi = dU - dW = 0 \qquad \textbf{(4.11)}$$

or

$$dU = dW \qquad \textbf{(4.12)}$$

The components of the Piola-Kirchhoff stress vector are given by the same relations used for small displacements which are defined in Chapter Three, as follows:

$$[F]=\begin{Bmatrix} N_x \\ N_y \\ N_{xy} \\ M_x \\ M_y \\ M_{xy} \end{Bmatrix}=[D][\varepsilon] \qquad \textbf{(4.13)}$$

Thus,

$$dU = \int_V d\bar{\varepsilon}^T \sigma \, dV = \int_A \int_{-\frac{h}{2}}^{\frac{h}{2}} (d\varepsilon_x \sigma_x + d\varepsilon_y \sigma_y + d\gamma_{xy}\tau_{xy} + d\gamma_{xz}\tau_{xz} + d\gamma_{yz}\tau_{yz})\, dz\, dA \qquad \textbf{(4.14)}$$

Substituting the strain expression from Equation (4.4) into Equation (4.14) and integrating over the thickness allows ***dU*** to be rewritten only as an area integral giving,

$$dU = \int_A d\bar{\varepsilon}^T \sigma \; dA \qquad \textbf{(4.15)}$$

in which the stress resultants vector are defined in chapter three, and as shown in Figure (4.1), where in-plane stress resultants are,

$$\left[N_x, N_y, N_{xy}\right]^T = \left[\int_{-h/2}^{h/2} \left(\sigma_x, \sigma_y, \tau_{xy}\right) dz\right]^T \qquad \textbf{(4.16)}$$

and bending stress resultants are:

$$\left[M_x, M_y, M_{xy}\right]^T = \left[\int_{-h/2}^{h/2} \left(\sigma_x, \sigma_y, \tau_{xy}\right) z\, dz\right]^T \qquad \textbf{(4.17)}$$

The transverse shear resultants are:

$$\left[Q_x, Q_y\right]^T = \left[\int_{-h/2}^{h/2} \left(\tau_{xz}, \tau_{yz}\right) dz\right]^T \qquad \textbf{(4.18)}$$

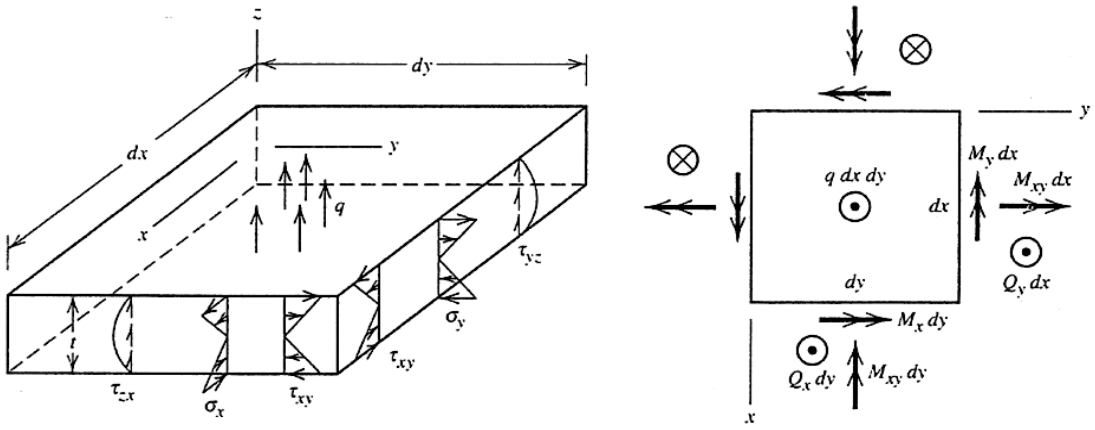

Figure (4.1): Differential element of a plate, (**a**) Stresses on cross sections and distributed lateral load $q=q(x,y)$, (**b**) Differential forces and moments. Arrows that represent forces normal to the plate mid-surface are viewed end-on.[**Cook,1995**][26]

The variation in the potential energy of the external load is:

$$dW = \int_V \rho\, du^T q\, dV + \int_A du^T P_t\, da \qquad \textbf{(4.19)}$$

where V is the undeformed volume, du is the virtual displacements, ρ is the mass density, q is the body forces per unit mass and P_t is the surface tractions acting over an undeformed area A.

The variation of strain $d\varepsilon$ due to the virtual displacements du, generally $d\varepsilon$ is given as the sum of the variation of the linear and nonlinear generalized strains as:

$$d\bar{\varepsilon} = d\varepsilon_o + d\varepsilon_L \qquad \textbf{(4.20)}$$

Since ε_o is a linear function of displacement,

$$d\varepsilon_o = [B_o]du \qquad \textbf{(4.21)}$$

Also,

$$d\varepsilon_L = [B_L]du \qquad \textbf{(4.22)}$$

Thus, the total strain-nodal displacement matrix for total strains is:

$$[\bar{B}] = [B_o] + [B_L] \qquad \textbf{(4.23)}$$

in which $[B_o]$ is the same matrix as in the linear strain analysis such as derived in Chapter 3, and only $[B_L]$ depends on the displacements.

$$[B_o] = \begin{bmatrix} B_o^p & 0 \\ 0 & B_o^b \end{bmatrix},\ [B_L] = \begin{bmatrix} 0 & B_L^b \\ 0 & 0 \end{bmatrix} \qquad \textbf{(4.24)}$$

where $[B_L]$ can be found by taking the variation of the nonlinear strain components $\{\varepsilon_L^p\}$ with respect to the displacements. This nonlinear strain components of Equation (4.3) can be written in a more convenient form as:

$$[\varepsilon_L^p] = \begin{Bmatrix} \frac{1}{2}\left(\frac{\partial w}{\partial x}\right)^2 \\ \frac{1}{2}\left(\frac{\partial w}{\partial y}\right)^2 \\ \left(\frac{\partial w}{\partial x}\right)\left(\frac{\partial w}{\partial y}\right) \end{Bmatrix} = \frac{1}{2}\begin{bmatrix} \frac{\partial w}{\partial x} & 0 \\ 0 & \frac{\partial w}{\partial y} \\ \frac{\partial w}{\partial y} & \frac{\partial w}{\partial x} \end{bmatrix} \begin{Bmatrix} \frac{\partial w}{\partial x} \\ \frac{\partial w}{\partial y} \end{Bmatrix} = \frac{1}{2}[A_\theta]\{\theta\} \qquad \textbf{(4.25)}$$

where the displacement gradients with respect to the lateral displacements (w) are:

$$\{\theta\} = \begin{bmatrix} \frac{\partial w}{\partial x} \\ \frac{\partial w}{\partial y} \end{bmatrix} \quad \textbf{(4.26)}$$

Then, the variation of the nonlinear component of the in-plane strain is obtained from Equation (4.25) in terms of the virtual gradients $d\theta$ as:

$$d\varepsilon_L^p = A_\theta \, d\theta \quad \textbf{(4.27)}$$

where

$$A_\theta = \begin{bmatrix} \frac{\partial w}{\partial x} & 0 \\ 0 & \frac{\partial w}{\partial y} \\ \frac{\partial w}{\partial y} & \frac{\partial w}{\partial x} \end{bmatrix} \quad \textbf{(4.28)}$$

in which, A_θ represents the gradients of total displacements and,

$$d\theta = d\begin{bmatrix} \frac{\partial w}{\partial x} \\ \frac{\partial w}{\partial y} \end{bmatrix} \quad \textbf{(4.29)}$$

represents the gradients of incremental displacements.

The displacement gradients (θ) of Equation (4.26) may now be written in terms of the nodal displacements ($\boldsymbol{u}$) and Cartesian derivatives of the shape functions as:

$$\{\theta\} = [G]\{u\} \quad \textbf{(4.30)}$$

where

$$[G] = [G_1 \quad G_2 \quad ..... \quad G_n] \quad \textbf{(4.31)}$$

and,

$$G_i = \begin{bmatrix} 0 & 0 & \frac{\partial N_i}{\partial x} & 0 & 0 \\ 0 & 0 & \frac{\partial N_i}{\partial y} & 0 & 0 \end{bmatrix} \quad \textbf{(4.32)}$$

The above equation represents the gradient for five degrees of freedom per node. Taking the variation of Equation (4.25) as follows:

$$d\left\{\varepsilon_L^p\right\} = \frac{1}{2} d[A_\theta]\{\theta\} + \frac{1}{2}[A_\theta] d\{\theta\} = [A_\theta] d\{\theta\} = [A_\theta][G] d\{u\} \quad \textbf{(4.33)}$$

hence immediately, by definition

$$\left[B_L^b\right]_o = [A_\theta][G] \quad \textbf{(4.34)}$$

In order to incorporate the imperfections in the formulation, the strain due to imperfections as given in Equation (4.9), thus can be written the imperfection strain components as follows:

$$\left\{\varepsilon_p^I\right\}=\frac{1}{2}\begin{bmatrix} 2\dfrac{\partial w_o}{\partial x} & 0 \\ 0 & 2\dfrac{\partial w_o}{\partial y} \\ 2\dfrac{\partial w_o}{\partial y} & 2\dfrac{\partial w_o}{\partial x} \end{bmatrix}\begin{Bmatrix} \dfrac{\partial w}{\partial x} \\ \dfrac{\partial w}{\partial y} \end{Bmatrix}=\frac{1}{2}[A_1]\{\theta\} \qquad \textbf{(4.35)}$$

Following the same analysis as for the nonlinear strains, the combination of the effects of the two strains into one $[B_L^b]$ is defined as:

$$[B_L^b]=[A_2][G] \qquad \textbf{(4.36)}$$

where

$$[A_2]=[A_\theta]+[A_1]$$

$$[A_2]=\begin{bmatrix} \dfrac{\partial w}{\partial x}+2\dfrac{\partial w_o}{\partial x} & 0 \\ 0 & \dfrac{\partial w}{\partial y}+2\dfrac{\partial w_o}{\partial y} \\ \dfrac{\partial w}{\partial y}+2\dfrac{\partial w_o}{\partial y} & \dfrac{\partial w}{\partial x}+2\dfrac{\partial w_o}{\partial x} \end{bmatrix} \qquad \textbf{(4.37)}$$

In the present study, the imperfection is assumed to be of sinusoidal function over the plate as:

$$w_o(x,y)=w_o\sin\left(\frac{n\pi x}{L_x}\right)\sin\left(\frac{n\pi y}{L_y}\right) \qquad \textbf{(4.38)}$$

where L_x, and L_y are the dimensions of the plate in the x, and y-direction, respectively. w_o is the maximum value of the initial imperfection at the plate center.

The variation in the potential energy of deformation for a plate element with large deflection can be written as:

$$dU=\int_V\left[\overline{B}\right]^T\sigma\,dV \qquad \textbf{(4.39)}$$

Substituting Equations (4.39) and (4.19) into Equation (4.11) can give the equilibrium equations written as:

$$\Psi(u)=\int_V\left[\overline{B}\right]^T\overline{\sigma}\,dV-dW=0 \qquad \textbf{(4.40)}$$

where Ψ represents the sum of external and internal generalized forces.

Clearly, the solution of Equation (4.40) will have to be approached iteratively. In order to use an incremental solution procedure, the relation between du and $d\Psi$ must be found. Thus, taking appropriate variation of Equation (4.40) with respect to du:

$$\frac{d\Psi}{du} = \int_V \frac{d\left[\bar{B}\right]^T}{du} \bar{\sigma}\, dV + \int_V \left[\bar{B}\right]^T \frac{d\bar{\sigma}}{du} dV \qquad \textbf{(4.41)}$$

where the variation of the external load with respect to displacements is equal to zero, and thus Equation (4.41) can be written at another form:

$$\frac{d\Psi}{du} = \int_V \frac{d\left[B_L\right]^T}{du} \bar{\sigma}\, dV + \left[\bar{K}\right] \qquad \textbf{(4.42)}$$

where

$$\left[\bar{K}\right] = \int_A \left[\bar{B}\right]^T [D]\left[\bar{B}\right] dA = \left[K_o\right] + \left[K_L\right] \qquad \textbf{(4.43)}$$

The first term of Equation (4.42) can be written as:

$$\int_V \frac{d\left[B_L\right]^T}{du} \bar{\sigma}\, dV = \left[K_\sigma\right] \qquad \textbf{(4.44)}$$

where $\left[K_\sigma\right]$ is a symmetric matrix dependent on the stress level. This matrix is known as initial stress matrix or geometric matrix. Thus,

$$d\Psi = \left(\left[K_o\right] + \left[K_L\right] + \left[K_\sigma\right]\right) du = \left[K_T\right] du \qquad \textbf{(4.45)}$$

with $\left[K_T\right]$ being the total, or tangent stiffness matrix.

4.4 Tangent Stiffness Matrix

The tangent stiffness matrix can be written as:

$$\left[K_T\right] = \left[K_o\right] + \left[K_L\right] + \left[K_\sigma\right] \qquad \textbf{(4.46)}$$

where $\left[K_o\right]$ is the constant linear elastic stiffness matrix and can be written as:

$$\left[K_o\right] = \int_A \left[B_o\right]^T [D]\left[B_o\right] dA \qquad \textbf{(4.47)}$$

$\left[K_L\right]$ is the initial or large displacement matrix which is quadratically dependent upon displacement $\boldsymbol{u}$, and can be written as:

$$\left[K_L\right] = \int_A \left[B_o\right]^T [D]\left[B_L\right] dA + \int_A \left[B_L\right]^T [D]\left[B_L\right] dA + \int_A \left[B_L\right]^T [D]\left[B_o\right] dA \qquad \textbf{(4.48)}$$

Finally $[K_\sigma]$ is the initial stress stiffness matrix which has to be found by using the definition of Equation (4.44). By taking the variation of Equation (4.23) then:

$$d[B_L]^T = \begin{bmatrix} 0 & 0 \\ d[B_L^b]^T & 0 \end{bmatrix} \tag{4.49}$$

This on substitution into Equations (4.44) and (4.37) gives:

$$[K_\sigma] = \int_A \begin{bmatrix} 0 & 0 \\ [G]^T d[A]^T & 0 \end{bmatrix} \begin{Bmatrix} N_x \\ N_y \\ N_{xy} \\ M_x \\ M_y \\ M_{xy} \end{Bmatrix} \tag{4.50}$$

However, using the mathematical properties of the matrix **[*A*]**, this matrix can be written as:

$$d[A]^T \begin{Bmatrix} N_x \\ N_y \\ N_{xy} \end{Bmatrix} = \begin{bmatrix} N_x & N_{xy} \\ N_{xy} & N_y \end{bmatrix} [G] da \tag{4.51}$$

and finally one can obtain

$$[K_\sigma] = \begin{bmatrix} 0 & 0 \\ 0 & [K_\sigma^b] \end{bmatrix} \tag{4.52}$$

Thus,

$$[K_\sigma] = \int_A [G]^T \begin{bmatrix} N_x & N_{xy} \\ N_{xy} & N_y \end{bmatrix} [G] da \tag{4.53}$$

It is recalled that the stresses resultants are defined in terms of the element strains and thus in terms of the element displacements and shape functions through Chapter Three.

4.5 Applied Load

For plate bending applications two forms of loading will be considered. Firstly, a uniformly distributed load acting normal to the plate (in ***z***-direction) may be applied. Secondly is a distributed loading per unit length in a normal and tangent direction, as shown in Figure (4.2). These distributed forces need not be constant but can vary (independently) along the element edge. Since the parabolic isoparametric elements are being employed the variation will be defined by prescribing the normal and

tangential values at the three nodal points forming the element edge to which the loads are applied. A pressure normal to a face is assumed to be positive if it acts in a direction towards the element. A tangential load is assumed to be positive if it acts in an counter-clockwise direction with respect to the loaded element. It is supposed that the three nodal values of normal and tangential distributed loads are $(p_n)_i$ and $(p_t)_i$ respectively, where i ranges from 1 to 3. The distributed loading intensity at any point along the loaded edge is given by[**Hinton** and **Owen**, **1977**][38]:

$$\begin{bmatrix} p_n \\ p_t \end{bmatrix} = \sum_{i=1}^{3} N_i \begin{bmatrix} (p_n)_i \\ (p_t)_i \end{bmatrix} \qquad \textbf{(4.54)}$$

The components of force acting in the x and y-directions respectively are:

$$\begin{aligned} dP_x &= \left(p_t ds \cos(\alpha) - p_n ds \sin(\alpha)\right) = \left(p_t dx - p_n dy\right) \\ dP_y &= \left(p_t ds \sin(\alpha) + p_n ds \cos(\alpha)\right) = \left(p_t dy + p_n dx\right) \end{aligned} \qquad \textbf{(4.55)}$$

To perform the integration along the element edge in terms of the curvilinear variable ξ, dx and dy are given by:

$$dx = \frac{\partial x}{\partial \xi} d\xi; \quad dy = \frac{\partial y}{\partial \xi} d\xi \qquad \textbf{(4.56)}$$

Using these in Equation (4.55) yields:

$$\begin{aligned} dP_x &= \left(p_t \frac{\partial x}{\partial \xi} - p_n \frac{\partial y}{\partial \xi} \right) d\xi \\ dP_y &= \left(p_t \frac{\partial y}{\partial \xi} + p_n \frac{\partial x}{\partial \xi} \right) d\xi \end{aligned} \qquad \textbf{(4.57)}$$

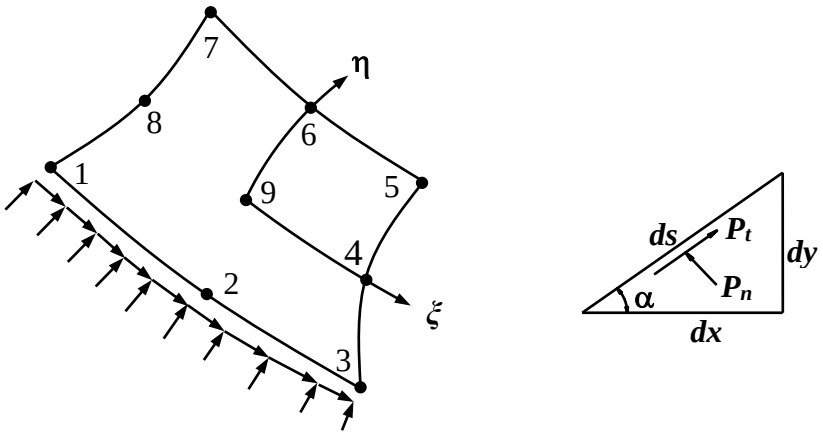

Figure (4.2): Normal and tangential loads/unit length applied to a parabolic isoparametric element [**Hinton** and **Owen**, **1977**][38]

Then by applying the integration along the loaded element edge as:

$$P_{xi} = \int_s N_i \left(p_t \frac{\partial x}{\partial \xi} - p_n \frac{\partial y}{\partial \xi} \right) d\xi$$
$$P_{yi} = \int_s N_i \left(p_t \frac{\partial y}{\partial \xi} + p_n \frac{\partial x}{\partial \xi} \right) d\xi \qquad \textbf{(4.58)}$$

These expressions are performed for the loads applied on an element edge along ξ. When the element is loaded along η-edge the integration becomes with η **(**local coordinate**).**

A uniformly distributed load acting normal to the plate (in ***z*** direction) must be converted into equivalent nodal forces before equation solution takes place, as shown in Figure (4.3).

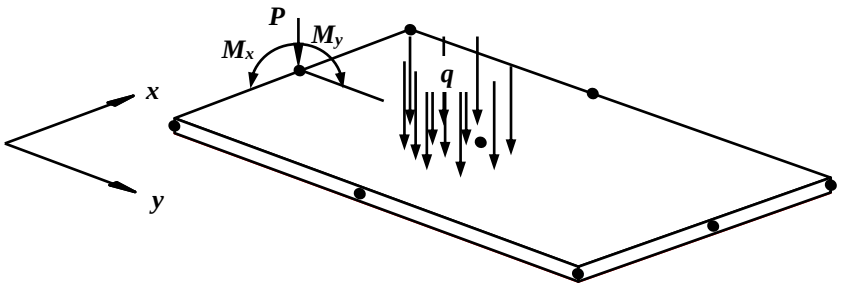

Figure (4.3): Generalized nodal forces for a plate bending element

This can readily be achieved by use of the general expression as:

$$F_i = \int_V [N]^T p\, dV = \begin{bmatrix} P \\ 0 \\ 0 \end{bmatrix} = \int_A N_i \begin{bmatrix} q \\ 0 \\ 0 \end{bmatrix} dA \qquad \textbf{(4.59)}$$

where ***q*** is the distributed load intensity and integration is taken over the element area.

4.6 Numerical Integration of Isoparametric Plate Element

It has become clear that, it is important to choose a suitable integration rule that is both accurate and computationally efficient because the numerical integration of plate elements affects the characteristic of the element efficiency.

The rules adopted in this study, and their advantages and disadvantages are briefly described as follows:

4.6.1 Full integration rule

The full integration rule consists of (m × m) Gauss points, where m is the number of nodes along each element side with proper number of nodes inside the element. This rule exhibits some disadvantages which appear in the quadrilateral plate and shell element applications. These disadvantages are in shear locking phenomenon which results in stiffening of the solution when the thickness is small compared with other dimensions. Such phenomenon takes place with applications of plate for different reasons. For shell it results from the inability of the full integrated shell element to undergo inextensional bending. This is more complicated than the same situation in plate, which is caused by the transverse shear energy. It does not diminish as desired when the plate becomes thin [**Baka**, **2002**][(13)].

4.6.2 Reduced integration rule

Reduced integration consists of (m-1) × (m-1) Gauss points. By using such integration rule, the solution accuracy for thin plates and shells may be significantly improved. On the other hand, the uniform application of reduced integration tends to diminish the rank of the stiffness matrix resulting in the occurrence of spurious mechanism in addition to the rigidity body modes.

4.6.3 Selective integration rule

In the selective integration technique, bending and membrane energies are integrated by using the full rule, while the shear terms are computed by using the reduced integration rule. The process involves the following two steps, which are particularized for the quadratic element:

1- The transverse shear strains (corresponding terms in the strain matrix [**B**]), are computed at the four Gauss points (I,II,III,IV) as shown in Figure (4.4) using (2 × 2) reduced integration rule.
2- The bending and membrane strains (corresponding terms in the strain matrix [**B**]) are computed at the nine Gauss points of the full (3 × 3) integration rule [**Baka**, **2002**][(13)].

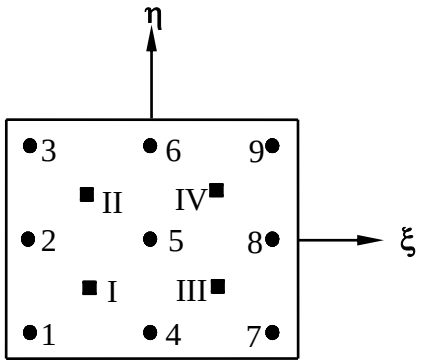

Figure (4.4): Four and nine-Gauss point position for selective integration

Thus, Equation (4.47) becomes by using the numerical integration as follows:

$$[K_o] = \int_A [B]^T [\mathrm{E}][B] dA = \int_{-1}^{1}\int_{-1}^{1} [B]^T [\mathrm{E}][B] |\mathrm{J}| d\xi d\eta \qquad \textbf{(4.60)}$$

In the present study the selective integration rule has been adopted to compute the integration of the matrices where (3×3) is used for bending and membrane energies and (2×2) for transverse shear energies.

4.7 Material Nonlinearity

Because of the wide use of thin-walled structures such as those used in bridges, cranes, and hoists, steel-building structures, ship structures, and airplane structures, it is very important in the designing process of these structures not only to determine the load-carrying capacity (the ultimate load), but also to analyze the structure's behavior up to collapse. It is very important to know in what way the structure fails, that means, either it happens rapidly without earlier signs of catastrophe (brittle structure) or it proceeds slowly with warning against catastrophe (ductile structure). It is obvious that the second character of failure is more desirable.

The determination of the failure stress of thin-walled structures under compressive loads is a topic, which has attracted considerable attention over the past hundred years. **Box [1883]** appears to be the first to propose a formula for the failure stress (σ_m) of a simply supported mild steel panel with uniform in-plane stress in one direction only. That is [**Murray**, **1989**][(72)]: -

$$\sigma_m = \frac{1236}{\sqrt{b/h}} \quad \text{MPa} \qquad \textbf{(4.61)}$$

where

b: is the width of the plate.

h: is the thickness of the plate.

Over the last 50 years there has been a proliferation of formulas which enable designers to estimate stresses but nearly all of these formulas to a lesser or greater extent are based on empirical rules. While it is obviously desirable for designers to have at their disposal simple rules such as Equation (4.61), the rules should be based upon sound theoretical concepts with a back-up of careful experiments. Failure of a mild steel panel is a complicated elastic-plastic process, which depends upon the geometry of the panel; its initial imperfections, the yield stress, and the boundary conditions (both in-plane and out-of-plane). It is self-evident that a simple formula such as Equation (4.61) cannot account for all these factors. An "exact" elastic-plastic analysis of a thin-walled structure up to and beyond (σ_m) is rather complex even with the aid of present day computing techniques.

There have so far been few attempts to follow the history of even a simple imperfect plate into the elastic-plastic range. Such analysis is expensive in computer time and it is unlikely that designers can use these techniques directly as design tools. Also, it is likely that design tables could not be produced to cover the whole range of problems likely to confront designers. This is introduced when material properties vary with the loading condition, i.e. the constitutive laws are a function of the current load so that the stress-strain relationship is nonlinear. Plate structures are fabricated from ductile materials or from composite materials whose behavior may be divided into elastic and plastic phases. It may also be assumed that the plastic strain does not grossly exceed the ultimate strain of the material.

Material nonlinearity does not require a formulation of the basic (governing) differential equations. The required elastic-plastic relationships between stresses and total strains may be derived from the

simple two dimensional relationships with the flow theory of plasticity being used to evaluate the plastic components of strains. To determine whether any given combination of stresses is sufficient to cause yield, it is necessary to define a yield criterion and elastic-plastic stress-strain relationships for isotropic and orthotropic materials.

4.7.1 Failure criteria for isotropic plate structure

A yield criterion must be able to define the onset of the plasticity under combination of stresses. The designer must assess the integrity of the structure with respect to strength for the determined state of stress. Most experimental determinations of the strength of a material are based on uniaxial stress states. However, the general practical problem involves biaxial, triaxial and other complex states of stress. The yield criterion established by **von-Mises** for plates of isotropic materials is given as follows:

$$f = \frac{1}{\sigma_o^{\,2}}\left(\sigma_x^{\,2} + \sigma_y^{\,2} - \sigma_x\sigma_y + 3\tau_{xy}^{\,2} + 3\tau_{xz}^{\,2} + 3\tau_{yz}^{\,2}\right) \leq 1.0 \qquad \textbf{(4.62)}$$

where σ_o is the uniaxial yield stress, σ_x and σ_y are the direct stress components in the ***x*** and ***y***-directions, τ_{xy} is the shear stress in ***xy***-plane, τ_{xz} is the transverse shear stress in ***xz***-section, and τ_{yz} is the transverse shear stress in ***yz***-section. Equation (4.62) neglects the normal stress σ_z.

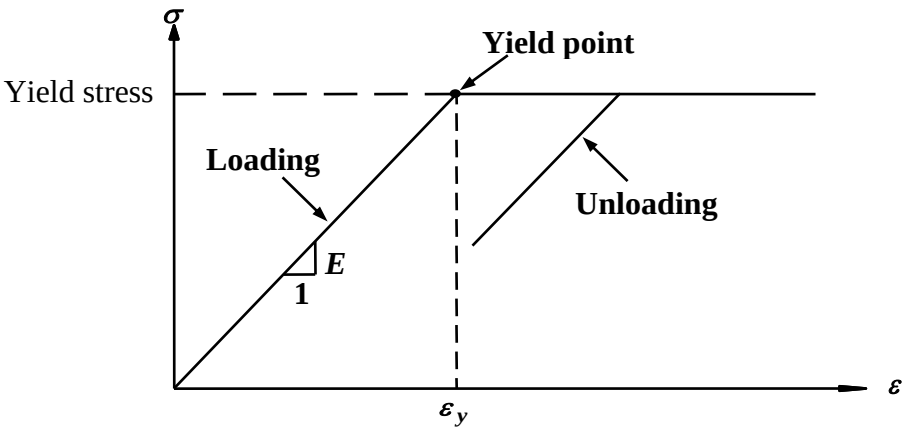

Figure (4.5): Idealizated stress-strain relationship of uniaxial loading behavior for isotropic plate

4.7.2 Failure criteria for laminated plate structure

The stresses in an individual lamina are fundamental to control the failure initiation and progression in the laminate. The strength of each individual lamina is assessed separately by considering the stresses acting on it along the material axes. The initial failure of a lamina is governed by exceeding the maximum limit prescribed by a failure criterion. The determination of failure load is very essential in understanding the failure process as well as the reliability and safety of structures. The ultimate load that makes the plate fail is calculated based on **Tsai-Wu** criterion for general composite materials and on **Hashin** criterion for fiber composite materials as follows [**Jones**, **1999**][50]:

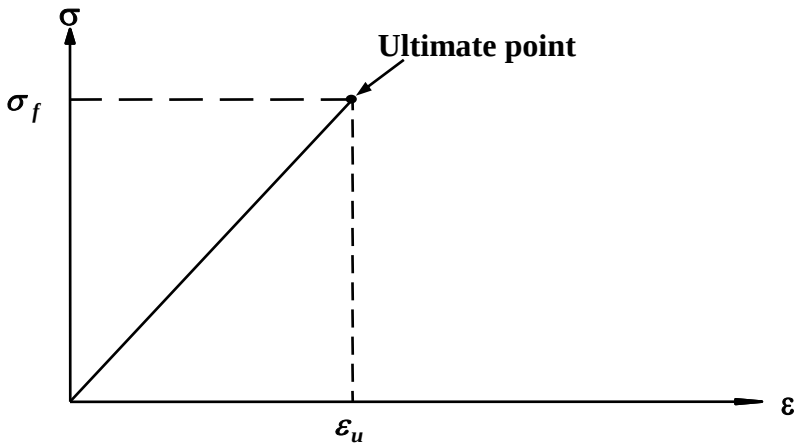

Figure (4.6): Idealizated stress-strain relationship of uniaxial loading behavior for orthrotropic plate[**Jones**, **1999**][50]

$$F_i\sigma_i + F_{ij}\sigma_i\sigma_j = 1; \qquad i,j = 1,.....6 \tag{4.63}$$

where F_i and F_{ij} are strength tensors of the second and fourth order respectively and the usual contracted tensor notation is used except that $\sigma_4 = \tau_{13}, \sigma_5 = \tau_{23}$, and $\sigma_6 = \tau_{12}$. Equation (4.63) is obviously very complicated thus it will restrict the above attention to the reduction of above equation for an orthotropic lamina under plane stress conditions:

$$\begin{aligned} &F_1\sigma_1 + F_2\sigma_2 + F_3\sigma_3 + F_{11}\sigma_1^2 + +F_{22}\sigma_2^2 + F_{33}\sigma_3^2 + F_{12}\sigma_1\sigma_2 \\ &+ F_{13}\sigma_1\sigma_3 + F_{23}\sigma_2\sigma_3 + F_{44}\sigma_4^2 + F_{55}\sigma_5^2 + F_{66}\sigma_6^2 = 1 \end{aligned} \tag{4.64}$$

The terms that are linear in the stresses are useful in representing different strengths in tension and in compression. The terms that are quadratic in the stresses are the more or less usual terms to represent an ellipsoid in stress space, where $F_3 = 0$ indicates that to the shear strength of a material in compression and in tension is similar, and $\sigma_3 = 0$ in ***z***-direction. Also, the shear strength of a material is equal in three dimensions and equal to ***S***. Thus, the terms of F_i is:

$$F_1 = \left(\frac{1}{X_t} - \frac{1}{X_c}\right), F_2 = \left(\frac{1}{Y_t} - \frac{1}{Y_c}\right), F_3 = \left(\frac{1}{Z_t} - \frac{1}{Z_c}\right)$$

$$F_{11} = \left(\frac{1}{X_t . X_c}\right), F_{22} = \left(\frac{1}{Y_t . Y_c}\right), F_{33} = \left(\frac{1}{Z_t . Z_c}\right)$$

$$F_{44} = \left(\frac{1}{R^2}\right), F_{55} = \left(\frac{1}{S^2}\right), F_{66} = \left(\frac{1}{T^2}\right) \qquad \textbf{(4.65)}$$

$$F_{12} = \frac{-1}{2}\left(\frac{1}{X_t . X_c . Y_t Y_c}\right)^{0.5}, F_{13} = \frac{-1}{2}\left(\frac{1}{X_t . X_c . Z_c . Z_t}\right)^{0.5}$$

$$F_{23} = \frac{-1}{2}\left(\frac{1}{Y_t . Y_c . Z_c . Z_t}\right)^{0.5}$$

$X_c, X_t =$ The axial or longitudinal strength in compression and tension.

$Y_c, Y_t =$ The transverse strength in compression and tension.

$Z_c, Z_t =$ The transverse strength in compression and tension.

$R, T, S =$ Shear strength of the material.

Equation (4.64) becomes as:

$$F_1\sigma_1 + F_2\sigma_2 + F_{11}\sigma_1^2 + + F_{22}\sigma_2^2 + F_{12}\sigma_1\sigma_2 + F_{44}\sigma_4^2 + F_{55}\sigma_5^2 + F_{66}\sigma_6^2 = 1 \qquad \textbf{(4.66)}$$

Equation (4.66) is suitable for the elastic-plastic analysis of anisotropic materials.

For matrix cracking failure, two different failure criteria are used depending on whether the transverse normal stress, σ_{22}, is in tension or in compression. The failure index, e_m^2, is defined in terms of transverse tensile strength, Y_t , transverse compressive strength, Y_c, and in-plane shear strength, ***R***, and is expressed as:

$$e_m^2 = \frac{\sigma_{22}}{Y_c}\left[\left(\frac{Y_c}{2R}\right)^2 - 1\right] + \left(\frac{\sigma_{22}}{2R}\right)^2 + \left(\frac{\tau_{12}}{R}\right)^2 \quad \text{for } \sigma_{22} < 0 \qquad \textbf{(4.67)}$$

and

$$e_m^2 = \left(\frac{\sigma_{22}}{Y_t}\right)^2 + \left(\frac{\tau_{12}}{R}\right)^2 \quad \text{for } \sigma_{22} > 0 \qquad \textbf{(4.68)}$$

where (e_m) is the failure index for matrix cracking. Matrix cracking is assumed to occur when the failure index (e_m) exceeds unity.

Fiber-matrix shear failure is assumed to be dependent on a combination of axial stress, σ_{11}, and shear stress, τ_{12}, and is expressed as follows:

$$e_s^2 = \left(\frac{\sigma_{11}}{X_t}\right)^2 + \left(\frac{\tau_{12}}{R}\right)^2 \quad \text{for } \sigma_{11} > 0 \text{ and } \left(\frac{\sigma_{11}}{X_t}\right)^2 < \left(\frac{\tau_{12}}{R}\right)^2 \qquad \textbf{(4.69)}$$

and,

$$e_s^2 = \left(\frac{\sigma_{11}}{X_c}\right)^2 + \left(\frac{\tau_{12}}{R}\right)^2 \quad \text{for } \sigma_{11} < 0 \text{ and } \left(\frac{\sigma_{11}}{X_t}\right)^2 < \left(\frac{\tau_{12}}{R}\right)^2 \qquad \textbf{(4.70)}$$

where (e_s) is the failure index for fiber-matrix shearing, X_t is the tensile strength along the fiber direction and X_c is the compressive strength along the fiber direction. Equations (4.69) and (4.70) predict that when the failure (e_s) exceeds unity, fiber-matrix shearing dominated failure occurs.

Fiber breakage failure occurs in tension due to the combination of axial stress and shear stress while the failure in compression is governed by buckling as expressed in terms of only axial stress. The criterion for breakage failure is expressed as follows:

$$e_f^2 = \left(\frac{\sigma_{11}}{X_t}\right)^2 + \left(\frac{\tau_{12}}{R}\right)^2 \quad \text{for } \sigma_{11} > 0 \qquad \textbf{(4.71)}$$

and,

$$e_f^2 = \left(\frac{\sigma_{11}}{X_c}\right)^{2^2} \quad \text{for } \sigma_{11} < 0 \qquad \textbf{(4.72)}$$

where (e_s) is the failure index for fiber breakage. The fiber breakage failure occurs when (e_s) exceeds unity.

4.8 Elastic-Plastic Stress-Strain Relationships

An ultimate strength analysis usually requires the nonlinear behavior of the material to be taken into consideration. The macroscopic behavior of the material can be described by a mathematical method (plasticity theory). The two major plasticity theories are the deformation theory and the flow theory. The deformation theory assumes a unique relation between total stresses and total strains.

In the flow theory the plastic deformations are "memorized" by integrating an equivalent plastic strain increment over the load history. It gives out an incremental relationship between stresses and strains. The mathematical model includes two major parts. The first part is that there exists a so-called loading function $f(\sigma)$ in stress space. This function is such that the state of the material is given by the volume of $f(\sigma)$ for structures composed of thin plates as in this study, the **Tsai-Wu** function may be used as the loading function. The other part of the flow theory is the flow rule, which gives the incremental stress-strain relation.

The flow theory is based on two major assumptions. The first is that elastic and plastic strain can be added. It is relevant here since the strains are small [**Mathlum**, **1997**][66].

$$\varepsilon_{ij} = \varepsilon_{ij}^{e} + \varepsilon_{ij}^{p} \qquad \textbf{(4.73)}$$

The elastic and plastic strains can therefore be treated separately. The plastic deformation is assumed to be incompressible: -

$$\varepsilon_{ii}^{p} = 0 \qquad \textbf{(4.74)}$$

The second assumption to be made is that the material is stable as defined by **Drucker** who considered an element initially in some state of stress to which by an external agency and additional set of stresses are slowly applied and slowly removed. In the cycle of application and removal of the added stresses, the work done by an external agency is non-negative. From the work of **Prandtl-Reuss**, the flow rule may be written as:

$$d\varepsilon_{ij}^{p} = d\lambda\sigma_{ij} \qquad \textbf{(4.75)}$$

where $d\varepsilon_{ij}^{p}$ is the plastic strain increment tensor, $d\lambda$ is a factor of proportionality, σ_{ij} is the deviatoric stress tensor.

The flow rule may be re-written as the associated flow rule:

$$d\varepsilon_{p} = d\lambda \frac{\partial f}{\partial \sigma_{ij}} \qquad \textbf{(4.76)}$$

For plastic flow to occur, a neutral loading condition must be maintained i.e.:

$$\frac{\partial f}{\partial \sigma_{ij}} - d\sigma_{ij} = 0 \qquad \textbf{(4.77)}$$

4.8.1 Strength of Composite Laminated Plate

A unidirectional fiber reinforced composite deforms as the load increases in the following four stages, more or less, depending on the relative brittleness or ductility of the fibers and matrix:

1- Both fibers and matrix deform elastically.
2- The fibers continue to deform elastically, but the matrix deforms plastically.
3- Both fibers and matrix deform plastically.
4- The fibers fracture followed by fracture of the composites.

Of course, for brittle fibers, stage (3) may not be realized. Similarly, a brittle matrix may not achieve either stage (2 or 3). Whether fracture of the composite occurs as a fiber failure or a matrix failure depends on the relative ductility of the fibers and the matrix.

Failure of the composite can then occur in two ways. First, the matrix shear stress around the fiber could exceed the allowable matrix shear stress. More precisely, the bond between the fiber and the matrix might be broken owing to high shear stress in the aforementioned mechanism for transfer of stress between broken fibers. Second, the fiber fracture could actually propagate across the matrix to other fibers and hence cause overall fracture of the composite. If a good bond is achieved between the fiber and the matrix and if the matrix fracture toughness is high, then the fiber fracture can continue until it causes gross composite fracture [**Jones**, **1999**][(50)].

The failure of one layer does not necessarily imply failure of the entire laminate; the laminate, in fact, can be capable of sustaining higher

loads despite a significant change in stiffness. An analogy to this phenomenon is the ability of an in-plane loaded plate to carry loads higher than the buckling load, but at an increase in the amount of the deformation per unit of load (a decreased stiffness), as shown in Figure (4.7).

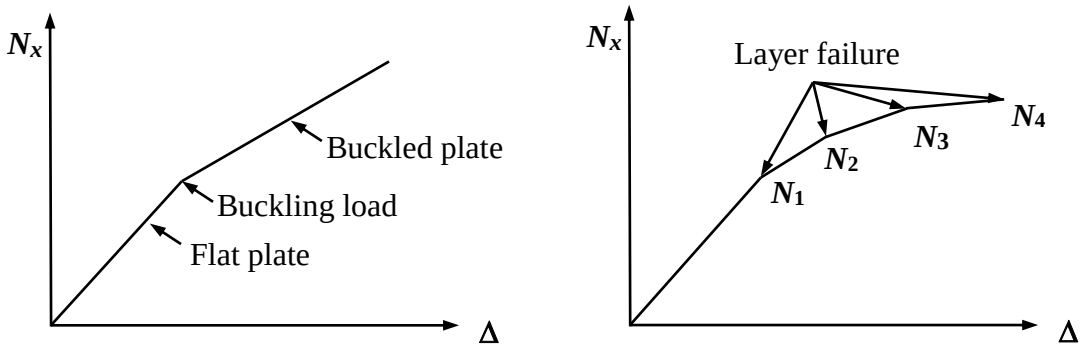

(a) Plate load-deformation behavior **(b)** Laminate load-deformation behavior

Figure (4.7): Analogy between buckled plate and laminate load-deformation behavior [**Jones, 1999**][(50)]

The overall procedure of the laminate strength analysis, showed at the same time yields the laminate load-deflection behavior. There, the load is taken to mean both forces and moments; similarly, deformations are meant to include both strains and curvatures. The analysis is composed of two different approaches that depend on whether any laminas have failed.

If no lamina has failed, the load must be determined at which the first lamina fails, that is, violates the failure criterion. In the process of this determination, the lamina stresses must be found as a function of the unknown magnitude of loads first in the laminate coordinates and then in the principal material directions. The properties of load parameter are increased until some lamina fails. That lamina is then eliminated, figuratively, from the laminate by assigning zero properties to the failed layer. Actually, because of the matrix manipulations involved in the analysis, the failed lamina properties must not be zero, but rather effectively zero values in order to avoid a singular matrix. The laminate strains are calculated from the known load and the stiffness prior to the failure of the lamina. If one or more laminas have failed, new laminate

extensional, coupling and bending stiffnesses are calculated, lamina stresses are recalculated to determine their distribution after a lamina has failed (the stresses will increase to maintain equilibrium). Then it must be verified that the remaining laminas, at their increased stress levels, do not fail at the same load that caused failure of the lamina in the preceding pass through the analysis. If no more lamina fails, then the load can be increased until another lamina fails and the cycle is repeated. In each cycle, the raised stresses caused by failure of a lamina must be verified not to cause a progressive failure that is where the laminas all successively fail at the same load. When such a progressive failure occurs, the laminate has suffered gross failure.

4.8.2 Yield Criterion Formulation

The present the elastic-plastic formulation is based on **von-Mises** criterion. The second part will introduce the formulation based on **Tsai-Wu** and **Hashin**[37] criteria.

4.8.2.1 Elastic-plastic formulation based on von-Mises criterion

The total strain increment $d\varepsilon$ is the sum of the elastic and plastic components:

$$d\varepsilon = d\varepsilon_e + d\varepsilon_p \qquad \textbf{(4.78)}$$

where $d\varepsilon_e$ is the elastic strain increment and $d\varepsilon_p$ is the plastic strain increment. The plastic strain increment is given by the flow rule, as mentioned in Equation (4.76):

$$d\varepsilon_p = d\lambda \frac{\partial f}{\partial \sigma} \qquad \textbf{(4.79)}$$

where $d\lambda$ is a non-negative scalar. For an associated flow, the potential f is taken as identical to a yield function $f(\sigma)$. The function $f(\sigma)$ may be defined in a similar manner to Equation (4.62), so that:

$$\bar{\sigma}^2 = \frac{1}{2}\left((\sigma_x - \sigma_y)^2 + \sigma_y^2 + \sigma_x^2 + 6(\tau_{xy}^2 + \tau_{xz}^2 + \tau_{yz}^2)\right) \qquad \textbf{(4.80)}$$

The effective stress ($\bar{\sigma}$) may be expressed in terms of principal stresses ($\sigma_1, \sigma_2, \sigma_3$) as:

$$\bar{\sigma}^2 = \frac{1}{2}\left((\sigma_1 - \sigma_2)^2 + (\sigma_2 - \sigma_3)^2 + (\sigma_3 - \sigma_1)^2\right) \quad \textbf{(4.81)}$$

where the subscripts **1**, **2**, **3** refer to the directions of the three principal axes. The differential form of the **von-Mises** law can be written as:

$$d\bar{\sigma} = \{Q\}^T \{d\sigma\} \quad \textbf{(4.82)}$$

where

$$\{Q\} = \frac{3}{\bar{\sigma}}\left[\frac{\sigma'_x}{2}, \frac{\sigma'_y}{2}, \tau'_{xy}, \tau'_{xz}, \tau'_{yz}\right] \quad \textbf{(4.83)}$$

$$\{d\sigma\} = \left[d\sigma_x, d\sigma_y, d\tau_{xy}, d\tau_{xz}, d\tau_{yz}\right] \quad \textbf{(4.84)}$$

in which,

$$\begin{aligned} \sigma'_x &= \sigma_x - \sigma_a \\ \sigma'_y &= \sigma_y - \sigma_a \\ \tau'_{xy} &= \tau_{xy} \\ \tau'_{xz} &= \tau_{xz} \\ \tau'_{yz} &= \tau_{yz} \end{aligned} \quad \textbf{(4.85)}$$

$$\sigma_a = \frac{\sigma_x + \sigma_y}{3} \qquad \text{(Mean or hydrostatic stress)}$$

According to **von-Mises**' theory, the effective plastic strain increment $d\bar{\varepsilon}_p$ is defined as a combination of the separate plastic strain increments as [**Alwash**, **1989**][9]:

$$d\bar{\varepsilon}_p = \frac{\sqrt{2}}{3}[(d\varepsilon_{xp} - d\varepsilon_{yp})^2 + d\varepsilon_{yp}^2 + d\varepsilon_{xp}^2 + \frac{3}{2}d\gamma_{xyp}^2 + \frac{3}{2}d\gamma_{xzp}^2 + \frac{3}{2}d\gamma_{yzp}^2]^{(1/2)} \quad \textbf{(4.86)}$$

and in terms of principal plastic strain increments ($d\varepsilon_{p1}, d\varepsilon_{p2}, d\varepsilon_{p3}$)

$$d\bar{\varepsilon}_p = \frac{\sqrt{2}}{3}[(d\varepsilon_{p1} - d\varepsilon_{p2})^2 + (d\varepsilon_{p2} - d\varepsilon_{p3})^2 + (d\varepsilon_{p3} - d\varepsilon_{p1})^2]^{(1/2)} \quad \textbf{(4.87)}$$

The mathematical form of flow rule (**Prandtle-Reuss** relation) is:

$$\frac{d\varepsilon_{xp}}{\sigma'_x} = \frac{d\varepsilon_{yp}}{\sigma'_y} = \frac{d\gamma_{xyp}}{2\tau'_{xy}} = \frac{d\gamma_{xzp}}{2\tau'_{xz}} = \frac{d\gamma_{yzp}}{2\tau'_{yz}} = d\lambda \quad \textbf{(4.88)}$$

Then, from Equation (4.88) considering principal stress directions,

$$\frac{d\varepsilon_{p1} - d\varepsilon_{p2}}{\sigma_1 - \sigma_2} = \frac{d\varepsilon_{p2} - d\varepsilon_{p3}}{\sigma_2 - \sigma_3} = \frac{d\varepsilon_{p3} - d\varepsilon_{p1}}{\sigma_3 - \sigma_1} = d\lambda \quad \textbf{(4.89)}$$

or in other from,

$$d\lambda\sqrt{(\sigma_1-\sigma_2)^2+(\sigma_2-\sigma_3)^2+(\sigma_3-\sigma_1)^2}=\sqrt{(d\varepsilon_{p1}-d\varepsilon_{p2})^2+(d\varepsilon_{p2}-d\varepsilon_{p3})^2+(d\varepsilon_{p3}-d\varepsilon_{p1})^2} \quad \textbf{(4.90)}$$

Hence, one gets:

$$d\lambda=\frac{3}{2}\frac{d\bar{\varepsilon}_p}{\bar{\sigma}} \quad \textbf{(4.91)}$$

By substituting from Equation (4.91) in Equation (4.88) and writing the resulting relation in matrix form, the following equation is obtained,

$$\{d\varepsilon_p\}=\{Q\}d\bar{\varepsilon}_p \quad \textbf{(4.92)}$$

where

$$\{d\varepsilon_p\}=\{d\varepsilon_{xp}\quad d\varepsilon_{yp}\quad d\gamma_{xyp}\quad d\gamma_{xzp}\quad d\gamma_{yzp}\} \quad \textbf{(4.93)}$$

Referring to Figure (4.8), the stress increments $\{d\sigma\}$ can be written in terms of strain increments as follows:

$$\{d\sigma\}=[D]\{d\varepsilon_e\} \quad \textbf{(4.94)}$$

or

$$\{d\sigma\}=[D](\{d\varepsilon_{ep}\}-\{d\varepsilon_p\}) \quad \textbf{(4.95)}$$

where

$\{d\varepsilon_e\}$: elastic strain increments.

$\{d\varepsilon_p\}$: plastic strain increments.

$\{d\varepsilon_{ep}\}$: total strain increments.

Premultiplying both sides of Equation (4.95) by $\{Q\}^T$ and substituting from Equation (4.83) and Equation (4.93) in the resulting equation give,

$$\{d\bar{\sigma}\}=\{Q\}^T[D](\{d\varepsilon_{ep}\}-\{Q\}\{d\bar{\varepsilon}_p\}) \quad \textbf{(4.96)}$$

But from Figure (4.8),

$$\{d\bar{\sigma}\}=H'\{d\bar{\varepsilon}_p\} \quad \textbf{(4.97)}$$

From Equation (4.95) and Equation (4.96), the following equation is obtained,

$$\{d\bar{\varepsilon}_p\}=\lfloor W\rfloor\{d\varepsilon_{ep}\} \quad \textbf{(4.98)}$$

where

$$\lfloor W \rfloor = \frac{\{Q\}^T [D]}{H' + \{Q\}^T [D]\{Q\}} \qquad \textbf{(4.99)}$$

and,

$H' = 0$ (for elastic-perfectly plastic material)

Then, to find the elasto-plastic stress-strain matrix $[D_{ep}]$, the stress increments $\{d\sigma\}$ could be expressed in terms of total strain increments $[d\varepsilon_{ep}]$ as follows:

$$\{d\sigma\} = [D_{ep}]\{d\varepsilon_{ep}\} \qquad \textbf{(4.100)}$$

But from Equation (4.92) and Equation (4.95), one can relate the plastic strain increments $\{d\varepsilon_p\}$ with the total strain increments $\{d\varepsilon_{ep}\}$ by the following equation,

$$\{d\varepsilon_p\} = \{Q\}\lfloor W \rfloor \{d\varepsilon_{ep}\} \qquad \textbf{(4.101)}$$

Then, substituting Equation (4.96) in Equation (4.101) gives,

$$\{d\sigma\} = ([D] - [D]\{Q\}\lfloor W \rfloor)\{d\varepsilon_{ep}\} \qquad \textbf{(4-102)}$$

by comparison Equation (4.100) and Equation (4.102), it is deduced that

$$[D_{ep}] = [D] - [D]\{Q\}\lfloor W \rfloor = [D] - \frac{[D]\{Q\}\{Q\}^T [D]}{\{Q\}^T [D]\{Q\}} \qquad \textbf{(4.103)}$$

where the matrix $[D_{ep}]$ is the constitutive elastic-plastic matrix for an isotropic material.

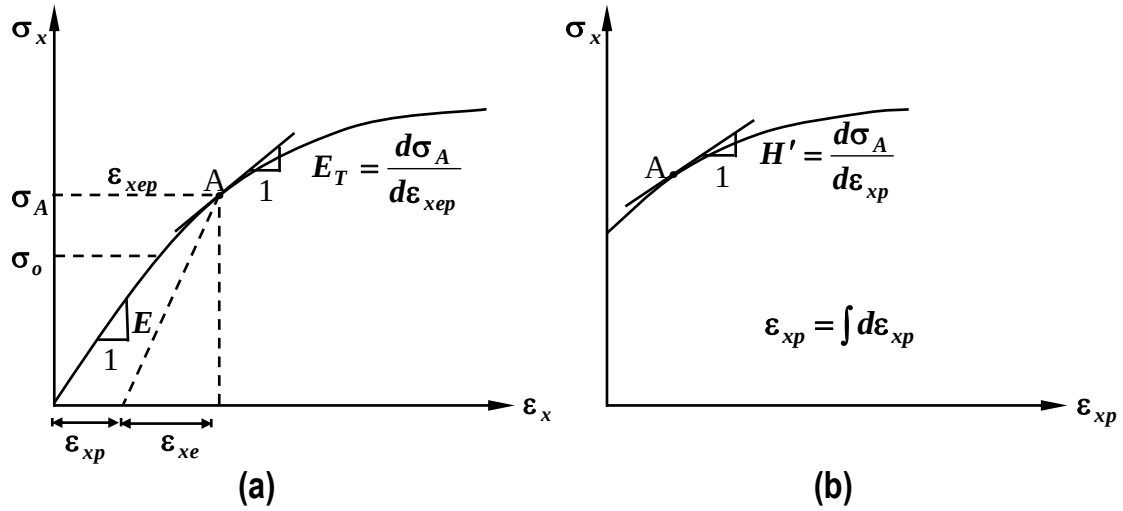

Figure (4.8): General stress-strain relations in uniaxial tension. (E: elastic modulus, E_T: tangent modulus). The second plot is obtained from first by substituting the elastic strains

4.8.2.2 Elastic-plastic formulation based on Tsai-Wu and Hashin criteria

The formulation in the previous section was dependent on the **von-Mises** criterion, but in the present section the formulation is based on **Tsai-Wu** criterion. The difference of the previous formulation is in the Equation (4.81), which becomes for laminated composite materials as:

$$\boldsymbol{F}_1\boldsymbol{\sigma}_1 + \boldsymbol{F}_2\boldsymbol{\sigma}_2 + \boldsymbol{F}_{11}\boldsymbol{\sigma}_1^2 + +\boldsymbol{F}_{22}\boldsymbol{\sigma}_2^2 + \boldsymbol{F}_{12}\boldsymbol{\sigma}_1\boldsymbol{\sigma}_2 + \boldsymbol{F}_{44}\boldsymbol{\sigma}_4^2 + \boldsymbol{F}_{55}\boldsymbol{\sigma}_5^2 + \boldsymbol{F}_{66}\boldsymbol{\sigma}_6^2 = 1 \quad \textbf{(4-104)}$$

The differential form of the **Tsai-Wu** law can be written as:

$$\{\boldsymbol{Q}\}^T \boldsymbol{d\sigma} = \boldsymbol{0} \quad \textbf{(4-105)}$$

where the flow vector $\{\boldsymbol{Q}\}=\partial \boldsymbol{f}/\partial\sigma$ is defined as follows:

$$\{\boldsymbol{Q}\}=\frac{\partial \boldsymbol{f}}{\partial \sigma}=\left[\frac{\partial \boldsymbol{f}}{\partial \sigma_1},\frac{\partial \boldsymbol{f}}{\partial \sigma_2},\frac{\partial \boldsymbol{f}}{\partial \tau_{12}},\frac{\partial \boldsymbol{f}}{\partial \tau_{13}},\frac{\partial \boldsymbol{f}}{\partial \tau_{23}}\right]^T \quad \textbf{(4-106)}$$

in which,

$$\begin{aligned}
\frac{\partial \boldsymbol{f}}{\partial \boldsymbol{\sigma}_1} &= \left(\boldsymbol{F}_1 + 2\boldsymbol{F}_{11}\boldsymbol{\sigma}_1 + \boldsymbol{F}_{12}\boldsymbol{\sigma}_2\right)\\
\frac{\partial \boldsymbol{f}}{\partial \boldsymbol{\sigma}_2} &= \left(\boldsymbol{F}_2 + 2\boldsymbol{F}_{22}\boldsymbol{\sigma}_2 + \boldsymbol{F}_{12}\boldsymbol{\sigma}_1\right)\\
\frac{\partial \boldsymbol{f}}{\partial \boldsymbol{\tau}_{12}} &= \left(6\boldsymbol{F}_{66}\boldsymbol{\tau}_{12}\right)\\
\frac{\partial \boldsymbol{f}}{\partial \boldsymbol{\tau}_{13}} &= \left(6\boldsymbol{F}_{44}\boldsymbol{\tau}_{13}\right)\\
\frac{\partial \boldsymbol{f}}{\partial \boldsymbol{\tau}_{23}} &= \left(6\boldsymbol{F}_{55}\boldsymbol{\tau}_{23}\right)
\end{aligned} \quad \textbf{(4-107)}$$

The elastic-plastic incremental stress-strain relationship for a composite material is:

$$\boldsymbol{d\sigma} = [\boldsymbol{D}]_{ep}\,\boldsymbol{d\varepsilon} \quad \textbf{(4-108)}$$

with

$$\boldsymbol{d\sigma} = [\boldsymbol{D}]_{ep}\,\boldsymbol{d\varepsilon} \quad \textbf{(4-109)}$$

$$[\boldsymbol{D}]_{ep} = [\boldsymbol{D}] - \frac{[\boldsymbol{D}]\{\boldsymbol{Q}\}\{\boldsymbol{Q}\}^T[\boldsymbol{D}]}{\{\boldsymbol{Q}\}^T[\boldsymbol{D}]\{\boldsymbol{Q}\}} \quad \textbf{(4-110)}$$

where the matrix $[\boldsymbol{D}]_{ep}$ is the constitutive elastic-plastic matrix for a general laminated composite material.

The progressive failure analysis is based on the assumption that the damage region can be substituted with an equivalent material with degraded properties. The amounts or degrees of property loss are dependent upon the failure mechanisms to cause damage. The property degradation model used in the present study depends on the failure modes predicted by the previous failure criterion. The degradation model is based on the rule of mixture and is applied at integration points of a finite element model. At every integration point that satisfies Tsai-Wu criterion and at least one of the failure criterion, the material properties are substituted with the degraded values as described below [**Park** and **Lee**, **2000**][(85)].

For matrix cracking failure, the laminate can be thought as a fiber bundle. The longitudinal modulus E_1 and shear modulus G_{12} will be degraded and transverse modulus E_2 and Poisson's ratio ν_{12} are reduced to zero. The matrix of in-plane elastic stiffness constants is modified as follows:

$$[D]_{ei} = \begin{bmatrix} \frac{E_1}{1-\nu_{12}\nu_{21}} & \frac{E_2\nu_{12}}{1-\nu_{12}\nu_{21}} & 0 \\ \frac{E_2\nu_{12}}{1-\nu_{12}\nu_{21}} & \frac{E_2}{1-\nu_{12}\nu_{21}} & 0 \\ 0 & 0 & G_{12} \end{bmatrix} \rightarrow [D]_{epi} = \begin{bmatrix} V_f E_f & 0 & 0 \\ 0 & 0 & 0 \\ 0 & 0 & 0 \end{bmatrix} \qquad \textbf{(4.111)}$$

where V_f is a fiber volume fraction and E_f is Young's modulus of fiber.

When fiber matrix shearing failure is predicted at an integration point, longitudinal modulus E_1 will remain unchanged and transverse modulus E_2 and Poisson's ratio ν_{12} and shear modulus G_{12} are reduced to zero. The matrix of in-plane stiffness constants is modified as follows:

$$[D]_{ei} = \begin{bmatrix} \frac{E_1}{1-\nu_{12}\nu_{21}} & \frac{E_2\nu_{12}}{1-\nu_{12}\nu_{21}} & 0 \\ \frac{E_2\nu_{12}}{1-\nu_{12}\nu_{21}} & \frac{E_2}{1-\nu_{12}\nu_{21}} & 0 \\ 0 & 0 & G_{12} \end{bmatrix} \rightarrow [D]_{epi} = \begin{bmatrix} E_1 & 0 & 0 \\ 0 & 0 & 0 \\ 0 & 0 & 0 \end{bmatrix} \qquad \textbf{(4.112)}$$

For fiber breakage failure, it is assumed that the fiber is completely broken; the failed region is thought to be an isotropic material made of only matrix. The matrix of in-plane elastic stiffness constants is then modified as follows:

$$[D]_{ei}=\begin{bmatrix} \frac{E_1}{1-\nu_{12}\nu_{21}} & \frac{E_2\nu_{12}}{1-\nu_{12}\nu_{21}} & 0 \\ \frac{E_2\nu_{21}}{1-\nu_{12}\nu_{21}} & \frac{E_2}{1-\nu_{12}\nu_{21}} & 0 \\ 0 & 0 & G_{12} \end{bmatrix} \rightarrow [D]_{epi}=\begin{bmatrix} \frac{V_m E_m}{1-(V_m\nu_m\nu_{21})} & \frac{V_m E_m \nu_m}{1-(V_m\nu_m\nu_{21})} & 0 \\ \frac{V_m E_m \nu_m}{1-(V_m\nu_m\nu_{21})} & \frac{V_m E_m \nu_m}{1-(V_m\nu_m\nu_{21})} & 0 \\ 0 & 0 & V_m G_m \end{bmatrix} \quad \textbf{(4.113)}$$

where V_m is a matrix volume fraction, E_m is Young's modulus of the matrix and G_m is the shear modulus of the matrix.

4.9 General Nonlinear Solution Procedure

The solution of linear elastic analysis for structural problems can be obtained directly from solving a set of algebraic equations in the following form

$$\{F\}=[K]\{u\} \quad \textbf{(4.114)}$$

where:

$\{F\}$: is the applied nodal force vector.

$[K]$: is the stiffness matrix.

$\{u\}$: unknown nodal displcemenet vector.

For the solution of a nonlinear structural problem, the state of equilibrium corresponding to the applied load must be found. These equilibrium equations can be written as:

$$\{R(u)\}=\{F\}-\{P(u)\} \quad \textbf{(4.115)}$$

where:

$\{R(u)\}$: is out of balance residual force vector.

$\{P(u)\}$: is the vector of the nodal forces equivalent to the internal stress level, and is given by,

$$\{P(u)\}=\int_V [B]^T\{\sigma\}dV \quad \textbf{(4.116)}$$

The satisfaction of equilibrium at the nodes requires that the external load vector be equal to the internal load vector, i.e. the out of balance force vector be zero.

$$\{R(u)\} = 0 \qquad \textbf{(4.117)}$$

The solution of Equation (4.104) is usually attempted by using one of the following three basic techniques.

- Iterative analysis
- Incremental analysis, or
- Iterative-incremental analysis.

These three techniques are shown for a single degree of freedom in Figure (4.9) a, b, and c respectively, and described briefly below.

In purely iterative techniques, the full load is applied in one increment, Figure (4.9,a), and an initial vector of unknown displacement, usually the linear solution, $\boldsymbol{u}_1$, is determined. Iterative corrections are performed then in order to get a progressively improved solution, $\boldsymbol{u}_2$, $\boldsymbol{u}_3$. This can be achieved as follows. The stresses corresponding to the predicted solution are calculated using the relevant constitutive laws. A vector of internal forces, $\boldsymbol{P}_1$, is calculated and compared with the external load vector, $\boldsymbol{F}$. The difference between these two vectors, the out of balance forces, $\boldsymbol{R}_i$, is then successively applied to the structure until the internal loads be equal, or very closely correspond to the externally applied load (convergence). The total displacements are calculated by summing the displacements from each iteration. In practice, the progress of iteration procedure is monitored with reference to a specified convergence criterion, the satisfaction of which indicates the approximate solution.

The problems where the entire response of the structure is required, purely iterative methods cannot be used because they fail to produce information about the intermediate stages. An incremental technique is essential in these cases.

The basis of the incremental technique is that the total load is sub-divided into smaller load increments. For each of these load increments linear constitutive and geometrical relationships are assumed. The simplest incremental procedure is the Euler method [**Cook, 1995**][26]. The incremental method does not account for force redistribution during the application of the load increments. Therefore it suffers from a

progressive and uncorrected tendency to drift from the true equilibrium path, see Figure (4.9,b).

In the mixed incremental-iterative method, the external loading is applied in increments and the solution corresponding to each load increment is obtained by iterating until convergence is achieved. Nowadays this technique is the most commonly used procedure in nonlinear finite element analyses, thus this method is adopted in the present work, Figure (4.9,c). In this approach the total external load is applied through small increments, and within each increment a number of iteration cycles are made in order to satisfy the equilibrium equations according to a specified tolerance. To satisfy the equilibrium equations within a sufficient accuracy, the number of iterations required depends on the structure.

4.10 Solution Technique

Different solution algorithms are used for calculating the incremental displacements ($\Delta \boldsymbol{u}$) at (ith) iteration during the (nth) load increment in the nonlinear solution system.

The computation time and the convergence to the correct solution are the measure of their effectiveness. There are many types of iterative methods such as:

1- Conventional Newton-Raphson (N-R) method.
2- Modified (N-R) method.
3- Combined conventional and modified (N-R) method.
4- Direct method.

4.10.1 Conventional Newton-Raphson (N-R) method

Conventional (N-R) method is one of the oldest and best known methods used in solving the nonlinear problems. A multi-degree of freedom system with a load level, $\{\boldsymbol{F}\}_i$ is considered and it is assumed and assume that the corresponding deformed configuration of the system which may be denoted symbolically by $\{\boldsymbol{u}\}_i$ is known, as shown in Figure (4.10).

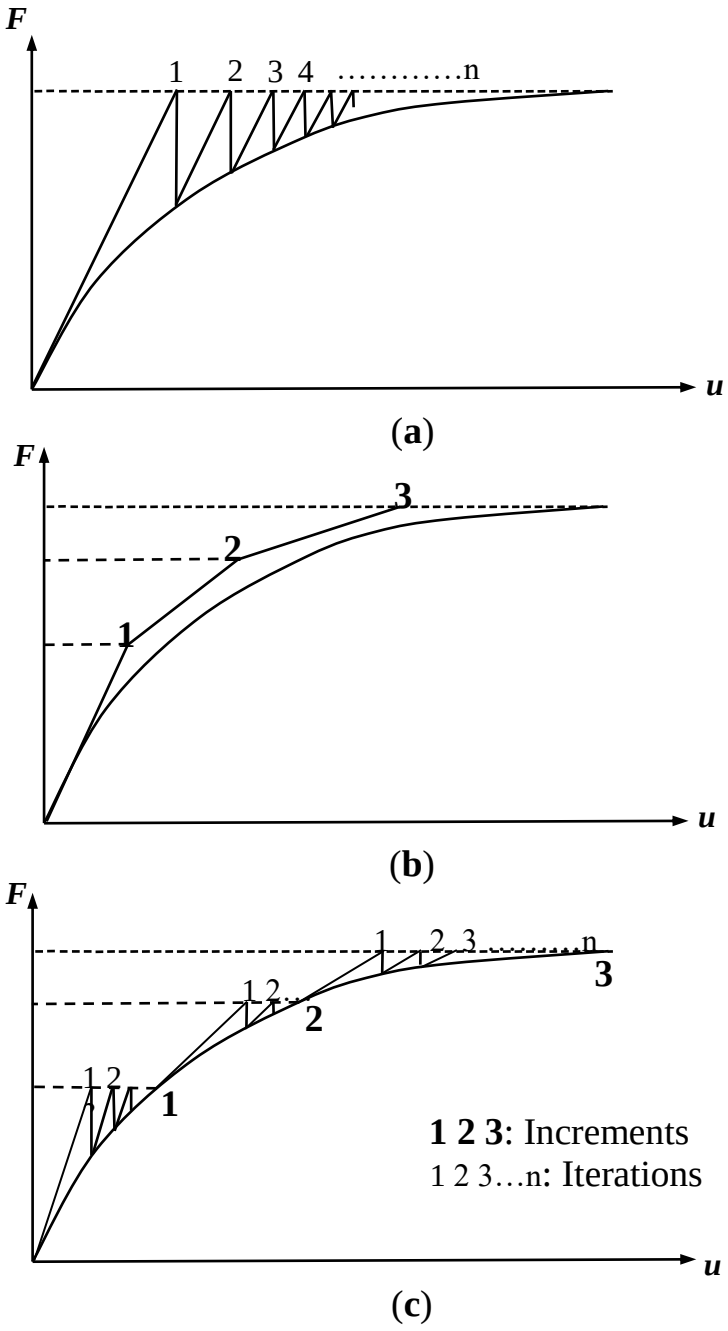

Figure (4.9): General methods for the solution of nonlinear equations: (**a**) Iterative, (**b**) Incremental, (**c**) Incremental-Iterative

Now to determine the configuration $\{\boldsymbol{u}\}_{i+1}$ corresponding to a load level $\{\boldsymbol{F}\}_{i+1}$, where:

$$\{\boldsymbol{F}\}_{i+1} = \{\boldsymbol{F}\}_i + \{\Delta\boldsymbol{F}\} \qquad \textbf{(4.118)}$$

and $\{\Delta\boldsymbol{F}\}$ is the additional applied load, by using a linearized analysis, the change in configuration $\{\Delta\boldsymbol{u}\}_1$ is computed first from:

$$\{\Delta F\} = [K_T]_0 \{\Delta u\}_1 \quad \textbf{(4.119)}$$

in which the tangent stiffness matrix $[K_T]_0$ is evaluated at the beginning of the load interval, i.e. at the load level $\{F\}_i$. $\{u\}_i + \{\Delta u\}_1$ represents an approximate configuration in the sense that joint equilibrium equations are not necessarily satisfied at the load level $\{F\}_{i+1}$. This approximate solution is then corrected by N-R iterations until equilibrium equations are satisfied within a prescribed tolerance.

From the approximate configuration $(\{u\}_i + \{\Delta u\}_1)$, a new tangent stiffness matrix is updated, and then the internal forces at the iteration corresponding to the configuration $\{F\}_j$ can be determined as:

$$\{P\}_j = [K_T]_j \{u\}_j \quad \textbf{(4.120)}$$

in which

$$\{u\}_j = \{u\}_i + \sum_{j=1}^{n} \{\Delta u\}_j \quad \textbf{(4.121)}$$

and $\{u\}_j$ is the vector of total displacements after n iterations, then, the out-of-balance forces $\{\Delta F\}_j$ can be obtained from:

$$\{\Delta R\}_j = \{F\}_{i+1} - \{P\}_j \quad \textbf{(4.122)}$$

The unbalanced joint forces are then treated as a load increment and the correction vector, $\{\Delta u\}_{j+1}$, is obtained from the incremental relationship

$$[K_T]_j \{\Delta u\}_{j+1} = \{\Delta R\}_j \quad \textbf{(4.123)}$$

a new approximate configuration is then obtained by making use of Equation (4.120). The process continues until the latest correction vector is sufficiently small.

The Newton-Raphson method requires that the tangent stiffness be formed and then triangularized for solution in each iteration. This is expensive if the problem has many degrees of freedom. Accordingly, various modifications have been proposed [**Cook**, **1995**][(26)].

4.10.2 Modified Newton-Raphson (N-R) method

This method differs from the conventional N-R method only in that the tangent stiffness matrix is not updated in each iteration (i.e., constant stiffness matrix). The process is depicted one dimensionally in Figure (4.11). As compared with the conventional N-R method, this method requires more iterations for convergence, but each iteration is done more quickly by avoiding the expensive repetitions of forming stiffness matrix $[K_T]$.

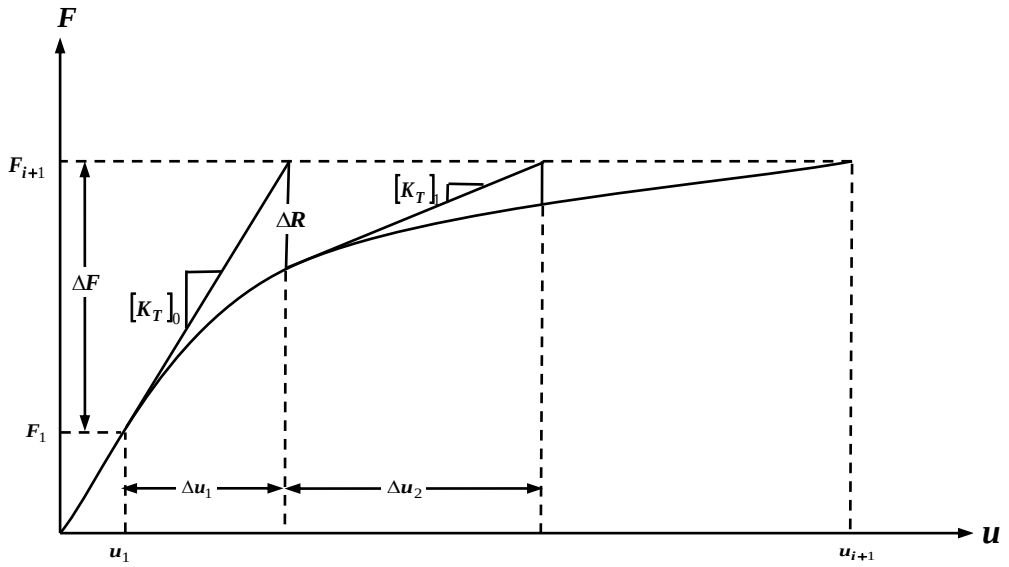

Figure (4.10): Conventional Newton-Raphson method

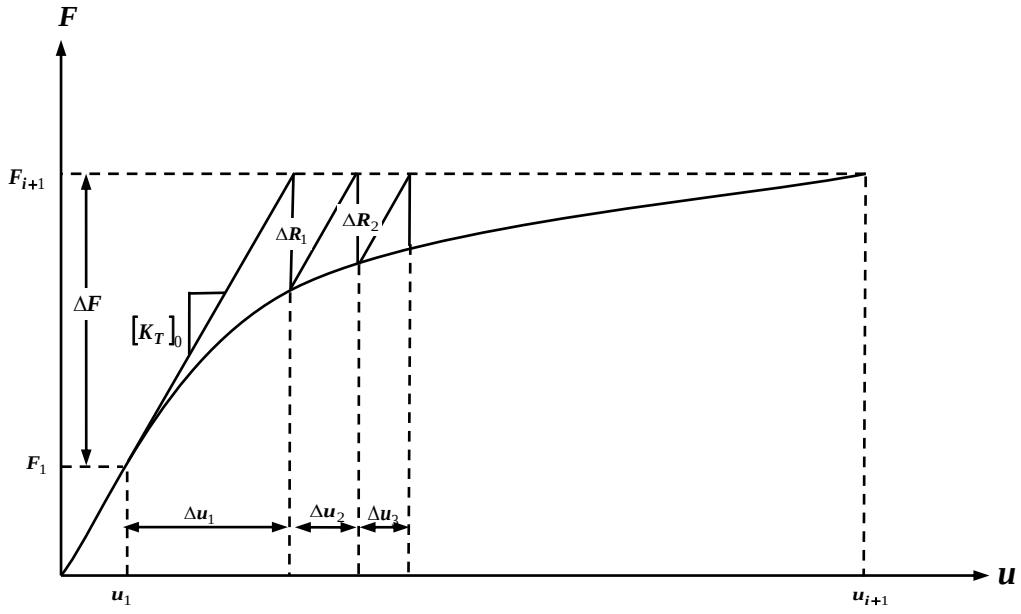

Figure (4.11): Modified Newton-Raphson method

4.10.3 Combined conventional and modified (N-R) method

In this method, the stiffness is held constant for several iterations and is updated when the rate of convergence begins to deteriorate (number of iterations exceeds the specified maximum limit), as shown in Figure (4.12).

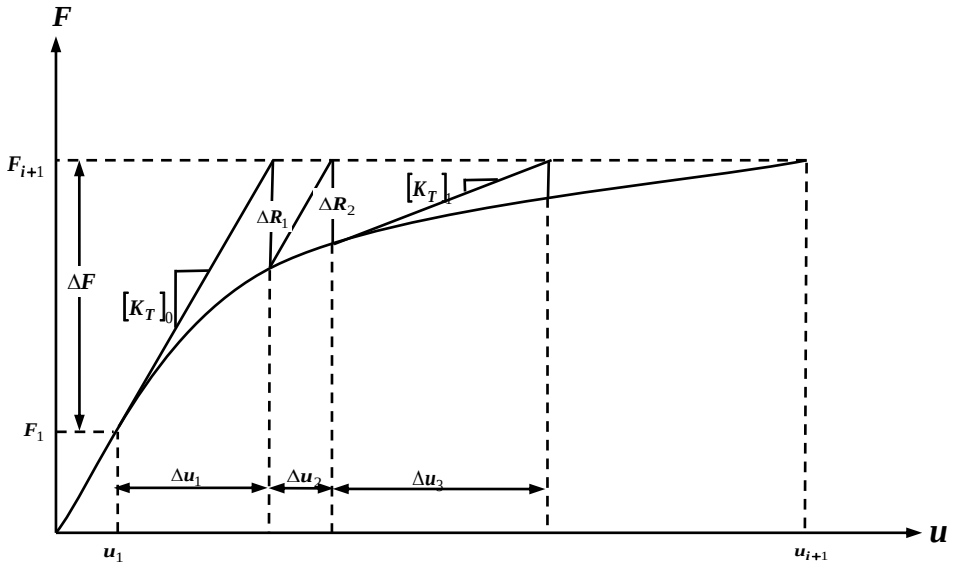

Figure (4.12): Combined conventional and modified (N-R) method

4.10.4 Direct method

In this method, the deformation corresponding to any load along the load-deformation curve is obtained by applying the load is a single step. The method thus deals with total deformations and total loads. The direct method can be used to obtain the deformations corresponding to a single value of the load and thus can be used to plot the entire load-deflection curve as shown in Figure (4.13).

In this method, the desired deformations are related to the applied load by the so-called secant stiffness matrix, i.e.:

$$[K_s]\{\Delta u\}_A = \{F\}_A \qquad \textbf{(4.124)}$$

Since $[K]_s$ depends on the internal forces and deformations that exist when the load is acting, and since quantities are not known at the beginning of calculations, the terms in $[K]_s$ must be determined by iteration. At the beginning, the linear stiffness matrix is used in Equation (4.124) to determine an approximate configuration. Then, from the

approximate configuration $\{u\}_1$ a new stiffness matrix is obtained. Equation (4.124) is solved again for the total displacement $\{u\}_A$. Then, another approximate solution is obtained $\{u\}_2$ until successive substitutions become negligible.

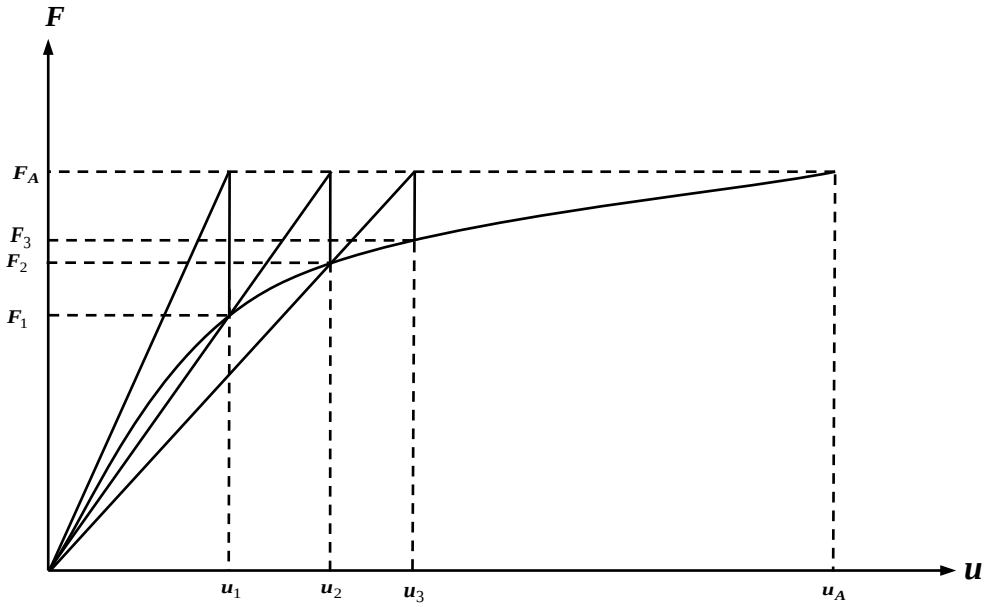

Figure (4.13): Direct method

4-11 Algorithm for the Solution of the Incremental Finite Element Method

The algorithm of the solution takes into account the nonlinearity in geometry and material of the element. The plasticity of the plate element is checked in the Gauss points and each Gauss point contains a number of layers and the stresses are checked in the centers of these layers. The external load is applied incrementally and at every load increment the stiffness matrix of the plate is updated. The solution has been achieved by using the modified Newton-Raphson iterations technique, as shown in Figure (4.11).

The process of analysis used in the present work is of the following pattern:

1. Input the data of the geometry of the plate and the properties of the material and input the number of layers and the value of initial imperfection and also input the boundary conditions of the plate and type of material for each layer.

2. Construct the vector of the nodal forces for each element after completing the numerical integration. Then, assemble the vectors of the nodal forces to find the total vector of nodal forces for the plate $\{F\}$.
3. Construct the linear stiffness matrix of the plate element and assemble these matrices of the elements where in the first step the plate is considered as a linear elastic plate and ($[K_\sigma]$, and $[B_L]$) will be neglected.
4. Calculate the nodal displacements vector after using the inverse matrix method to solve the unknown equations ($\{u\} = [K_o]^{-1}\{F\}$).
5. Calculate the strain increments at each Gauss point in the natural system and then, find the stress increments in each layer for each Gauss point at the center of each layer.
6. Calculate the effective stress ($\bar{\sigma}$) for the isotropic plate from Equation (4.80); while for the composite plate, find the yield unity from Equation (104) at each layer for each Gauss point in each element corresponding to the applied load vector.
7. At ***i***-th load increment; find ($[D_i]$,$[B_L]$, and $[K_\sigma]$) for each element corresponding to the stress history $\{\sigma_{i-1}\}_L$ of each layer for all Gauss points in that element.

For Gauss points having effective stress exceeding the yield limit (σ_o), the matrix $[D]$ is replaced by $[D_{ep}]$ by using Equation (4.110) for the isotropic plate and Equations (4.111)-(4.113) for the fiber composite plate. Then, update the stiffness matrix at the beginning of each load increment and this will be used in all iterations in that load increment.

8. At ***i***-th load increment, apply the residual forces from the previous iteration to be:

$$\{P\} = \int_V [\bar{B}]^T \{\sigma\} dV + [K_\sigma]\{u\} \qquad \textbf{(4-125)}$$

$$\{R\} = \{F\} + \{P\} \qquad \textbf{(4-126)}$$

where

$$[\bar{B}] = [B_o] + [B_L]$$

$[\sigma]$: Vector of total stresses at any ***j***-iteration.

$[u]$: Vector of element displacements at any ***j***-iteration.

$\{F\}$: Vector of external forces applied at the beginning of analysis.

$\{P\}$: Vector of internal forces for the plate.

$\{R\}$: Vector of residual forces at any ***j***-iteration.

9. Find the resulting strain increments at each Gauss point,

$$\{d\varepsilon_{epj}\} = [\bar{B}]\{du\}$$

After that, find the effective elastic-plastic strain increment $d\bar{\varepsilon}_{epj}$ from Equation (4.87) for a steel plate only; while the fiber composite plate has no $d\bar{\varepsilon}_{epj}$, as shown in Figure (4.6).

10. Find the stress increments from Equation (4.100) and add the resulting increment stress vector to the total stress vector from the previous iteration (σ_{j-1}) to find (σ_j) at the end of the increment. Then, compute the effective stress $(\bar{\sigma})$ from Equation (4.80).

Finite size stress increments produced from each iteration for each load increment may depart from the yield surface as shown in Figure (4.14). This discrepancy is particularly eliminated since in each iteration these stress increments are sufficiently small. However, the point of finding the stress can be reduced to the yield surface simply by scaling the stress vector $\{\sigma_i\}$ as given in Figure (4.14)

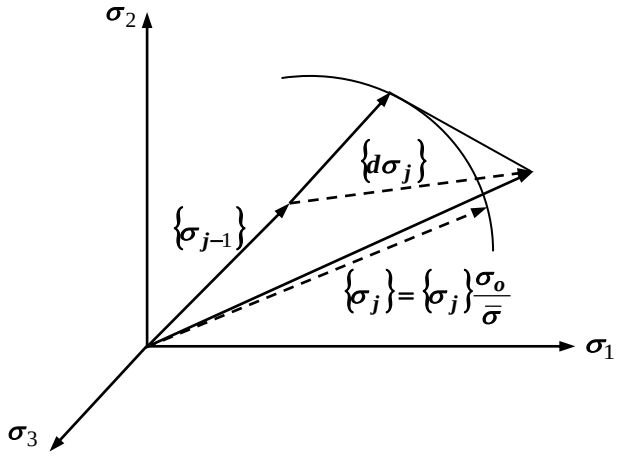

Figure (4.14): Scaling the stress $\{\sigma_j\}$ vector at the end of iteration so as to satisfy the yield criterion

At the end of iteration, update ($\{Q\}$ and $\lfloor W \rfloor$) as given in Equation (4.83) and (4.99) respectively by utilizing the stress history $[\sigma]$ for the considered layer at Gauss point.

11. Find the norm of residual forces at the end of iteration (***j***) as follows:

$$\text{norm}_j = \left[\sqrt{\frac{\sum (dR_{i+1})^2}{\sum (dR_i)^2}} \right] * 100 \qquad \textbf{(4-127)}$$

Then,

a- If $\text{norm}_j \leq \text{norm}_{j-1}$ and $\text{norm}_j \leq (0.1\%)$, print the total applied load and print the total nodal displacements $(\{u_j\} = \{u_{j-1}\} + \{du_j\})$ which represent $\{u_j\}$ at the end of ***i***-th load increment. Also, print the effective stress $\bar{\sigma}_j$ at all Gauss points which are corresponding to the stresses $(\{\sigma_j\} = \{\sigma_{j-1}\} + \{d\sigma_j\})$. Such effective stresses represent the stress $\bar{\sigma}_j$ at the end of *i*th load increment. Then, go to step (6) with next load increment (***i***+1).

b- If $\text{norm}_j \leq \text{norm}_{j-1}$ and $\text{norm}_j > (0.1\%)$ go to step (7) for next iteration (***j***+1).

c- Otherwise (if $\text{norm}_j > \text{norm}_{j-1}$), the solution has diverged and may indicate the collapse state. The termination of the analysis depends on any of the following.

1- The number of iterations exceeds a preselected maximum number. It must be mentioned here that this criterion is not always sufficient to indicate the failure of the plate; since it could happen that the solution is slowly converging because, for example, if large increments of load are used or very tight convergence tolerance is specified.

2- The stiffness matrix is no longer positive definite.

3- The strain exceeds the ultimate strain permitted ($2\varepsilon_y$) in steel material.

CHAPTER FIVE

Nonlinear Dynamic Analysis of Plate

5.1 General

Certain civil engineering structures are designed to carry their own dead load plus superimposed loads which are immovable and unvarying with time, that is, superimposed static loads. In such cases, the stress analysis involves only principles of statics. More often the design of a civil engineering structure involves not only static loads but also superimposed loads which are either moving or movable and may vary with time as in superimposed dynamic loads. In such cases, the stress analysis properly should involve principles of dynamics to determine the effect of dynamic loading.

However, in many of these cases, experience has shown that the dynamic effect makes a minor contribution to the total load which must be provided for the design and therefore the dynamic effect need not be evaluated precisely. In such cases, the dynamic effect may be handled by the use of an equivalent static load, or by an impact factor or by a modification of the factor of safety.

There have been a number of developments which have led to growing interest in a more precise evaluation of the effects produced by the dynamic portion of the loading. Among these are the imposition of more severe live load conditions (that is, machinery and vehicles moving at high speeds), the construction of high towers and long bridges involving more severe and important wind-loading conditions, the necessity of developing blast resistant constructions, and the desire to improve earthquake resistance of constructions. These are some aspects where it may be necessary to consider more precisely the response produced by dynamic loading.

The ability of thin-walled structures to absorb the energy of dynamic transient loading has led to its utilization for several classes of important structures, such as aerodynamic structures, power plant structure, bridge structures, etc. These types of structures are designed under these loads to maintain the overall structural integrity with irreversible deformation analysis. In the present chapter a computational modeling is developed for the nonlinear dynamic analysis of isotropic and laminated composite plates using finite element method. The dynamic equilibrium Equation and the derivation of mass and damping matrices will be presented. Two direct time integration methods (Newmark method and Harmonic acceleration method) are adopted.

5.2 Dynamic Equilibrium Equation

The dynamic equilibrium Equations are obtained by using the principle of virtual work which states that for any arbitrary kinematically consistent set of displacements, the internal virtual work done by stresses through virtual strains must be equal to that done by the external forces irrespective of the material behavior as [**Cook**, **1995**][(26)]:

$$\int_v (d\varepsilon)^T \sigma \, dv = \int_{s_t} (du)^T P_t \, ds + \int_v (du)^T (P_b - \rho \ddot{u} - C\dot{u}) dv \qquad \textbf{(5.1)}$$

where du is a vector of virtual displacements, $d\varepsilon$ is the vector of associated virtual strains and σ is the vector of actual stresses. The term P_t is a vector of surface tractions acting on the portion s_t of the boundary S. Vectors $P_b, \rho \ddot{u}$ and $C\dot{u}$ are the body, inertial and damping forces respectively. The symbol (·) denotes differentiation with respect to time. ρ is the mass density and C is the damping parameter.

For the finite element representation, the displacements, velocities and accelerations $u, \dot{u}$ and $\ddot{u}$ can be defined in terms of the nodal variables $d, \dot{d}$ and $\ddot{d}$ by the expressions:

$$u = \sum_{i=1}^{m} N_i(\xi,\eta) d_i = Nd \ , \ du = N\,\delta d \tag{5.2}$$

$$\dot{u} = \sum_{i=1}^{m} N_i(\xi,\eta) \dot{d}_i = N\,\dot{d} \tag{5.3}$$

$$\ddot{u} = \sum_{i=1}^{m} N_i(\xi,\eta) \ddot{d}_i = N\,\ddot{d} \tag{5.4}$$

where $u = \sum_{i=1}^{m} N_i(\xi,\eta) d_i = Nd$, N_i is the shape functions for i node, and m is the number of nodes.

With standard strain-nodal displacement matrix $[B]$, the virtual strain vector can be related to the nodal displacements as:

$$d\varepsilon = \sum_{i=1}^{m} [B]_i \delta d_i = [B]\delta d \tag{5.5}$$

Upon substitution of Equations (5.2-5.5) into Equation (5.1) then:

$$\delta d^T \left[[M]\ddot{d} + [C]\dot{d} + [K]d \right] = \delta d^T \{ f_e(t) \} \tag{5.6}$$

in which the mass matrix $[M]$, the damping matrix $[C]$, the stiffness matrix $[K]$ and the external applied vector $\{f_e(t)\}$ have the following element contributions:

$$[M_e] = \int_{Ve} N^T \rho\, N\, dV \tag{5.7}$$

$$[C_e] = \int_{Ve} N^T C\, N\, dV \tag{5.8}$$

$$[K_e] = \int_{Ve} [B]^T [D][B] dV \tag{5.9}$$

$$f_e(t) = \int_{se} N^T P_t\, ds + \int_{Ve} N P_b\, dV \tag{5.10}$$

where s_e and V_e denote the surface and volume of the element under consideration. As δd^T is arbitrary, then Equation (5.6) may be written as:

$$[M]\{\ddot{d}\} + [C]\{\dot{d}\} + [K]\{d\} = \{ f_e(t) \} \tag{5.11}$$

Equation (5.11) is the dynamic equilibrium Equation for a single or multi-degree of freedom system.

5.3 Formulation of Element Mass Matrix

When the shape functions used for the derivation of the mass matrix are identical to those used in formulating the element stiffness matrix; matrix $[M]$ is called the consistent mass matrix. This matrix was first derived by **Archer**, in **1963** [**Ali**, **2004**][6].

To derive the consistent mass matrix, one can consider the kinetic energy of the total solution domain discretized into a number of elements (NE) such that:

$$TI(\dot{d}) = \sum_{e=1}^{NE} TI^e(\dot{d}) \qquad \textbf{(5.12)}$$

where TI and TI^e are the kinetic energy of the total solution domain and the sub-domain respectively. The kinetic energy of the element (e) can be expressed as follows:

$$TI^e = \frac{1}{2}\int_A \{\dot{d}\}^T [m]\{\dot{d}\} dA \qquad \textbf{(5.13)}$$

The velocity vector within an element is discretized such that:

$$\{\dot{d}\} = \sum_{i=1}^{NN} N_i \{\dot{d}\}, \text{ NN: number of nodes.} \qquad \textbf{(5.14)}$$

By substituting Equation (5.14) into Equation (5.13), one gets:

$$TI^e = \frac{1}{2}\sum_{i=1}^{NN} \{\dot{d}\}^T \int_A N_i^T [m] N_i \, dA \{\dot{d}\} \qquad \textbf{(5.15)}$$

or in a matrix form:

$$TI^e = \frac{1}{2}\{\dot{d}\}^T \int_A [N][m][N] dA \{\dot{d}\} = \frac{1}{2}\{\dot{d}\}^T [M]\{\dot{d}\}^T \qquad \textbf{(5.16)}$$

Thus,

$$[M]^e = \int_A [N]^T [m][N] dA = \int_{-1}^{1}\int_{-1}^{1} [N]^T [M][N] |\mathbf{J}| \, d\xi \, d\eta \qquad \textbf{(5.17)}$$

where

$$[N] = [N_1, N_2, N_3, ..., N_{NN}] \qquad \textbf{(5.18)}$$

The mass matrix for five degrees of freedom per node is:

$$[m]_{5\times5} = \begin{bmatrix} I_1 & & & & 0 \\ & I_1 & & & \\ & & I_1 & & \\ & & & I_2 & \\ 0 & & & & I_2 \end{bmatrix} \tag{5.19}$$

for seven degrees of freedom per node,

$$[m]_{7\times7} = \begin{bmatrix} I_1 & & & & & & 0 \\ & I_1 & & & & & \\ & & I_1 & & & & \\ & & & I_2 & & & \\ & & & & I_2 & & \\ & & & & & I_3 & \\ 0 & & & & & & I_3 \end{bmatrix} \tag{5.20}$$

and for nine degrees of freedom per node, one can get:

$$[m]_{9\times9} = \begin{bmatrix} I_1 & & & & & & & & 0 \\ & I_1 & & & & & & & \\ & & I_1 & & & & & & \\ & & & I_2 & & & & & \\ & & & & I_2 & & & & \\ & & & & & I_3 & & & \\ & & & & & & I_3 & & \\ & & & & & & & I_4 & \\ 0 & & & & & & & & I_4 \end{bmatrix} \tag{5.21}$$

For layered plates, the element mass matrix can be written as follows:

$$[M] = \sum_{L=1}^{NL} [M]^e \tag{5.22}$$

where in the above three Equations (5.19), (5.20), and (5.21), I_1, I_2, I_3, and I_4 are translation inertia, rotary inertia, and respectively higher order inertia terms, and these are given by:

$$(I_1, I_2, I_3, I_4) = \sum_{L=1}^{NL} \int_{h_{L-1}}^{h_L} (1, z^2, z^4, z^6) \rho^L dz \tag{5.23}$$

where ρ^L is material density of L-th layer.

Instead of the consistent mass matrix, a lumped mass matrix $[M_L]$ may be used. This matrix is obtained by assuming that the element is

concentrated, or lumped, at the nodes of the element. Although the lumped mass matrix is more convenient for computational purposes, the consistent mass matrix is more efficient than the lumped mass matrix because the latter does not take into account the effect of plate element rotation [**Cook**, **1995**][26].

5.4 Formulation of Damping Properties

In the analysis of dynamic problems, it is sometimes assumed that the amplitude of free vibration remains constant with time, but experience shows that the amplitude diminishes with time and that the vibration is gradually damped out.

To bring the vibration analysis into better agreement with reality, the Equation of motion for a discretized body or structure often must include a term to account for energy dissipation, i.e. damping forces. These forces may arise from several causes, such as friction, air or fluid resistance, internal friction due to imperfect elasticity of materials, and so on. Among all of these sources of energy dissipation, the case where the damping forces are proportional to velocity which is called viscous damping, is the simplest to deal with mathematically. For this reason resisting forces of a complicated nature are usually replaced, for purpose of analysis, by equivalent viscous damping [**Cook**, **1995**][26].

5.4.1 Effect of damping

In most cases the effect of damping on the response of a vibratory system is minor and thus, it can be ignored. However, for vibratory system with a periodic excitation and a frequency at or near the natural frequency, i.e. the resonance phenomena, damping will be of primary importance and must be taken into account.

Figure (5.1) shows the relationship between the magnification factor (β) which represents the ratio of dynamic response to static response (function of dynamic response of the system) as:

$$\beta = \frac{1.0}{\sqrt{\left[[1-(\frac{\Omega}{\omega})^2]^2 + [2\gamma\frac{\Omega}{\omega}]^2\right]}}$$

and the ratio (Ω/ω) which represents the ratio of the angular frequency (Ω) of a simple harmonic force function ($P_o \cos(\Omega t)$ or $P_o \sin(\Omega t)$) to the natural frequency of the system (ω) plotted for various levels of damping ratios (γ). So typical values of damping ratio (γ) range from about (0.02) for piping systems to about (0.07) for bolted structures and reinforced concrete. As for undamped case, the value of (β) is approximately unity for small values of (Ω/ω), and approaches zero for large values of (Ω/ω). However, as the value of (Ω) approaches (ω) (i.e. approaches unity), the magnification factor grows rapidly. Furthermore, the value of (β) at or near resonance is very sensitive to the amount of damping. Thus, while damping has only a minor effect when the system is remote from resonance, it has a dramatic effect at or near resonance. In structural dynamics the influence of damping is critical for this case and represents its most important application [**Cook**, **1995**][26].

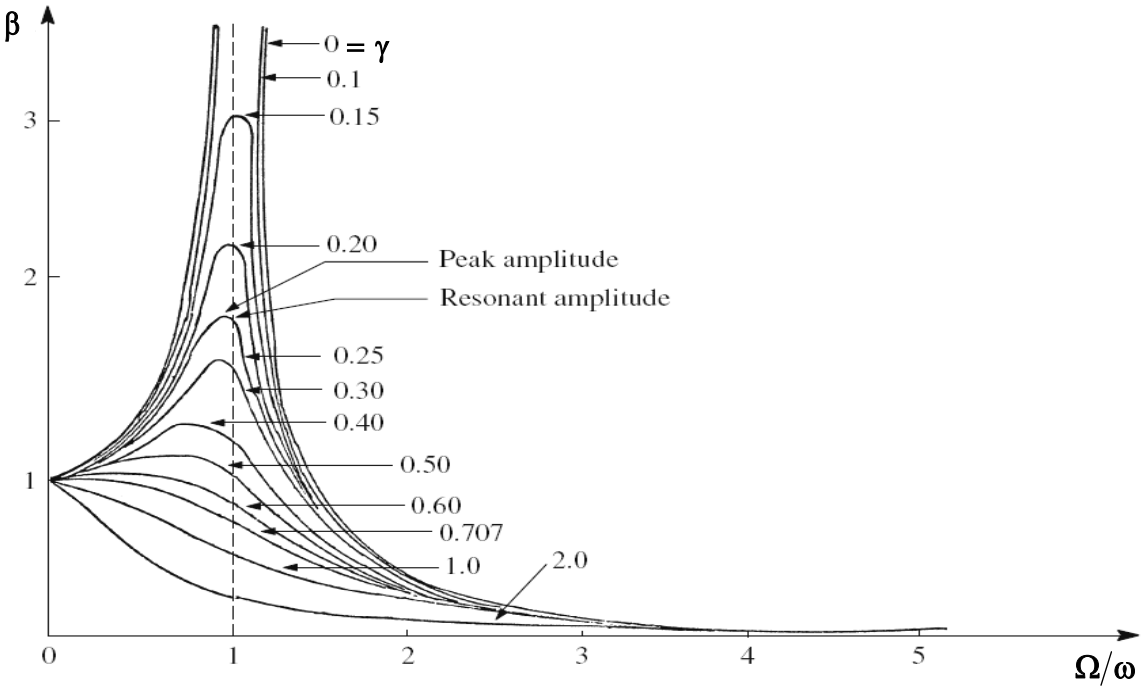

Figure (5.1): Effect of damping on the magnification factor [**Cook**, **1995**][26]

5.4.2 Damping matrix

With the present understanding in structures, it is not possible to formulate an explicit damping matrix for distributed damping throughout a structure, in a manner similar to that followed for the stiffness [$\boldsymbol{K}$] and mass [$\boldsymbol{M}$] matrices. In practice, damping is usually expressed in terms of damping ratios for each of the natural frequency modes. These ratios are established from experiments on similar structures. A number of alternative methods for generating the damping matrix [$\boldsymbol{C}$], however, exist and include discrete viscous damping and structural damping [**Cook**, **1995**][(26)].

The most common form for the representation of the damping matrix [$\boldsymbol{C}$] is the so-called Rayleigh-type damping [**Timoshenko** and **Gere**, **1961**][(107)] which was given as;

$$[C] = a_o[M] + a_1[K] \qquad \textbf{(5.24)}$$

in which (a_o and a_1) are arbitrary proportionality factors, which make the damping matrix satisfy the orthogonality condition with respect to the modal matrix [Φ] in the same way of the orthogonality conditions for the mass and stiffness matrices that is [**Bathe**, **1996**][(17)]:

$$\begin{aligned} \{\Phi\}^T[M]\{\Phi\} &= [I] \\ \{\Phi\}^T[K]\{\Phi\} &= [\Lambda] \\ \{\Phi\}^T[C]\{\Phi\} &= 2[\gamma][\Lambda]^{1/2} \end{aligned} \qquad \textbf{(5.25)}$$

where

$\{\Phi\}$: The modal matrix whose columns represent the natural modal shapes and the superscript ($\boldsymbol{T}$) denotes transpose.

$[I]$: Identity matrix.

$[\Lambda]$: Spectral matrix, which is a diagonal matrix with elements representing the squares of the natural frequencies (ω_i^2).

$[\gamma]$: Modal damping matrix which is also a diagonal matrix with elements representing the damping ratios for the system modes (γ_i)

Premultiplying Equation (5.24) by $\{\Phi\}^T$ and postmultiplying it by $\{\Phi\}$ yields:

$$\{\Phi\}^T[C]\{\Phi\} = a_o\{\Phi\}^T[M]\{\Phi\} + a_1\{\Phi\}^T[K]\{\Phi\} \quad \textbf{(5.26)}$$

Substituting Equations (5.25) into Equation (5.26) gives;

$$2[\gamma][\Lambda]^{1/2} = a_o[I] + a_1[\Lambda] \quad \textbf{(5.27)}$$

The two factors, a_o and a_1 can be determined by specifying the damping ratios for two modes for example 1 and 2, and substituting into Equation (5.27) as [**Pytet**, **1990**][89]:

$$2\gamma_1\omega_1 = a_o + a_1\omega_1^2 \quad \textbf{(5.28)}$$

$$2\gamma_2\omega_2 = a_o + a_1\omega_2^2 \quad \textbf{(5.29)}$$

where ω_1 and ω_2 are the natural frequencies for modes 1 and 2 respectively. By solving the above two Equations one can get:

$$a_o = \frac{2\omega_1\omega_2(\omega_2\gamma_1 - \omega_1\gamma_2)}{(\omega_2^2 - \omega_1^2)} \quad \textbf{(5.30)}$$

$$a_1 = \frac{2(\omega_2\gamma_2 - \omega_1\gamma_1)}{(\omega_2^2 - \omega_1^2)} \quad \textbf{(5.31)}$$

Then, the values of a_o and a_1 are substituted into Equation (5.24) to get the required damping matrix. Natural frequencies (ω_i) which are used in the Equations above are obtained from the solution of the eigenvalue problem for the undamped case [**Timoshenko** and **Gere**, **1961**][107]. As will be shown later, the corresponding damping ratios (γ_i) can be obtained by finding the damping ratio γ_1, related to the first mode of vibration, by using the field of a structure or from previous experience or even by assuming it within an acceptable range according to the type of the structure. With the value γ_1 on hand, other values (γ_i) can be extrapolated by using the approximate formula [**Ali**, **2004**][6]:

$$\gamma_i \approx \gamma_1\left(\frac{\omega_i}{\omega_1}\right)^{el} \quad ; (0.5 \le el \le 0.7) \quad \textbf{(5.32)}$$

Rewriting Equation (5.27) for an arbitrary mode (*i*), it gives:

$$2\gamma_i\omega_i = a_o + a_1\omega_1^2 \quad \textbf{(5.33)}$$

from which the damping ratio (γ_i) can be defined as:

$$\gamma_i = \frac{a_o + a_1 \omega_i^2}{2\omega_i} \qquad \textbf{(5.34)}$$

The relationship of Equation (5.34) between the natural frequency (ω_i) and the damping ratio (γ_i) is illustrated in Figure (5.2).

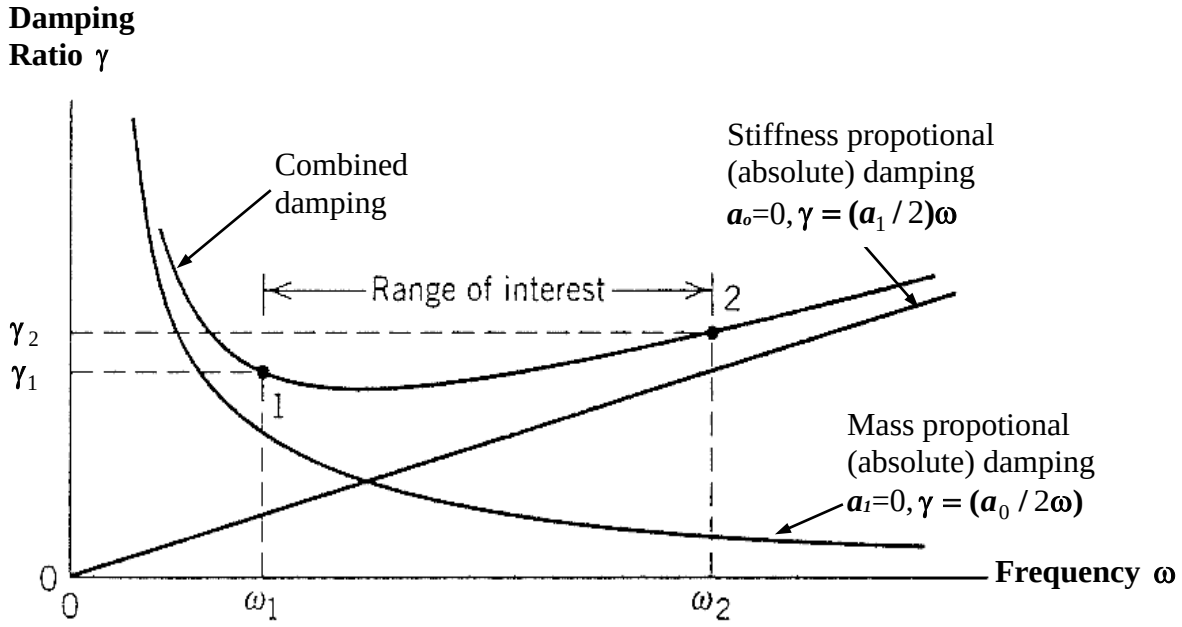

Figure (5.2): Relationship between damping ratio and frequency for Rayleigh damping [**Cook, 1995**][26]

5.5 Numerical Methods for Dynamic Analysis

5.5.1 Free vibration analysis

In the dynamic analysis, the natural frequency (ω) of the vibration is important to give an idea about the oscillation of the system with time, and to determine the natural period (T) of the vibration which represents the time for which the vibration repeats itself, where:

$$T = \frac{2\pi}{\omega} \qquad \textbf{(5.35)}$$

where ω is the natural circular (or angular) frequency.

In addition, the natural frequencies for more than one mode of vibration are used in constructing the damping matrix [C] as given previously.

To determine the natural frequencies of a structure, a free vibration problem (no external applied loads) for the undamped case is assumed:

$$[M]\{\ddot{d}\}+[K]\{d\}=\{0\} \qquad \textbf{(5.36)}$$

The problem of vibration analysis consists of determining the conditions under which Equation (5.36) will permit motions to occur.

Assuming harmonic motion:

$$\{d\}_i=\{y\}_i \sin(\omega_i t) \qquad (i=1,2,.....,n) \qquad \textbf{(5.37)}$$

where n is the number of D.O.F. in this harmonic expression, and $\{y\}_i$ is a vector of nodal amplitudes (the mode shape) for the i-th mode vibration. The symbol ω_i represents the angular frequency of mode i. When the second order derivative of Equation (5.37) is taken, the accelerations in free vibration are:

$$\{\ddot{d}\}_i=-\omega_i^2\{y\}_i \sin(\omega_i t) \qquad \textbf{(5.38)}$$

Substituting Equation (5.37) and (5.38) into Equation (5.36) gives:

$$\left([K]-\omega_i^2[M]\right)\{y\}_i=\{0\} \qquad \textbf{(5.39)}$$

From the theory of homogeneous Equations, nontrivial solution exists if the determinant of the coefficient matrix is equal zero. Thus,

$$\left|[K]-\omega_i^2[M]\right|=0 \qquad \textbf{(5.40)}$$

or

$$\left|[K_c]\right|=0 \qquad \textbf{(5.41)}$$

where

$$[K_c]=[K]-\omega_i^2[M] \qquad \textbf{(5.42)}$$

The symmetrical $n\times n$ matrix $[K_c]$ can be called the dynamic stiffness matrix of the finite degree system. Every element of $[K_c]$ is a linear function of ω^2.

Expansion of Equation (5.41) would give a polynomial of n called the characteristic Equation, whose roots yield the n natural frequencies of vibration of the system. It is known that since [K] and [M] are symmetrical and positive definite the n roots of the polynomial are all real

and positive, so that the natural frequencies are all real. Substitution of these roots (one at each time) into the homogeneous Equations (Equation (5.39)) produces the characteristic vectors, or eigen vectors $\{y\}_i$ within arbitrary constants.

A number of solution algorithms have been developed for the solution of the eigenvalue problem. However, only two techniques which are the most important will be presented here, namely the inverse iteration method and the matrix deflation method.

A- Inverse iteration method

This technique is very effective in calculating the smallest eigenvalue and the corresponding eigenvector, which are the most important eigen pair in structural dynamics.

The basic steps for solving the eigenvalue problem of the form ($[D]\{\Phi\} = \lambda[I]\{\Phi\}$) by using the inverse iteration method are [**Wang, 1966**][(115)]:

1- Computing the dynamic matrix [D] as follows:

$$[D] = [M]^{-1}[K] \qquad \textbf{(5.43)}$$

2- Assuming an initial trial vector $\{\Phi\}_1$ almost with all terms equal to 1.0.

3- Substituting the vector $\{\Phi\}_1$ in the following Equation:

$$\left([D] - \left(\frac{1}{\lambda}\right)[I]\right)\{\Phi\}_1 = 0 \qquad \textbf{(5.44)}$$

4- An approximate value of $(1/\lambda)$ is obtained by dividing the first element of the column matrix [D]{Φ}$_1$ by Φ_{11}, that is:

$$\lambda^1 = \frac{(\text{ First row of } D) \times \{\Phi\}_1}{\Phi_{11}} \qquad \textbf{(5.45)}$$

where Φ_{11} is the first element of the matrix $\{\Phi\}_1$.

5- The second approximate value of the characteristic vector $\{\Phi\}_1$ is obtained by:

$$\{\Phi\}_{approx} = \frac{[D]\{\Phi\}_1}{(1/\lambda)} \qquad \textbf{(5.46)}$$

These steps can be continued until the errors become sufficiently small where the used error criterion is the absolute differences, such that:

$$\varepsilon_r = \frac{\sum|\Phi_i - \Phi_{i-1}|}{\sum|\Phi_i|} \qquad \textbf{(5.47)}$$

B- Matrix deflation method

This method is used to determine any desired number of eigen pairs. Its technique is based on matrix deflation, that is, after finding the first eigen pair, (λ_1) and $\{\Phi\}_1$ by the inverse or any other iteration method, a new matrix has to be constructed from the original matrix by a deflation process in such a way that it contains only the remaining unknown eigenvalues of the original matrix.

To solve a generalized eigenvalue problem by this method it must first construct the deflation matrix $[B_{22}]$ of order (n-1) from the original matrix $[D]$ of order n. The following steps show the complete procedure of the present method [**Wang**, **1966**][(115)].

1- Forming the matrix $[B]$ such that

$$[B]=[T][D][T]^{-1} \qquad \textbf{(5.48)}$$

where [T] is a transformation matrix.

2- Partitioning $[B]$ matrix into:

$$[B]=\begin{bmatrix} b_{11} & B_{12} \\ 0 & B_{22} \end{bmatrix} \qquad \textbf{(5.49)}$$

3- Then the first eigenvalue of the matrix $[B]$ is the second eigenvalue (λ_2) of matrix $[D]$:

Then,

$$[C]=[B_{22}] \qquad \textbf{(5.50)}$$

In the above Equation, $[B]$ is a matrix that has the same eigenvalue as $[D]$, b_{11} is a single element equal to (λ_1), and $[B_{12}]$ is a row identical with the first row of matrix $[D]$ excluding the first element, while $[B_{22}]$ is a

matrix which possesses the eigenvalues $\lambda_1, \lambda_2, ..., \lambda_n$, also matrix $[T]$ that satisfies the requirement of Equation (5.48) is found to be:

$$[T]=\begin{bmatrix} 1 & 0 & . & . & . & 0 & 0 \\ \Phi_{12} & 1 & . & . & . & 0 & 0 \\ \Phi_{13} & 0 & . & . & . & . & 0 \\ . & . & . & . & . & . & . \\ . & . & . & . & . & . & . \\ . & . & . & . & . & 1 & . \\ \Phi_{1n} & 0 & . & . & . & . & 1 \end{bmatrix} \quad \textbf{(5.51)}$$

where the first column of matrix $[T]$ is the characteristic vector corresponding to the eigenvalue λ_1.

Also, the procedure to find the characteristic vector corresponding to λ_2 is as follows:

1- computing the characteristic vector $\{Y_2\}$ of $[B]$ matrix from the relationship:

$$[B]\{Y_2\}=\lambda_2\{Y_2\} \quad \textbf{(5.52)}$$

or

$$\begin{bmatrix} \lambda_1 & B_{12} \\ 0 & C \end{bmatrix}\begin{Bmatrix} y_{12} \\ Y_2^* \end{Bmatrix} = \lambda_2 \begin{Bmatrix} y_{12} \\ Y_2^* \end{Bmatrix} \quad \textbf{(5.53)}$$

2- then, the characteristic vector $\{\Phi\}_2$ of matrix $[D]$ can be obtained as:

$$\{\Phi\}_2 = [T]\{Y_2\} \quad \textbf{(5.54)}$$

In the above Equations, y_{12} is the first element of the characteristic vector $\{Y_2\}$, and $\{Y_2^*\}$ is the characteristic vector of matrix $[C]$, because $[C]\{Y_2^*\}=\lambda_2\{Y_2^*\}$. From Equation (5.52), one can find that:

$$\lambda_1 y_{12} + B_{12}\{Y_2^*\} = \lambda_2 y_{12} \quad \textbf{(5.55)}$$

Then,

$$y_{12} = -\frac{B_{12}\{Y_2^*\}}{\lambda_1 - \lambda_2} \quad \textbf{(5.56)}$$

The succeeding eigen pairs can be obtained in a way similar to the above procedures.

5.5.2 Forced vibration analysis

The dynamic equilibrium Equation, Equation (5.11) represents a system of linear differential Equations of second order and, in principle; the solution of the Equations can be obtained by standard procedures for the solution of differential Equations with constant coefficients. However, the procedures proposed for the solution of a general system of differential Equations become very expensive if the order of the matrices is large. In a practical finite element analysis, there are few effective methods. These are mainly, the direct time integration and the mode superposition. In the direct integration methods, the dynamic equilibrium Equations are integrated using a numerical step-by-step procedure. The term "direct" means that prior to the numerical integration, no transformation of the Equations into a different form is carried out [**Ali**, **2004**][(6)]. In essence, the direct numerical integration is based on two ideas. First, Equation (5.11) is satisfied at discrete time intervals (Δt) apart. The second idea is that a variation of displacements, velocities and accelerations within each time interval (Δt) is assumed. The available direct procedures can be further subdivided into implicit and explicit methods.

The implicit algorithms are more effective for structural dynamic problems. In the implicit method the response is controlled by a relatively small number of low frequency modes, while the explicit algorithms are very efficient for wave propagation problems, in which the contribution of intermediate and high frequency structural modes to the response is important [**Subbaraj** and **Dokainish**, **1989**][(102)].

The calculation of the nonlinear dynamic response of structure of structures including instability or buckling phenomena has received considerable attention and a good amount of literature has appeared on this subject. The nonlinear dynamic analysis depends largely on solving the following Equations:

$$[M]\{\ddot{d}(t)\}+[C]\{\dot{d}(t)\}+[K_T]\{d(t)\}=\{F(t)\} \qquad \textbf{(5.57)}$$

in which $[K_T]$ is the tangent stiffness matrix of the plate (or structure) and depends on the current displacements and stresses as derived in Chapter Four and takes into account the geometrical and the material nonlinearity. It is noted that the most efficient numerical methods for solving Equation (5.57) are the direct time integration methods (or step-by-step integration method). Any method for direct numerical integration of the differential Equations of motion may be visualized as some type of finite difference formulation. Clearly, artificial damping plays an important role in the numerical method, since the dynamic buckling load increases with an increase in artificial damping. It is also important that a time integration scheme be used that is stable and accurate, since otherwise buckling loads are predicted numerically but are physically nonexistent. In direct integration, the approach is to write the Equation of motion, Equation (5.57), at a specific instance of time:

$$[M]_n \{\ddot{d}(t)\}_n + [C]_n \{\dot{d}(t)\}_n + \{f\}_n = \{F(t)\}_n \qquad \textbf{(5.58)}$$

where

$$\{f\}_n = [K_T]_n \{d(t)\}_n \qquad \textbf{(5.59)}$$

and,

$\{f\}_n$: is the internal forces vector at time $n\Delta t$,
$[K_T]_n$: is the tangent stiffness matrix at time $n\Delta t$,
$\{d(t)\}_n$: is the displacement vector at time $n\Delta t$,
$\{\dot{d}(t)\}_n$: is the velocity vector at time $n\Delta t$,
$\{\ddot{d}(t)\}_n$: is the acceleration vector at time $n\Delta t$.

The subscript n denotes time level $n\Delta t$ and Δt is the size of the time increment or time step. It may be seen that all the terms in Equation (5.58) are time dependent; the damping matrix is also considered in the Equation. The most conventional implicit time integration procedures are **Newmark** method, and **Harmonic acceleration** method and these are considered in the present study.

5.5.2.1 Newmark method

This method is based on using the equilibrium conditions given by Equation (5.11) at time $(t+\Delta t)$ in order to calculate the displacements at this time. This method is also a modification of the linear acceleration method, as shown in Figure (5.3).

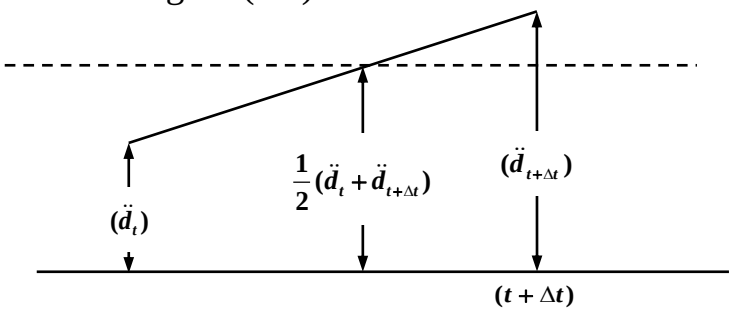

Figure (5.3) Newmark's constant-average acceleration scheme[**Rao**,**1968**][(90)]

The following Equations are used [**Newmark**, **1959**]:

$$\{\dot{d}\}_{t+\Delta t} = \{\dot{d}\}_t + \Delta t\left((1-\gamma)\{\ddot{d}\}_t + \gamma\{\ddot{d}\}_{t+\Delta t}\right) \qquad \textbf{(5.60)}$$

and,

$$\{d\}_{t+\Delta t} = \{d\}_t + \Delta t\{\dot{d}\}_t + (\Delta t)^2\left((\frac{1}{2}-\beta)\{\ddot{d}\}_t + \beta\{\ddot{d}\}_{t+\Delta t}\right) \qquad \textbf{(5.61)}$$

where β and γ parameters determine the stability and accuracy of the algorithm and Δt is the time interval.

To solve Equation (5.58) at time $(t+\Delta t)$ for displacements, velocities, and accelerations, the following procedure must be followed. First Equation (5.61) may be solved for $\{\ddot{d}\}_{t+\Delta t}$ in terms $\{d\}_{t+\Delta t}$ and $\{\dot{d}\}_{t+\Delta t}$ as:

$$\{\ddot{d}\}_{t+\Delta t} = a_o\left(\{d\}_{t+\Delta t} - \{d\}_t\right) - a_2\{\dot{d}\}_t - a_3\{\ddot{d}\}_t \qquad \textbf{(5.62)}$$

Substitution Equation (5.62) into Equation (5.60) yields:

$$\{\dot{d}\}_{t+\Delta t} = a_2\left(\{d\}_{t+\Delta t} - \{d\}_t\right) - a_4\{\dot{d}\}_t - a_5\{\ddot{d}\}_t \qquad \textbf{(5.63)}$$

where a_0 , a_2, a_3, a_4, and a_5 are defined later.

Substitution of Equation (5.62) into Equation (5.58) at time $(t+\Delta t)$ gives a system of simultaneous Equations which can be solved for $\{d\}_{t+\Delta t}$:

$$\begin{aligned}\left([K_T] + a_o[M] + a_1[C]\right)\{d\}_{t+\Delta t} = \{F(t)\}_{t+\Delta t} &+ [M]\left(a_2\{\dot{d}\}_t + a_3\{\ddot{d}\}_t\right) \\ &+ [C]\left(a_4\{\dot{d}\}_t + a_5\{\ddot{d}\}_t\right)\end{aligned} \qquad \textbf{(5.64)}$$

where $\boldsymbol{a}_1$ is defined later.

For convenience, the following is used:

$$[\boldsymbol{K}_T]_{eff} = [\boldsymbol{K}_T] + \boldsymbol{a}_o[\boldsymbol{M}] + \boldsymbol{a}_1[\boldsymbol{C}] \qquad \textbf{(5.65)}$$

and,

$$\{\boldsymbol{F}(\boldsymbol{t})\}_{eff} = \{\boldsymbol{F}(\boldsymbol{t})\}_{t+\Delta t} + [\boldsymbol{M}]\left(\boldsymbol{a}_2\{\dot{\boldsymbol{d}}\}_t + \boldsymbol{a}_3\{\ddot{\boldsymbol{d}}\}_t\right) + [\boldsymbol{C}]\left(\boldsymbol{a}_4\{\dot{\boldsymbol{d}}\}_t + \boldsymbol{a}_5\{\ddot{\boldsymbol{d}}\}_t\right) \qquad \textbf{(5.66)}$$

So, Equation (5.66) may be written in the form:

$$[\boldsymbol{K}_T]_{eff}\{\boldsymbol{d}\}_{t+\Delta t} = \{\boldsymbol{F}(\boldsymbol{t})\}_{eff} \qquad \textbf{(5.67)}$$

For a linear system, $[\boldsymbol{K}_T]_{eff}$ will be constant during the analysis at any time (see Chapter four), while in the nonlinear analysis, $[\boldsymbol{K}_T]_{eff}$ is a function of current displacement vector $\{\boldsymbol{d}\}$. Therefore, an iterative procedure must be used to define $[\boldsymbol{K}_T]_{eff}$. In the nonlinear analysis, it is more useful to put Equation (5.67) in increment form. For such purpose, Equation (5.67) may be rewritten as:

$$[\hat{\boldsymbol{K}}_T]\{\Delta\boldsymbol{d}\} = \{\Delta\hat{\boldsymbol{F}}(\boldsymbol{t})\} \qquad \textbf{(5.68)}$$

in which $[\hat{\boldsymbol{K}}_T]$ is the effective stiffness matrix and $\{\Delta\hat{\boldsymbol{F}}(\boldsymbol{t})\}$ is the effective load vector. Equation (5.68) is solved by an iterative procedure like Equation (5.64). It may be noted that Equation (5.64) may be used for solving linear problems, while for nonlinear problems, Equation (5.68) should be used.

Solving Equation (5.68) for $\{\Delta\boldsymbol{d}\}$, approximate values for accelerations, velocities and displacements may be given as:

$$\begin{aligned}
\{\ddot{\boldsymbol{d}}\}_{t+\Delta t} &= \boldsymbol{a}_o\{\Delta\boldsymbol{d}\} - \boldsymbol{a}_2\{\dot{\boldsymbol{d}}\}_t - \boldsymbol{a}_3\{\ddot{\boldsymbol{d}}\}_t \\
\{\dot{\boldsymbol{d}}\}_{t+\Delta t} &= \boldsymbol{a}_1\{\Delta\boldsymbol{d}\} - \boldsymbol{a}_4\{\dot{\boldsymbol{d}}\}_t - \boldsymbol{a}_5\{\ddot{\boldsymbol{d}}\}_t \\
\{\boldsymbol{d}\}_{t+\Delta t} &= \{\boldsymbol{d}\}_t + \{\Delta\boldsymbol{d}\}\ ;
\end{aligned} \qquad \textbf{(5.69)}$$

where

$$\boldsymbol{a}_o = \frac{1}{\beta(\Delta t)^2},\ \boldsymbol{a}_1 = \frac{\gamma}{\beta(\Delta t)},\ \boldsymbol{a}_2 = \frac{1}{\beta(\Delta t)},\ \boldsymbol{a}_3 = \frac{1}{2\beta} - 1$$

$$\boldsymbol{a}_4 = \frac{\gamma}{\beta} - 1,\ \boldsymbol{a}_5 = \frac{\Delta t}{2}\left(\frac{\gamma}{\beta} - 2\right)$$

5.5.2.2 Stability aspects

The two factors γ and β used in **Newmark** method have great effect on the stability and accuracy of the method. The method is unconditionally stable if [**Subbraj** and **Dokainish**, **1989**][102]:

$$\gamma \geq 0.5 \qquad \textbf{(5.70)}$$

and,

$$\beta \geq \frac{(1+2\gamma)}{16} \qquad \textbf{(5.71)}$$

These conditions assure that the diagonal elements of stiffness matrix are positive (positivity condition). The parameter γ, used in Equation (5.60), produces positive logarithmic damping with time step Δt if $\gamma > 0.5$ and negative logarithmic damping eventually to an unbounded response if $\gamma < 0.5$. Thus in most applications, $\gamma = 0.5$ is used in Equation (5.60) to follow becomes the trapezoidal rule.

The parameter β in Equation (5.61) controls the variation of acceleration within the time step Δt. For this reason the technique is referred to as Newmark's generalized acceleration method (or Newmark β-method).

The time step must be chosen to satisfy the accuracy and the algorithmic stability requirements of the analysis. The possible errors in amplitude and in the period time of each method of Newmark's family were considered by a number of researchers. A summary of algorithmic stability for the Newmark method [**Subbraj** and **Dokainish**, **1989**][102] will be given:

The method is unconditionally stable when

$$2\beta \geq \gamma \geq 0.5 \qquad \textbf{(5.72)}$$

and conditionally stable when

$$\gamma \geq 0.5$$

$$\beta < \frac{\gamma}{2} \qquad \textbf{(5.73)}$$

$$\omega \Delta t \geq \Omega_{cr}$$

where ω is the undamping frequency of vibration and Ω_{cr} for undamping system may be given by

$$\Omega_{cr} = \frac{1}{\sqrt{0.5\gamma - \beta}} \qquad \textbf{(5.74)}$$

The use of γ greater than 0.5 introduces spurious damping which can be used to good advantage in suppressing the undesirable higher modes with highly erroneous time periods caused by discretization of continuous systems coupled with the use of large time step. The amount of this artificial viscosity to be introduced into the solution can be controlled through choice of (δ) parameter, i.e.

$$\gamma = 0.5 + \delta$$

where δ is a positive value. It has been shown that the free parameter β shall be chosen such that[**Nagarajan** and **Popov**,**1975**][(73)]:

$$\beta \geq 0.25(1+\delta)^2$$

in order to preserve unconditional stability for linear analyses.

5.5.2.3 Harmonic acceleration method

A recent method for the step-by-step direct integration of the dynamic Equations of motion has been adopted. In this method a harmonic relationship for the acceleration time is assumed, as shown in Figure (5.4).

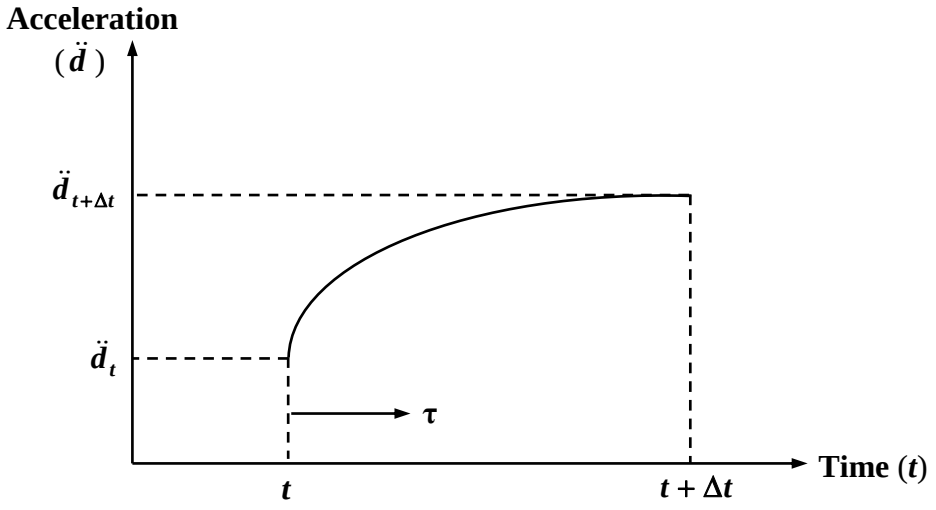

Figure (5.4): Harmonic variation of acceleration during time interval[(30)]

The actual response of linear or nonlinear systems has a harmonic relation with time, while in the linear acceleration method; a cubic time-displacement relation is obtained.

The basic Equation for the assumed harmonic acceleration at any time (τ) where ($t < \tau < t + \Delta t$)[30]:

$$\ddot{d}_t = A\sin(\omega(\tau - t) + B) \qquad \textbf{(5.75)}$$

where A and B are constants, and ω is the frequency of the system.

The coefficients A and B can be found by applying the boundary conditions:

$$\begin{aligned} &1\text{- at } \tau = t \quad , \ddot{d}_\tau = \ddot{d}_t \\ &2\text{- at } \tau = t + \Delta t \ , \ddot{d}_\tau = \ddot{d}_t + \Delta\ddot{d}_t \end{aligned} \qquad \textbf{(5.76)}$$

Substituting Equations (5.76) into Equation (5.75) and solving for A and B, yields:

$$\tan(B) = \frac{\ddot{d}_t \sin(\omega\Delta t)}{\left[\ddot{d}_t + \Delta\ddot{d}_t - \ddot{d}_t \cos(\omega\Delta t)\right]} \qquad \textbf{(5.77)}$$

and,

$$A = \frac{\ddot{d}_t}{\sin(B)} \qquad \textbf{(5.78)}$$

Now, integrating Equation (5.75) twice between the limits (t) and (τ), yields:

$$\dot{d}_\tau = \dot{d}_t - \frac{A}{\omega}\left[\cos(\omega(\tau - t) + B) - \cos(B)\right] \qquad \textbf{(5.79)}$$

and,

$$d_\tau = d_t + \dot{d}_t(\tau - t) - \frac{A}{\omega}\left[\frac{1}{\omega}\sin(\omega(\tau - t) + B) - \frac{1}{\omega}\sin(B) - (\tau - t)\cos(B)\right] \qquad \textbf{(5.80)}$$

Then, the evaluation of Equations (5.79) and (5.80) at time $(t + \Delta t)$, gives:

$$\Delta\dot{d}_t = -\frac{A}{\omega}\left[\cos(\omega\Delta t + B) - \cos(B)\right] \qquad \textbf{(5.81)}$$

and,

$$\Delta d_t = \dot{d}_t\Delta t - \frac{A}{\omega}\left[\frac{1}{\omega}\sin(\omega\Delta t + B) - \frac{1}{\omega}\sin(B) - \Delta t.\cos(B)\right] \qquad \textbf{(5.82)}$$

Making use of Equations (5.77) and (5.79) with Equations (5.81) and (5.82), gives:

$$\Delta\dot{d}_t = -\left(\frac{2\ddot{d}_t + \Delta\ddot{d}_t}{\omega}\right)\left(\frac{\cos(\omega\Delta t) - 1}{\sin(\omega\Delta t)}\right) \qquad \textbf{(5.83)}$$

$$\Delta d_t = \dot{d}_t \Delta t - \left(\frac{\Delta t\, \ddot{d}_t}{\omega}\right)\left(\frac{\cos(\omega \Delta t)-1}{\sin(\omega \Delta t)}\right) - \left(\frac{\Delta \ddot{d}_t}{\omega^2} - \frac{\Delta t\, \Delta \ddot{d}_t}{\omega \sin(\omega \Delta t)}\right) \quad \textbf{(5.84)}$$

For simplicity, the following will be defined:

$$a_o = \frac{1}{\omega^2} - \frac{\Delta t}{\omega \sin(\omega \Delta t)}$$
$$a_1 = \frac{\Delta t \cos(\omega \Delta t) - \Delta t}{\omega \sin(\omega \Delta t)} \quad \textbf{(5.85)}$$

Substituting Equation (5.85) into Equations (5.83) and (5.84), yields after using a matrix form:

$$\{\Delta \dot{d}\}_t = -\frac{a_1}{\Delta t}\left(2\{\ddot{d}\}_t + \{\Delta \ddot{d}\}_t\right) \quad \textbf{(5.86)}$$

$$\{\Delta d\}_t = \{\dot{d}\}_t \Delta t - a_1\{\ddot{d}\}_t - a_o\{\Delta \ddot{d}\}_t \quad \textbf{(5.87)}$$

5.5.3 Algorithm solution of nonlinear dynamic analysis

The nonlinear dynamic analysis of plates which takes into account the nonlinearity of geometry and material is considered in this study. The Newmark and Harmonic acceleration methods are utilized in the present study. The illustrated procedure of the solution will explain for Harmonic acceleration method (H.A.M.), and the same procedure is used for another method.

1- Solving the Equations of acceleration and velocity vectors at time $(t + \Delta t)$ for $\{\Delta \ddot{d}\}_t$ and $\{\Delta \dot{d}\}_t$ respectively in terms of $\{\Delta d\}_t$. For (H.A.M.) solving Equation (5.87) for $\{\Delta \ddot{d}\}_t$ and substituting into Equation (5.86), to yield:

$$\{\Delta \ddot{d}\}_t = \frac{1}{a_o}\left(-\{\Delta d\}_t + \Delta t\{\dot{d}\}_t - a_1\{\ddot{d}\}_t\right) \quad \textbf{(5.88)}$$

$$\{\Delta \dot{d}\}_t = \frac{a_1}{\Delta t\, a_o}\left((a_1 - 2a_o)\{\Delta d\}_t + \{\Delta d\}_t - \Delta t\{\dot{d}\}_t\right) \quad \textbf{(5.89)}$$

2- Rewriting the basic Equation of motion, Equation (5.58), at time $(t + \Delta t)$

$$[M]_{t+\Delta t}\{\ddot{d}\}_{t+\Delta t} + [C]_{t+\Delta t}\{\dot{d}\}_{t+\Delta t} + [K_T]\{d\}_{t+\Delta t} = \{F(t)\}_{t+\Delta t} \quad \textbf{(5.90)}$$

This can be written in other form:

$$[M]_{t+\Delta t}\left(\{\ddot{d}\}_t + \{\Delta \ddot{d}\}_t\right) + [C]_{t+\Delta t}\left(\{\dot{d}\}_t + \{\Delta \dot{d}\}_t\right) + [K_T]\left(\{d\}_t + \{\Delta d\}_t\right) = \{F(t)\}_{t+\Delta t}$$

3- Substituting $\{\Delta \ddot{d}\}_t$ and $\{\Delta \dot{d}\}_t$ evaluated in step 1 into the basic Equation of motion. For (H.A.M.), substituting Equations (5.88) and (5.89) into Equation (5.91) to give a system of simultaneous Equations which can be solved for $\{\Delta d\}_t$:

$$\left[a_o[K_T]_{t+\Delta t}-[M]_{t+\Delta t}+\frac{a_1}{\Delta t}[C]_{t+\Delta t}\right]\{\Delta d\}_t = a_o\{F(t)\}_{t+\Delta t}-a_o[K_T]_{t+\Delta t}\{d\}_t$$
$$-[C]_{t+\Delta t}\left[(a_o-a_1)\{\dot{d}\}_t+\frac{a_1}{\Delta t}(2a_1-a_o)\{\ddot{d}\}_t\right] \qquad \textbf{(5.92)}$$
$$-[M]_{t+\Delta t}\left[\Delta t\{\dot{d}\}_t+(a_o-a_1)\{\ddot{d}\}_t\right]$$

At the beginning of the analysis, the matrices $[K_T]_{t+\Delta t}$, $[C]_{t+\Delta t}$, and $[M]_{t+\Delta t}$ may be taken at the time (t) as an approximation, and for convenience Equation (5.92) may be written in the form:

$$[K_T]_{eff}\{\Delta d\}_t = \{\Delta F\}_{eff} \qquad \textbf{(5.93)}$$

in which $[K_T]_{eff}$ is the effective stiffness matrix which is defined as:

$$[K_T]_{eff} = \left[a_o[K_T]-[M]+\frac{a_1}{\Delta t}[C]\right] \qquad \textbf{(5.94)}$$

and $\{\Delta F\}_{eff}$ is the effective load vector which after making use of Equation (5.58) is defined as:

$$\{\Delta F\}_{eff} = a_o\{F(t)\}-a_o\{f\}-[C]_{t+\Delta t}\left[(a_o-a_1)\{\dot{d}\}_t+\frac{a_1}{\Delta t}(2a_1-a_o)\{\ddot{d}\}_t\right] \qquad \textbf{(5.95)}$$
$$-[M]_{t+\Delta t}\left[\Delta t\{\dot{d}\}_t+(a_o-a_1)\{\ddot{d}\}_t\right]$$

In linear analysis, $[K_T]_{eff}$ will be constant during the analysis at any time, while in nonlinear analysis, $[K_T]_{eff}$ is a function of displacement vector $\{d\}$. Therefore, an iterative procedure must be used to define $[K_T]_{eff}$.

4- Solving the effective Equation and computing the total values of displacement, velocity and acceleration vectors.

For (H.A.M.), solving Equation (5.91) for $\{\Delta d\}_t$, approximate values for acceleration and velocity increments can be obtained from Equations (5.86) and (5.87) and the total values for displacement, velocity and acceleration vectors can be found from:

$$\begin{aligned}\{d\}_{t+\Delta t} &= \{d\}_t+\{\Delta d\}_t\\ \{\dot{d}\}_{t+\Delta t} &= \{\dot{d}\}_t+\{\Delta \dot{d}\}_t\\ \{\ddot{d}\}_{t+\Delta t} &= \{\ddot{d}\}_t+\{\Delta \ddot{d}\}_t\end{aligned} \qquad \textbf{(5.96)}$$

The approximate solution above is then improved step-by step by using an iterative process until the out-of-balance forces become negligible and the equilibrium is satisfied to a prescribed tolerance.

5- Determining the unbalanced joint forces.

For (H.A.M), the unbalanced joint force vector, $\{\Delta Q\}_j$, during the j-th cycle of iteration can be calculated from Equation (5.65) as:

$$\{\Delta Q\}_j = \{F(t)\}_{t+\Delta t} - [M]_j \{\ddot{d}\}_t - [C]_j \{\dot{d}\}_t - \{f\}_j \quad \textbf{(5.97)}$$

6- Determining the corrections that $\{\Delta Q\}_j$ implies for $\{\Delta d\}_t$, $\{\Delta \dot{d}\}_t$, and $\{\Delta \ddot{d}\}_t$, respectively.

Assuming that $\{\Delta\Delta d\}_t$, $\{\Delta\Delta \dot{d}\}_t$, and $\{\Delta\Delta \ddot{d}\}_t$ denote the corrections that $\{\Delta Q\}_j$ implies for $\{\Delta d\}_t$, $\{\Delta \dot{d}\}_t$, and $\{\Delta \ddot{d}\}_t$ respectively, then (also for H.A.M.) from Equations (5.88) and (5.89):

$$\{\Delta\Delta \ddot{d}\}_j = \frac{-1}{a_o}\{\Delta\Delta d\}_j$$
$$\{\Delta\Delta \dot{d}\}_j = \frac{a_1}{a_o \Delta t}\{\Delta\Delta d\}_j \quad \textbf{(5.98)}$$

and from Equation (5.91)

$$[M]_j \{\Delta\Delta \ddot{d}\}_j + [C]_j \{\Delta\Delta \dot{d}\}_j + [K_T]_j \{\Delta\Delta d\}_j = \{\Delta Q\}_j \quad \textbf{(5.99)}$$

Substituting Equations (5.98) into Equation (5.99), yields:

$$\left[-[M]_j + \frac{a_1}{\Delta t}[C]_j + a_o [K_T]_j\right]\{\Delta\Delta d\}_j = a_o \{\Delta Q\}_j \quad \textbf{(5.100)}$$

or, in other form:

$$[\hat{K}]_{eff} \{\Delta\Delta d\}_j = a_o \{\Delta Q\}_j \quad \textbf{(5.101)}$$

After solving Equation (5.101) for $\{\Delta\Delta d\}_t$ and computing $\{\Delta\Delta \dot{d}\}_t$, and $\{\Delta\Delta \ddot{d}\}_t$ from Equations (5.98), new approximate values for the displacement, velocity and acceleration vectors may be obtained.

7- Adding the correction vectors:

$$\{\Delta d\}_j = \{\Delta d\}_{j-1} + \{\Delta\Delta d\}_j$$
$$\{\Delta \dot{d}\}_j = \{\Delta \dot{d}\}_{j-1} + \{\Delta\Delta \dot{d}\}_j \quad \textbf{(5.102)}$$
$$\{\Delta \ddot{d}\}_j = \{\Delta \ddot{d}\}_{j-1} + \{\Delta\Delta \ddot{d}\}_j$$

This process is continued until the residual forces, $\{\Delta Q\}_j$ computed from Equation (5.97) becomes too small, thus convergence occurs.

8- Checking the tolerance, if convergence does not occur, then going to step 5, otherwise going to 3.

5.6 Properties and Abilities of the Program

The computer program (FENSDAAP)(Finite element nonlinear static and dynamic analysis of anisotropic plate) is designed to deal with large displacement elastic and elastic-plastic post-buckling analysis of plates with inclusion of transverse shear effect and with different boundary conditions and subjected to static and dynamic loads. The properties and abilities of this program may be summarized as follows:

1- Static (or dynamic) analysis with geometrical and material nonlinearities.
2- Nonlinear analysis by incremental-iterative method using either N-R or modified N-R method for iteration process.
3- Using two different types of mass representation, consistent and lumped mass matrix.
4- Including damping properties by using the Rayleigh type damping. The program includes updating the damping matrix after each incremental load in the large displacement analysis of plates.
5- Solving the eigenvalue problem using the matrix deflation with the inverse iteration method to determine any desired number of system's natural frequencies.
6- Using different time-integration methods for dynamic analysis, which are the Newmark family and the harmonic acceleration method.
7- Using an iteration process in the dynamic part of analysis to obtain the dynamic equilibrium. The methods used for the iteration process are the conventional and the modified N-R methods.
8- Using different types of elements; four-node element, eight-node element, and nine-node element.
9- Using different types of degrees of freedom per node as (five degrees of freedom, seven degrees of freedom, and nine degrees of freedom).
10- The possibility to analyze plates with different end conditions by introducing the degrees of freedom for any type of end condition.
11- Using different types of initial curvature in the analysis of plates.
12- Using two types of fibers (straight fibers and sine wave fibers), and sine wave fibers can have different amplitudes and different modes.

5.7 Structure of the Program

The FENSDAAP computer program is coded in FORTRAN 90 language executed by PC Pentium IV 2800 MHz full cache Intel processor compatible computer with 512 MB RAM. The structure chart of this program is shown in Figure (5.5).

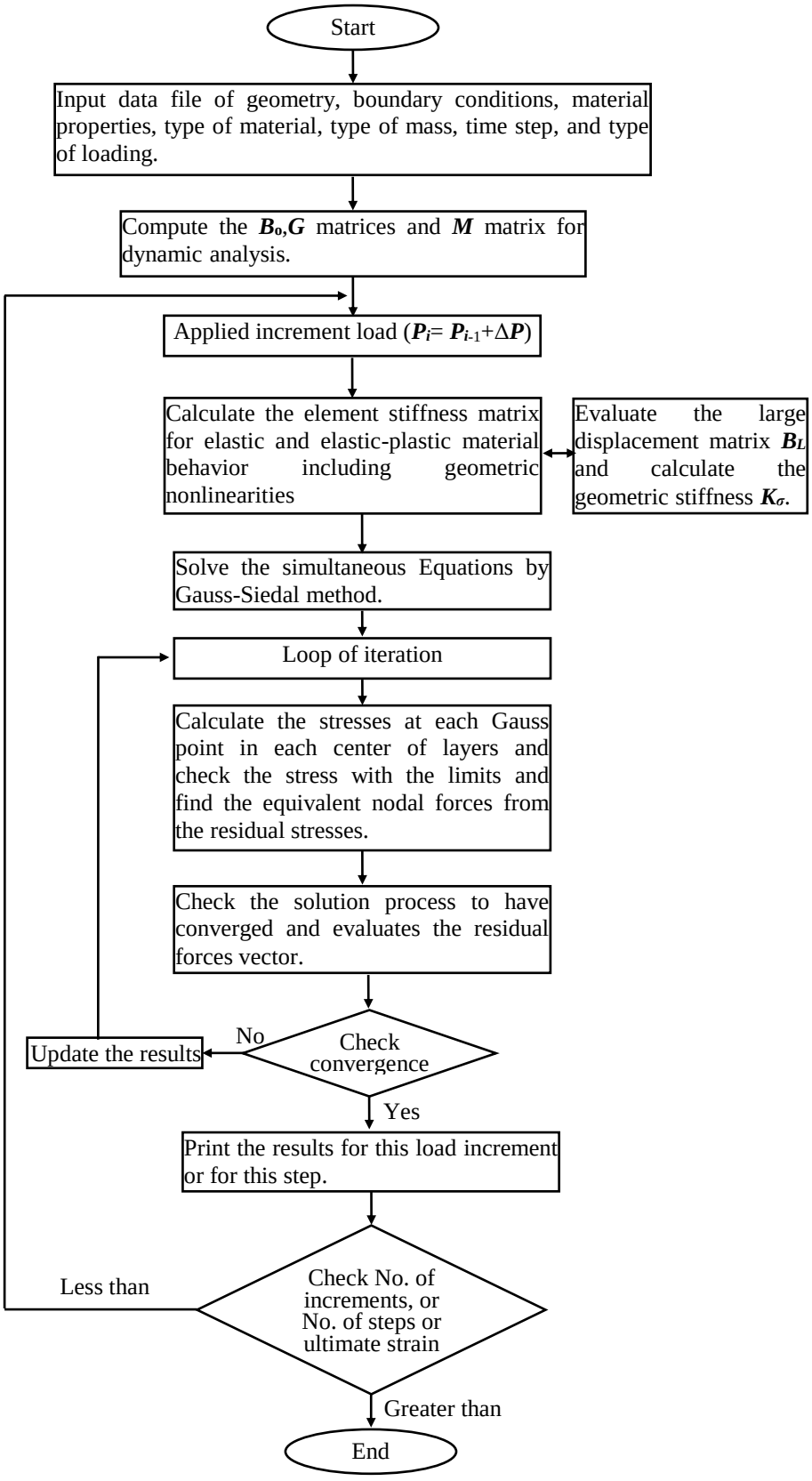

Figure (5.5): Structure chart of computer program (FENSDAAP) for static analysis

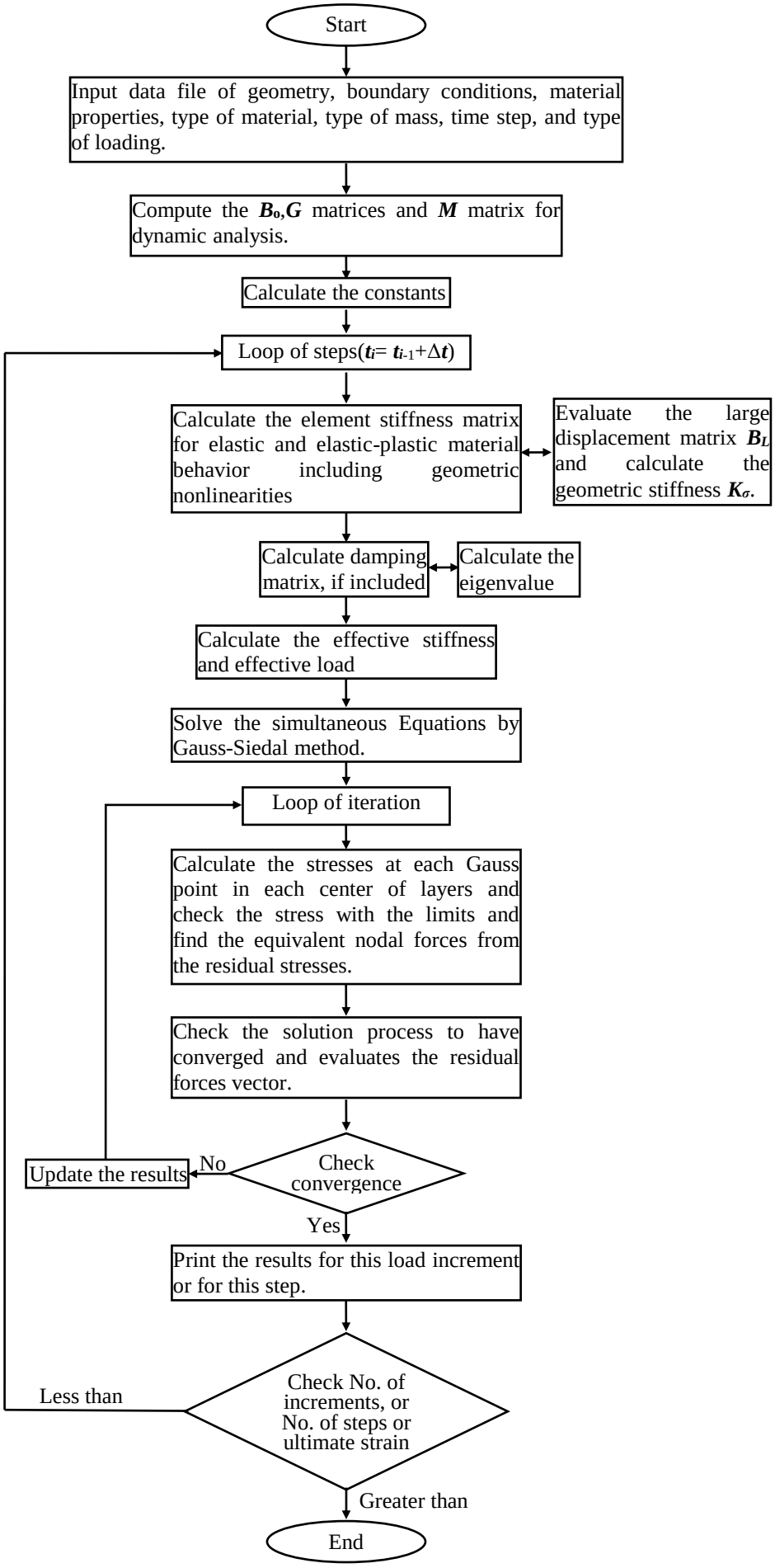

Figure (5.5): Structure chart of computer program (FENSDAAP) for dynamic analysis

CHAPTER SIX

Applications and Discussions on Nonlinear Static Analysis

6.1 General

This chapter deals with the large displacement elastic-plastic static analysis of anisotropic plates under in-plane compressive load by using the isoparametric Lagrangian nine-node finite elements. Several effects were considered such as: slenderness ratio, aspect ratio, initial imperfection, boundary conditions, number of layers, number of degrees of freedom per node, type of fiber (straight fibers or sine wave fibers) in the study of the large displacement elastic-plastic analysis of rectangular plates.

The analysis is carried out into two categories:

1. Studying the large displacement elastic-plastic behavior of steel plates under in-plane compressive load with different boundary conditions, different aspect ratios, different slenderness ratios, and various initial imperfections. Non-dimensional relationships of load-deflection curves for the out-of-plane displacements and also ultimate strength-slenderness ratio curves are presented.
2. Studying the large displacement elastic-plastic behavior of composite laminated plates under in-plane compressive load with different slenderness ratios, different initial imperfections, different orthotropy ratios, direction of in-plane compressive load, and two types of fibers (straight fibers or sine wave fibers). Non-dimensional relationships of load -deflection curves for the out-of-plane displacements and also ultimate strength-slenderness ratio curves are introduced.

6.2 Numerical Examples

In order to verify the reliability of the adopted numerical method, some case studies reported by other researchers are utilized. The study of the steel plate and then the study of the composite plate will be introduced.

6.2.1 Convergence study

At first, in order to select the more suitable mesh, number of layers, and number of degrees of freedom per node, the following convergence study is carried out.

6.2.1.1 Mesh size

The finite element equations are solved for a given value of load and amplitude of initial imperfection, using the successive iteration method. The rate of convergence depends on the mesh size and on the time consumption in the analysis. The mesh effect and time consumption has been investigated for a square simply supported plate under in-plane compressive load. The material properties of the analyzed plate are (E=210 GPa, v=0.3, a=b=1.0 m, h=0.01 m, w_o/h=0.00 (no initial imperfection)). Nine-node elements and two layers through thickness are used in the analysis of this plate. Table (6.1) gives a measure of convergence as a function of mesh size, CPU, and amount of error. **Yamaki**[120] used Fourier series to solve the present problem and the exact solution is (w/h=1.038) .

Figure (6.1) presents the percentage of error in maximum deflection versus the number of elements. It can be seen that (4×4) mesh of a full plate more suitable from the accuracy and the CPU so that it is considered.

Table (6.1): Finite element solution for a square simply supported plate subjected to in-plane compressive load, ($P_x/P_{cr}=1.38$, $w_o/h=0$)

Mesh size for (full plate)	Max. Def. (w/h)	Error %	CPU (sec)
2×2	1.167	12.42	76.94
3×3	1.065	2.600	225.62
4×4	1.048	0.960	433.67
5×5	1.043	0.482	994.73
6×6	1.041	0.290	1437.54

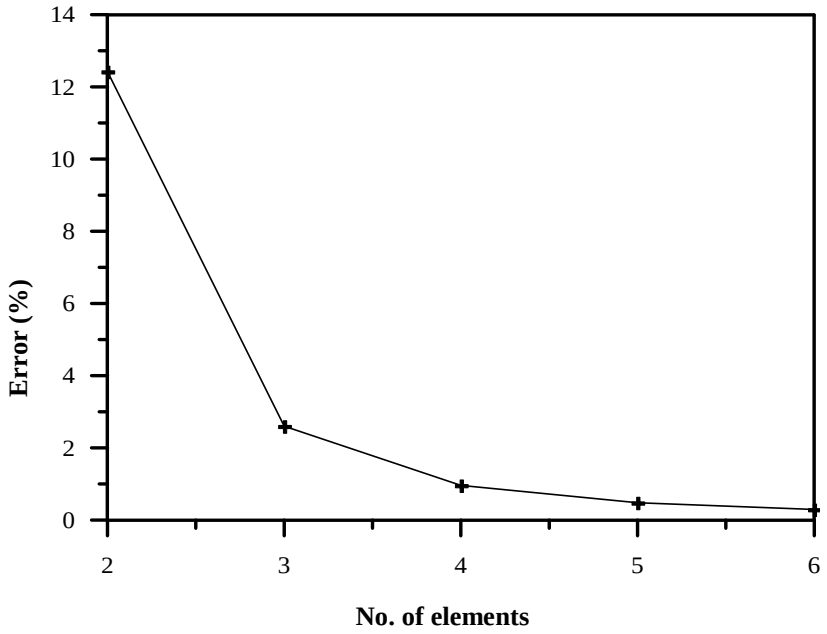

Figure (6.1): Convergence tests for simply supported square plate under in-plane compressive load

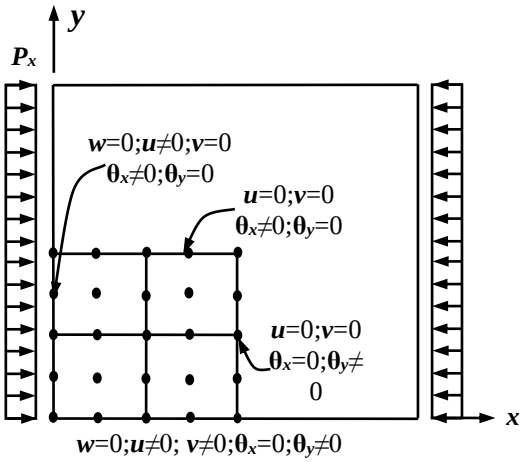

Figure (6.2): Finite element mesh and boundary condition for the quarter of the plate

6.2.1.2 Number of layers

To investigate the behavior of the simply supported square thin plate under in-plane loading up to the ultimate strength, the effect of the number of layers was studied.

Figure (6.3) shows the load-deflection curve of the simply supported plate obtained by using (2×2) mesh for the quarter plate and different number of layers (2-10) layers. This figure reveals the finite element results obtained by the nine-node isoparametric Lagrangian

elements. From this plate, the predicted ultimate load is (1397.5kN/m,1303 kN/m,1289 kN/m,1288 kN/m,1287 kN/m) for 2, 4, 6, 8, and 10 layers respectively. From this figure one can select the six layers where this number of layers gives good stability of results and suitable consumption time. In this example, the material properties of the analyzed plate are (E=200 GPa, v=0.3, a=b=1.0 m, h=0.01 m, w_o/h=0.01, yield stress σ_o= 250 MPa)

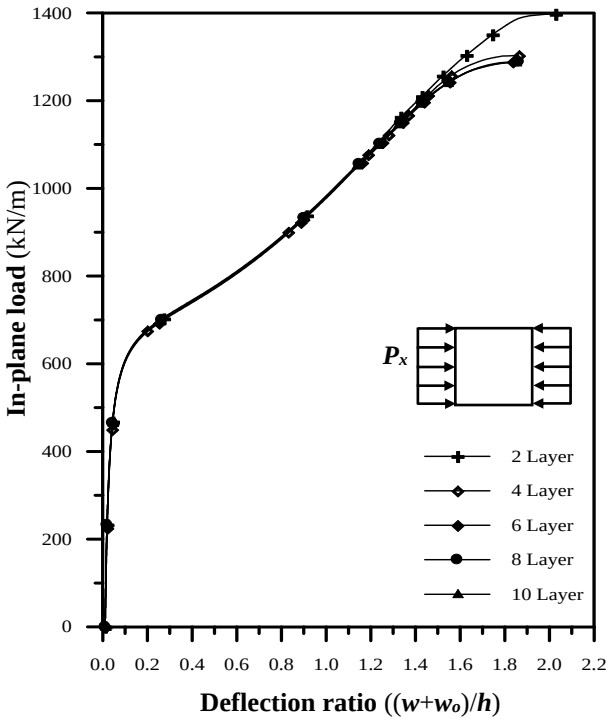

Figure (6.3): Effect of number of layers on the large displacement elastic-plastic analysis a square simply supported plate under in-plane compressive load

6.2.1.3 Number of degrees of freedom (per node)

The effect of the number of degrees of freedom per node (NDOF) was studied in order to select the more suitable number.

Figure (6.4) shows the load-deflection curve of a simply supported plate as was obtained by using different NDOF (5, 7, and 9) degrees. The numerical analysis was obtained by using the nine-node isoparametric Lagrangian element. The quarter of the plate is divided into (2×2) mesh and the thickness is divided into six layers. The plate has initial imperfection (w_o/h) of (0.1) by which the initial shape is considered to be

a sinusoidal curve. The geometry and material properties of analyzing this plate are (***E***=200 GPa, ***v***=0.3, ***a***=***b***=1.0 m, ***h***=0.05 m, ***b***/***h***=20). From this figure, one can select the five degrees of freedom where this number of degrees gives a difference from the nine degrees of freedom not more than (3%) and it is sufficient to give good stability of results and suitable consumption time.

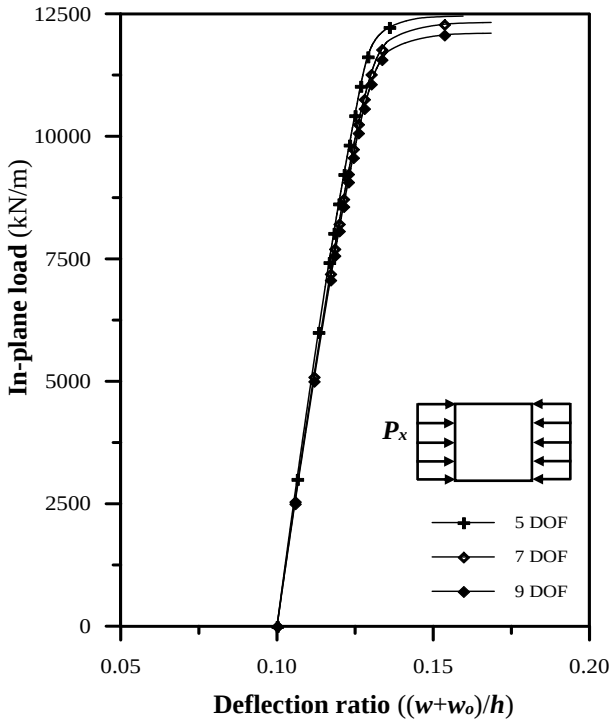

Figure (6.4): Effect of number of degrees of freedom on the large displacement elastic-plastic analysis of rectangular steel plate under in-plane compressive load

6.2.2 Comparison with experimental investigation of steel plate

a- Simply supported rectangular plate under in-plane loading (with *a*/*b*=2.0)

The accuracy of the results of the present analysis of real panels is checked through comparing with the experimental and numerical results studied by **Mirambell**, **et al.** [**1994**][(67)] on simply supported panels and with the others studied by **Amash**[**2003**][(11)].

The properties of specimen are given in Figure (6.5). The numerical analysis of **Mirambell**, **et al.** is based on the displacement

formulation of the finite element method for the nonlinear analysis of general steel shell structures and they divided the full plate into (4×4) by using nine-node Ahmed shell element, while, **Amash**'s numerical analysis was based on the finite difference method and he divided the full plate into (24×12) divisions and five layers through thickness.

In the present study, this plate is analyzed by using isoparametric Lagrangian nine-node elements with five degrees of freedom per node and the quarter of the plate is divided into (2×2) mesh and the thickness is divided into six layers.

Figure (6.6) shows a comparison with the experimental and the numerical results for the out-of-plane displacements. The results obtained from the present study give good agreement with the experimental and theoretical results obtained by **Mirambell**, **et al.** and by **Amash** with difference not more than (16%) with the experimental investigation. On the other hand, the present results are closer to that based on experimental investigation of **Mirambell**, **et al.[1994]**(67). The load-deflection results are listed in Table (6.2).

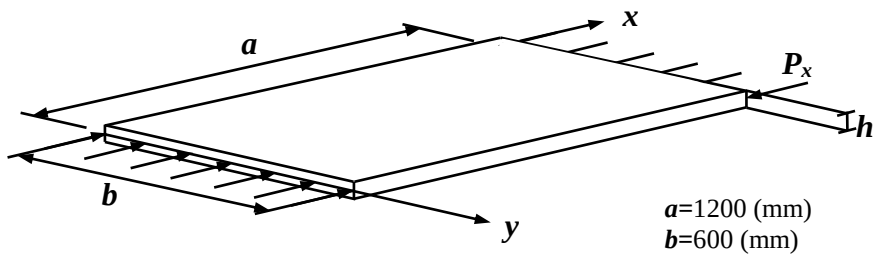

a=1200 (mm)
b=600 (mm)
h=3 (mm)
E= 210000 MPa
v= 0.3
w_o=1.92 sin (2π ***x***/***a***) sin (π ***y***/***b***)
σ_o=250 MPa (yield stress)

Figure (6.5): Details of a rectangular simply supported thin steel plate under in-plane compressive load with aspect ratio (***a/b***=2.0)

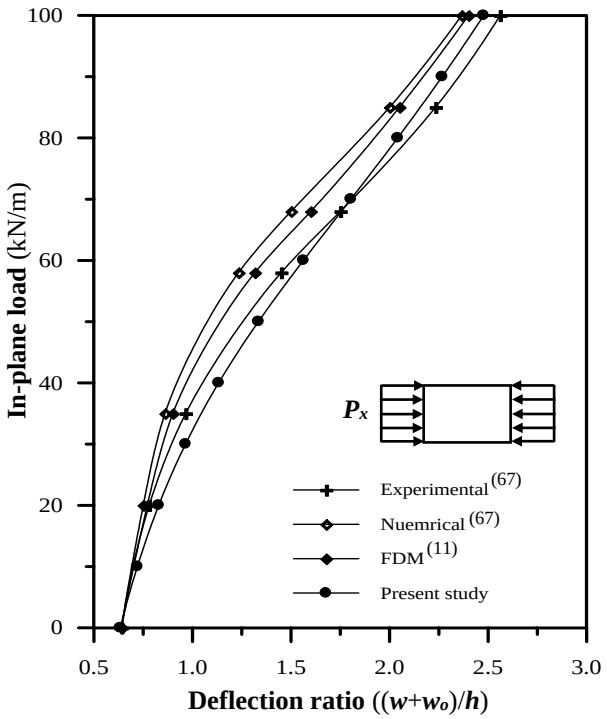

Figure (6.6): Post-buckling behavior of a rectangular simply supported thin steel plate under in-plane compressive load with aspect ratio (***a/b***=2.0)

Table (6.2): Comparison of results with experimental and theoretical studies of a rectangular simply supported thin steel plate under in-plane compressive load and with aspect ratio (***a/b***=2.0)

Load ***(***kN/m**)**	**Max. Deflection** $((w+w_o)/h)$			
	Experimental results(67)	**Theoretical results**(67)	**Finite Difference method**(11)	**Present study**
0	0.640	0.640	0.640	0.640
20	0.780	0.750	0.770	0.828
35	0.900	0.790	0.850	1.044
60	1.450	1.250	1.340	1.515
70	1.770	1.550	1.620	1.750
85	2.240	2.000	2.040	2.155
100	2.600	2.366	2.400	2.477

b- Simply supported rectangular plate under in-plane loading with a/b=0.875

A simply supported rectangular plate subjected to uniform compressive load is analyzed. The unloaded edges can be moved in the in-plane direction but remain straight. **Moxham**[71] tested two plates with slenderness ratio (b/h=55 and b/h=80) and with initial imperfection (w_o/h=0.055 and w_o/h=0.080), respectively. So, he presented a theoretical formulation through comparing his theoretical results with the experimental values. Many researchers presented theortical studies in comparison with **Moxham**'s experimental test such as **Little**[64],**Crisfield**[27], **Mathlum**[66], and **Amash**[11]. **Moxham**[71] and **Little** used energy methods in their analysis. **Amash** used the finite difference method. **Crisfield** and **Mathlum** used the finite element method.

Moxham suggested that (a/b=0.875) is a suitable figure for a general application, basing this conclusion on a limited number of calculations for very small (w_o) values. He also concluded that the minimum collapse load occurs when (a/b=0.875). **Little**[64], **Crisfield**[27], and **Mathlum**[66] supported this conclusion. Consequently, the theoretical results produced by **Moxham**, **Little**, **Crisfield**, **Mathlum**, and **Amash** for the elastic-plastic analysis of plates in compression were presented for plates with an aspect ratio (a/b=0.875).

Again, in the present study, this plate is analyzed using isoparametric Lagrangian nine-node elements with five degrees of freedom per node and the quarter of the plate is chosen and divided into (2×2) mesh and the thickness is divided into six layers.

Here, it is sufficient to notice that the results obtained from the various solutions differ in detail from one to other, but that, in general, the agreement between the solutions is good when account is taken from the different approaches in using the different approximations required in the analyses.

Figure (6.7) presents the geometry and the properties of the material of the plate that was tested by **Moxham**[71].

Figures (6.8) and (6.9) present the load-deflection curves of two slender plates with two different initial imperfections under compressive load and with the edges of the plate simply supported. From these figures, one can notice the good agreement of the present study with **Moxham**[71] theoretical study.

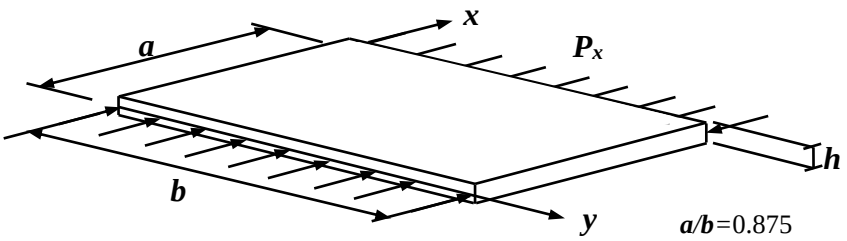

a/b=0.875
a=481.25 (mm)
b=550 (mm)
E= 207000 MPa
σ_o=250 MPa (yield stress)
v= 0.3
w_o/h=0.055

Figure (6.7): Details of geometry and material properties of a rectangular simply supported thin steel plate under in-plane compressive load with aspect ratio (***a/b***=0.875) [71]

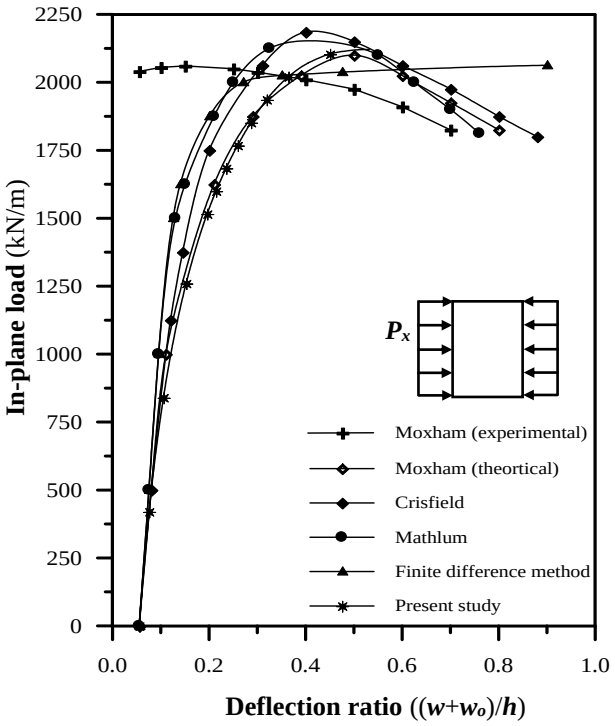

Figure (6.8): Load - deflection curve of a rectangular simply supported steel plate under compressive load, (***b***/***h***=55,***a***/***b***=0.875,w_o/***h***=0.055,***h***=10 mm)

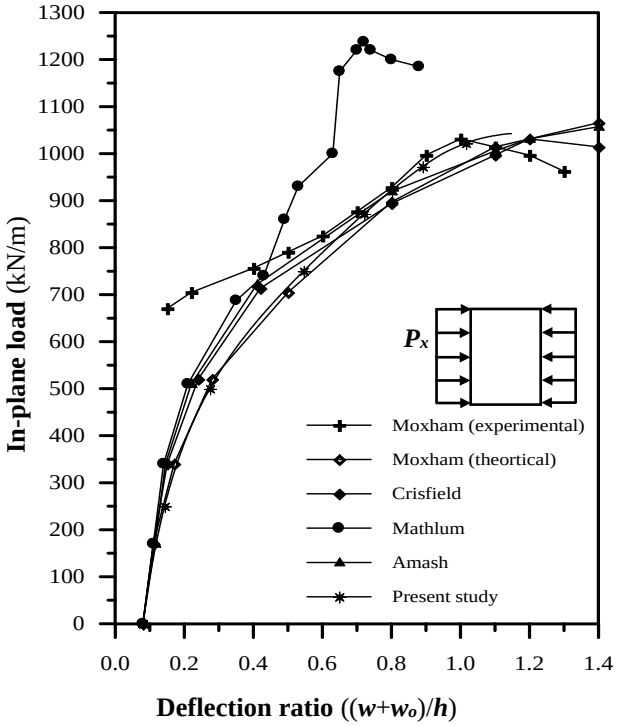

Figure (6.9): Load - deflection curve of a rectangular simply supported steel plate under compressive load, (b/h=80,a/b=0.875,w_o/h=0.080,h=6.875 mm)

6.2.3 Comparison with theoretical investigation of steel plate

Simply supported square plate under in-plane loading (with a/b=1.0)

Two simply supported square plates subjected to uniform in-plane loading were analyzed. The unloaded edges can be moved in the in-plane direction but remain straight. Only one quarter of each plate is modeled by (2×2) mesh due to symmetry and the thickness is divided into six layers. The plate have very small initial deflection of (w_o/h=0.01) by which the shape is considered to be a sinusoidal curve.

The numerical analysis of **Ueda**, **et al.**[109] is based on the displacement formulation of the finite element method and they applied (10×10) mesh model for a quarter of the plate by using a triangular plane shell element with three corner nodal points and subdivided the plate thickness into twenty layers. **Paik** and **Kim**[76] used four-node shell elements and they divided the quarter plate into (5×5) mesh model and applied plastic node model through thickness.

Figure (6.10) and (6.11) show the load-deflection curve for the typical thin and thick plates, respectively. The present results are compared to the conventional finite element solution by **Ueda**, **et. al.** [109], and by **Paik** and **Kim**[76]. From these figures, one can notice the good agreement of the present study with other studies. The following

properties of the thin plates are (h=0.0045 m, E=210×10^6 kN/m^2, v=0.3, b=0.5 m, σ_o=153 MPa) and for thick plates they are (h=0.00675 m, E=210×10^6 kN/m^2, v=0.3, b=0.5 m, σ_o=153 MPa).

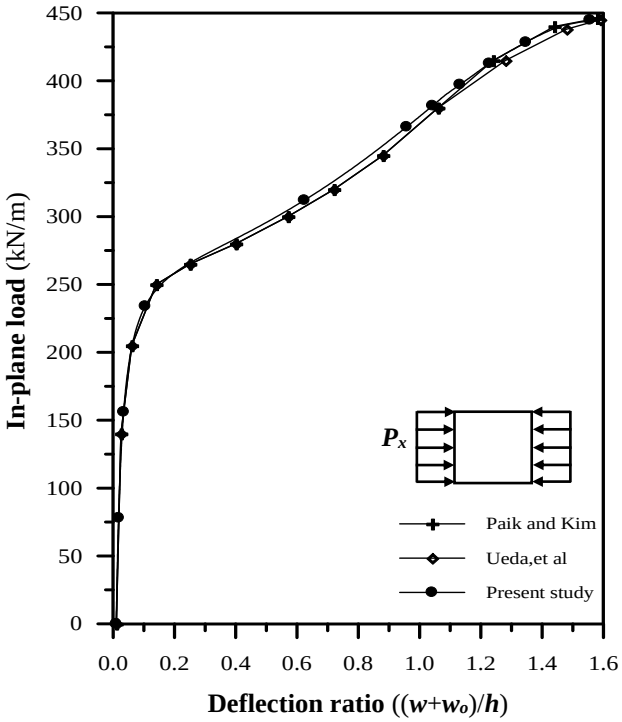

Figure (6.10): Load - deflection curve of a square simply supported thin plate under in-plane compressive load, (b/h=111.1, w_o/h=0.01,a/b=1.0)

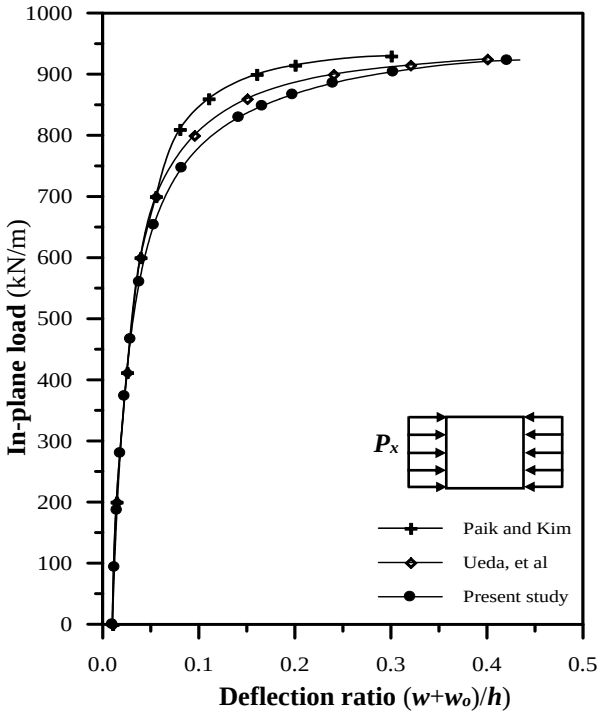

Figure (6.11): Load - deflection curve of a square simply supported thick plate under in-plane compressive load, (b/h=74.07, w_o/h=0.01,a/b=1.0)

6.2.4 Influence of the magnitude of the initial deflection on the ultimate strength of steel plate

The elastic-plastic large deformation behavior of a plate subjected to uniform in-plane compressive load is also analyzed with varying the magnitude of the initial deflection whose shape is also considered to be a sinusoidal curve as shown in Figures (6.12), (6.13), and (6.14), with different values of aspect ratio (a/b=1.0, 0.8, and 0.6), respectively. The boundary condition of the plate is simple support and the in-plane displacements of the unloaded edges are unrestrained so that little membrane stresses in the transverse direction may occur. The quarter plate is modeled by (2×2) mesh and the thickness is divided into six layers. The material properties of the plates are (E=200 GPa, ν=0.3, σ_o=250 MPa (yield stress)).

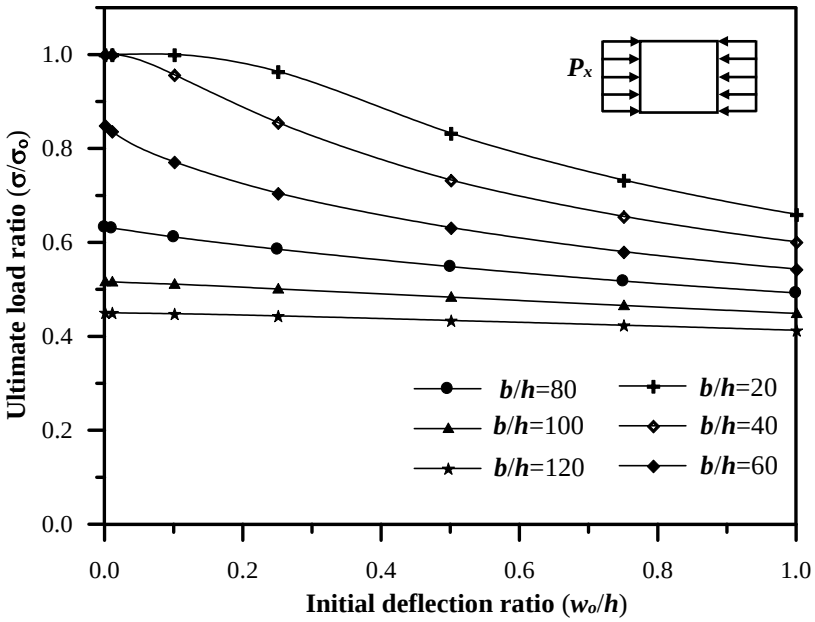

Figure (6.12): Effect of initial imperfection on ultimate strength of a simply supported plate under in-plane compressive load and with aspect ratio (a/b=1.0)

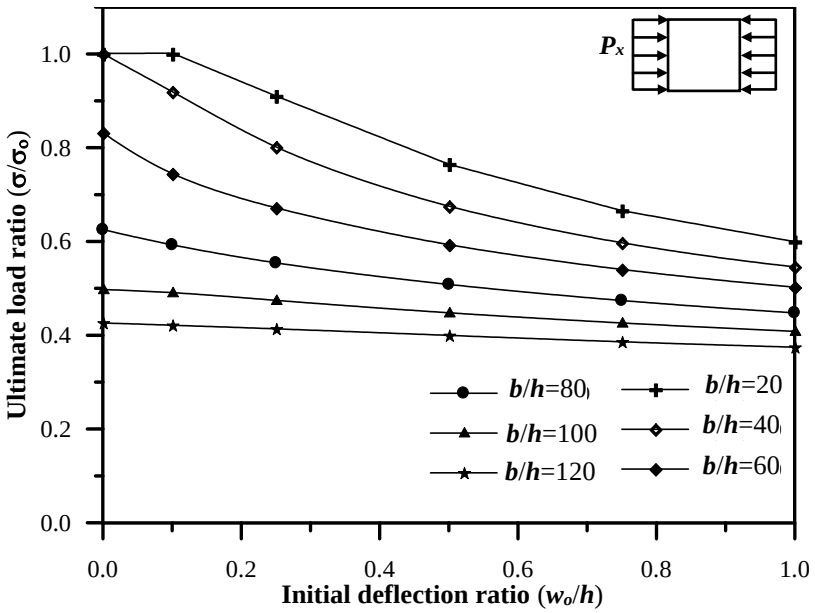

Figure (6.13): Effect of initial imperfection on ultimate strength of a simply supported plate under in-plane compressive load and with aspect ratio (a/b=0.8)

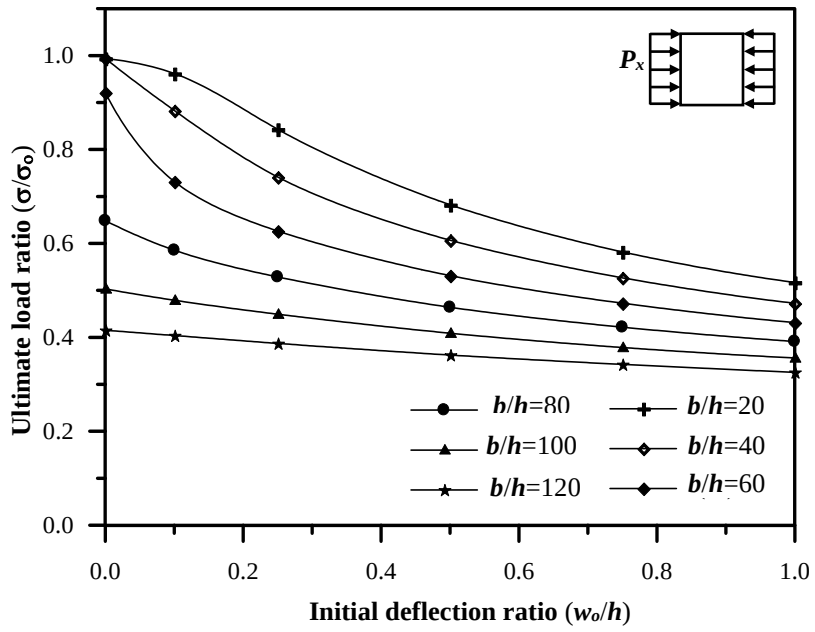

Figure (6.14): Effect of initial imperfection on ultimate strength of a simply supported plate under in-plane compressive load and with aspect ratio (a/b=0.6)

Figures (6.15), (6.16), and (6.17) show the ultimate strength-slenderness ratio curves of the simply supported plate under in-plane loading and with different values of initial deflection ratio (w_o/h) and for different aspect ratios (a/b) (1.0, 0.8, and 0.6), respectively.

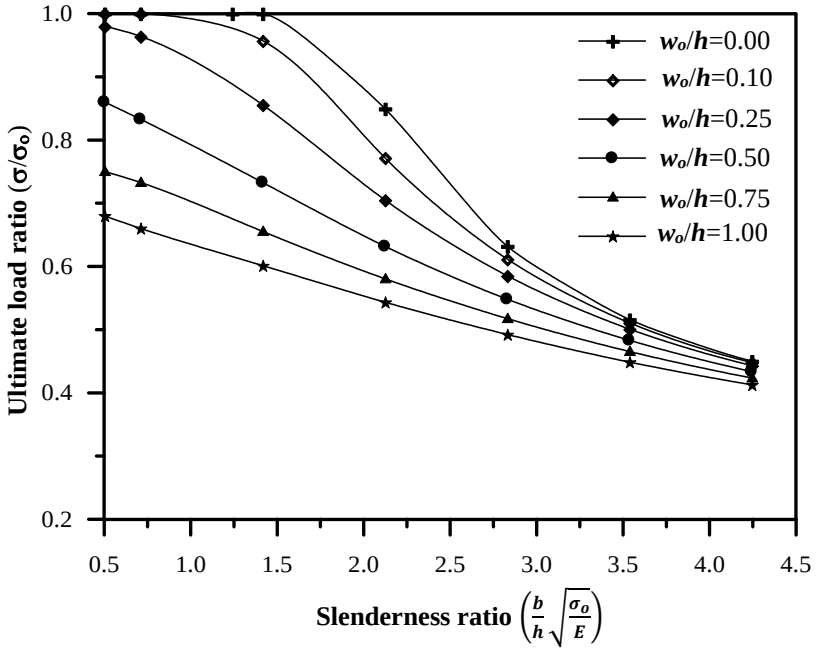

Figure (6.15): Ultimate load – slenderness ratio curve of a simply supported steel plate under in-plane compressive load and with aspect ratio (a/b=1.00)

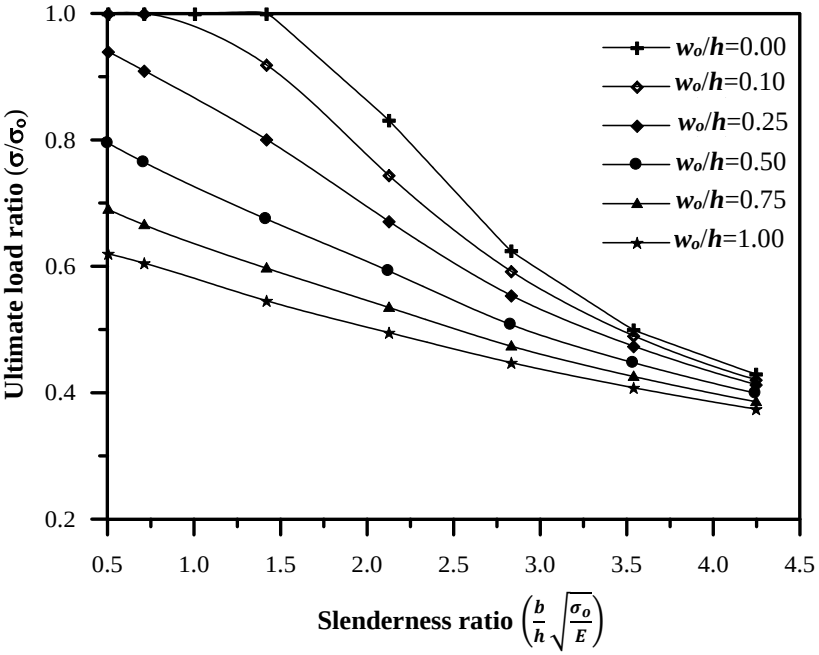

Figure (6.16): Ultimate load – slenderness ratio curve of a simply supported steel plate under in-plane compressive load and with aspect ratio (a/b=0.80)

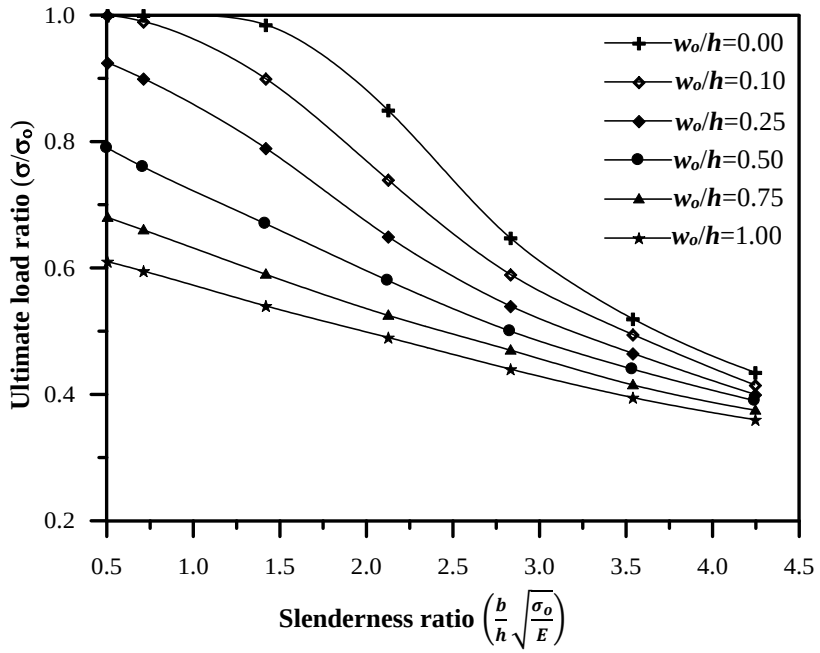

Figure (6.17): Ultimate load – slenderness ratio curve of a simply supported steel plate under in-plane compressive load and with aspect ratio (a/b=0.60)

From these figures, the conclusions are as follows:

1. The ultimate strength of plates under in-plane compressive load is decreasing with increasing of initial imperfection ratio. Table (6.3) shows the approximate values of decrease of the ultimate strength for many types of plates with a range of initial imperfection ratio (w_o/h) (0.0-1.0).

Table (6.3): Approximate decreasing percentage of ultimate strength of plates with change of initial imperfection ratio (w_o/h)(from 0.0 to 1.0)

Slenderness ratio $\left(\frac{b}{h}\sqrt{\frac{\sigma_o}{E}}\right)$	Aspect ratio (a/b)		
	1.0	**0.8**	**0.6**
0.500	32%	38%	39%
0.707	34 %	38%	43%
1.414	40 %	45%	52%
2.121	36 %	42%	46%
2.828	21%	30%	40%
3.535	13%	18%	29%
4.242	9%	12%	21%

2. The decreasing of the ultimate strength due to increase of initial imperfection ratio (w/h) will drop rapidly as soon as the slenderness is ratio increased.
3. The maximum decrease of the ultimate strength occurs at a plate with slenderness ratio (1.414) for all types of aspect ratio.

4. Plates with aspect ratio (0.6) give maximum decrease of ultimate strength for a range of slenderness ratio (0.5-4.242).
5. Plates with slenderness ratio $\left(\frac{b}{h}\sqrt{\frac{\sigma_o}{E}}\right)$ less than (1.414) are considered thick plates where this type of plates yields without buckling while the very slender plates (slenderness ratio greater than 1.414) buckles elastically. In plates with slenderness ratio (1.414), "critical buckling plate", both buckling and yielding occur almost simultaneously.

6.2.5 Influence of boundary condition on the ultimate strength of a steel plate

To study the effect of the boundary condition on the elastic-plastic large displacement analysis of a square plate subjected to in-plane compressive load, three types of boundary conditions are considered (all edges simply supported, all edges clamped, two edges simply supported and others clamped), as shown in Figure (6.18). In the present study, these plates are analyzed by using the isoparametric Lagrangian nine-node elements with five degrees of freedom per node and the quarter of the plate is divided into (2×2) mesh and the thickness is divided into six layers.

Figure (6.19) shows the effect of initial imperfection on the ultimate strength of a square plate with aspect ratio (***a***/***b***=1) and slenderness ratio (***b***/***h***=100) and under in-plane loading for three types of boundary conditions.

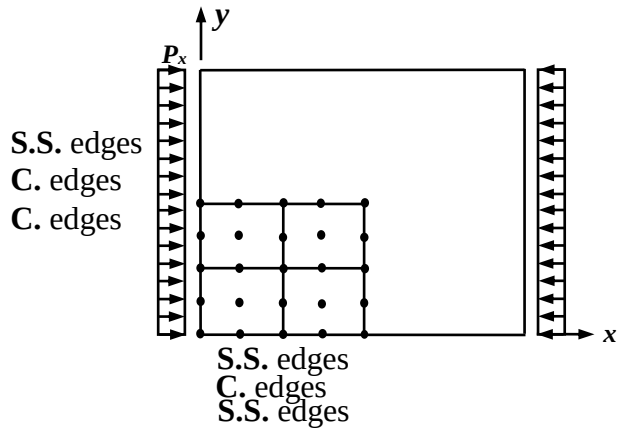

a=1000 (mm)
b=1000 (mm)
E= 200000 MPa
v= 0.3
w_o=5.0 sin (***π x***/***a***) sin (***π y***/***b***)
σ_o=250 MPa (yield stress)

Figure (6.18): Details of a sqaure plate under in-plane compressive load and with different boundary conditions

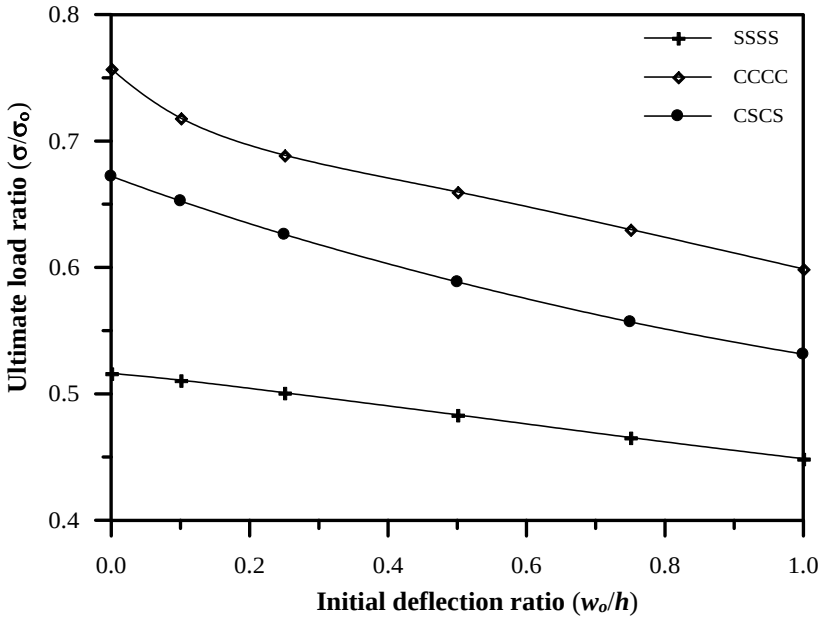

Figure (6.19): Effect of initial imperfection on ultimate strength of a square plate under in-plane compressive load and with different boundary conditions ($\boldsymbol{a}/\boldsymbol{b}$=1.0, $\boldsymbol{b}/\boldsymbol{h}$=100)

Figure (6.20) presents the ultimate strength-slenderness ratio curves of a square plate under in-plane compressive load and with different boundary conditions and for initial imperfection ratio ($\boldsymbol{w_o}/\boldsymbol{h}$=0.5).

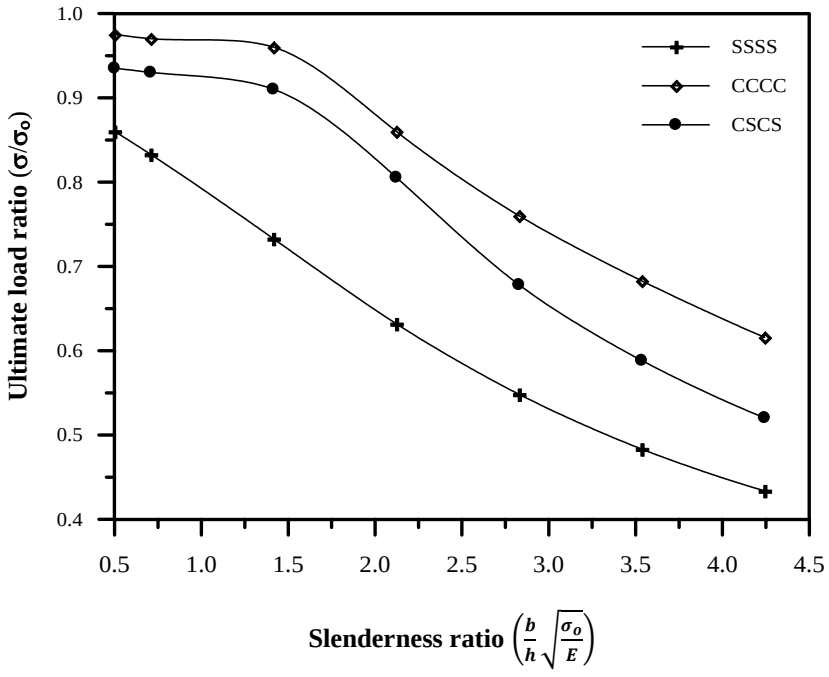

Figure (6.20): Ultimate load – slenderness ratio curve of a square plate with different boundary conditions and under compressive load ($\boldsymbol{a}/\boldsymbol{b}$=1.0, $\boldsymbol{w_o}/\boldsymbol{h}$=0.5)

Table (6.4): Ultimate strength results for different types of boundary conditions of a square steel plate under in-plane compressive load and with initial imperfection (w_o/h=0.5)

Slenderness ratio $\left(\frac{b}{h}\sqrt{\frac{\sigma_o}{E}}\right)$	Boundary conditions		
	SSSS	CCCC	CSCS
0.500	0.860	0.973	0.935
0.707	0.833	0.970	0.930
1.414	0.733	0.960	0.910
2.121	0.632	0.860	0.806
2.828	0.548	0.760	0.678
3.535	0.483	0.683	0.588
4.242	0.434	0.616	0.520

6.2.6 Comparison with experimental investigation of composite plate

The post-buckling and failure characteristics of flat, rectangular graphite-epoxy panels with and without holes that are loaded in axial compression have been examined in an experimental study by **Starnes** and **Rouse** [**1981**] and in a theoretical study by **Elseifi** [**1998**][(31)]. The panels were fabricated from commercially available unidirectional Thornel 300 graphite-fiber tapes preimpregnated with 450 K cure Narmco 5208 thermosetting epoxy resin. Typical lamina properties for this graphite-epoxy system are 131.0 GPa for the longitudinal Young's modulus, 13.0 GPa for the transverse Young's modulus, 6.4 GPa for the in-plane shear modulus, 0.38 for the major Poisson's ratio (v_{12}), and 0.14 mm for the lamina thickness. The loaded ends of the panel were clamped by fixtures during testing, and the unloaded edges were simply supported by knife-edge restrains to prevent the panels from buckling as wide columns. The in-plane compressive load is applied on the composite laminated plate in ***x***-direction.

Elseifi used four-node elements and divided the plate into six elements along the width, and twelve elements along the length.

In the present study, the plate is analyzed by using nine-node isoparametric Lagrangian finite elements with nine degrees of freedom

per node and the results are compared with the available experimental and theoretical results. The panel is 0.508 m long, 0.178 m wide, and 24-ply orthotropic laminate with $[(45^o/0^o/-45^o)_2, (45^o/0^o/-45^o)_2, (45^o/0^o/90^o)_4]$ stacking sequence. The modeling approach of the quarter plate was based on using two elements in the short direction, and three elements in the long direction. The finite element mesh used is shown in Figure (6.21). In order to efficiently proceed beyond the critical buckling point in the post-buckling analysis of the panel, an initial geometric imperfection in the same shape as the first buckling mode was assumed. The amplitude of this initial imperfection is (1%) of the total laminate thickness. A good correlation is observed between the experimental and the finite element results of the present study. Figure (6.22) shows the out-of-plane deflection (***w***) near a point of maximum deflection (node ***i***) normalized by the panel thickness ***h*** as a function of the normalized load. From this figure, it can be noticed that good agreement exists with the experimental results with a difference not more than (6%). On the other hand, the present results are closer to the experimental investigation.

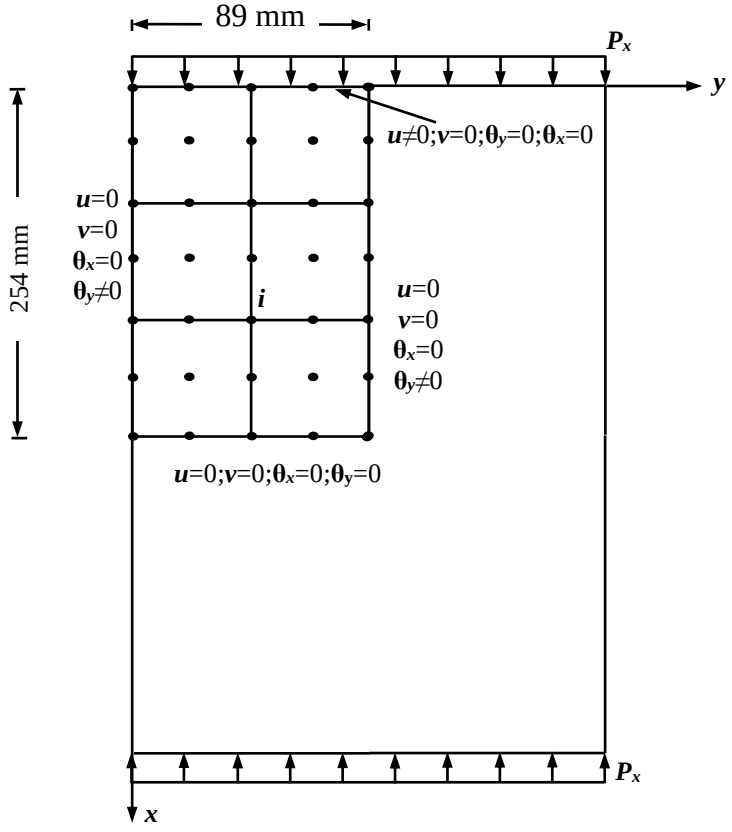

Figure (6.21): Finite element mesh and boundary condition for the quarter of the composite plate under in-plane compressive load in ***x***-direction

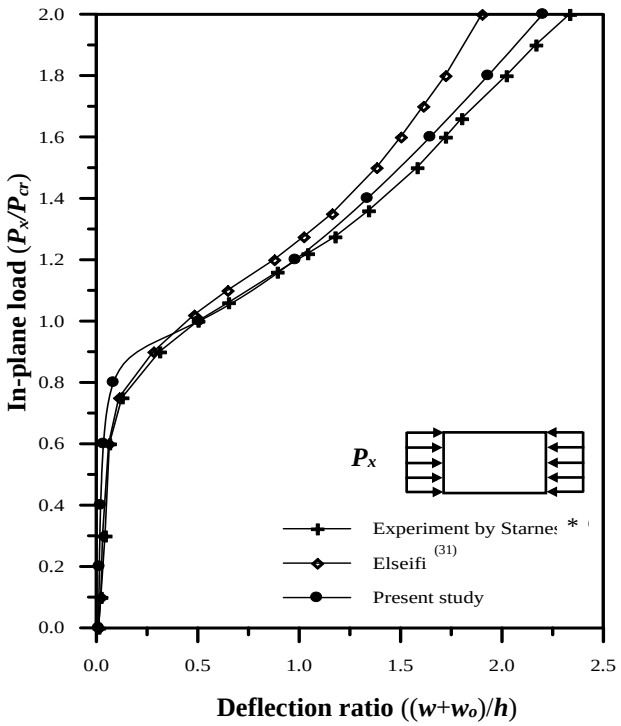

Figure (6.22): Post-buckling curve for a rectangular thin composite laminated plate under in-plane compressive load in ***x***-direction

Table (6.5): Comparison of results with experimental and theoretical studies of composite laminated plate under in-plane compressive load in ***x***-direction, (a/b=2.854, w_o/h=0.1)

Load (P_x/P_{cr})	**Max. Deflection** ($(w+w_o)/h$)		
	Experimental results(*)	**Theoretical results**(31)	**Present study**
0.00	0.010	0.010	0.010
0.10	0.021	0.020	0.013
0.30	0.042	0.030	0.017
0.60	0.063	0.060	0.035
0.75	0.125	0.110	0.064
0.90	0.310	0.280	0.210
1.10	0.850	0.645	0.770
1.28	1.176	1.021	1.122
1.50	1.580	1.380	1.495
1.60	1.720	1.500	1.645
1.80	2.020	1.720	1.930
1.90	2.166	1.810	2.068
2.00	2.333	1.900	2.203

* : Given by **Starnes** and **Rouse** [**1981**] as mentioned in **Elseifi** [**1998**](31).

6.2.7 Comparison with theoretical investigation of composite plate

A square cross-ply laminated plate with simply supported edges and initial imperfection was analyzed by **Zou** and **Qiao** [**2002**][(125)]. Lateral in-plane expansion is allowed at the loaded ends and the unloaded edges can be moved in the plane but remain straight. The layer material and geometry properties are presented in Figure (6.23). The slenderness ratio is set as (b/h=20), and it represents a moderately thick laminate[(125)]. The laminated plate contains eight equal-thickness layers in $[0^o/90^o]_4$ layup. The initial imperfection (w_o/h) is given by (0.0 and 0.1) by which the shape is considered to be a sinusoidal curve. **Zou** and **Qiao** used higher order finite strip method and solved the nonlinear equations by **Newton-Raphson** method. In the present study, a quarter of the laminate is modeled with (2×2) mesh of nine-node isoparametric Lagrangian element with nine degrees of freedom per node. Numerical results and response comparisons with **Zou** and **Qiao** [**2002**][(125)] are shown in Figures (6.24) and (6.25) for axial load versus total deflection and axial load versus end shortening strain (ε). The present results are really close to those of **Zou** and **Qiao** [**2002**][(125)] with a difference of not more than (15%).

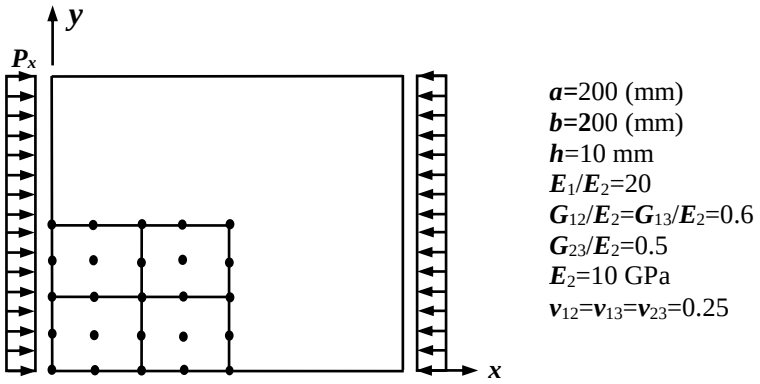

Figure (6.23): Details of a square laminated composite plate under in-plane compressive load and material properties.

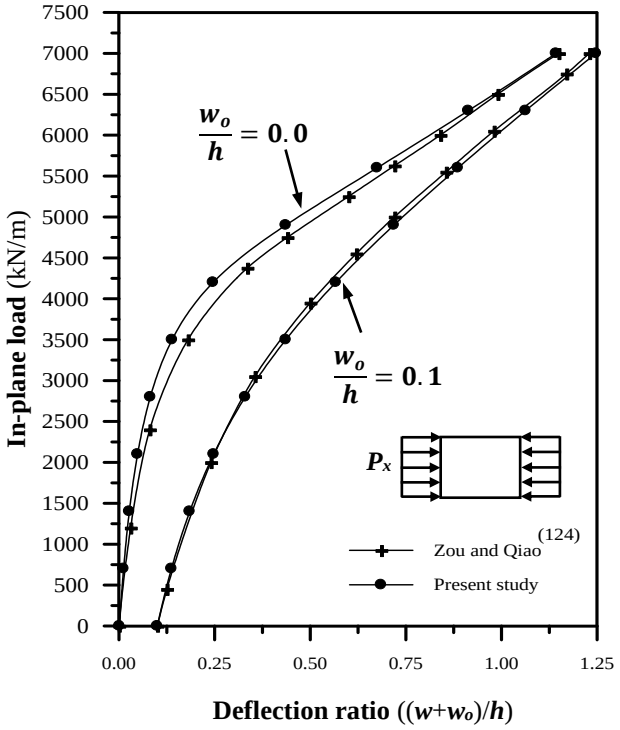

Figure (6.24): Load-deflection curve of antisymmetric cross-ply imperfect rectangular thick composite laminated plate under compressive load,($\boldsymbol{b}/\boldsymbol{h}$=20, $\boldsymbol{a}/\boldsymbol{b}$=1)

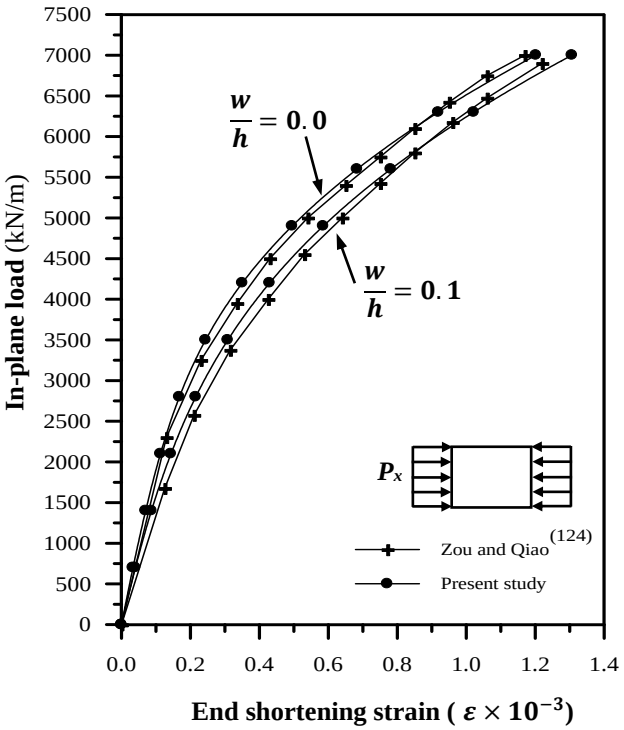

Figure (6.25): Load-end shortening strain curve of antisymmetric cross-ply imperfect rectangular thick composite laminated plate under compressive load,($\boldsymbol{b}/\boldsymbol{h}$=20, $\boldsymbol{a}/\boldsymbol{b}$=1)

6.2.8 Parametric Study

A parametric study is performed to assess the influence of several important parameters on the elastic-plastic large displacement analysis of a composite laminated plate subjected to in-plane compressive load.

The selected parametric studies are summarized as follows:

1. The effect of number of layers.
2. The effect of through-thickness shear deformation.
3. The effect of fiber's orientation angle.
4. The effect of degree of orthotropy of individual layers.
5. The effect of type of lamination.
6. The effect of fiber waviness.

Each one of the above parameters was studied individually by analyzing a type of laminated composite plate. In all cases, a nine-node element was used and also one quadrant of the plate was analyzed due to symmetry and (2×2) mesh is used in the cross-ply and straight fiber plates while for angle-ply and sine wave fiber plates, were analyzed by considering the full plates with (4×4) element mesh. Lateral in-plane expansion is allowed at the loaded ends and the unloaded edges can be moved in the in-plane direction but remain straight. The initial imperfection shape is considered to be a sinusoidal curve. The following geometry and layer material properties of high graphite epoxy are used in the analysis: (E_1=172.5 GPa; E_2=7.08 GPa; G_{12}=G_{13}=3.45 GPa, G_{23}=1.38 GPa; E_f=341.42 GPa; E_m=3.58 GPa; V_f=0.5; V_m=0.5; ν_{12}=ν_{13}=ν_{23}=0.25, X_t=X_c=1450 MPa, Y_t=36 MPa, Y_c=230 MPa, S=62 MPa)[**Parhi**, **et al.**, **2001**][83]. The geometry properties are (a=1.0 m, a/b=1).

1. Effect of number of layers

A simply supported square plate with slenderness ratio (b/h=100), and with symmetric cross-ply and antisymmetric cross-ply, was chosen to study the effect of number of layers on the large displacement elastic-plastic behavior of laminated composite plate under in-plane compressive load. The plate has initial imperfection of (w_o/h=0.00).

Figures (6.26) and (6.27) show that for the same volume of the plate, the ultimate load will increase only by about (2%) for the symmetric cross-ply plate and by about (5%) for the antisymmetric cross-ply plate when increasing the number of layers (3-10) for the symmetric cross-ply and (4-10) for the antisymmetric cross-ply plates. The stiffness increase may be related to the increase of the number of reinforced layers. Also, the increase of the number of layers will give a better orthogonal stiffness through thickness. From these figures, it can be seen that increasing the number of layers more than (6 layers) for the symmetric cross-ply and the antisymmetric cross-ply plates has a slight effect on increasing the stiffness of the plate.

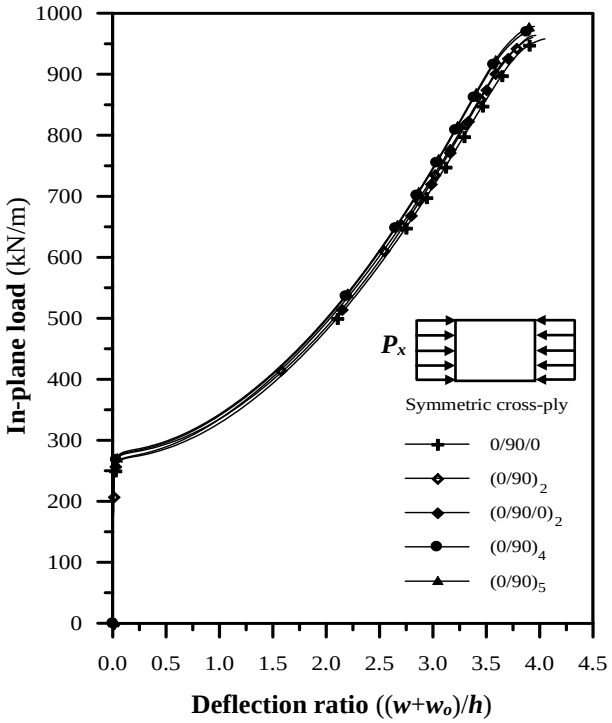

Figure (6.26): Effect of number of layers on the large elastic-plastic analysis of symmetric cross-ply imperfect square composite laminated plate under in-plane compressive load

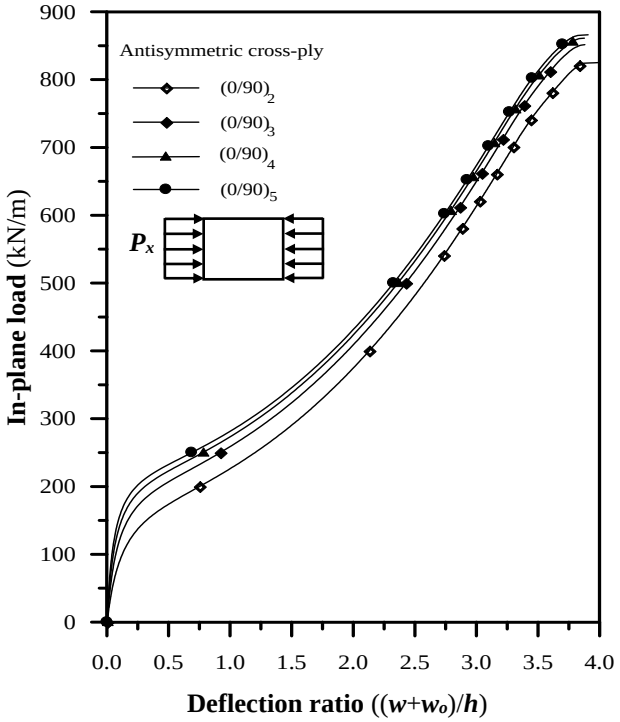

Figure (6.27): Effect of number of layers on the large elastic-plastic analysis of antisymmetric cross-ply imperfect square composite laminated plate under in-plane compressive load

2. Effect of through-thickness shear deformation

To show the effect of transverse shear deformation on the large displacement elastic-plastic analysis of laminated composite plate under in-plane compressive load, a simply supported plate with a range of slenderness ratio (***b***/***h***) from (20) to (120), with symmetric cross-ply and antisymmetric cross-ply arrangement and with six layers was analyzed. The initial imperfection is (w_o/h= 0.1) by which the shape is considered to be a sinusoidal curve.

Figures (6.28) and (6.29) present the load-deflection curves of the symmetric cross-ply, and the antisymmetric cross-ply laminated composite plate under in-plane loading and with slenderness ratio (***b***/***h***=20) by taking the effects of transverse shear deformation through the degrees of freedom per node of the element.

Figures (6.30) and (6.31) show the effect of shear deformation of symmetric cross-ply, and antisymmetric cross-ply laminated composite

plate under in-plane loading with range of slenderness ratio(***b***/***h***) (20-120).

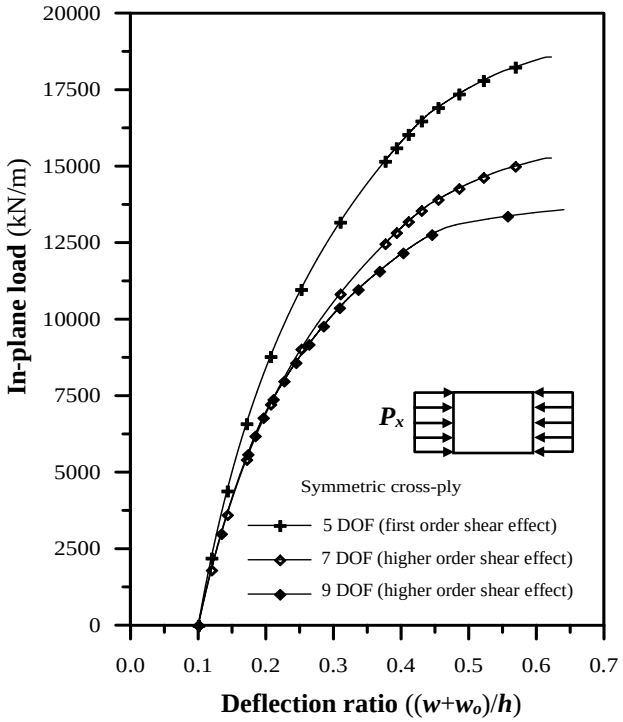

Figure (6.28): Load-deflection curve of symmetric cross-ply imperfect square composite laminated plate under in-plane compressive load with (***b***/***h***=20;***a***/***b***=1; w_o /***h***=0.1)

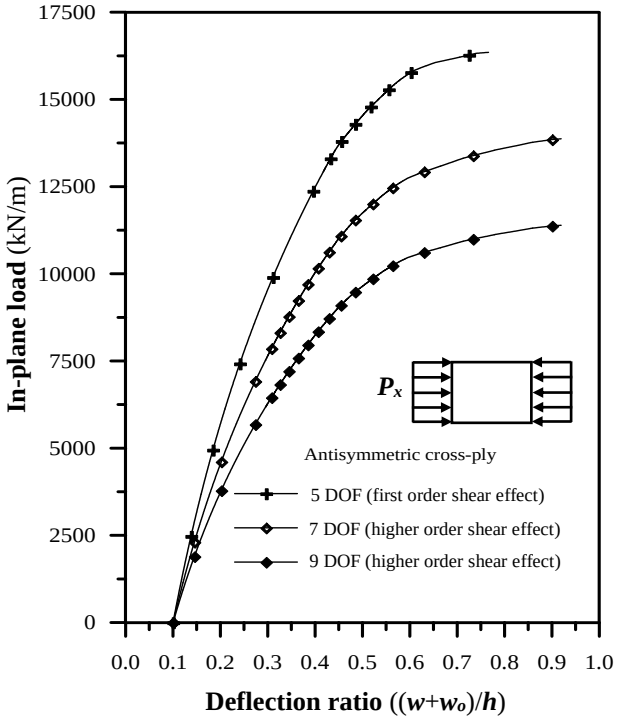

Figure (6.29): Load-deflection curve of antisymmetric cross-ply imperfect square composite laminated plate under in-plane compressive load with (***b***/***h***=20;***a***/***b***=1; w_o /***h***=0.1)

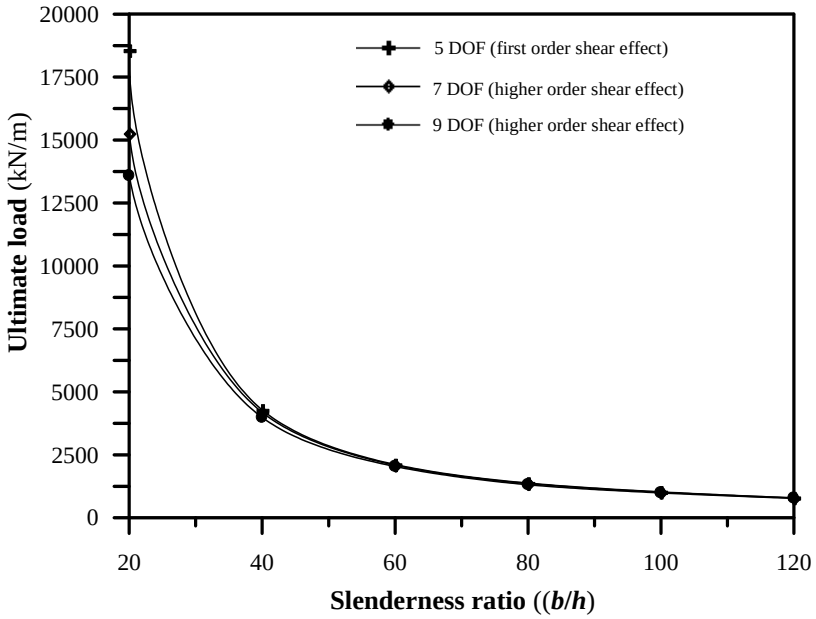

Figure (6.30): Effect of number of degrees of freedom on the large elastic-plastic analysis of symmetric cross-ply composite laminated plate under in-plane compressive load with a range of slenderness ratio (***b***/***h***)

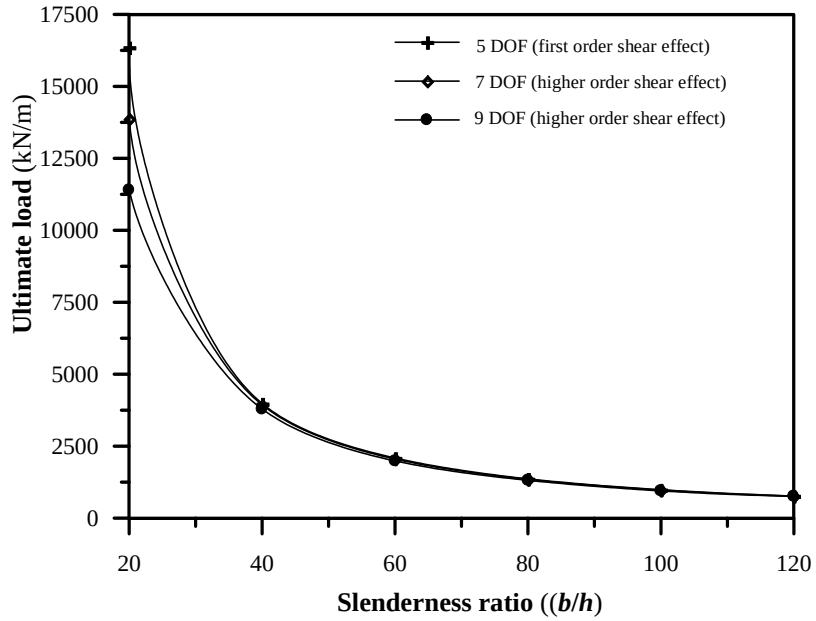

Figure (6.31): Effect of number of degrees of freedom on the large elastic-plastic analysis of antisymmetric cross-ply composite laminated plate under in-plane compressive load with a range of slenderness ratio (***b***/***h***)

3. Effect of fiber's orientation angle

To study the effect of fiber's orientation angle on the large displacement elastic-plastic analysis of laminated composite plates under in-plane compressive load, a square simply supported laminated plate with two layers was analyzed. The initial imperfection is neglected in the present study.

Figure (6.32) shows the effect of fiber's orientation on the nonlinear analysis of composite laminated plate under in-plane compressive load. From this figure, it could be noticed that the ultimate strength of the plate with ($0^o/90^o$) gives ultimate load (651.2 kN/m). This orientation's fiber means that it is the optimum for a plate under in-plane compressive load.

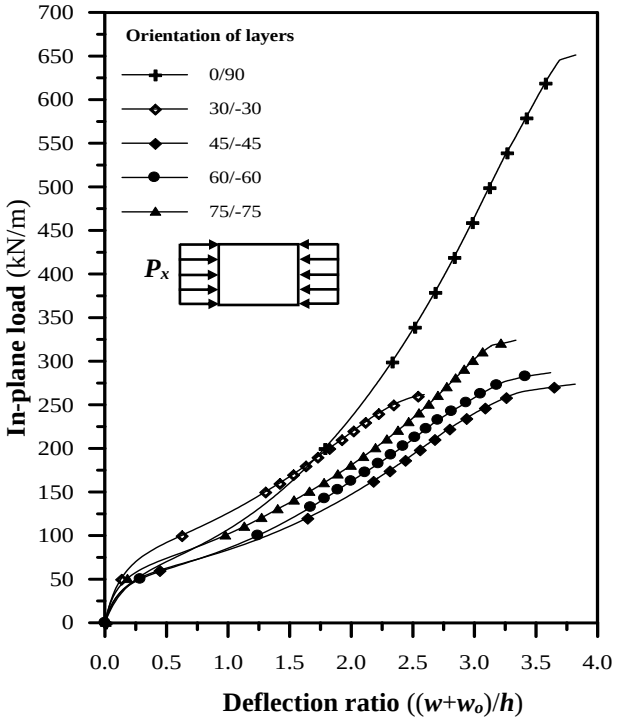

Figure (6.32): Effect of orientation's fiber on the large displacement elastic-plastic analysis of composite laminated plate under in-plane compressive load (b/h=100; w_o/h=0.0;a/b=1)

4. Effect of degree of orthotropy of individual layers

To show the effect of degree of orthotropy of individual layers on the large displacement elastic-plastic analysis, a square simply supported plate, with symmetric cross-ply, and antisymmetric cross-ply arrangement, and with six layers, was analyzed. The initial imperfection is neglected in the present study. The modulus of elasticity of the material in the main direction was varied in the analysis and the modulus of elasticity of the material in the secondary direction is keeping (E_2=7.08 GPa).

Figures (6.33) and (6.34) present the load-deflection curves of the symmetric cross-ply and the antisymmetric cross-ply laminated composite plates under in-plane compressive load and with slenderness ratio (b/h=80), and a range of orthotropy ratio (1-20).

Figures (6.35) and (6.36) show the effect of degree of orthotropy of individual layers on the ultimate strength of the symmetric cross-ply and the antisymmetric cross-ply laminated composite plates under in-plane compressive load with a range of slenderness ratio (b/h) (20-120).

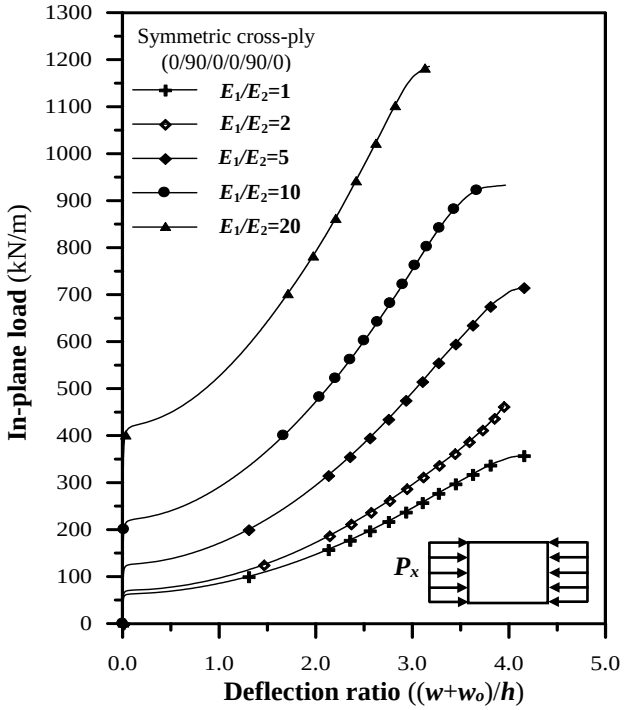

Figure (6.33): Load-deflection curve of the symmetric cross-ply square composite laminated plate under in-plane compressive load with (b/h=80;w_o/h=0.0:a/b=1) and with range of orthotropy ratio (1-20)

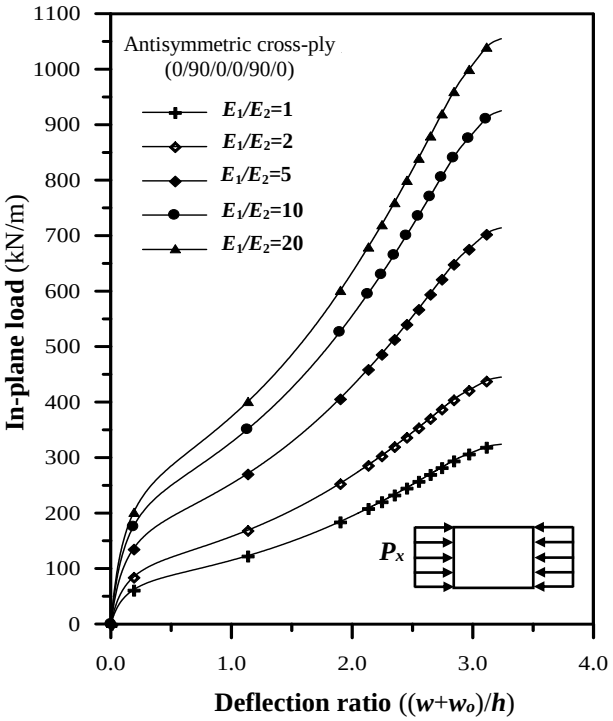

Figure (6.34): Load-deflection curve of the antisymmetric cross-ply square composite laminated plate under in-plane compressive load with (b/h=80; w_o/h=0.0;a/b=1) with range of orthotropy ratio (1-20)

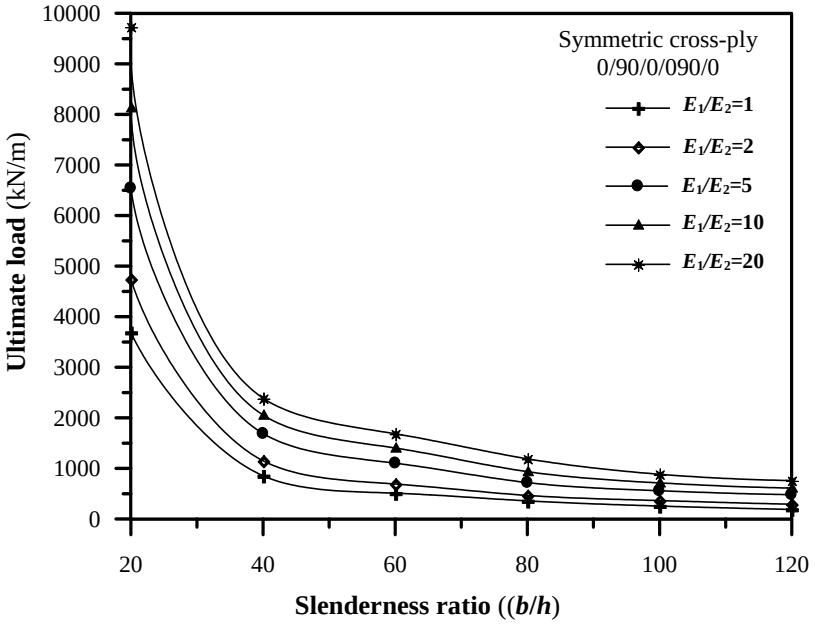

Figure (6.35): Effect of orthotropy of individual of layers on the large elastic-plastic analysis of symmetric cross-ply composite laminated plate under in-plane compressive load with range of slenderness ratio (b/h)(20-120)

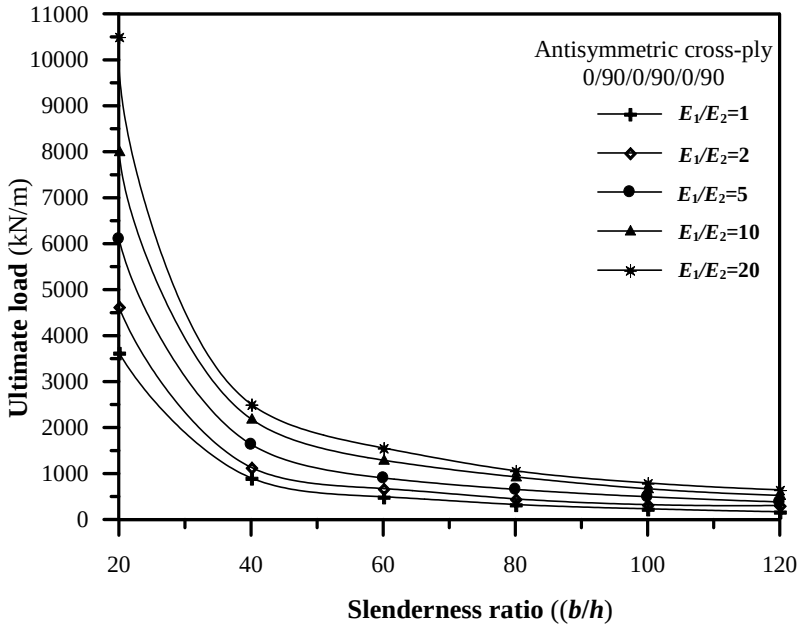

Figure (6.36): Effect of orthotropy of individual of layers on the large elastic-plastic analysis of antisymmetric cross-ply composite laminated plate under in-plane compressive load with range of slenderness ratio (b/h)(20-120)

5. Effect of type of lamination

To study the effect of lamination on the large displacement elastic-plastic analysis of laminated plate under in-plane compressive load, four types of simply supported composite plates (symmetric cross-ply, symmetric angle-ply, antisymmetric cross-ply, and antisymmetric angle-ply arrangements) were considered in the analysis. The initial imperfection is (w_o/h= 0, and 0.1) by which the shape is considered to be a sinusoidal curve.

Figures (6.37) and (6.38) present the load-deflection curve of the four types of simply supported composite plate (with symmetric cross-ply, symmetric angle-ply, antisymmetric cross-ply, and antisymmetric angle-ply arrangements). From these figures, it could be noticed that the ultimate strength of the symmetric cross-ply and antisymmetric cross-ply laminated plates give ultimate load (972.4 kN/m, and 960 kN/m), respectively which are more than the ultimate load of the symmetric and antisymmetric angle-ply plates. This means that the orthogonal arrangement of layers gives higher ultimate load. This is because the loading is in the main direction of the layers.

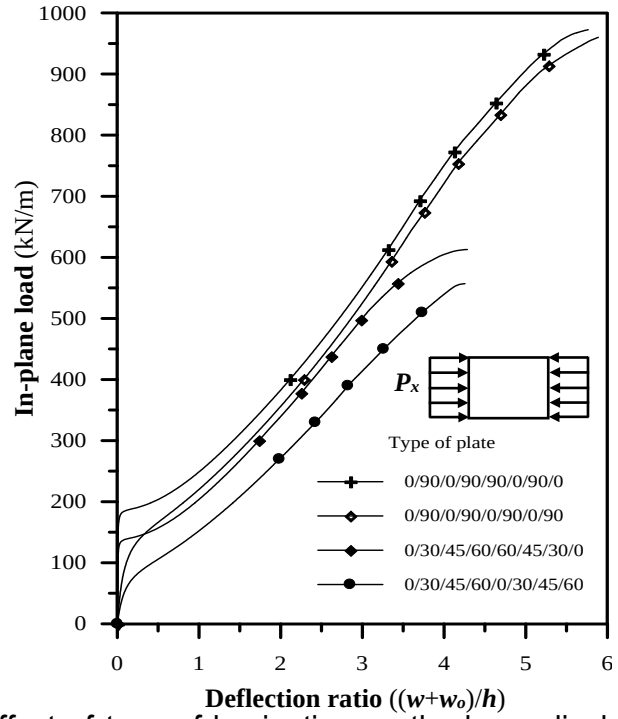

Figure (6.37): Effect of type of lamination on the large displacement elastic-plastic analysis of composite laminated plate under in-plane compressive load, (***a/b***=1, w_o/h= 0.0, ***b***/***h***=100)

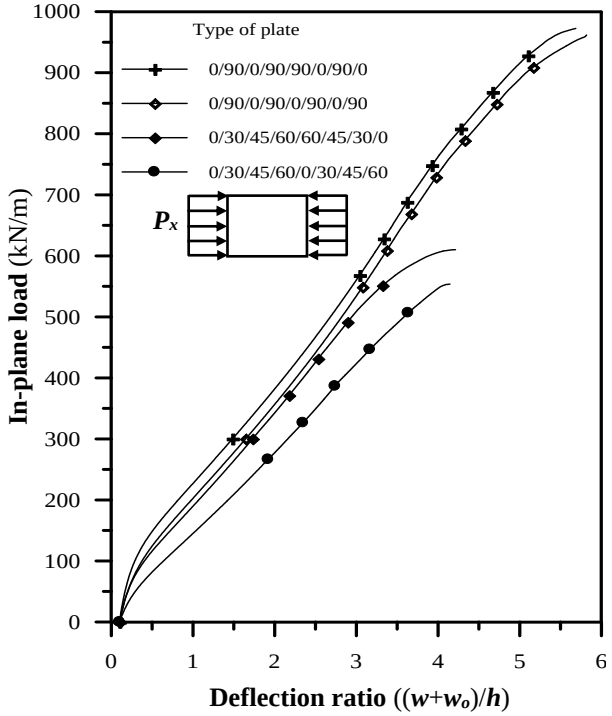

Figure (6.38): Effect of type of lamination on the large displacement elastic-plastic analysis of composite laminated plate under in-plane compressive load, (***a/b***=1, w_o/h= 0.1, ***b***/***h***=100)

6. Effects of fiber waviness

To show the effect of fiber waviness on the large displacement elastic-plastic analysis of laminated composite plate, a square simply supported plate, with six layers was considered. The shape of fiber was considered to follow a sinusoidal curve. The effects of this type are (number of sequence (***k***), amplitude of wave (Δ), and fiber's orientation (θ)), as mentioned in Chapter Three. The initial imperfection (w_o/h= 0.1) by which the shape is considered to be sinusoidal curve. The value of amplitude of sine wave fiber is varying (Δ=0.05-0.5) and the number of sequences of the sine wave fiber (***k***) was considered changeable in the range of (1-12).

Figures (6.39) and (6.40) present the load-deflection curves of laminated with symmetric cross-ply composite plate under in-plane compressive load and with sine wave fibers with a range of amplitude (0.05-0.5).

Figures (6.41)-(6.44) present the ultimate strength-fiber path amplitude (Δ) curves for the laminated, with symmetric cross-ply, and antisymmetric cross-ply composite plates under in-plane compressive load and with a range of number of sequences (***k***) (1-12).

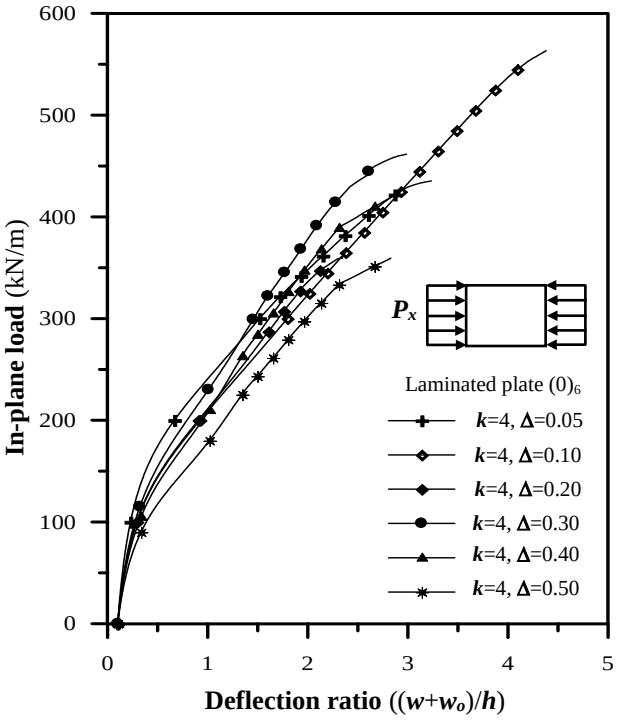

Figure (6.39): Load-deflection curve of simply supported square laminated composite plate with sine wave fiber with a range of fiber amplitude (0.05-0.50) and under in-plane compressive load, (w_o/h =0.1;b/h=100;a/b=1.0;k=4)

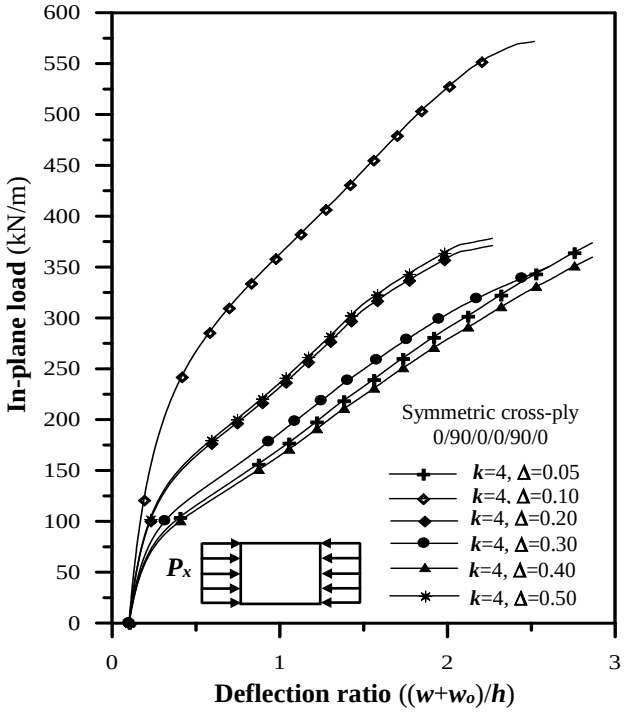

Figure (6.40): Load-deflection curve of simply supported square symmetric cross-ply composite plate with sine wave fiber with a range of fiber amplitude (0.05-0.50) and under in-plane compressive load, (w_o/h =0.1;b/h=100;a/b=1.0;k=4)

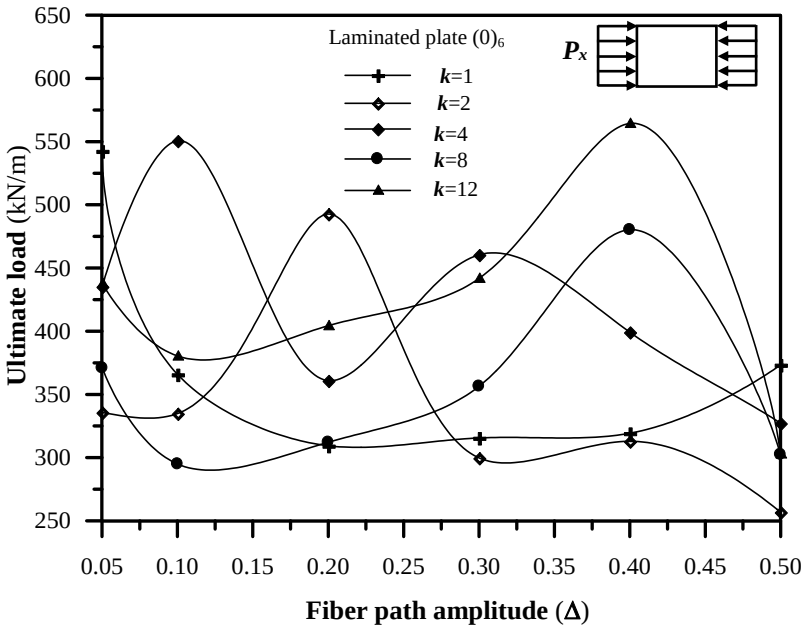

Figure (6.41): Ultimate load-fiber path amplitude curve of simply supported square laminated composite plate under in-plane compressive load in x-direction and with a range of number of sequences (1-12),(w_o/h= 0.1, b/h=100, a/b=1.0)

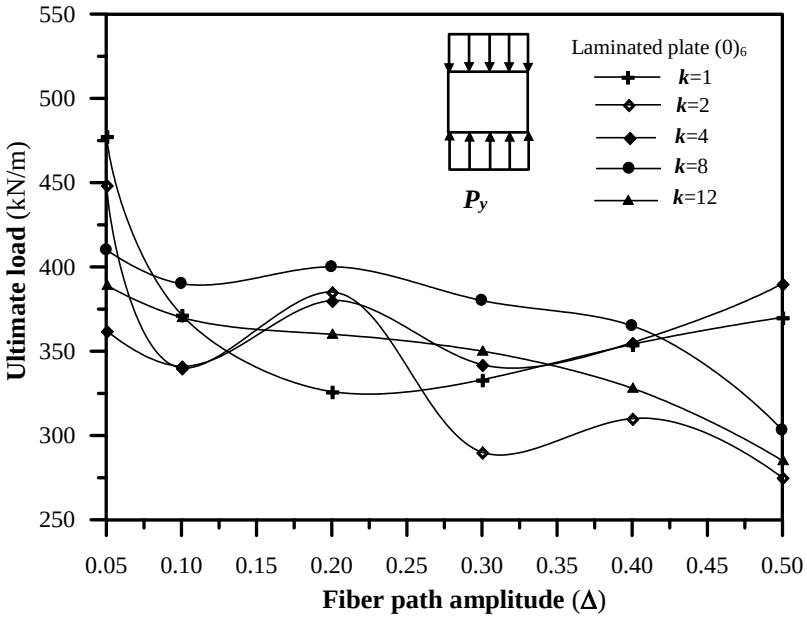

Figure (6.42): Ultimate load-fiber path amplitude curve of simply supported square laminated composite plate under in-plane compressive load in ***y***-direction and with a range of number of sequences (1-12),(w_o/h= 0.1, b/h=100, a/b=1.0)

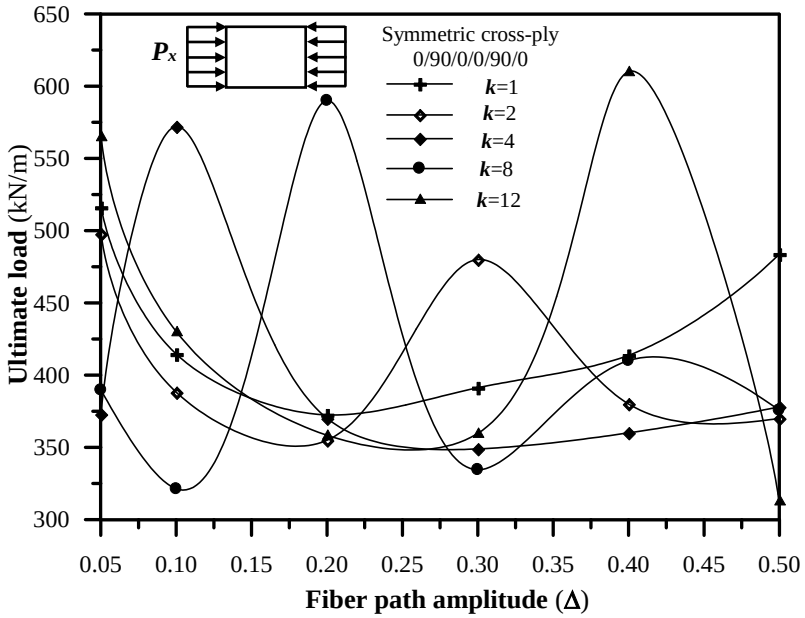

Figure (6.43): Ultimate load-fiber path amplitude curve of simply supported square symmetric cross-ply composite plate under in-plane compressive load and with a range of number of sequences (1-12),(w_o/h= 0.1, b/h=100, a/b=1.0)

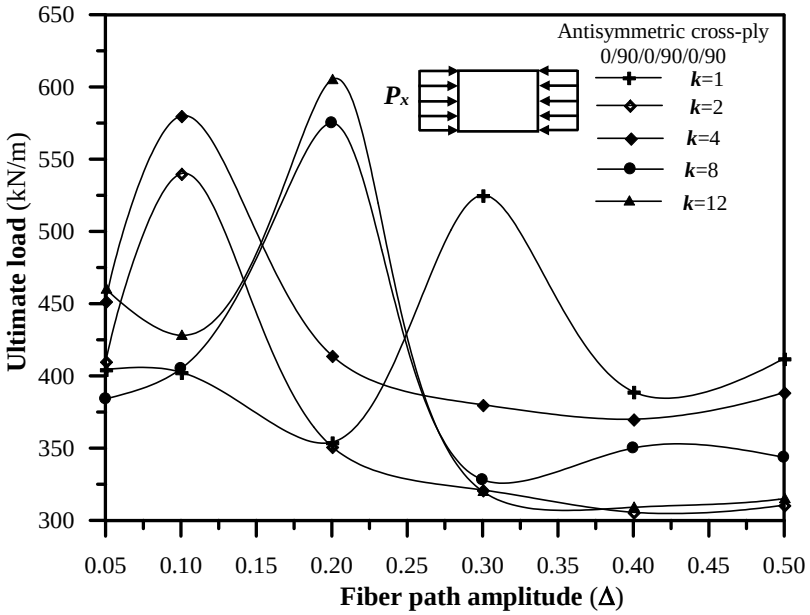

Figure (6.44): Ultimate load-fiber path amplitude curve of simply supported square antisymmetric cross-ply composite plate under in-plane compressive load and with a range of number of sequences (1-12),(w_o/h= 0.1, b/h=100, a/b=1.0)

6.2.9 Summary

From these figures in the parametric study, the following points can be noticed:

1. The ultimate strength of plates under in-plane compressive load is decreasing with increasing the number of degrees of freedom per node where the increasing of number of degrees will increase the effect of transverse shear deformation and the increasing of transverse shear deformation will cause decreasing of stiffness matrix of the plate and consequently will decrease the ultimate strength of the plate. The decreasing percentage of the ultimate strength of the symmetric cross-ply plate is about (2.5%) for slenderness ratio (120) and is about (27%) for the plate with slenderness ratio (20); while for the antisymmetric cross-ply plate, the decreasing percentage of the ultimate strength is about (2%) for the plate with slenderness ratio (120) and about (30%) for the plate with slenderness ratio (20).
2. The ultimate strength of laminated plate will be increased as soon as the orthotropy ratio is increased, because of the increased stiffness of

the laminated plate with the same volume and number of layers. For a range of orthotropy ratio (1-20), the ultimate strength of the symmetric cross-ply plate will increase about (4.0) times for slenderness ratio (120) and about (2.5) times for slenderness ratio (20).

3. The capacity of a laminated plate with sine wave fiber under in-plane compressive load in the direction of waviness is more than the capacity of the plate under in-plane compressive load orthogonal to the direction of waviness by (42%) for a plate with sine wave fiber ($\boldsymbol{k}$=12, Δ=0.4).
4. The ultimate strength of a cross-ply laminated plate is greater than the ultimate strength of an angle-ply laminated plate with the same laminas.
5. The ultimate strength of a symmetric cross-ply laminated plate is greater than the ultimate strength of an antisymmetric cross-ply laminated plate with the same laminas.
6. A symmetric cross-ply laminated plate with sine wave fiber ($\boldsymbol{k}$=12, Δ=0.4) gives in-plane loading (610 kN/m) and this represents the peak capacity and this case is the best.

CHAPTER SEVEN

Applications and Discussions on Nonlinear Dynamic Analysis

7.1 General

This chapter deals with the large displacement elastic-plastic dynamic analysis of laminated composite plates under in-plane dynamic load by using the finite element method. The effect of time step, number of degrees of freedom per node, number of layers, initial imperfection, type of loading, damping effect, type of mass, fiber waviness, type of time integration method, and others are considered in the present study. Firstly, the large displacement elastic-plastic analysis of a metal plate under in-plane dynamic loading will be studied with certain effects. Time history curves are presented to show the oscillation in the metal plate. Secondly, the large displacement elastic-plastic dynamic analyses of laminated composite plates under in-plane dynamic loading with different effects are studied. Also, time history curves are presented to show the oscillation of the composite laminated plates.

Numerical examples, representing different types of plates, as reported by other researchers are utilized in the present study to verify the reliability of the computer program.

7.2 Numerical Examples

Several plates are analyzed to study the different effects on the large displacement elastic-plastic dynamic behavior of plates with some comparison with other researchers.

7.2.1 Comparison with available theoretical investigation of plate

a- Simply supported square plate under transverse suddenly applied constant dynamic loading

In order to test the accuracy and efficiency of the developed algorithm, a simply supported plate under a uniform transverse constant dynamic loading is analyzed. The plate geometry, applied transverse loading, and a typical mesh used over the quarter plate are given in Figure (7.1).

The numerical analysis of **Akay** [**1980**][(10)] is based on the displacement formulation of the finite element method and he applied (2×2) mesh model for a quarter of the plate using the four-node isoparametric mixed quadrilateral element with time step (Δt=0.0025 sec) and used **Newmark** linear acceleration method with α=1/2, and β=1/6 and neglected the damping effect.

In the present study, this plate is analyzed using the isoparametric Lagrangian nine-node elements with five degrees of freedom per node and the quarter of the plate is divided into (2×2) element mesh with time step (Δt=0.0025 sec). Also, **Newmark** constatnt average acceleration method is used in the present study with α=1/2, and β=1/4 and neglecting damping effect. A consistent mass matrix was considered in the present study.

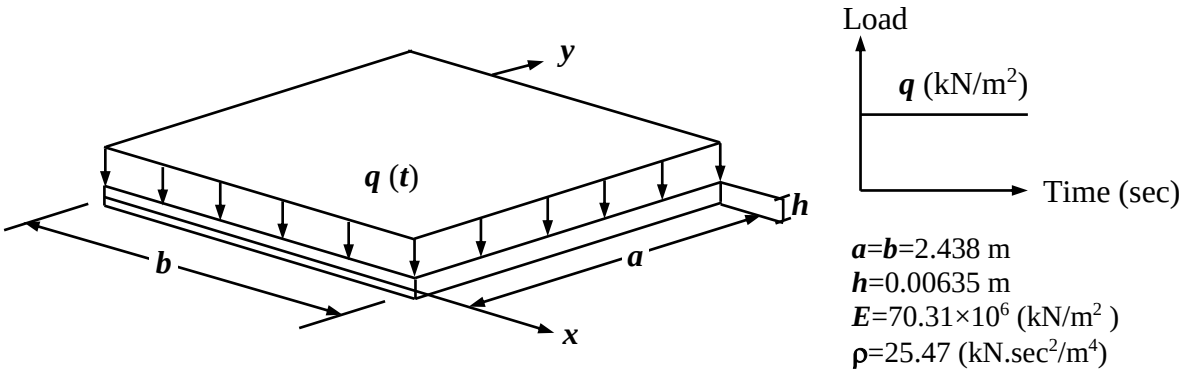

a=b=2.438 m
h=0.00635 m
E=70.31×10^6 (kN/m^2)
ρ=25.47 (kN.sec^2/m^4)
v= 0.25
q=0.04882 (kN/m^2)
Δt=0.0025 (sec)

Figure (7.1): Details of a square simply supported plate under transverse suddenly applied constant dynamic loading

Figure (7.2) shows a comparison of the present study with **Akay**'s[10] study for the central deflection ratio. The results obtained from the present study give good agreement with the theoretical results obtained by **Akay**[10] with a difference of not more than (2%).

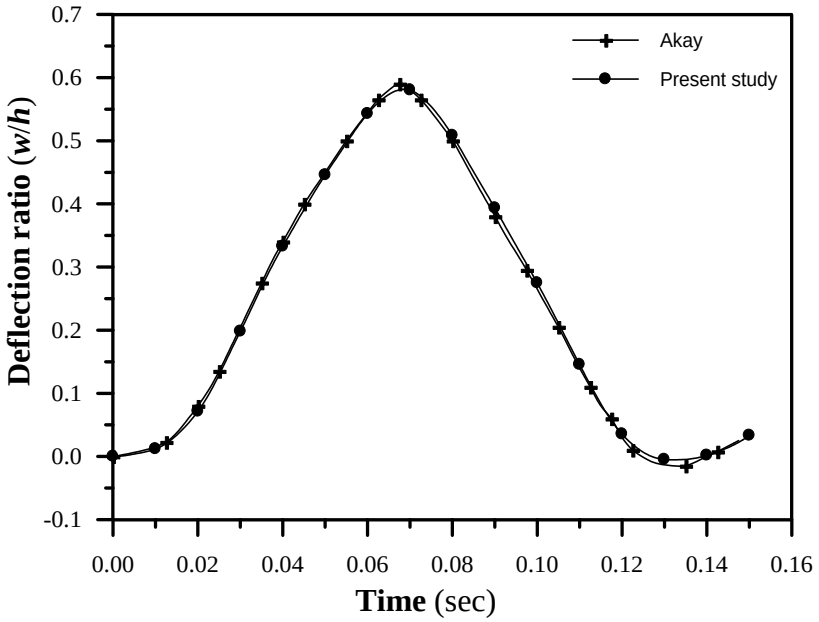

Figure (7.2): Time history curve of a square simply supported plate under transverse suddenly applied constant dynamic loading

b- Simply supported square plate under in-plane parabolic pulse dynamic loading

For dynamic buckling of plate under in-plane dynamic loading, the example results are presented for the plate under in-plane impact dynamic loading and compared with **Tao**, **et al.** [**2004**][(105)] results and with finite element software ADINA program used by some authors[(105)] in order to validate the present study.

The plate is simply supported along all its edges, and the load was introduced as an impact load which had characteristics of a half sine wave with peak value of $\boldsymbol{P_x(t)}$, as given in following equation:

$$\boldsymbol{P_x(t)} = \begin{Bmatrix} \boldsymbol{\eta_1 t^2 + \eta_2 t} & \boldsymbol{(0 \le t \le T_d)} \\ \boldsymbol{0} & \boldsymbol{(t > T_d)} \end{Bmatrix}$$

where $\boldsymbol{\eta_1 = \frac{-4P_{max}}{T_d^2}, \eta_2 = \frac{4P_{max}}{T_d}}$, $\boldsymbol{P_{max}}$ is the peak value of the in-plane dynamic pulse loading and $\boldsymbol{T_d}$is the duration of the impact loading and represents the first period of lateral free vibration of the unloaded plate ($2\boldsymbol{\pi/\omega}$). The initial geometrical imperfection of the plate sinusoidal profile is: $\boldsymbol{w_o = w_1.\sin(x).\sin(y)}$. The geometry and material properties of the plate specimen are ($\boldsymbol{a=b}$=0.15 m, $\boldsymbol{h}$=0.0016m, $\boldsymbol{E}$=70.6 GPa, $\boldsymbol{\sigma_o}$=240 MPa, $\boldsymbol{\nu}$=0.25, $\boldsymbol{\rho}$=27 kN.sec^2/m^4, $\boldsymbol{w_1/h}$=0.15625**,** $\boldsymbol{P_{max}}$=78.4 kN/m, $\boldsymbol{T_d}$=0.0035 sec).

Tao, **et al.** applied Hamilton's principle to obtain the motion equations of the plate and took the deflection of the plate as a Fourier series and used Galerkin method with these equations to be solved numerically by Runge-Kutta method.

In the present study, this plate is analyzed by using isoparametric Lagrangian nine-node elements and the quarter of the plate is divided into (2×2) mesh with time step ($\boldsymbol{\Delta t}$=0.00005 sec). A consistent mass matrix was considered in the present study.

Figure (7.3) shows the time history curve for the square simply supported thin plate under in-plane impact dynamic loading with aspect ratio

(***a/b***=1.0). From this figure, the present study gives good agreement with the theoretical results obtained by **Tao**, **et. al**[105] with a difference not more than (5%).

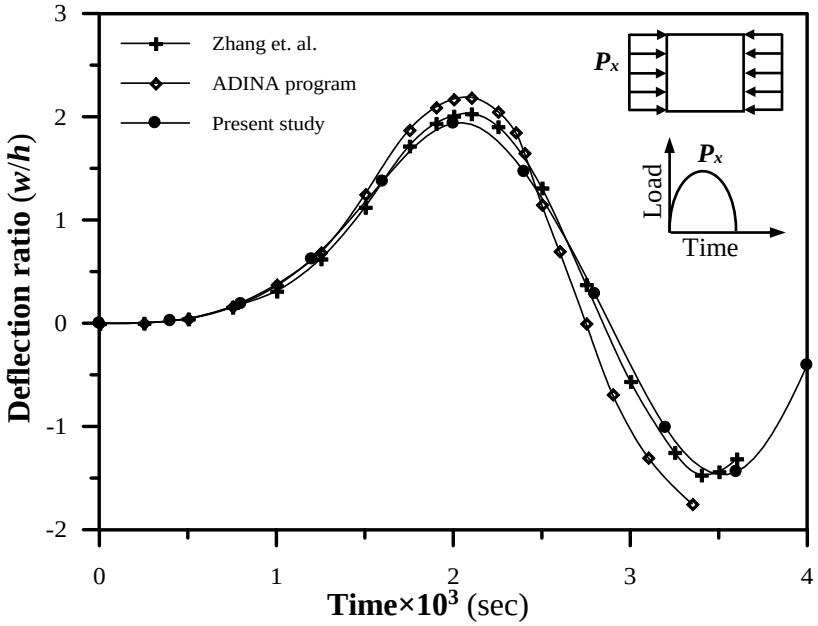

Figure (7.3): Time history curve for a square simply supported plate under in-plane parabolic pulse dynamic loading, (***b/h***=93.75,w_o/h=0.15625, P_x=78.4 kN/m, T_d=0.0035 sec)

7.2.2 Parametric study

The effect of the number of degrees of freedom per node, initial imperfection, time step, loading type, boundary conditions, viscous damping, mass matrix type, method of integration (**Newmark** method or harmonic acceleration method) and load magnitude are considered to study the large displacement elastic-plastic dynamic analysis of steel plate under in-plane dynamic loading. Each one of the parameters above was studied individually by analyzing a type of steel plate under in-plane loading. In all cases, the nine-node isoparamteric Lagrnagian element was used and one quadrant of the plate was analyzed due to symmetry and (2×2) mesh was used and the thickness was divided into six layers.

1. Effect of time step

A square simply supported plate under in-plane constant dynamic loading was analyzed to study the effect of time step on the large displacement elastic-plastic dynamic analysis of steel plate. A set of time step (0.0005 sec-0.00005 sec) were considered in the present study. The plate has initial imperfection (w_o/h) of (0.1) by which the shape is considered to be a sinusoidal curve. The geometry and material properties of the analyzed plate are (a=b=1.0 m, h=0.01m, E=200 GPa, σ_o=240 MPa, v=0.30, ρ=78 kN.sec^2/m^4, P_x=504 kN/m,). A consistent mass matrix and **Newmark** integration method with α=1/2, and β=1/4 were considered in the present study.

Figure (7.4) shows the central deflection ratio-time curve for the square simply supported plate under impact in-plane loading. From this figure, one can select the time step as (Δt=0.0001sec) where this time step gives good stability of results and suitable consumption time with a difference not more than (1%) from the time step (Δt=0.00005 sec).

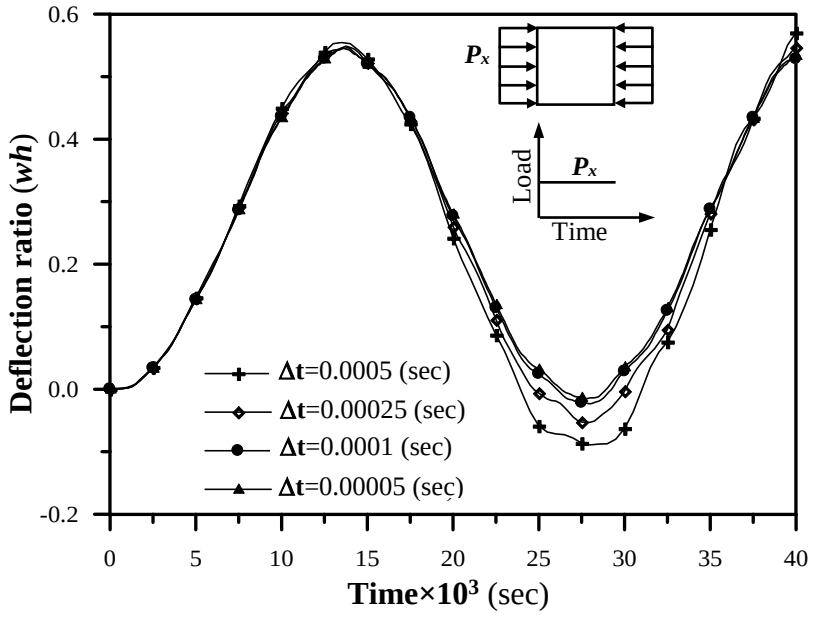

Figure (7.4): Effect of time step on the large displacement elastic-plastic dynamic analysis of a square simply supported plate under suddenly applied in-plane constant dynamic loading with a range of time steps, (b/h=100, P_x=504 kN/m,w_o/h=0.1)

2. Effect of number of degrees of freedom per node

A simply supported square steel plate subjected to in-plane constant dynamic loading is analyzed to study the effect of shear deformation through thickness. The unloaded edges can move in the in-plane direction but remain straight. The plate has initial imperfection (w_o/t=0.1) by which the shape is considered to be a sinusoidal curve. The geometry and material properties of the analyzed plate are (E=200 GPa, σ_o=240 MPa, v=0.30, ρ=78 kN.sec^2/m^4, a=b=1.0 m, h=0.05 m, b/h=20, P_x=6250 kN/m, P_x/P_u=0.5, Δt=0.0001sec). A consistent mass matrix and **Newmark** integration method with α=1/2, and β=1/4 were considered in the present study.

Figure (7.5) shows the time history curve for the simply supported plate under in-plane constant dynamic loading as obtained by using different numbers of degrees of freedom per node (5, 7, and 9). From this figure, one can select the five degrees of freedom where this number of degrees gives a difference with nine degrees of freedom not more than (6%) and gives suitable consumption time.

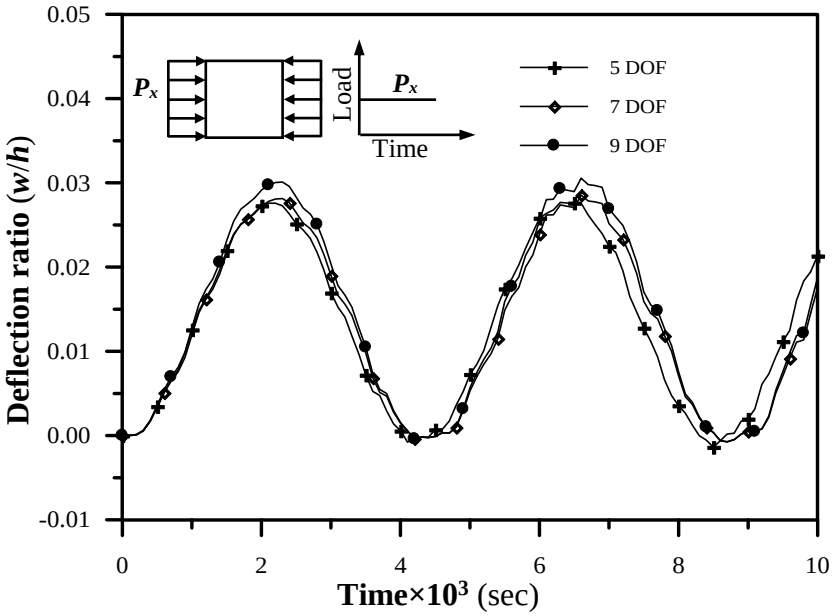

Figure (7.5): Effect of number of degrees of freedom on the large displacement elastic-plastic dynamic analysis of a square simply supported plate under suddenly applied in-plane constant dynamic loading, (b/h=20,w_o/h=0.1, Δt=0.0001 sec, P_x=6250 kN/m)

3. Effect of initial imperfection

A square simply supported plate under in-plane constant dynamic loading was analyzed to study the effect of initial imperfection on the large displacement elastic-plastic dynamic analysis of steel plate. The plate has a range of initial imperfection (w_o/h) of (0.0-1.0) by which the shape is considered to be a sinusoidal curve. The analyzed plate is subjected to a uniform in-plane constant dynamic loading of less than the buckling load to show the effect of initial imperfection on the nonlinear dynamic behavior. The unloaded edges of the plate can move in the in-plane direction but remain straight. Only a quarter of the plate is modeled by (2×2) element mesh due to the symmetry. The following properties of the thin plate are (a=b=1.0 m, h=0.01m, E=200 GPa, σ_o=240 MPa, v=0.30, ρ=78 kN.sec^2/m^4, $P_{buckling}$=723 kN/m, P_{max}=504 kN/m, Δt=0.0001 (sec)). A consistent mass matrix and **Newmark** integration method with α=1/2, and β=1/4 were considered in the present study.

Figure (7.6) shows time history curve with a range of initial imperfections (0.0-1.0). From this figure, it can be noticed that increasing the initial imperfection will decrease the time period of the plate. So, if the plate has no initial imperfection then an in-plane dynamic loading of less than the buckling load of the plate will cause the plate to have no oscillation.

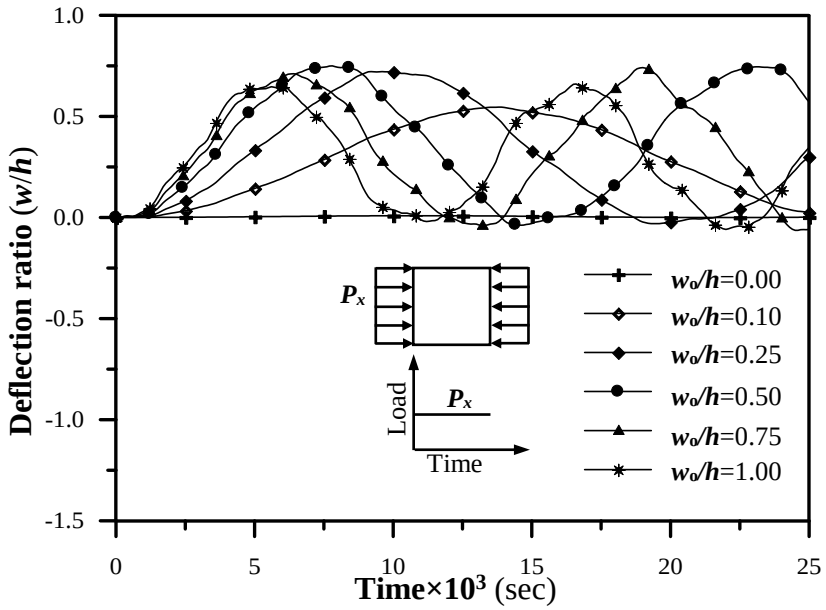

Figure (7.6): Effect of initial imperfection on the large displacement elastic-plastic dynamic analysis of a square simply supported plate under suddenly applied in-plane impact dynamic loading, (b/h=100, Δt=0.0001 sec, P_x=504 kN/m, a/b=1.0)

4. Effect of mass matrix

To study the effect of mass matrix type on the large displacement elastic-plastic dynamic analysis of a square plate subjected to in-plane dynamic loading, the two types of mass matrix were considered (consistent mass matrix, and lumped mass matrix). The plate has an initial imperfection (w_o/h) of (0.1) by which the shape is considered to be a sinusoidal curve. The geometry and material properties of the analyzed plate are (E=200 GPa, σ_o=240 MPa, v=0.3, a=b=1.0 m, h=0.01 m, b/h=100, P_x=504 kN/m, ρ=78 kN.sec^2/m^4, Δt=0.0001sec). **Newmark** integration method with α=1/2, and β=1/4 was considered in the present study.

Figure (7.7) shows the effect of mass matrix type on the nonlinear dynamic analysis of a square plate with aspect ratio (a/b=1) and slenderness ratio (b/t=100) under in-plane dynamic loading.

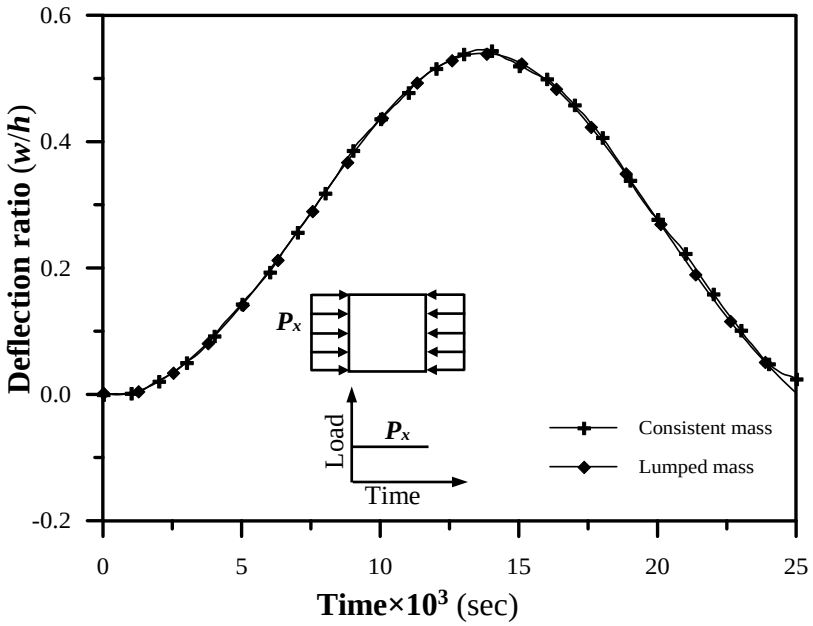

Figure (7.7): Effect of mass matrix type on the large displacement elastic-plastic dynamic analysis of a square simply supported plate under suddenly applied in-plane constant dynamic loading, (b/h=100,w_o/h=0.1, Δt=0.0001 sec, P_x=504 kN/m)

5. Effect of method of integration

To study the effect of integration method on the large displacement elastic-plastic dynamic analysis of a square plate subjected to in-plane dynamic loading, two methods of integration were considered (**Newmark** integration method, and harmonic acceleration method). The plate has an initial imperfection (w_o/h) of (0.1) by which the shape is considered to be a sinusoidal curve. The geometry and material properties of analyzed plate are (E=200 GPa, σ_o=240 MPa, v=0.3, a=b=1.0 m, h=0.01 m, b/h=100, P_x=504 kN/m, ρ=78 kN.sec^2/m^4, Δt=0.00010 sec). A consistent mass matrix was considered in the present study.

Figure (7.8) shows the effect of type of integration method on the nonlinear dynamic analysis of a square plate with aspect ratio (a/b=1) and slenderness ratio (b/h=100), under in-plane dynamic loading. One can see that the difference between the two methods is very small but the harmonic acceleration method needs more time by the iterative solution than **Newmark** method and so it needs to calculate the free vibration frequency.

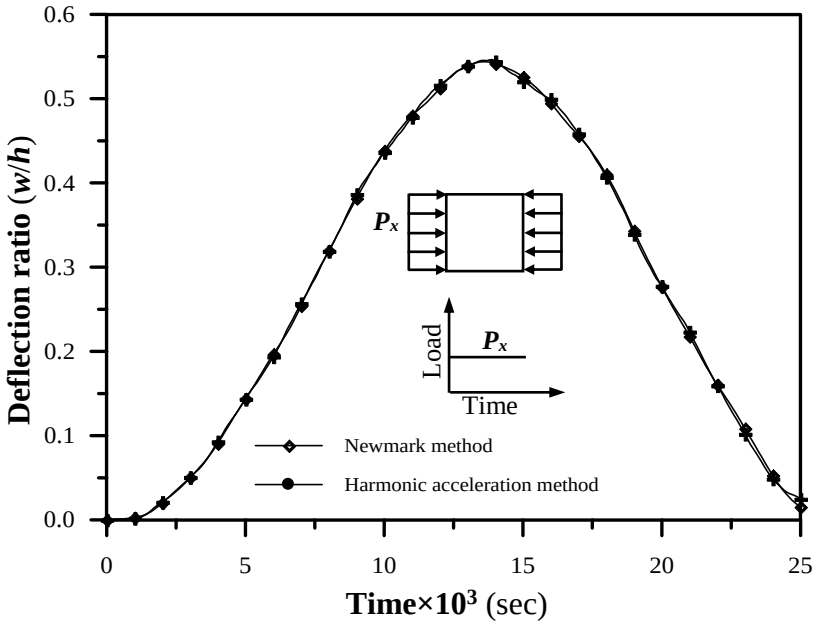

Figure (7.8): Effect of type of integration method on the large displacement elastic-plastic dynamic analysis of a square simply supported plate under suddenly applied in-plane constant dynamic loading, (b/h=100,w_o/h=0.1, Δt=0.0001 sec, P_x=504 kN/m)

6. Effect of boundary conditions

To study the effect of boundary conditions on the large displacement elastic-plastic dynamic analysis of steel plate, a square plate under in-plane dynamic loading with various boundary conditions was analyzed. Three types of boundary conditions (all edges simply supported, all edges clamped, two edges in load direction clamped and other two edges simply supported) were considered. The plate has an initial imperfection (w_o/h=0.25) by which the shape is considered to be a sinusoidal curve. Only a quarter of the plate is modeled by (2×2) element mesh due to the symmetry. The following properties of the thin plate are (a=b=1.0m, h=0.01m, E=200 GPa, σ_o=240 MPa, ν=0.30, ρ=78 kN.sec^2/m^4, P_{max}=504 kN/m, Δt=0.0001 (sec)). A consistent mass matrix and **Newmark** integration method with α=1/2, and β=1/4 were considered in the present study.

Figure (7.9) presents the time history of the square steel plate with slenderness ratio (b/h=100) under in-plane constant dynamic loading and with initial imperfection (w_o/h=0.25). As it is explained from this figure, it can be noticed that the oscillation of the plate will decrease as the restrains of the edges increase.

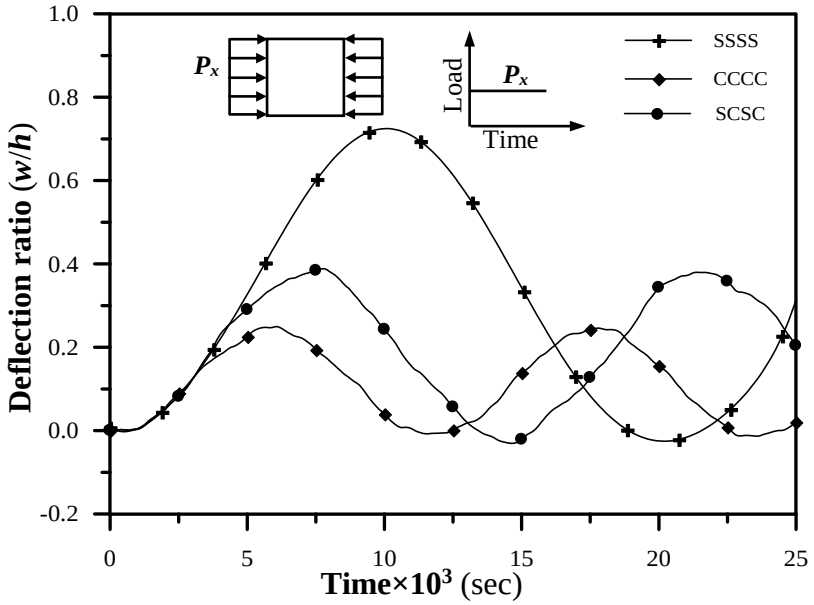

Figure (7.9): Effect of boundary condition on the large displacement elastic-plastic dynamic analysis of a square simply supported plate under suddenly applied in-plane constant dynamic loading, (b/h=100,w_o/h=0.25, Δt=0.0001 sec, P_x=504 kN/m)

7. Effect of loading type

A square simply supported plate under different types of in-plane pulse dynamic loading was analyzed to study the effect of type of loading for the same duration of time and the same peak value of loading on large displacement elastic-plastic dynamic analysis of steel plate. The plate has an initial imperfection (w_o/h) of (0.25) by which the shape is considered to be a sinusoidal curve. The geometry and material properties of the analyzed plate are (a=b=1.0 m, h=0.01m, E=200 GPa, σ_o=240 MPa, ν=0.30, ρ=78 kN.sec^2/m^4, P_{max}=504 kN/m, T_d=0.005 (sec)), Δt=0.0001 (sec)). A consistent mass matrix and **Newmark** integration method were considered in the present study. Different types of in-plane dynamic loading were considered, as given in Figure (7.10). An in-plane exponential pulse loading as a function of time as ($P_x(t) = P_{max}\left(1-\frac{t}{T_d}\right).exp\left(-0.35\frac{t}{T_d}\right)$) where P_{max} is the peak value and the parabolic in-plane pulse loading is a function of time as

$$P_x(t) = \begin{cases} \eta_1 t^2 + \eta_2 t & (0 \le t \le T_d) \\ 0 & (t > T_d) \end{cases}$$

where $\eta_1 = \frac{-4P_{max}}{T_d^2}, \eta_2 = \frac{4P_{max}}{T_d}$, P_{max} is the peak value of the in-plane pulse dynamic loading.

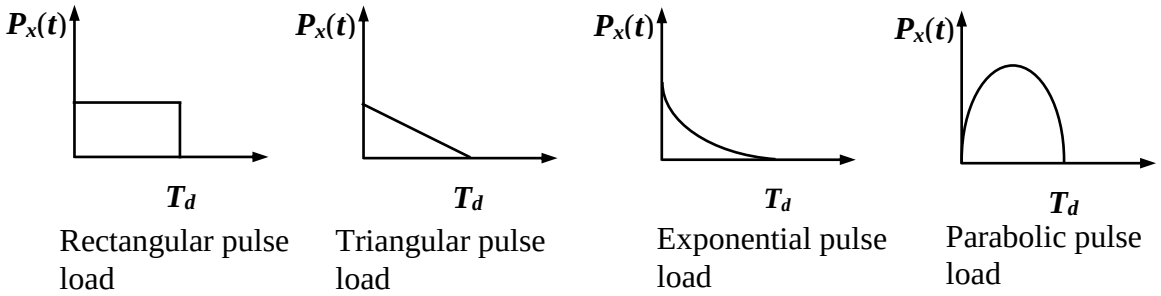

Figure (7.10): Types of in-plane dynamic loading.

Figure (7.11) shows the central deflection ratio-time curve of simply supported square plate under different in-plane loading with the same duration of time. From this figure it can be noticed that dynamic buckling occurs in the plate under the rectangular in-plane loading at early steps and gives maximum central deflection. This reveals that the pulse rectangular loading is very significant than other types of loading.

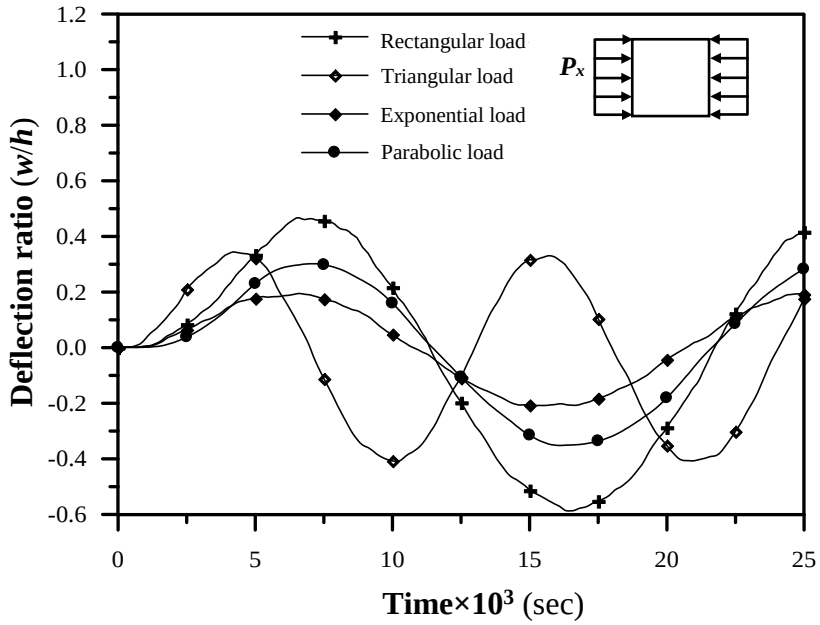

Figure (7.11): Effect of type of in-plane dynamic loading on the large displacement elastic-plastic dynamic analysis of a simply supported square plate, (b/h=100, T_d=0.005 sec, Δt=0.0001 sec, P_x=504 kN/m, w_o/h=0.25)

8. Effect of load magnitude

The large displacement elastic-plastic dynamic analysis of a steel plate subjected to uniform in-plane dynamic loading is also analyzed with varying range of in-plane dynamic loading taken as a ratio of the static ultimate load. The initial imperfection shape is considered to be a sinusoidal curve. The following material properties are used in the analysis: (E=200 GPa, ν= 0.30; σ_o=240 MPa, and ρ=78 kN.sec^2/m^4), and the geometry properties are (a=1.0 m, a/b=1, and h=0.01m). Constant in-plane dynamic loading (constant with time), and time step (Δt=0.0001 (sec)) were considered. The analyzed plate is simply supported and subjected to a uniform in-plane load with the unloaded edges able to move in the in-plane direction but remain straight. A consistent mass matrix and **Newmark** integration method with α=1/2, and β=1/4 were considered in the present study.

Figures (7.12) presents the time history curve of simply supported plate under in-plane loading with a range of loading ratio (P_x/P_u)(0.5-0.7), where P_u is the ultimate in-plane loading of the plate at static analysis. The ultimate in-plane loading for the plate with no initial imperfection (w_o/h=0.0) is (1273 kN/m).

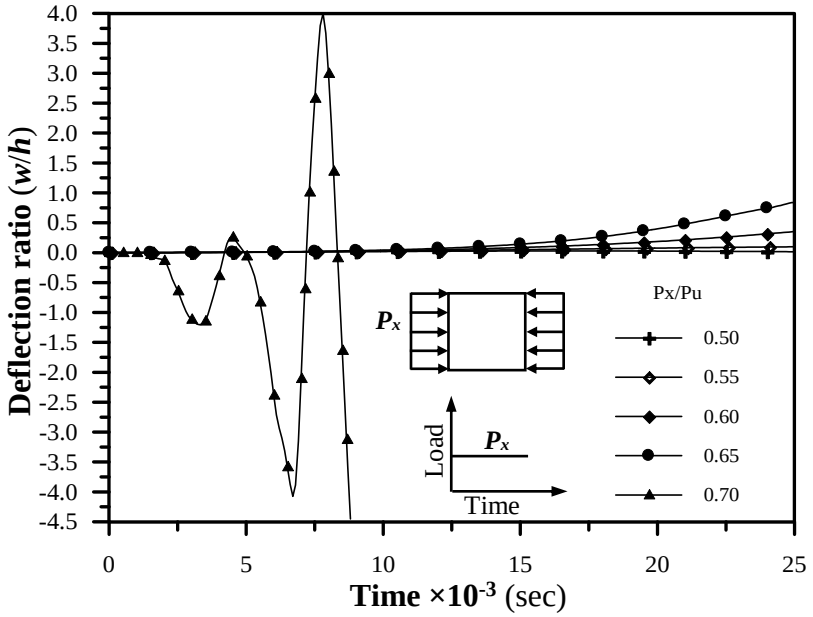

Figure (7.12): Effect of load magnitude on the large displacement elastic-plastic dynamic analysis of a square simply supported plate with range of in-plane constant dynamic loading ratio (0.5-0.7),(b/h=100, Δt=0.0001 sec, w_o/h=0.0).

Figure (7.13) presents the time history curve of the simply supported plate under in-plane constant dynamic loading with a range of loading ratio (P_x/P_u)(0.4-0.6). The ultimate in-plane loading for the plate with initial imperfection (w_o/h=0.1) is (1260 kN/m).

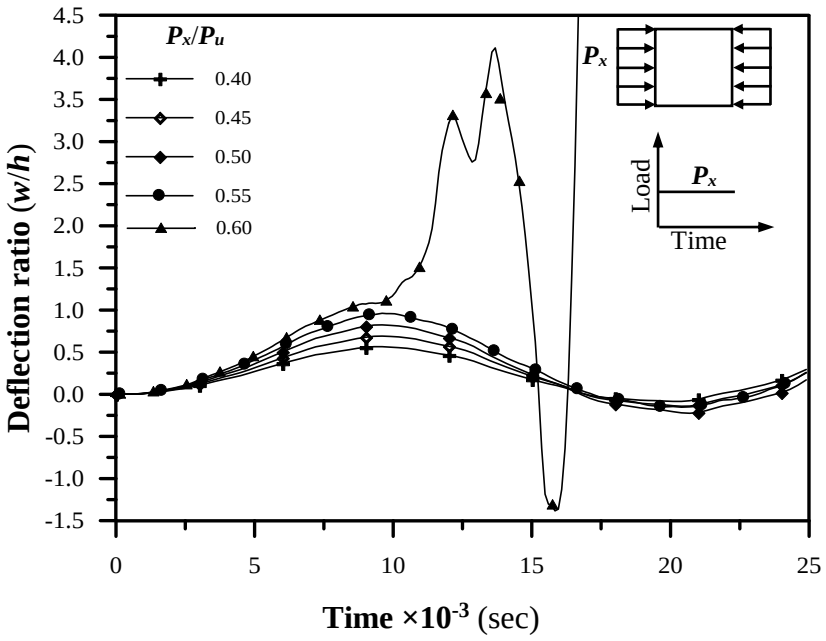

Figure (7.13): Effect of load magnitude on the large displacement elastic-plastic dynamic analysis of a square simply supported plate with range of in-plane constant dynamic loading ratio (0.4-0.6),(b/h=100, Δt=0.0001 sec, w_o/h=0.1).

Figure (7.14) presents the time history curve of simply supported plate under in-plane loading with range of loading ratio (P_x/P_u)(0.4-0.6). The ultimate in-plane loading for the plate with initial imperfection (w/h=0.25) is (1236 kN/m).

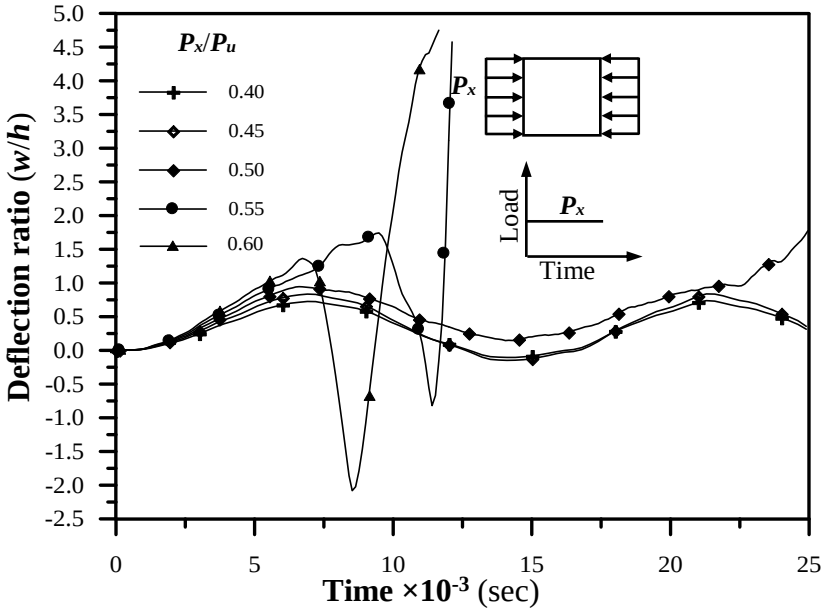

Figure (7.14): Effect of load magnitude on the large displacement elastic-plastic dynamic analysis of a simply supported square plate with range of in-plane constant dynamic loading ratio (0.4-0.6),($\boldsymbol{b/h}$=100, $\Delta \boldsymbol{t}$=0.0001 sec, $\boldsymbol{w_o/h}$=0.25).

9. Effect of damping

As in the previous parametric studies, the same plate was analyzed to study the effect of damping on the large displacement elastic-plastic dynamic behavior of the steel plate. Different values of damping factor (0.01-0.1) were considered in the present study. The initial imperfection shape is considered to be a sinusoidal curve. The following material properties are used in the analysis: ($\boldsymbol{E}$=200 GPa; σ_o=240 MPa; $\boldsymbol{v}$= 0.30, and ρ=78 kN.sec^2/m^4, $\boldsymbol{w_o/t}$=0.10), and the geometry properties are ($\boldsymbol{a}$=1.0 m, $\boldsymbol{a/b}$=1, and $\boldsymbol{h}$=0.01m). In-plane dynamic loading (constant with time), and time step ($\Delta \boldsymbol{t}$=0.0001 (sec)) were used. A consistent mass matrix and **Newmark** integration method with α=1/2, and β=1/4 were considered in the present study.

Figures (7.15) and (7.16) present the time history curve of the simply supported plate under in-plane constant dynamic loading with range of loading ratio ($\boldsymbol{P_x/P_u}$) (0.6-0.75). Two values of damping factor were considered (0.01 and 0.05), respectively.

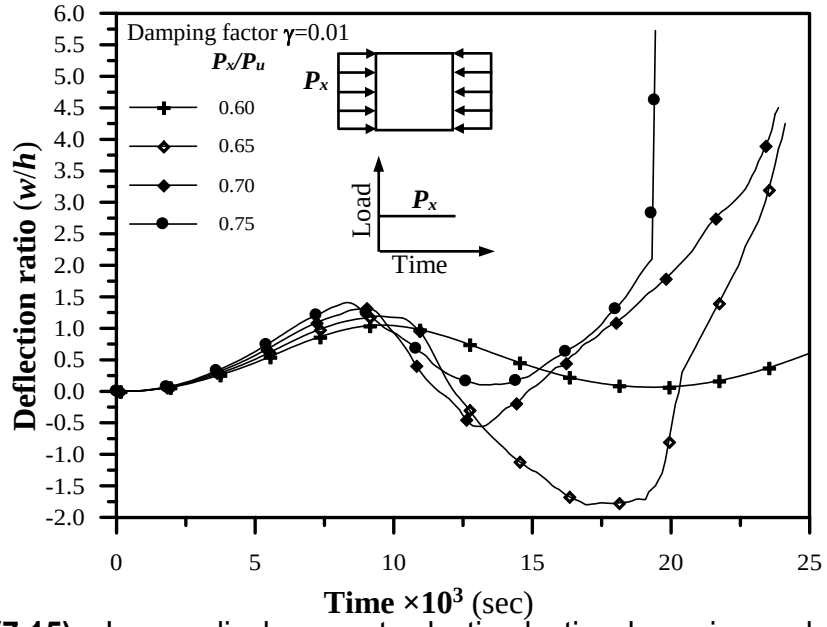

Figure (7.15): Large displacement elastic-plastic dynamic analysis of a simply supported square plate with range of in-plane constant dynamic loading ratio (0.6-0.75) and damping factor (γ=0.01),($\boldsymbol{b/h}$=100, $\Delta \boldsymbol{t}$=0.0001 sec, $\boldsymbol{w_o/h}$=0.10)

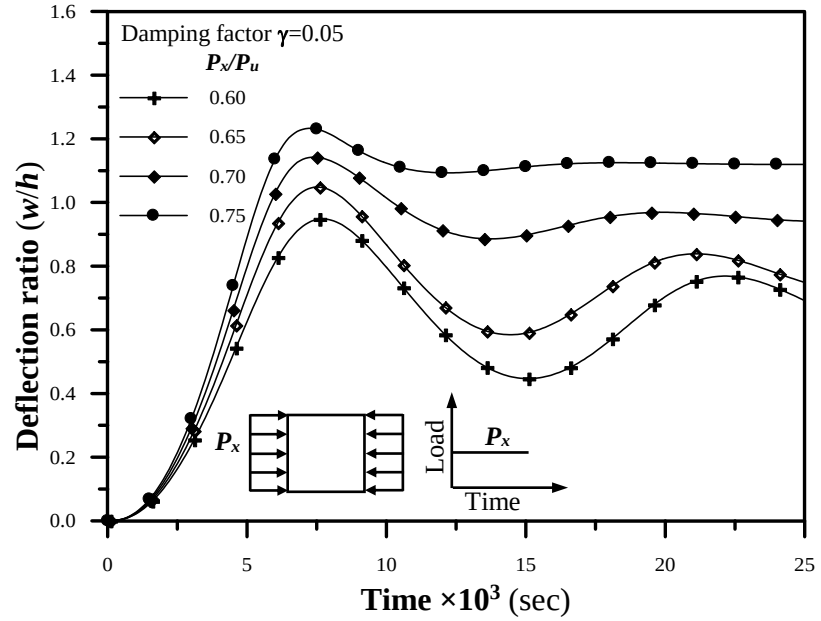

Figure (7.16): Large displacement elastic-plastic dynamic analysis of a simply supported square plate with range of in-plane constant dynamic loading ratio (0.6-0.75) and damping factor (γ=0.05),($\boldsymbol{b/h}$=100, $\Delta \boldsymbol{t}$=0.0001 sec, $\boldsymbol{w_o/h}$=0.10)

Figures (7.17) and (7.18) present the time history curve for the simply supported plate under in-plane dynamic loading with a range of damping

factors (γ) (0.01-0.10). The value of the in-plane dynamic loading ratio (P_x/P_u) was taken (0.75) and the plate has two cases of initial imperfections (w_o/h) (0.10 and 0.25) were considered.

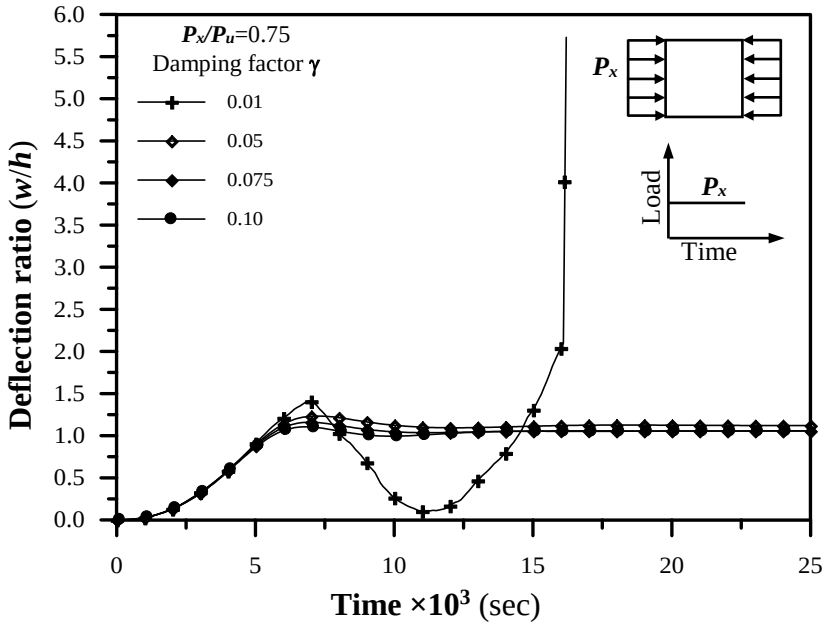

Figure (7.17): Effect of damping factor on the large displacement elastic-plastic dynamic analysis of a square simply supported plate under in-plane constant dynamic loading, (b/h=100, Δt=0.0001 sec, w_o/h=0.10, P_x/P_u=0.75)

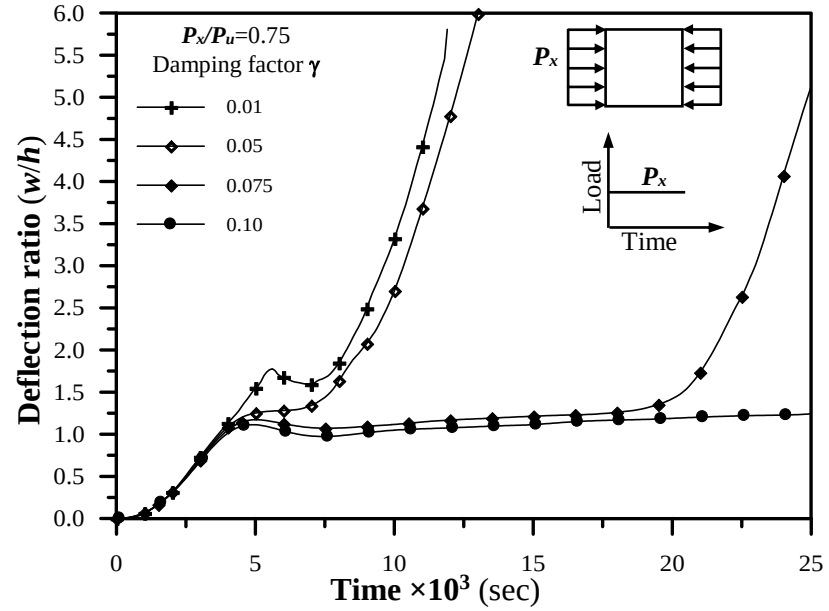

Figure (7.18): Effect of damping factor on the large displacement elastic-plastic dynamic analysis of a square simply supported plate under in-plane constant dynamic loading,(b/h=100, Δt=0.0001 sec, w_o/h=0.25, P_x/P_u=0.75)

From these figures, the following can be noticed that:

1. The perfect plate does not reveal any oscillation when the in-plane dynamic loading is less than the buckling load of the plate.
2. The dynamic capacity of the plate decreases with the increase of the initial imperfection and the duration time decreases too.
3. The increase in damping factor will decrease more rapidly the amplitude of the response gradually with time and causes rapid slowing of the oscillation of the plate.
4. The dynamic capacity of a plate will increase with increasing the damping factor. By increasing the damping factor, the plate behavior will approach to that of static behavior.
5. If the response of the plate shows no oscillation about the static deflection position, it means that the damping factor is below the critical damping ratio.

7.2.3 Comparison with available theoretical investigation of composite plate

Clamped supported square angle-ply laminated plate under transverse suddenly applied constant dynamic loading

A square angle-ply ($0^o/45^o/90^o$/core/$90^o/45^o/30^o/0^o$) sandwich laminated plate with clamped edges and subjected to a suddenly applied uniformly transverse load was analyzed and compared with **Kommineni** and **Kant** [**1993**][(57)]. The following layer material properties are used in the analysis: for face sheets (Graphite/epoxy prereg system) ($\boldsymbol{E}_1$=130.8 GPa; $\boldsymbol{E}_2$=10.6 GPa $\boldsymbol{G}_{12}$=$\boldsymbol{G}_{13}$=6 GPa; $\boldsymbol{G}_{23}$=3.9 GPa; $\boldsymbol{v}_{12}$=0.28; and ρ=15.8 kN.sec^2/m^4); for core sheet (US Commercial al. honeycomb, ¼ in cell size, 0.003 in foil) ($\boldsymbol{G}_{13}$=0.5206 GPa; $\boldsymbol{G}_{23}$=0.1772 GPa; ρ=1.009 kN.sec^2/m^4). The time step is ($\Delta\boldsymbol{t}$=0.000025 sec),and applied load ($\boldsymbol{q}$=50 kN/m^2). The geometry properties are ($\boldsymbol{a}$=1.0 m, $\boldsymbol{a}/\boldsymbol{b}$=1, and $\boldsymbol{h}$=0.01m, at top three stiff layers, thickness of each layer=0.025 $\boldsymbol{h}$, at bottom four stiff layer, thickness of each layer=0.08125 $\boldsymbol{h}$, and thickness of core=0.6 $\boldsymbol{h}$). **Kommineni** and **Kant** used nine-node isoparametric Lagrangian elements with nine-node degrees of freedom per node and divided the full plate into (4×4) element mesh.

In the present study, the full laminated plate is modeled by (4×4) element mesh with nine-node isoparametric Lagrangian element and nine degrees of freedom per node. A consistent mass matrix and **Newmark** integration method with α=1/2, and β=1/4 were used in the present study.

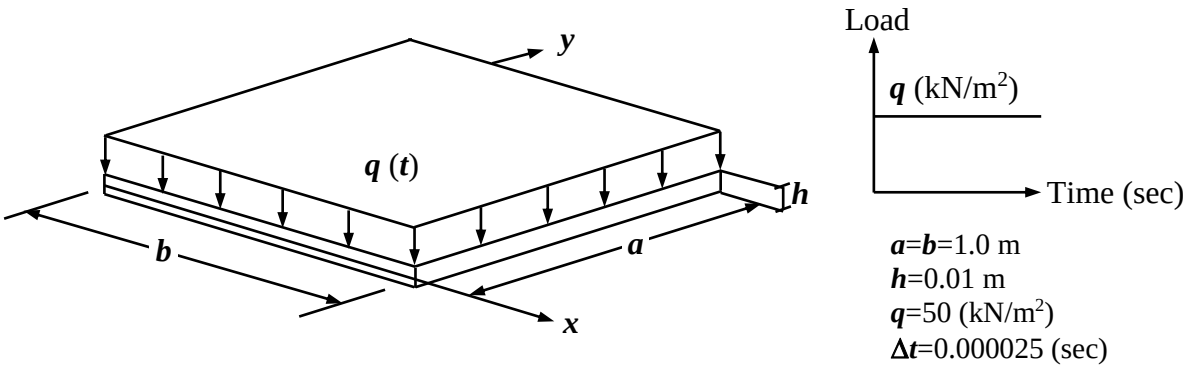

Figure (7.19): Details of a clamped square sandwich composite plate under transverse constant dynamic loading

Figure (7.20) shows the time history curve for the clamped angle-ply laminated plate under transverse suddenly applied load. From this figure, it can be noticed that good agreement with other study exists with a difference not exceeding (1%).

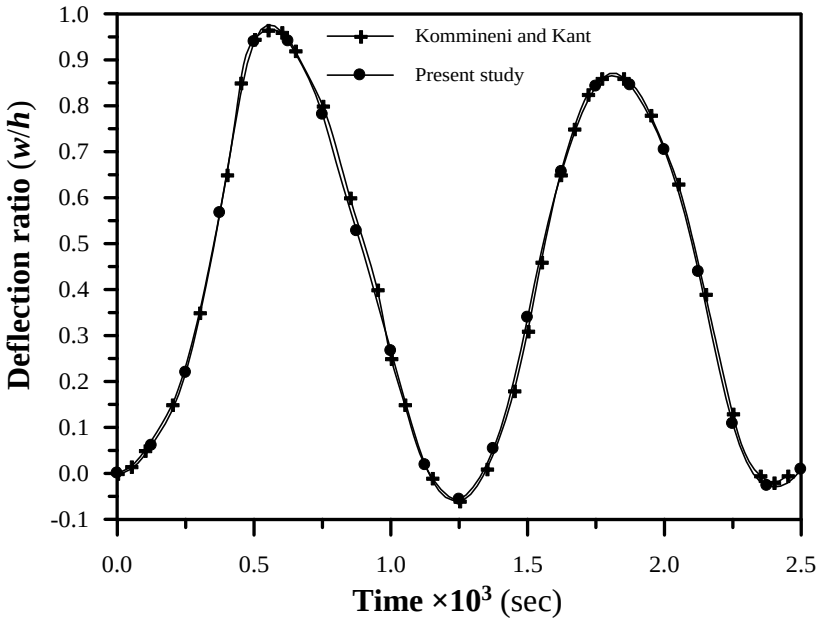

Figure (7.20): Central deflection ratio-time curve of a clamped square sandwich composite plate under transverse constant dynamic loading,(***b/h***=100, Δt=0.000025sec, ***q***=50 kN/m^2)

7.2.4 Parametric Study

To investigate the large displacement elastic-plastic dynamic behavior of laminated composite plate under in-plane dynamic loading, effects of several important parameters were studied.

The selected parametric studies can be summarized as follows:

1. The effect of number of layers.
2. The effect of through-thickness shear deformation.
3. The effect of degree of orthotropy of individual layers.
4. The effect of fiber's orientation angle.
5. The effect of load magnitude.
6. The effect of damping.
7. The effect of fiber waviness.

Each one of the above parameters was studied individually by analyzing a type of laminated composite plate. In all cases, the nine-node isoparametric Lagrangian element was used and one quadrant of the plate was analyzed due to symmetry and (2×2) element mesh which was used for the cross-ply laminated plates while the angle-ply and sine wave fiber plates were analyzed by considering full plates with (4×4) element mesh. Lateral in-plane expansion is allowed at the loaded ends and the unloaded edges were allowed to move in the in-plane direction but remain straight. The following geometry and layer material properties of high graphite epoxy are used in the analysis: ($\boldsymbol{E}_1$=172.5 GPa***;*** $\boldsymbol{E}_2$=7.08 GPa; $\boldsymbol{G}_{12}$=$\boldsymbol{G}_{13}$=3.45 GPa, $\boldsymbol{G}_{23}$=1.38 GPa; $\boldsymbol{E}_f$=341.42 GPa; $\boldsymbol{E}_m$=3.58 GPa; $\boldsymbol{V}_f$=0.5; $\boldsymbol{V}_m$=0.5; $\boldsymbol{\nu}_{12}$=$\boldsymbol{\nu}_{13}$=$\boldsymbol{\nu}_{23}$=0.25, ρ=15.8 kN.sec^2/m^4 $\boldsymbol{X}_t$=$\boldsymbol{X}_c$=1450 MPa, $\boldsymbol{Y}_t$=36 MPa, $\boldsymbol{Y}_c$=230 MPa, $\boldsymbol{S}$=62 MPa)[83]. The geometry properties are ($\boldsymbol{a}$=1.0 m, $\boldsymbol{a}$/$\boldsymbol{b}$=1).

1. Effect of number of layers

A simply supported square plate with slenderness ratio ($\boldsymbol{b}$/$\boldsymbol{h}$=100), and with symmetric cross-ply and antisymmetric cross-ply arrangements, were chosen to study the effect of number of layers on the large displacement elastic-plastic dynamic behavior of a laminated composite plate under in-plane constant dynamic loading. The initial imperfection is ($\boldsymbol{w}_o$/$\boldsymbol{h}$= 0.1) by which

the shape is considered to be a sinusoidal curve. The consistent mass matrix and **Newmark** integration method with α=1/2, and β=1/4 were used in the present study.

Figures (6.21) and (6.22) present the time history curve and show that for the same volume of the plate, the response (deflection) will decrease about (15%) for the symmetric cross-ply and about (29%) for the antisymmetric cross-ply plates where with increasing the number of layers (3-10) for the symmetric cross-ply and (2-10) for the antisymmetric cross-ply arrangements, the stiffness increase may be related to the increase of the number of the reinforced layers. Thus, extension and bending stiffness will increase; and therefore, the amplitude will decrease. Also, the increase of the number of layers will give a better distribution of orthogonal stiffness through the depth. From these figures, it can be seen that the increase of the number of layers more than (8 layers) for the symmetric cross-ply and the antisymmetric cross-ply plates have slight effect on increasing the stiffness of the plate.

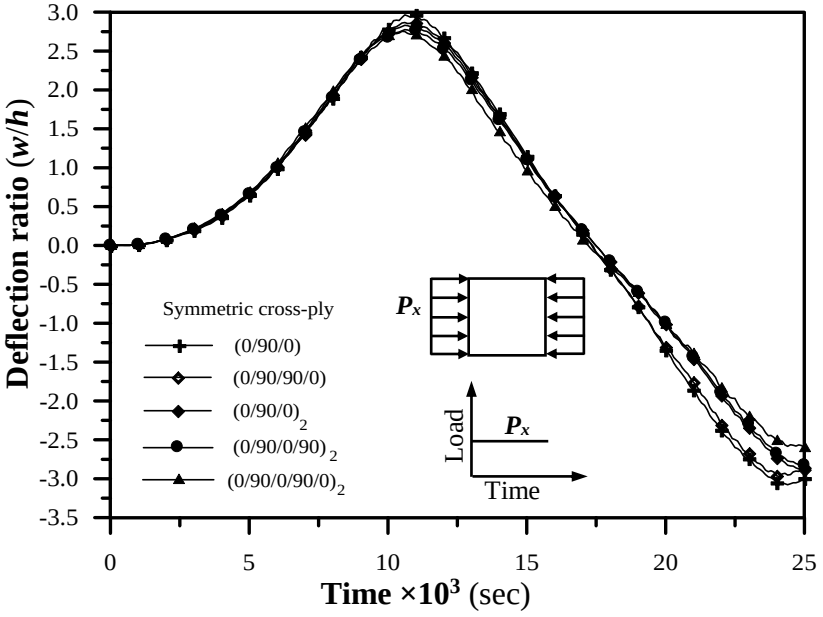

Figure (7.21): Effect of number of layers on the large displacement elastic-plastic analysis of symmetric cross-ply laminated plate under in-plane constant dynamic loading ratio (P_x/P_u=0.4), (b/h=100,Δt=0.0001, w_o/h=0.1)

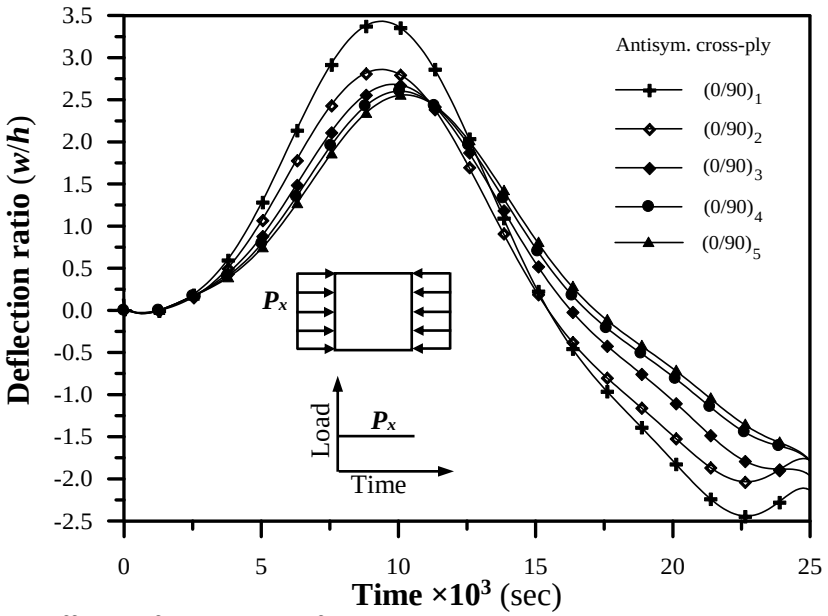

Figure (7.22): Effect of number of layers on the large displacement elastic-plastic analysis of antisymmetric cross-ply laminated plate under in-plane constant dynamic loading ratio (P_x/P_u=0.4), (b/h=100,Δt=0.0001, w_o/h=0.1)

2. Effect of through-thickness shear deformation

To study the effect of shear deformation on the large displacement elastic-plastic dynamic analysis of a laminated composite plate under in-plane constant dynamic loading, a simply supported square plate with slenderness ratio (b/h=20), and with symmetric cross-ply and antisymmetric cross-ply arrangements and with eight layers was analyzed. The initial imperfection is (w_o/h= 0.1) by which the shape is considered to be a sinusoidal curve. The consistent mass matrix and **Newmark** integration method with α=1/2, and β=1/4 were used in the present study.

Figures (7.23) and (7.24) present the time history curves for the symmetric cross-ply, and for the antisymmetric cross-ply laminated composite plates by taking the through-thickness shear deformation through the degrees of freedom of the element. From these figures, it can be noticed that increasing the number of degrees of freedom per node from five degrees to nine degrees will increase the central deflection about (16%) for symmetric cross-ply and about (20%) for antisymmetric cross-ply plates.

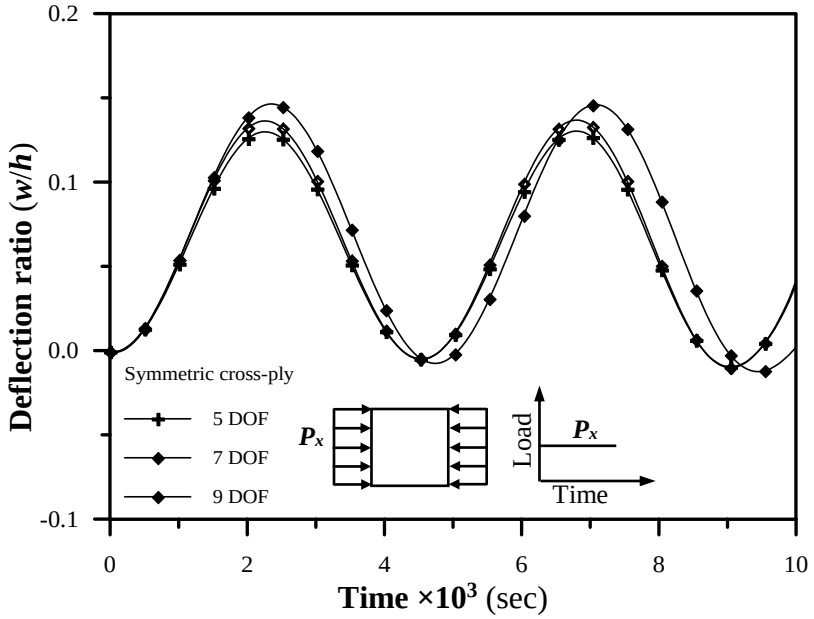

Figure (7.23): Effect of transverse shear deformation on the large displacement elastic-plastic analysis of symmetric cross-ply laminated plate under in-plane constant dynamic loading ratio (P_x/P_u=0.3), (b/h=20,Δt=0.0001, w_o/h=0.1,P_u=18563 kN/m)

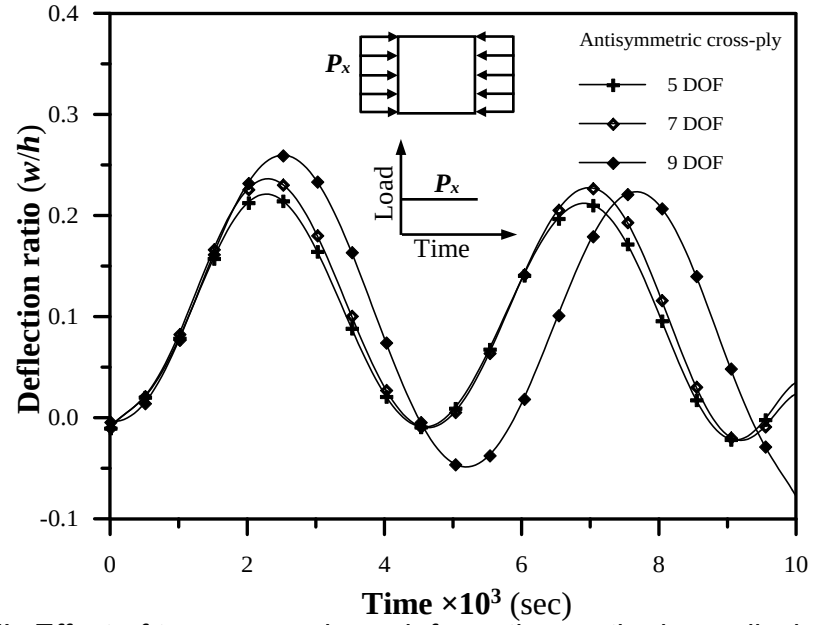

Figure (7.24): Effect of transverse shear deformation on the large displacement elastic-plastic analysis of antisymmetric cross-ply laminated plate under in-plane constant dynamic loading ratio (P_x/P_u=0.3), (b/h=20,Δt=0.0001, w_o/h=0.1,P_u=16347 kN/m)

3. Effect of degree of orthotropy of individual layers

To show the effect of degree of orthotropy of individual layers on the response of the laminated composite plate under in-plane dynamic loading, a simply supported square plate with symmetric cross-ply and antisymmetric cross-ply arrangements and with slenderness ratio (b/h=40) was analyzed. The modulus of elasticity in the direction orthogonal to the fibers used in the analysis was: (E_2=7.08 GPa) and the time step was (Δt=0.0001 sec). The suddenly applied in-plane loading ratio was (P_x/P_u=0.40)). The static ultimate in-plane compressive loading (P_u) for the symmetric cross-ply plate was (4275 kN/m) and the ultimate in-plane compressive loading for the antisymmetric cross-ply plates was (3968 kN/m). The initial imperfection was (w_o/h= 0.1) by which the shape was considered to be a sinusoidal curve. Again, a consistent mass matrix and **Newmark** integration method with α=1/2, and β=1/4 were used in the present study. A quarter of the laminated plate was modeled by (2×2) element mesh with nine-node isoparametric Lagrangian elements having nine-degrees of freedom per node.

Figures (7.25) and (7.26) present the time history curves for the considered plates of symmetric cross-ply and antsymmetric cross-ply arrangements under in-plane dynamic loading, respectively with a range of orthotropy ratio (E_1/E_2) (1-20). It can be noticed that the response (deflection) of the laminated plates will decrease as soon as the orthotropy ratio is increased, because of increasing stiffness of laminated plate with the same volume and number of layers. For a range of orthotropy ratio (1-20), the central deflection will decrease about (78%) for the symmetric cross-ply and about (70%) for the antisymmetric cross-ply plates. The degree of orthotropy ratio may be changed by using different types of fibers such as boron, graphite, glass, …etc.

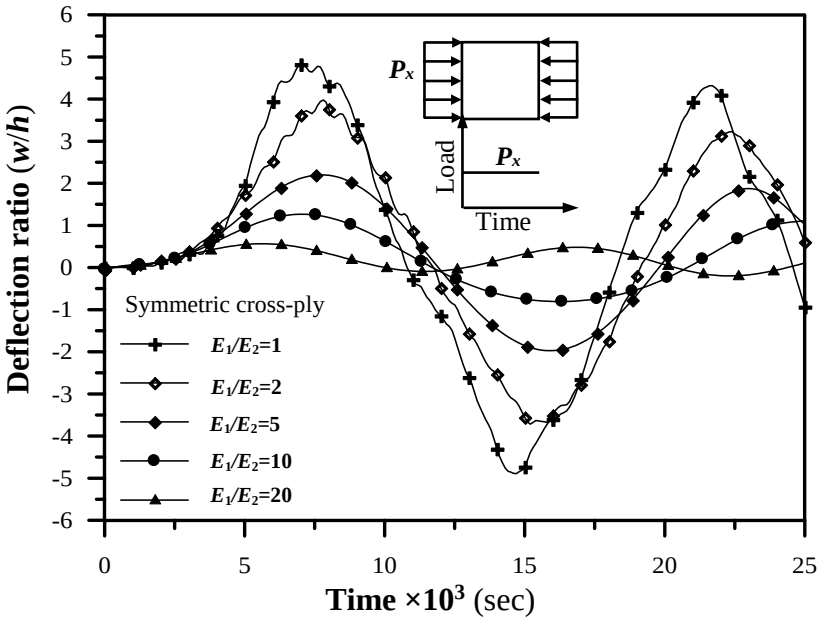

Figure (7.25): Effect of orthotropy of layers on the large displacement elastic-plastic dynamic analysis of symmetric cross-ply simply supported square plate under in-plane constant dynamic loading (P_x/P_u=0.4), (b/h=40,Δt=0.0001, w_o/h=0.1)

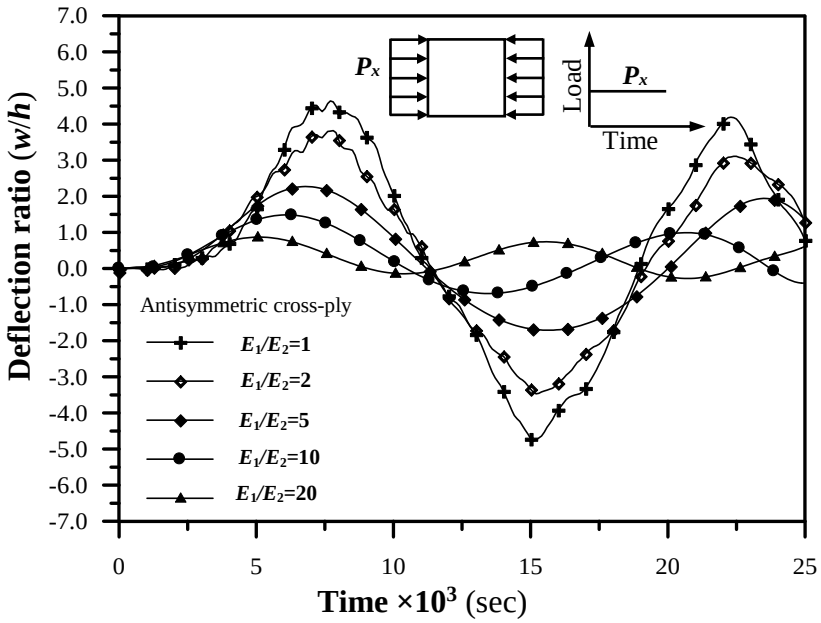

Figure (7.26): Effect of orthotropy of layers on the large displacement elastic-plastic dynamic analysis of antisymmetric cross-ply simply supported square plate under in-plane constant dynamic loading ratio(P_x/P_u=0.4),(b/h=40,Δt=0.0001,w_o/h=0.1)

4. Effect of fiber's orientation angle

To show the effect of fiber's orientation angle on the large displacement elastic-plastic dynamic analysis of laminated composite plates under in-plane constant dynamic loading, a simply supported square plate with slenderness ratio (***b/h***=60) was considered. The initial imperfection was (***w*****o*****/h*****=** 0.1) by which the shape was considered to be a sinusoidal curve. A consistent mass matrix and **Newmark** integration method with α=1/2, and β=1/4 were used in the present study. A quarter of the laminated plate was modeled (2×2) element mesh with nine-node isoparametric Lagrangian elements having nine degrees of freedom per node.

Figure (7.27) presents the time history curve for the laminated simply supported square plate under in-plane dynamic loading and with many types of fiber's orientation angle. From this figure, it could be noticed that the central deflection of the plate with (0^o/90^o) is less than the deflections of others, this orientation's fiber is the optimum for a plate under in-plane dynamic loading.

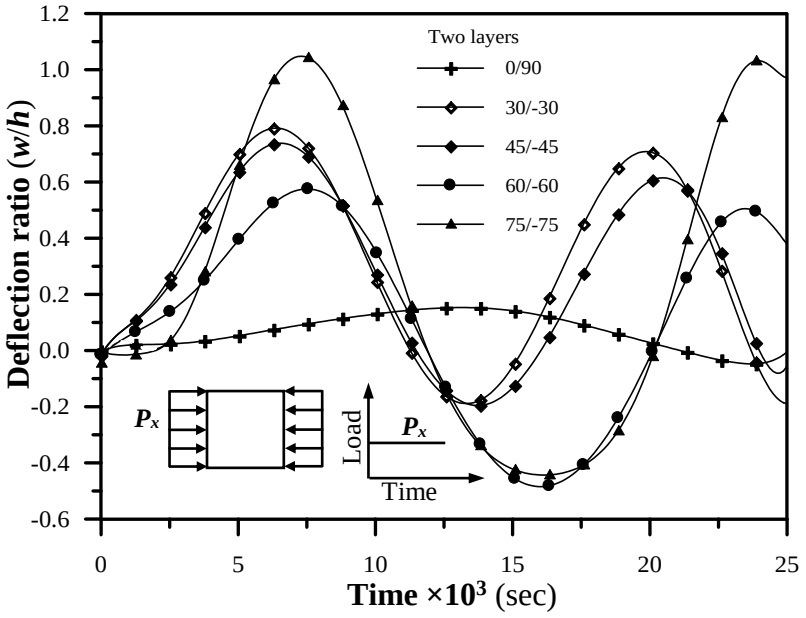

Figure (7.27): Effect of fiber's orientation angle on the large displacement elastic-plastic analysis of a laminated simply supported square plate under in-plane constant dynamic loading (***P*****x**=700 kN/m), (***b/h***=60, Δt=0.0001, ***w*****o*****/h***=0.1)

5. Effect of load magnitude

To study the effect of load magnitude on the large displacement elastic-plastic behavior of laminated composite plates under in-plane constant dynamic loading, a simply supported square plate with slenderness ratio (b/h=100) was analyzed with a range of in-plane constant dynamic loading ratio (P_x/P_u). The initial imperfection shape was considered to be a sinusoidal curve. The consistent mass matrix and **Newmark** integration method with α=1/2, and β=1/4 were used in the present study. A quarter of the laminated plate was modeled by (2×2) element mesh with nine-node isoparametric Lagrangian elements having nine degrees of freedom per node.

Figures (7.28) and (7.29) present the central deflection ratio-time curve of the simply supported square plate with symmetric cross-ply composite lamination under in-plane constant dynamic loading. The values of the static ultimate strength of the symmetric cross-ply plates are (P_u=972.4 kN/m) for plate with initial imperfection (w_o/h=0.0) and (P_u=960 kN/m) for plate with initial imperfection (w_o/h=0.1).

Figures (7.30) and (7.31) present the central deflection ratio-time curve of simply supported square plate with antisymmetric cross-ply composite lamination under in-plane dynamic loading. The values of the static ultimate strength of the symmetric cross-ply plates are (P_u=960 kN/m) for plate with initial imperfection (w_o/h=0.0) and (P_u=955 kN/m) for plate with initial imperfection (w_o/h=0.1). It is noticed that the time capacity decreases with increasing the loading ratio and also with increasing the initial imperfection.

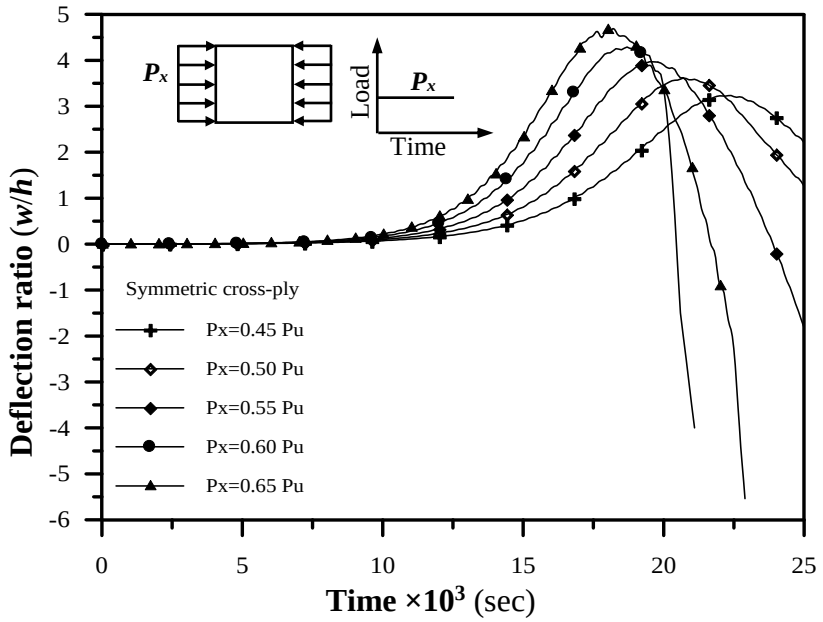

Figure (7.28): Effect of load magnitude on the large displacement elastic-plastic analysis of a simply supported square symmetric cross-ply plate under in-plane constant dynamic loading, (b/h=100, Δt=0.0001, w_o/h=0.0, P_u=972.4 kN/m)

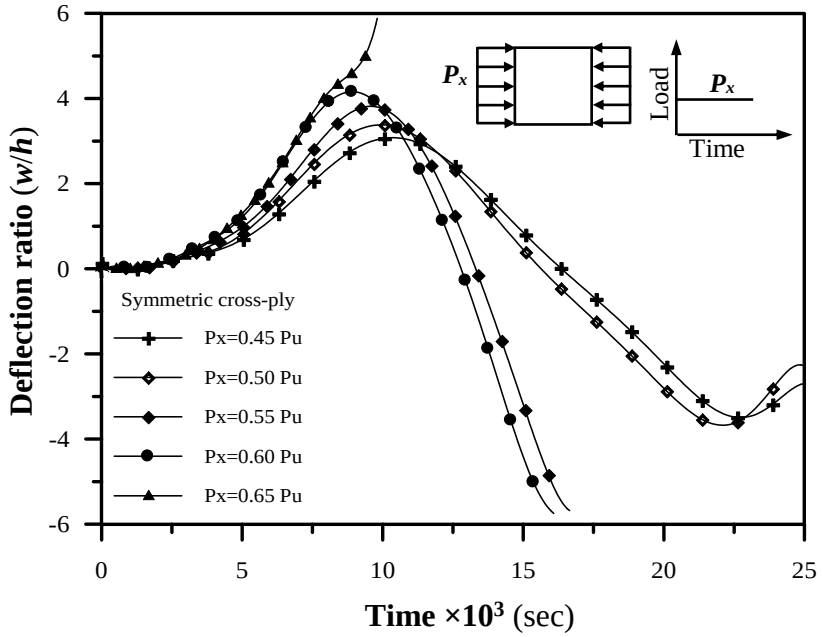

Figure (7.29): Effect of load magnitude on the large displacement elastic-plastic analysis of a simply supported square symmetric cross-ply plate under in-plane constant dynamic loading, (b/h=100, Δt=0.0001, w_o/h=0.1, P_u=960 kN/m)

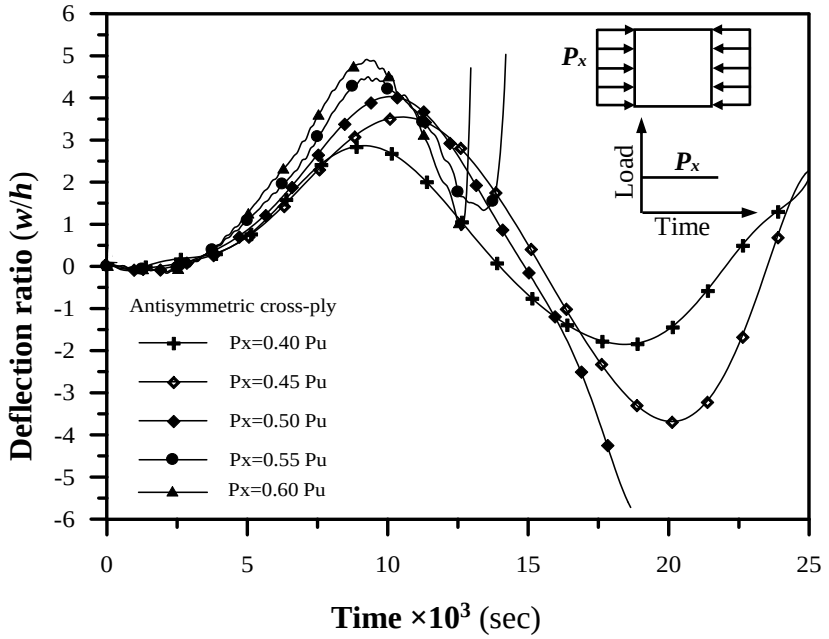

Figure (7.30): Effect of load magnitude on the large displacement elastic-plastic analysis of a simply supported square antisymmetric cross-ply plate under in-plane constant dynamic loading, (b/h=100, Δt=0.0001, w_o/h=0.0, P_u=960 kN/m)

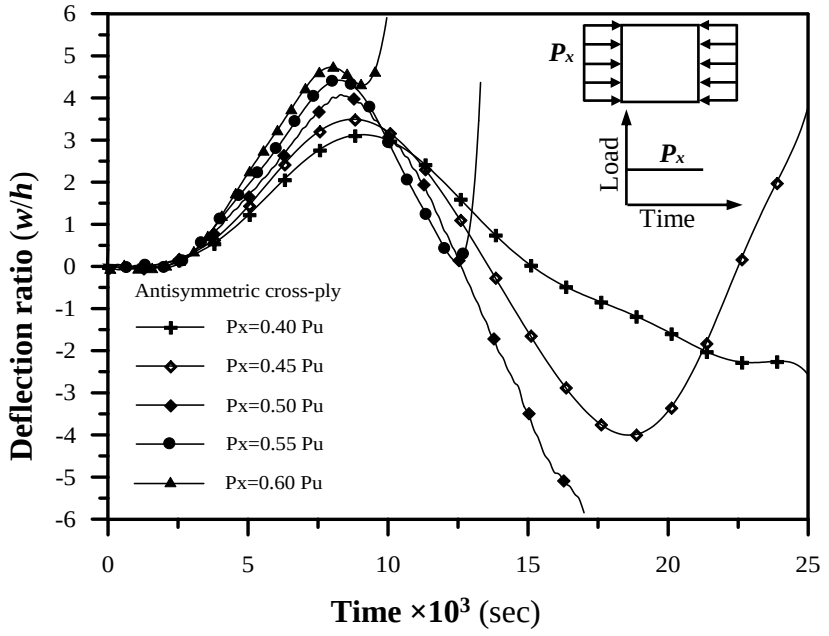

Figure (7.31): Effect of load magnitude on the large displacement elastic-plastic analysis of a simply supported square antisymmetric cross-ply plate under in-plane constant dynamic loading, (b/h=100, Δt=0.0001, w_o/h=0.1, P_u=955 kN/m)

6. Effect of damping

To study the effect of damping on the large displacement elastic-plastic dynamic behavior of composite plates, two examples are considered. The first one is a simply supported square plate with symmetric cross-ply lamination with eight layers and under in-plane dynamic loading. The second one is a simply supported square plate with antisymmetric cross-ply lamination with eight layers and under in-plane dynamic loading. Different values of damping factor (0.0-0.1) are considered in the present study. The initial imperfection shape is considered to be a sinusoidal curve. The consistent mass matrix and **Newmark** integration method with α=1/2, and β=1/4 were used in the present study. A quarter of the laminated plate is modeled by (2×2) element mesh with nine-node isoparametric Lagrangian elements having nine degrees of freedom per node. The plates were analyzed under in-plane constant dynamic loading ratio (P_x/P_u=0.65) for the symmetric cross-ply plate and (P_x/P_u=0.6) for the antisymmetric cross-ply plate.

Figure (7.32) presents the time history curve for a simply supported square plate with symmetric cross-ply lamination under in-plane constant loading with a range of damping factor (γ) (0.0-0.1).

Figure (7.33) presents the time history curve for a simply supported square plate with antisymmetric cross-ply lamination under in-plane constant loading with range of damping factor (γ) (0.0-0.1). It is noticed that the response (deflection) decreases with the increase of the damping factor. Also, the plate shows no oscillation about the static deflection position for damping factors greater than or equal to (0.05). This means that the plate is under the critical damping ratio. So, it can be seen that the antisymmetric lamination of plates has a rate of damping faster than symmetric lamination. This type of lamination can be used in places that need damping property.

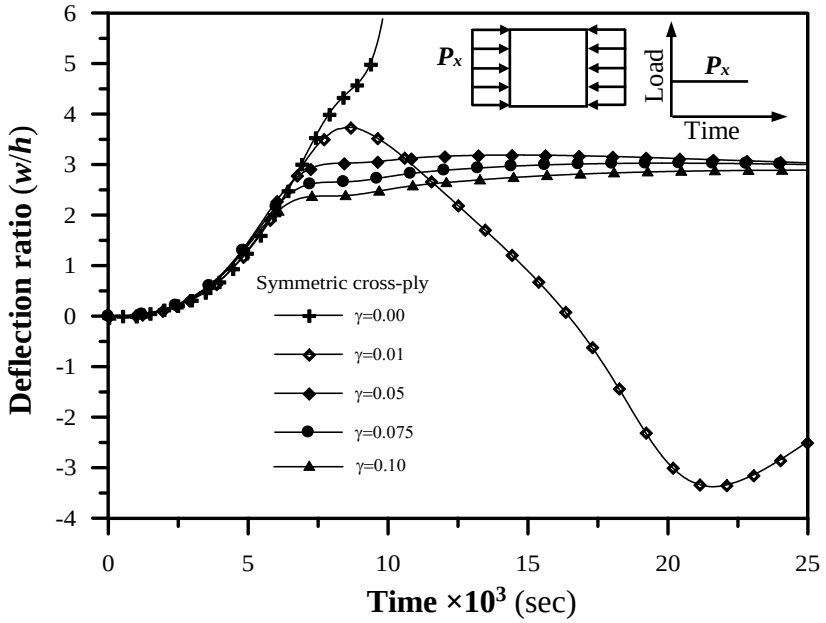

Figure (7.32): Effect of damping factor on the large displacement elastic-plastic analysis of a simply supported square symmetric cross-ply plate under in-plane constant dynamic loading, (b/h=100, Δt=0.0001, w_o/h=0.1, P_x/P_u=0.65)

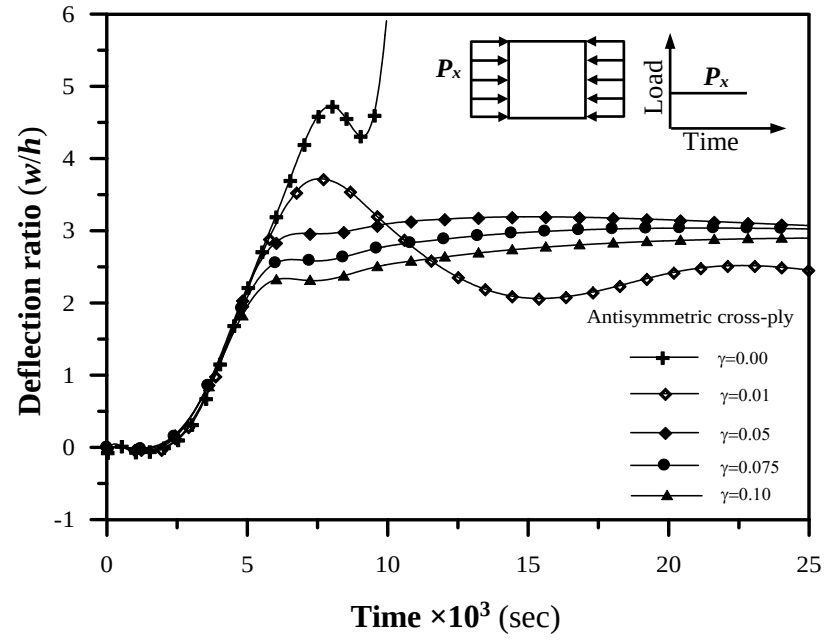

Figure (7.33): Effect of damping factor on the large displacement elastic-plastic analysis of a simply supported square antisymmetric cross-ply plate under in-plane constant dynamic loading, (b/h=100, Δt=0.0001, w_o/h=0.1, P_x/P_u=0.60)

7. Effect of fiber waviness

To study the effect of fiber waviness on the large displacement elastic-plastic dynamic behavior of composite (laminated) plate, two types of lamination were considered. The first one is a simply supported square plate, laminated plate with eight layers under in-plane constant dynamic loading. The second one is a simply supported square symmetric cross-ply laminated plate with eight layers under also constant dynamic loading. Different values of fiber path amplitude (Δ) (0.05-0.5) and different numbers of sequences (***k***) (4-12) were considered. The plates were under in-plane constant dynamic loading (250 kN/m). In the present study, the full laminate plate was modeled with (4×4) element mesh with nine-node isoprametric Lagrangian elements having nine degrees of freedom per node. A consistent mass matrix and **Newmark** integration method with α=1/2, and β=1/4 were used in the present study.

Figures (7.34)-(7.36) show the time history curves for the simply supported composite laminated plate with eight layers having sine wave fiber $(0)_8$ and under in-plane constant dynamic loading.

Figures (7.37)-(7.39) show the time history curves for the square symmetric cross-ply composite laminated plate under in-plane suddenly applied constant dynamic loading and having eight layers with sine wave fiber.

From these figures, the following can be noticed:

1. The oscillation of the symmetric cross-ply laminated composite plate with sine wave fiber (***k***=12,Δ=0.4) is less than that of other plates.
2. The time capacity of the laminated plate with symmetric cross-ply lamination and with sine wave fiber (***k***=4 and ***k***=12) is greater than the time capacity of the laminated plate with symmetric cross-ply lamination and with sine wave fiber (***k***=8).
3. The time capacity of the laminated plate with sine wave fiber (***k***=8,Δ=0.4) is greater than that of the others and also the time capacity of

the symmetric cross-ply plate with sine wave fiber (k=8,Δ=0.2) is greater than that of the others.

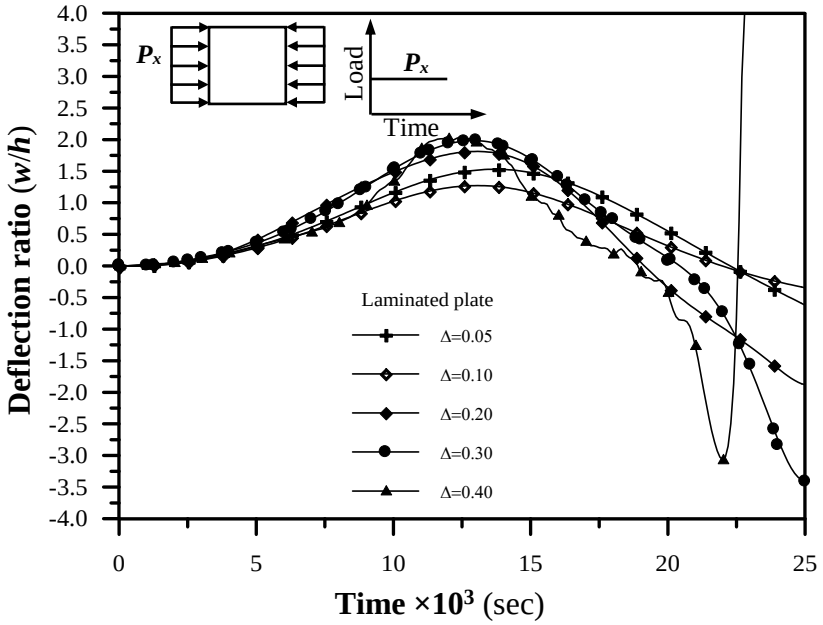

Figure (7.34): Effect of fiber waviness on the large displacement elastic-plastic analysis of a simply supported square laminated plate under in-plane constant dynamic loading, (b/h=100, Δt=0.0001, w_o/h=0.1, P_x=250 kN/m, k=4)

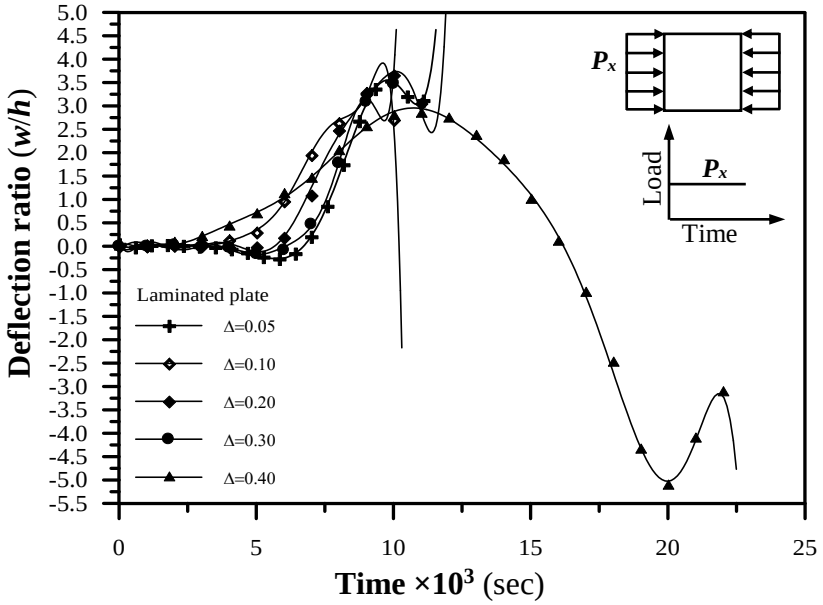

Figure (7.35): Effect of fiber waviness on the large displacement elastic-plastic analysis of a simply supported square laminated plate under in-plane constant dynamic loading, (b/h=100, Δt=0.0001, w_o/h=0.1, P_x=250 kN/m, k=8)

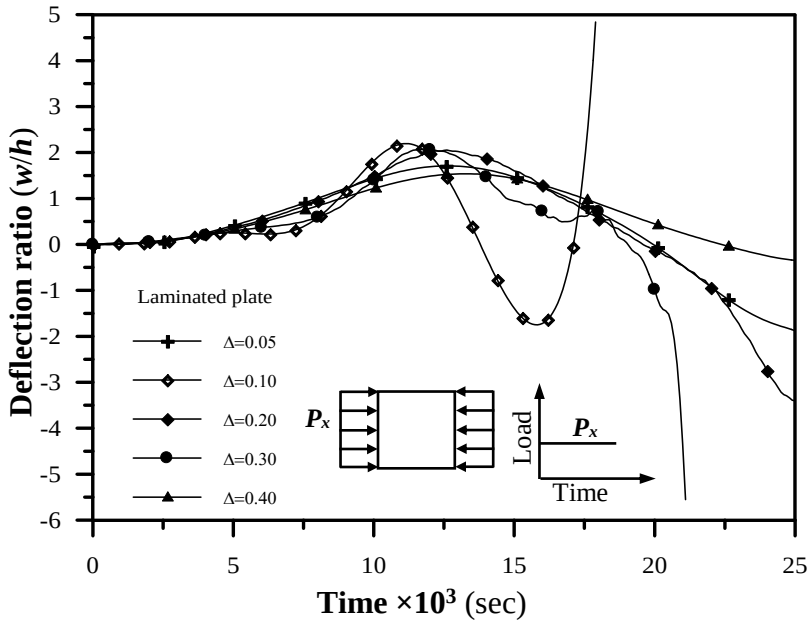

Figure (7.36): Effect of fiber waviness on the large displacement elastic-plastic analysis of a simply supported square laminated plate under in-plane constant dynamic loading, (b/h=100, Δt=0.0001, w_o/h=0.1, P_x=250 kN/m, k=12)

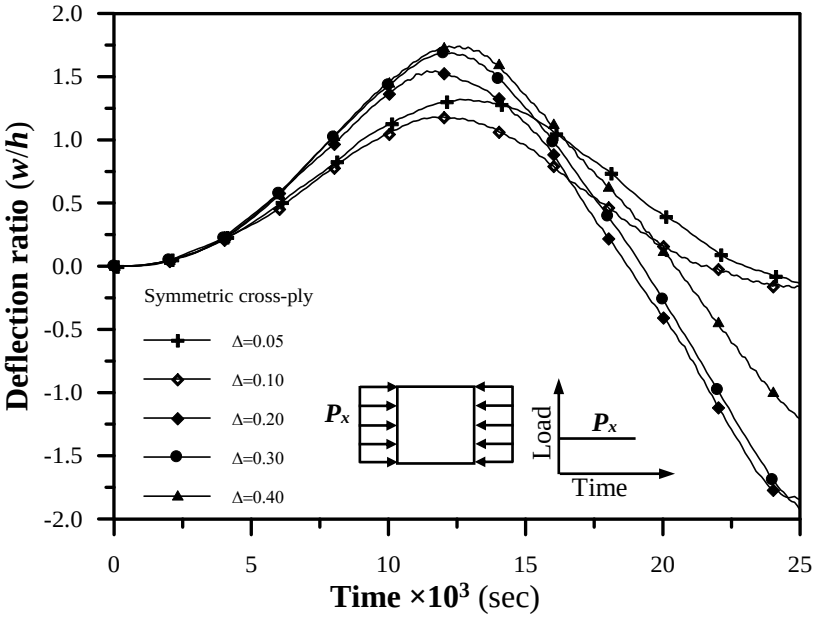

Figure (7.37): Effect of fiber waviness on the large displacement elastic-plastic analysis of a simply supported square symmetric cross-ply plate under in-plane constant dynamic loading, (b/h=100, Δt=0.0001, w_o/h=0.1, P_x=250 kN/m, k=4)

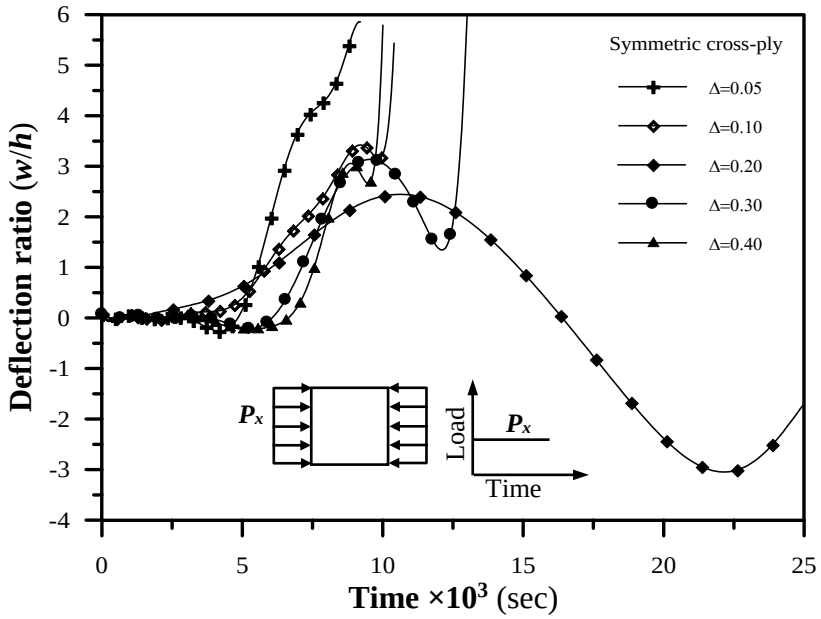

Figure (7.38): Effect of fiber waviness on the large displacement elastic-plastic analysis of a simply supported square symmetric cross-ply plate under in-plane constant dynamic loading, (b/h=100, Δt=0.0001, w_o/h=0.1, P_x=250 kN/m, k=8)

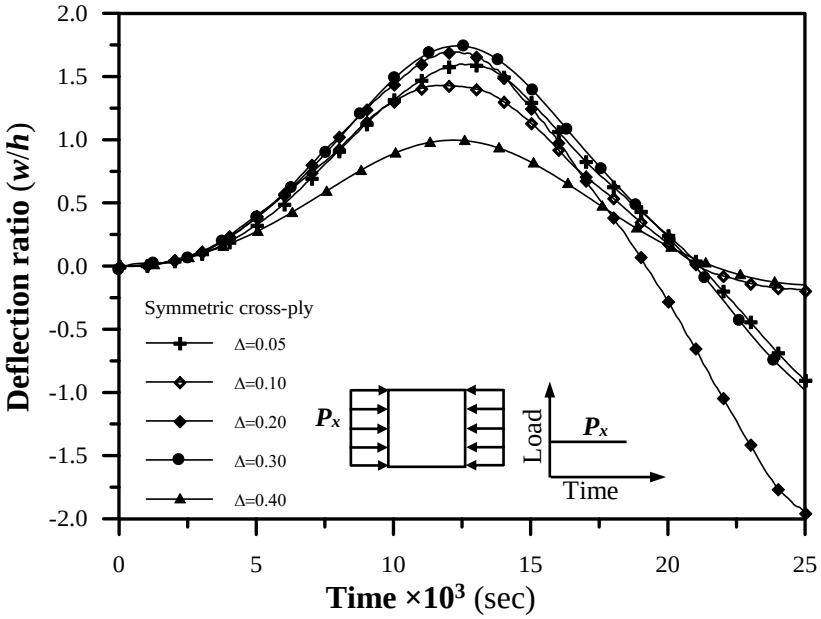

Figure (7.39): Effect of fiber waviness on the large displacement elastic-plastic analysis of a simply supported square symmetric cross-ply plate under in-plane constant dynamic loading, (b/h=100, Δt=0.0001, w_o/h=0.1, P_x=250 kN/m, k=12)

CHAPTER EIGHT

Conclusions and Recommendations

8.1 General

In this chapter, the conclusions based on the numerical solutions described in the previous chapters are given. The following conclusions are drawn with regard to the results obtained for the anisotropic plates under in-plane static and dynamic loading. Suggestions for future work are also presented.

8.2 Conclusions

8.2.1 Static analysis

1. The results of the present approach (two-dimensional layered approach) associated with the finite element method show that this approach is suitable to carry out the large displacement elastic-plastic analysis of anisotropic plates under transverse and in-plane loading.
2. The present higher order theory represents an efficient theory in the analysis of laminated plates when compared with the first order shear deformation theory and with the classical lamination theory. However, these theories are not necessary for the analysis of thin steel plates. These higher order and first order shear deformation theories lead to realistic parabolic variation of transverse shear stress through the plate thickness.
3. The behavior of thin plates is very sensitive to the amount of initial imperfection, slenderness ratio and aspect ratio. The decrease of ultimate strength of steel plates will increase with decreasing the aspect ratio such as the plate with slenderness ratio ($\frac{b}{h}\sqrt{\frac{\sigma_o}{E}}$=1.414) and aspect ratio ($\boldsymbol{a}/\boldsymbol{b}$=1.0, 0.8, and 0.6). The decreasing percentage of ultimate strength is (40%, 45%, and 52%), respectively with respect to the ($\boldsymbol{a}/\boldsymbol{b}$) ratios above.

4. The maximum decrease of the ultimate strength occurs in plates with slenderness ratio ($\left(\frac{b}{h}\sqrt{\frac{\sigma_o}{E}}\right) = 1.414$) for all types of aspect ratio.
5. Plates with slenderness ratio $\left(\frac{b}{h}\sqrt{\frac{\sigma_o}{E}}\right)$ less than (1.414) are considered to be thick plates where such plates yields without buckling while the very slender plates (slenderness ratio greater than 1.414) buckles elastically (without yielding). The plate with slenderness ratio (1.414) "critical buckling plate", shows buckling and yielding almost simultaneously.
6. Plates with aspect ratio (0.6) give maximum decrease of ultimate strength for a range of slenderness ratio (0.5-4.242).
7. The decreasing percentage of the ultimate strength of a steel plate increases with the decrease of slenderness ratio where plates with high slenderness the decreasing percentage of the ultimate strength will be little.
8. The ultimate strength of plates under in-plane compressive load decreases with the increase in the number of degrees of freedom. The decreasing percentage of ultimate strength of symmetric cross-ply plates is about (2.5%) for slenderness ratio (120) and is about (27%) for plates with slenderness ratio (20); while for antisymmetric cross-ply plates, the decreasing percentage of ultimate strength is about (2%) for plates with slenderness ratio (120) and about (30%) for plates with slenderness ratio (20).
9. The effect of fiber's orientation angle is found to be significant on the large displacement elastic-plastic behavior of laminated composite plates. It is found that the best angle at which one gets minimum deflection and maximum ultimate strength occurs at ($0^o/90^0$).
10. The increasing number of layers for the same volume of plate shows a pronounced effect on reducing the central deflection of plates. However, for symmetric cross-ply plates the decreasing percentage is about (2%) for the number of layers from (3) to (10), while the decreasing percentage

in antisymmetric cross-ply plates is about (5%) for the number of layers from (4) to (10). The decrease of central deflection of plates with symmetric lamination will die away when the number of layer becomes more than (6).

11. The behavior of a laminated plate is very sensitive to the shape of fibers (straight or sine wave). The behavior of a plate with sine wave fiber depends on the amplitude of the fiber and the number of sequences of fiber.
12. The ultimate strength of a laminated plate will increase as soon as the orthotropy ratio is increased, because of increasing the stiffness of the laminated plate with the same volume and number of layers. For a range of orthotropy ratio (1-20), the ultimate strength of a symmetric cross-ply plates will increase about (4.0) times for slenderness ratio (120) and about (2.5) times for slenderness ratio (20).
13. Symmetric cross-ply laminated plate with sine wave fiber ($\boldsymbol{k}$=12, Δ=0.4) represents the peak capacity and the best one.
14. The capacity of a laminated plate with sine wave fiber under in-plane compressive load in the direction of waviness is more than the capacity of the plate with sine wave fibers under in-plane compressive load orthogonal to the direction of waviness by (42%) for a plate with sine wave fiber ($\boldsymbol{k}$=12, Δ=0.4).
15. The ultimate strength of a symmetric cross-ply laminated plate is greater than the ultimate strength of an antisymmetric cross-ply laminated plate about (2%).

8.2.2 Dynamic analysis

1. The **Newmark**'s average acceleration represents the most efficient method in solving the nonlinear dynamic equilibrium equations for anisotropic plates.

2. The main conclusion of the large displacement elastic-plastic dynamic analysis is that a perfect plate does not reveal any oscillation when under in-plane dynamic loading of less than the buckling load of this plate.
3. The large displacement elastic-plastic dynamic analysis of a plate is very sensitive to the initial imperfection where the ultimate dynamic capacity and the time of failure will decrease as the initial imperfection is increased.
4. The increasing damping factor will decrease the amplitude of the response gradually with time and cause slowing in the oscillation of the plate.
5. If the response of the plate shows no oscillation about the static deflection position, it means that the damping factor is under the critical damping ratio.
6. The large displacement elastic-plastic dynamic analysis is very sensitive to the orthotropy ratio. For a range of orthotropy ratio (1-20), the central deflection will decrease about (78%) for a symmetric cross-ply plate and about (70%) for an antisymmetric cross-ply plate.
7. The effect of fiber's orientation angle is found to be significant on the large displacement elastic-plastic dynamic analysis of laminated composite plates under in-plane dynamic loading. It is found that the central deflection of a plate with ($0^o/90^o$) gives response less than others; this orientation of fibers is optimum for plates under in-plane pulse dynamic loading.
8. The dynamic capacity of a plate and the time of duration will decrease as the loading ratio ($\boldsymbol{P_x/P_u}$) is increased.
9. The antisymmetric cross-ply laminated plate has a damping rate faster than the symmetric cross-ply laminated plate. Therefore, this lamination may be used in plates which are subject to high intensity impact load and need to damp this oscillation in a shorter time of duration.

10. The time of capacity of a laminated plate with symmetric cross-ply lamination and with sine wave fibers (***k***=4 and ***k***=12) is greater than the time of capacity of a laminated plate with symmetric cross-ply lamination and with sine wave fibers (***k***=8).
11. The oscillation of a symmetric cross-ply laminated composite plate with sine wave fibers (***k***=12, Δ=0.4) is less than that in other plates and this represents the peak capacity and this case is the best one.

8.3 Recommendations

From the present study the following recommendations are suggested for further studies.

1. Studying the large displacement elastic-plastic dynamic analysis of stiffened steel plates with initial cracking.
2. Studying the large displacement elastic-plastic dynamic analysis of anisotropic plates under thermal and in-plane loading.
3. Studying the large displacement elastic-plastic dynamic analysis of anisotropic plates under thermal and in-plane loading with delamination through thickness.
4. Studying the free vibration of laminated composite plates with sine wave fibers.
5. Studying the large displacement elastic-plastic dynamic analysis of laminated composite plates with varying sine wave fibers through thickness.
6. Studying the wave propagation effect in laminated composite plates.
7. This subject needs to be supplemented by experimental results to be obtained from laboratory tests under dynamic loads.

REFERENCES

1. Aalami, B., and Chapman, J. C., "Large Deflection Behavior of Orthotropic Plates under Transverse and In-plane Loads", Proc. ICE, London, England, Vol.42, Mar., 1969, pp.347-382.

2. Abbas, F. K., and Mathlum, M. K., "Large Deflection Elasto-Plastic Analysis of Plates by Finite Element Methods", Eng. and Tech., Vol.19, No.4, 2000, Baghdad, pp.88-108.

3. Abdel-Sayed, G., "Effective Width of Thin Plates in Compression", ASCE, J. Struct. Eng., Vol.95, No.ST10, Oct., 1969, pp.2183-2203.

4. Abid-Ali, A. K., "Stress Analysis of Laminated Fiber Reinforced Composite Cylinder", M.Sc. Thesis, University of Babylon, Hilla, Iraq, 2000.

5. Ali, A. A., "Vibration and Stability Analysis of Frame-Type Structures and Plates Using Beam-Column Analogy", PhD. Thesis, University of Technology, Building and Construction Department, Baghdad, Iraq, 2004.

6. Ali, N. H., "Finite Element Dynamic Analysis of Laminated Composite Plates Including Damping Effect", M.Sc. Thesis, University of Babylon, Hilla, Iraq, 2004.

7. Al-Khafaji, S. O. W., "Dynamic Analysis of Fiber Reinforced Composite Shell Structure under Action of Impulsive Excitation" M.Sc. Thesis, University of Babylon, Hilla, Iraq, 2005.

8. Al-Mutairy, H. M. K., "Large Displacement and Post-Buckling Analysis of Non-Prismatic Members in Plane Frames under Static and Dynamic Loads", M.Sc. Thesis, University of Babylon, Hilla, Iraq, 2000.

9. Alwash, N. A., "Elasto-Plastic and Limit Analyses of Thick plates", M.Sc. Thesis, University of Baghdad, Baghdad, Iraq, 1989.

10. Akay, H. "Dynamic Large Deformation Analysis of Plates Using Mixed Finite Elements" Comp. & Struct., Vol.11, 1980, pp1-11.

11. Amash, H. K., "Post-buckling and Post-Yielding Analysis of Imperfect Thin Plate by Finite Difference method", M.Sc. Thesis, University of Babylon, Hilla, Iraq, 2003.

12. Azevedo, R.L. and Awruch, A.M. "Geometric Nonlinear Dynamic Analysis of Plates and Shells Using Eight-Node Hexahedral Finite Element with Reduced Integration", J. Braz. Soc. Mech. Sci., Vol.21, No.3, 1999, pp.1-22.

13. Baka, H. A., "Nonlinear Finite Element Analysis of Flat and Slightly Curved Reinforced Concrete Slabs" Thesis, University of Babylon, Hilla, Iraq, 2002.

14. Bathe, K.J., and Ozdemir, H. "Elastic-Plastic Large Deformation Static and Dynamic Analysis.", Comp. & Struct., Vol.6, No.2, 1975, pp81-92.

15. Bathe, K.J., Ramm, E., and Wilson, E. "Finite Element Formulations for Large Deformation Dynamic Analysis." Int. J. Num. Meth. Eng., Vol.9, 1975, pp355-386.

16. Bathe, K.J., and Bolourchi, S. "A Geometric and Material Nonlinear Analysis of Plate and Shell Element." Comp. & Struct., Vol.11, 1980, pp23-48.

17. Bathe, K.J., "Finite Element Procedures in Engineering Analysis", Perntice-Hall, Englewood Cliffs, N.T., 1996

18. Bradfield, C.D., "An Evaluation of The Elastic-Plastic Analysis of Plates Loaded by Uniaxial In-Plane Compression", Int. J. Mech. Sci., Vol.24, No.3, 1982, pp.127-146.

19. Chajes, A., "Principles of Structural Stability Theory", Printice- Hall, Inc., Englewood Cliffs, New Jersey, 1974.

20. Chen, H., and Virgin, L.N. “Finite Element Analysis of Post-Buckling Dynamics in Plates Part II: Non-stationary Analysis” Int. J. Solids and Struct., Vol.-, No.-, 2005, pp--, at web site search.

21. Chia, C.Y., “Nonlinear Analysis of Plates”, McGraw-Hill International Book Company, 1980.

22. Clough, R.W., “Dynamics of Structures”, McGraw-Hill, 1982.

23. Coan, J.M., “Large Deflection Theory for Plates with Small Initial Curvature Loaded in Edge Compression”, J. Appl. Mech., Vol.18, June, 1951, pp.143-151.

24. Colville, J., Becker, E.B., and Furlong, R.W., “Large Deflection Analysis of Thin Plates”, ASCE, J. Struct. Div., Vol.99, No.ST3, Mar., 1973, pp.349-364.

25. Colville, J., and Kuen-Yaw Shye, “Post-Buckling Finite Element Analysis of Flat Plates”, ASCE, J. Struct. Div., Vol.105, No.ST2, Feb., 1979, pp.297-311.

26. Cook, R.D., “Finite Element Modeling for Stress Analysis”, John Wiley & Sons, Inc., 1995.

27. Crisfield, M.A., “Full-Range Analysis of Steel Plates and Stiffened Plating under Uniaxial Compression”, Proc. ICE, Vol.59, Part 2, Dec., 1975, pp.593-624.

28. Crisfield, M.A., “Nonlinear Finite Element Analysis of Solids and Structures”, Vol.1: Essentials, John Wiley & Sons, Inc., 2000.

29. Crisfield, M.A., “Nonlinear Finite Element Analysis of Solids and Structures”, Vol.2: Advanced Topics, John Wiley & Sons, Inc., 2000.

30. “Dynamic Analysis by Harmonic Acceleration Method”, For evaluation by Al-Sarraf, S., to be published, 1996.

31. Elseifi, M., “A New Scheme for the Optimum Design of Stiffened Composite Panels with Geometric Imperfections”, Ph.D. Thesis, Virginia Polytechnic Institute, U.S.A., 1998.

32. Fok, C. D. “Effects of Initial Imperfections on the Elastic Post-Buckling Behavior of Flat Plates.”, Ph. D. Thesis, Monash University, Cited in [71].

33. Fok, W.C., “Evaluation of Experimental Data of Plate Buckling”, ASCE, J. Eng. Mech., Vol.110, No.4, 1984, pp.577-588.

34. Frieze, P.A., Hobbs, R.E., and Dowling, P.J., “Application of Dynamic Relaxation to The Large Deflection Elasto-Plastic Analysis of Plates”, Comp. & Struc., Vol.8, 1978, pp.301-310.

35. Gallagher, R.H., “Finite Element Analysis Fundamentals”, Prentice-Hall, Englewood Cliffs, New Jersey, 1973.

36. Harding, J.E., Hobbs, R.E., and Neal, B.G., “The Elasto-Plastic Analysis of Imperfect Square Plates under In-Plane Loading”, Proc. ICE, London, Part 2, Vol.63, Mar., 1977, pp.137-158.

37. Hashin, Z. “Failure Criteria for Unidirectional Fiber Composites”, ASME, J. Appl. Mech., Vol.47, 1980, pp.329-334.

38. Hinton, E., and Owen, D.R.J., “Finite Element Programming”, First Edition, Academic Press Inc., London, 1977.

39. Hinton, E., and Owen, D.R.J., “Finite Element in Plasticity: Theory and Practice”, Pineridge Press Limited, Swansea, U.K., 1980.

40. Hinton, E., and Owen, D.R.J., “Finite Element Software for Plates and Shells”, Pineridge Press Limited, Swansea, U.K., 1984.

41. Hodge, P. G., “Plastic Analysis of Structures” McGraw-Hill, New York, 1959.

42. Houlston, R. “Finite Strip Analysis of Plates and Stiffened Panels Subjected to Air-Blast Load.”, Comp. & Struct., Vol.32, No.3/4, 1989, pp647-659.

43. Husain, H.M., Al-Daami, H., and Amash, H.K., "Buckling Behavior of Rectangular Plate with Variable Thickness." Eng. and Tech., Baghdad, Vol.21, No.10, 2002, pp.736-745.

44. Ishizoki, and Bathe, K.J. "Finite Element Large Displacement and Elastic-Plastic Dynamic Analysis of Shell Structures." Comp.&Struct., Vol.11, 1980, pp309-318.

45. Jaeger, L.G., "Elementary Theory of Elastic Plates", Pergamon Press Headington Hill Hall, Oxford, 1964.

46. Stegman, J., and Lind, E., "Notes on Structural Analysis of Composite Shell Structures", First Edition, 2001.

47. Jayachardalan, S.A., Gopalakrishnan, S., and Narayana, R., "Explicit Incremental Matrices for the Post-Buckling Analysis of Thin Plates with Small Initial Curvature", Int. J. Struct. Eng. and Mech., Vol.12, No.30, 2001, pp.283-295.

48. Johnson, W., and Mellor, P.B., "Engineering Plasticity" Van Nastrand Reinhold Company, 1973.

49. Jones, R.M., "Mechanics of Composite Materials", First Edition, Scripta Book Company, U.S.A., 1975.

50. Jones, R.M., "Mechanics of Composite Materials", Second Edition, Taylor and Francis Inc., U.S.A., 1999.

51. Kao, R., and Perrone, N. "Dynamic Buckling of Axisymmetric Spherical Caps with Initial Imperfection." Comp. & Struct., Vol.9, 1978, pp463-473.

52. Kao, R., "Nonlinear Dyanmic Buckling of Spherical Caps with Initial Imperfections", Comp. & Struct., Vol.12, 1980, pp49-63.

53. Kaw, A., "Mechanics of Composite Materials", Second Edition, Taylor and Francis Group, LLC, 2006.

54. Kielb, R. E., and Han, L. S., "Vibration and Buckling of Rectangular Plates under In-plane Hydrostatic Loading" J. Sound and Vibration, Vol.70, No.4, 1980, pp543-555.

55. Khante, S. N., Rode, V., and Kant, T., "Nonlinear Transient Dynamic Response of Damping Plates Using a Higher Order Shear Deformation Theory", Nonlinear Dynamics, Vol.47, 2007, pp38-403.

56. Koh, C.G., Owen,D.R., and Peric, D. "Explicit Dynamic Analysis of Elasto-Plastic Laminated Composite Shells: Implementation of Non-Iterative Stress Update Schemes for The Hoffman Yield Criterion" Computation Mechanics, Vol.16, 1995, pp307-314.

57. Kommineni, J. R., and Kant, T. "Geometrically Non-linear Transient C^o Finite Element Analysis of Composite and Sandwich Plates with a Refined Theory." Struct. Eng. And Mech., Vol.1, No.1, 1993, pp87-102.

58. Lee, S.C., and Yoo, C.H., "Strength of Plate Girder Web Panels under Pure Shear", ASCE, J. Struct. Eng., Vol.124, No.2, Feb., 1998, pp.184-194.

59. Lee, S.C., and Yoo, C.H., "Experimental Study on Ultimate Shear Strength of Web Panels", ASCE, J. Struct. Eng., Vol.128, No.8, Aug., 1999, pp.838-846.

60. Lee, S.C., and Yoo, C.H., and Yoon, D.Y., "Behavior of Intermediate Transverse Stiffness Attached on Web Panels", ASCE, J. Struct. Eng., Vol.128, No.3, March, 2002, pp.337-345.

61. Levine, H.S., Armen, H., Jr., Winter, R., and Pieko, A. "Nonlinear Behavior of Shells of Revolution under Cyclic Loading", Comp. & Struct., Vol.3, 1973, pp589-617.

62. Li, Z.H., and Owen, R.J. "Elastic-Plastic Analysis of Laminated Anisotropic Shells by a Refined Finite Element Laminated Model", Comp. & Struct., Vol.32, No.5, 1989, PP1005-1024.

63. Lin, T.H., Lin, S.R., and Mazelsky, B., "Elasto-Plastic Bending of Rectangular Plates with Large Deflection", Trans. ASME, Vol.39, Dec., 1972, pp.978-982.

64. Little, G.H., "Rapid Analysis of Plate Collapse by Live-Energy Minimization", Int. J. Mech. Sci., Vol.19, 1977, pp.728-744.

65. Mallikarjuna, and Kant, T. “Dynamics of Laminated Composite Plates with a Higher-Order Theory and Finite Element Discretization.” J. Sound and Vibration, Vol.126, No.3, 1988, pp463-475.

66. Mathlum, M.K., “Large Deflection Elasto-Plastic Analysis of Plates by Finite Element Method”, M.Sc. Thesis, Department of Building and Costruction, Universty of Technology, Iraq, 1997.

67. Mirambell, E., Costa, J., and Arnedo, A., “Analytical and Experimental Study on the Behavior of Steel Panels under Plane Compression”, Proc. Int. Conf. On Steel Struct., CI-Premier Pte. Ltd, Jakarta, Indonesia, 1994, pp.205-212

68. Mirambell, E., Zarate, A.V., “Web Buckling of Tapered Plate Girders”, Proc. ICE, Structs & Bldgs, Vol.140, Feb., 2000, pp.51-60.

69. Mohammed, A.M., “Effect of Initially Imperfect and Boundary Condition on The Buckling and Post-Buckling Behavior of Steel Plates”, M.Sc. Thesis, Department of Building and Construction, University of Technology, Iraq, 2001.

70. Moy, S. S., “Plastic Methods for Steel and Concrete Structures”, MacMillan Publishers, Ltd., 1985.

71. Moxham, K.E. “Theoretical Prediction of The Strength of Welded Steel Plates in Compression” Cambridge University Report No. CUED/C-Struct. TR2, 1971, cited in [7].

72. Murray, N.W., “Introduction to Theory of Thin-Walled Structures”, Oxford University Press, 1986.

73. Nagarajan, S., and Popov, E. P. “Elastic-Plastic Dynamic Analysis of Axisymmetric Shells.” Comp. & Struct., Vol.4, 1974, pp1117-1134.

74. Nagarajan, S., and Popov, E. P. “Nonlinear Dynamic Analysis of Axisymmetric Shells” Int. J. Num. Meth. Eng., Vol.9, 1975, pp535-550.

75. Ng, G.F. "The Analysis of Nonlinear Dynamic Behavior (Including Snap-Through) of Post-Buckling Plates by Simple Analytical Solution" NASA Memorandom, April, 1988, pp1-29.

76. Paik, J.K., and Kim, Y., "A Simplified Finite Element Method for The Ultimate Strength Analysis of Plates with Initial Imperfection", Journal of The Society of Naval Architects of Korea, Vol.26, No.1, Mar., 1989, pp.24-38.

77. Paik, J.K., "A New Concept of the Effective Shear Modulus for a Plate Buckled in Shear", J. Ship Research, Vol.39, No.1, Mar., 1995, pp.70-75.

78. Paik, J.K., Ham, J.H., and Ko, J.H., "A New Plate Buckling Design Formula", Journal of The Society of Naval Architects of Japan, Vol.172, 2nd Report, Dec., 1992, pp.417-428.

79. Paik, J.K., Thayamballi, A.K., Wang, G., and Kim, B.J., "On Advanced Buckling and Ultimate Strength Design of Ship Plating", The Society of Naval Architects and Marine Engineers, 2000.

80. Pandya, B. N., and Kant, T. "Finite Element Analysis of Laminated Composite Plates Using a Higher Order Displacement Model", Composite Science and Technology, Vol.32, 1988, pp.137-155.

81. Pandya, B.N., and Kant, T. "Higher Order Shear Deformable Theories for Flexure of Sandwich Plates-Finite Element Evaluations", Int. J. Solids and Structures, Vol.24, 1988, pp.1267-1286.

82. Pandey, M. D., "Effect of Fiber Waviness on Buckling Strength of Composite Plates." ASCE, J. Eng. Mech., Vol.125, No.10, 1999, pp.1173-1179.

83. Parhi, P.K., Bhattacharyya, S.K., and Sinha, P.K. "Failure Analysis of Multiple Delaminated Composite Plates Due to Bending and Impact" Bull. Mater. Sci., Vol.24, No.2, 2001, pp143-149.

84. Park, H., and Lee, S.W. "Dynamic Analysis of Geometrically Nonlinear Composite Structures under Time-Dependent Pressure Loading",2000.

85. Paz, M. “Structural Dynamics: Theory and Computation”, Von Nostrand Reinhold Comapny, NewYork, 1980.

86. Phan, N.D., and Reddy, J.N. “Analysis of Laminated Composite Plates Using a Higher Shear Deformation Theory.” Int. J. Num. Meth. Eng., Vol.21, 1985, pp2201-2219.

87. Pica, A., Wood, R.D., and Hinton, E. “Finite Element Analysis of Geometrically Nonlinear Plate Behavior Using a Mindlin Formulation.” Comp. & Struct., Vol.11, 1979, pp.203-215.

88. Pica, A., Wood, R.D “Post-Buckling Behavior of Plates and Shells Using a Mindlin Shallow Shell Formulation.” Comp. & Struct., Vol.12, 1980, pp.759-768.

89. Pytet, M., “Introduction to Finite Element Vibration Analysis”, 1990, cited in [31].

90. Rao, S.S., “Mechanical Vibrations”, 1st Edition, Addison-Wesely Publishing Company, Inc., U.S.A., 1986.

91. Reddy, J.N. “Dynamic (Transient) Analysis of Layered Anisotropic Composite Material Plates.” Int. J. Num. Meth. Eng., Vol.19, 1983, pp237-255.

92. Reddy, J.N., “On Laminated Composite Plates with Integrated Sensors and Actuators”, Eng. Struct., Vol.21, 1999, pp.568-593.

93. Rerkshanandana, N., Usami, T., and Karasudhi, P., “Ultimate Strength of Eccentrically Loaded Steel Plates and Box Sections”, Comp. & Struct., Vol.13, 1981, pp.467-481.

94. Rudrapatna, N.S., Vaziri, R., and Olson, M.D. “Deformation and Failure of Blast Loaded Square Plates.” Int. J. Impact Engineering, Vol.22, 1999, pp449-467.

95. Rudrapatna, N.S., Vaziri, R., and Olson, M.D. “Deformation and Failure of Blast Loaded Stiffened Plates.” Int. J. Impact Engineering, Vol.24, 2000, pp457-474.

96. Rushton, K.R., "Post-Buckling of Tapered Plates", Int. J. Mech. Sci., Vol.11, 1969, pp.461-480.

97. Save, M.A., and Massonnet, C. E., "Plastic Analysis and Design of Plates, Shells and Disks", North-Holland Publishing Company-Amsterdam, 1972.

98. Shukla, K.K., and Nath, Y., "Thermomechanical Post-Buckling of Cross-Ply Laminated Rectangular Plates", ASCE, J. Eng. Mech., Vol.128, No.1, 2002, pp.93-101.

99. Sridharan, S., and Graves-Smith, T.R., "Post-Buckling Analysis with Finite Strips", ASCE, J. Eng. Mech. Div., Vol.107, No.EM5, Oct., 1981, pp.869-888.

100. Stein, M., "Behavior of Buckling Rectangular Plates", ASCE, J. Eng. Mech. Div., Vol.86, No.EM2, Apr., 1960, pp.59-76.

101. Stricklin, J.A., Martinez, J.E., Hong, J.H., and Haisler, W. E., "Nonlinear Dynamic Analysis of Shells of Revolution by Matrix Displacement Method." J. AIAA, Vol.9, No.4, 1971, pp629-636.

102. Subbaraj, K., and Dokaniish, M. A., "A Survey of Direct Time-Integration in Computational Structural Dynamics-II Implicit Methods. " Comp.&Struct., Vol.32, No.6, 1989, pp1387-1401.

103. Sun, G., and Williams, F.W., "An Initial Post-Buckling Analysis for Prismatic Plate Assemblies under Axial Compression", Int. J. Solids and Structures, Vol.34, No.28, 1997, pp.3705-3725.

104. Szilard, R., "Theory and Analysis of Plates: Classical and Numerical Methods", Prentice- Hall, Inc., Englewood Cliffs, New York, 1974.

105. Tao, Z., Tu-guang, L., Yao,Z., and Jio-zhi,L. "Nonlinear Dynamic Buckling of Stiffened Plates under In-plane Impact Load.", J. Zhejiang University Science, Vol.5, No.5, 2004, pp609-617.

106. Timoshenko, S.P., and Woinowsky-Krieger, S., "Theory of Plates and Shells", 2nd Ed, McGraw-Hill Book Co., Inc., New York, 1959.

107. Timoshenko, S.P., and Gere, J.M., "Theory of Elastic Stability", 2nd Ed, McGraw-Hill Book Co., Inc., New York, 1961.

108. Turvey, G.J., and Salehi, M., "Elasto-Plastic Response of Uniformly Loaded Sector Plates: Full-Section Yield Model Predictions and Spread of Plasticity", Comp. & Struct., Vol.79, 2001, pp.2335-2348.

109. Ueda, Y., and Yao, T., "The Plastic Node Method: A New Method of Plastic Analysis", Computer Methods in Applied Mechanics and Engineering, Vol.34, 1982, pp.1089-1104.

110. Ueda, Y., Rashed, S.M.H., and Paik, J.K., "An Incremental Galerkin Method for Plates and Stiffened Plates", Comp. & Struct., Vol.27, No.1, 1987, pp.147-156.

111. Ugral, A.C., "Stresses in Plates and Shells", McGraw-Hill, Inc, 1981.

112. Usami, T., "Post-Buckling of Plates in Compression and Bending", ASCE, J. Struc. Eng., Vol. 108, No. ST3, Mar., 1982, pp.591-609.

113. Usami, T., "Effectve Width of Locally Buckled Plates in Compression and Bending", ASCE, J. Struct. Eng., Vol.119, No.5, May, 1993, pp.1358-1373.

114. Wah, T., "Large Deflection Theory of Elasto-Plastic Plates", ASCE, J. Eng. Mech. Div., Vol.84, No. EM4, Oct., 1958, pp.1-24.

115. Wang, P.C., "Numerical Matrix Method in Structural Mechanics", John Wiley & Sons, Inc., 1966.

116. Weller, T., Abramovich, H., and Yaffe, R., "Dynamic Buckling of Beams and Plates Subjected to Axial Impact", Comp. & Struct., Vol.32, No.3/4, 1989, pp835-851.

117. Williams, D.G. and Walker, A. C., "Explicit Solution for The Design of Initially Deformed Plates Subject to Compression", Proc. ICE, London, Vol.59, Part 2, 1975, pp.763-787.

118. Williams, D.G., and Aalami, B., "Thin Plate Design for In-Plane Loading", Halsted Press, A Division of John Wiley & Son, Inc., New York, 1979.

119. Wilson, E.L., and Penzien, J., "Evaluation of Orthogonal Damping Matrices.", Int. J. Num. Meth. Eng., vol.4, 1972, pp5-10.

120. Yamaki, N., "Post-Buckling Behavior of Rectangular Plates with Small Initial Curvature Loaded in Edge Compression", ASME Trans., J. Appl. Mech., Vol.26, 1959, pp.407-414.

121. Zienkiewicz, O.C., and Taylor, R.L. "The Finite Element Methods", Fifth Edition, McGraw-Hill Book Company, London, 1977.

122. Zienkiewicz, O.C., "The Finite Element Methods", Third Edition, Vol.1:The Basis, McGraw-Hill Book Company, London, 2000.

.123

124. Zienkiewicz, O.C., "The Finite Element Methods", Third Edition, Vol.2: Solid Mechanics, McGraw-Hill Book Company, London, 2000.

125. Zou, G., and Qiao, P., "Higher Order Finite Strip Method for Post-Buckling Analysis of Imperfect Composite Plates" J. Eng. Mech., Vol.128, No.9, Sep., 2002, pp.1008-1015.